Analysis and control of self-sustained instabilities in a cavity using reduced order modelling

Kaushik Kumar Nagarajan

THÈSE

En vue de l'obtention du

DOCTORAT DE L'UNIVERSITÉ DE TOULOUSE

Délivré par :
Institut National Polytechnique de Toulouse (INP Toulouse)

Discipline ou spécialité :

Dynamique des fluides

Présentée et soutenue par :
Kaushik Kumar NAGARAJAN

le : lundi 8 février 2010

Titre :
Analysis and control of self-sustained instabilities in a cavity
using reduced order modelling
Analyse et contrôle des instabilités dans une cavité
par modélisation d'ordre réduit

JURY
Jean-Pierre RAYMOND, Professeur, Université Paul Sabatier, IMT, Toulouse, Président
Christophe AIRIAU, Professeur, Université Paul Sabatier, Toulouse, Directeur
Laurent CORDIER, Chargé de recherche CNRS, LEA/CEAT, Poitiers, Examinateur
Angelo IOLLO, Professeur, Université Bordeaux, IMB, Bordeaux, Rapporteur
Bernd. R NOACK, Directeur de Recherche CNRS, LEA/CEAT, Poitiers, Rapporteur

---

Ecole doctorale :
Mécanique, Energétique, Génie civil et Procédés (MEGeP)

Unité de recherche :
Institut de Mécanique des Fluides de Toulouse (IMFT)

Directeur(s) de Thèse :
Christophe AIRIAU, Professeur, Université Paul Sabatier, Toulouse
Azeddine KOURTA, Professeur, Polytech Orléans, PRISME, Orléans

Rapporteurs :
Angelo IOLLO, Professeur, Université Bordeaux, IMB, Bordeaux
Bernd. R NOACK, Directeur de Recherche CNRS, LEA/CEAT, Poitiers

Acknowledgments

Thomas Alva Edison once said: ”100% Success = 99% perspiration + 1% inspiration” ! for me, the ratio of perspiration to inspiration didn’t trigger my thoughts as much as the truth that inspiration is more dense, deeper and carries equal weight! Without being ‘calculative’ in expressing myself, I would still have to admit my anxiety of making understatements:

I cannot thank enough my supervisors Christophe Airiau and Azeddine Kourta who have motivated me to stretch my forte and my competence beyond limits and thereby helped me discover my inner strength which I was not aware of. I owe the success of my efforts and the brightness of my future to them. Christophe brought to this work the insight and rigor in many parts especially concerning ‘Control’. I am very indebted to him for having instilled in me a sense of rigor in my research, as well as in presenting this work. His concern to make his students learn the state-of-art was very well ref ected in the many workshops I attended during the three years.

Words fail to express my gratitude to Laurent Cordier from LEA Poitiers, who has for the most part of the work served as a virtual supervisor. His knowledge in POD based Reduced Order Modelling was indispensible. His rigor and never-say-die attitude has rubbed off on me for life. He has held the guiding light for me to tread this path and has encouraged me all-through. His guidance and constructive criticism have been like stepping stones in the process. Thanks for his great patience in talking to me practically everyday and advising me. Apart from this, I enjoyed the moments of long discussions I had with him on almost every topic.

I sincerely thank Bernd Noack and Angelo Iollo for accepting to be a part of the jury. Their deep knowledge of the state-of-art was ref ected in the many questions they posed and has encouraged me to pursue this f eld further in my career. I would also like to thank Jean-Pierre Raymond for agreeing to preside over the defence presentation. I would also like to remember him for the good lunches I had at his home, his lively spirit and love for Mathematics. I would also like to acknowledge Professor Pierre Comte of LEA Poitiers for providing me with a copy of his DNS code and his help during the initial days of the work.

Thanks for the support I received from the Service Informatiques during the last three years. Special thanks to Nicolas Renon of CICT for providing me various tips on large-scale computation. Thanks to Marie Christiani secretory of the group for coordinating the various activities of the project. Her enthusiasm to help foreign students in many day-to-day activities is noteworthy. I would also like to thank Véronique Cassin, the new secretory, for her help during the last days of the work.

Special thanks to the various partners of the AeroTraNet project who gave a new direction on solving a problem by combining the various aspects of work like numerical, experimental. The bi-annual meetings gave me an unique opportunity to network with various researchers working on different aspects of the same problem. I would also like to thank peers in the f eld whom I met during many conferences and workshops. Thanks to Clancy Rowley, Dietmar Rempfer, Ravindran for providing many exciting perspectives of thought. A special acknowledgment goes to John Burkardt from Florida State University for maintaining the best collection of libraries of various programs which have been used in this work. I have copied his style of programming!

Thanks to Laia and Sivam, mes amies in this long sejour of three years, who have stood by me and encouraged all along. Laia has been a great support till the last days of my thesis. Her

uncanny ability to organise things leaves me awe-struck. Sivam by sharing his treasure of Tamil songs made my days lively. Thanks to my other friends Karim, Anais, Houssam, Remi, Wafa, Marguerite, Thibaud, Benjamin, Romain, Xavier, Rudy, Mariyana, Bernard, Dirk, Yannick, Marie, Omar, Luigi, Sheetal and Aalap for their support and encouragement. I would like to acknowledge Yogesh for suggesting many improvements in the write-up. Thanks to David for giving me various tips for my f nal presentation.

I owe my heart f lled thanks to my parents; especially my mother (Smt. Girija Nagarajan), brother and sister-in-law (Ishwar & Ramya), sisters - Rani, Preethi, Gowri (Chinni included) for their encouragements, forbearance, support and prayers and having stood by me during 'high and low tides', for the unfaltering faith they had in me, which was an essential base to the victorious atmosphere I'm breathing in, right now.

Thanks to my friends the Badri-boys (Dilip, Guru, JP, Kiran, Parag, Sriram, Sreenidhi, Vivek), Divya and Swathi for their constant encouragement and prayers for my betterment. I would like to thank Raghoothamachar for cultivating in me a sense of unbiasedness while pursuing knowledge. Thanks to Dr. Ramesh (NAL) for encouraging me in my pursuits. I would also like to thank Dr Kirti Malhotra and Dr N. Balasubramanya my undergraduate professors. Thanks to Professor A.S.Vasudevamurthy of TIFR for his words of motivation to come abroad for a PhD.

There is no greater blessing than to have the guidance of an enlightened personality. All our knowledge, inspiration and wisdom are dormant within us as seeds. The proper watering through spiritual guidance nurtures these seeds to grow into deep-rooted, majestic trees. That kind of initiation is what I have received from Shrila Prabhupada. This seed was further cultivated and enriched by Shri Bannanje Govindacharya by showing me a new light, leading to the path of Shri Madhwacharya, who is immanent in every soul, the preceptor of all the worlds and the embodiment of all virtues.

Last but not the least, all these thanks-giving would have no real meaning if I fail to recognise the Supreme Lord Shri Krishna, immanent in all of them. I humbly dedicate this work unto His lotus feet with heart-felt prayers. I would like to admit that I too am a mere instrument in this progression.

This thesis has been supported by a Marie Curie Early Stage Research Training Fellowship of the European Community's Sixth Framework Programme under contract number MEST CT 2005 020301.

Contents

General Introduction

Motivation

Les émissions acoustiques représentent un des problèmes majeures du transport aérien qui concernent l'environnement. Généralement on classe les bruits émis en fonction de leur origine mécanique, aérodynamique et ceux liésaux systèmes secondaires. On s'intéresse ici au bruit émis au voisinage des aéroports, et il provient pour l'essentiel (voir figures 1 et 2) de l'écoulement autour du train d'atterrissage, de celui des jets de réacteurs et de différentes cavités présentes sur l'avion. Nous allons dans la suite considéré uniquement la géométrie de la cavité dont l'écoulement est schématiquement donné sur la figure 3 et 4, en fonction du rapport d'aspect. Le travail présenté ici consiste à analyser la physique de l'écoulement et de la propagation du bruit et surtout à chercher à réduire les émissions acoustiques.

Différents approches expérimentales par un contrôle passif ou actif de l'écoulement ont pu déjà être testées avec plus ou moins de succès, grâce en particulier aux avancées techniques dans les moyens de mesures et de de contrôle, et dans le domaine des ressources informatiques. Actuellement, en utilisant les Simulations Numériques Directes (DNS) ou les Simulations à Grandes Echelles (LES) nous sommes en mesure de mieux comprendre la physique de cet écoulement. Par contre, compte tenu de l'énorme dimension du problème, les études numériques et théoriques du contrôle acoustique doivent nécessairement passer par la réduction de modèle (ROM, voir figure 5). Ici nous appliquerons la Décomposition en Valeurs Propres Orthogonales (POD), qui permettent finalement de réduire la complexicité des équations de Navier-Stokes à la résolution et donc au contrôle, d'un systèmes d'équations au dérivées ordinaires (ODE, voir figure 6), plus simple à manipuler et résoudre. En se basant sur les travaux précédents de Rowley et al. (2003), Gloerfelt (2008), Kasnakoğlu (2007), Samimy et al. (2007) et de Cordier et al. (2009), nous allons proposer un contrôle du système réduit, une fois celui-ci calibré et l'appliquer ensuite sur le système complet issu des Simulations Numériques Directes.

Ce travail a été effectué dans le cadre d'un projet Marie-Curie appelé AeroTraNet, mené en collaboration avec 3 universités étrangères. Le LEA de Poitiers a largement contribué aux différentes parties: L. Cordier pour ce qui concerne la réduction de modèle, P. Compte pour les DNS.

Organisation du document

La chapitre 1 introduit l'outil de simulation numérique de base (DNS). Les éléments de la théorie du contrôle utilisés plus tard sont présentés dans le chapitre 2. Le chapitre suivant est consacré à la réduction de modèle et son application sur l'écoulement de cavité. Le système dynamique obtenu est fortement instable aussi le chapitre 5 est dédié à la calibration et la stabilisation du modèle réduit. De multiples approches sont abordées. Le contrôle du système dynamique forcé et son effet sur l'écoulement complet, sur la base de la théorie du contrôle linéaire quadratique gaussien sont finalement présentés dans le chapitre 5. Une conclusion suivi de quelques annexes achèvent le document.

Motivation

The recent rise in the air travel has given rise to a number of environmental concerns of which an important issue is the noise. Exposure to noise, particularly near the airports have been known to cause a number of health problems, like stress, hearing problems, hypertension, cardio-vascular problems, sleeping disorders. A constant exposure to noise levels beyond $65 - 70$ dB is known to cause life term health effects.

Noise emitted from an aircraft can be broadly classif ed as mechanical noise, aerodynamic noise and aircraft system noise. Mechanical noise is usually caused due to propeller, jet engines. The main source of mechanical noise in an aircraft occurs during cruise conditions, due to the high velocity of jet from the engine. The aerodynamic noise arises due to the airf ow around the different geometric conf gurations such as fuselages, high lift devices devices, landing gears, head and tail rotors of a helicopter etc. Aircraft system noise is mainly due to the cabin pressurisation as well as due to the auxiliary power units used to start the main engines, to provide power during ground conditions. Although during cruise conditions the mechanical noise dominates, the aerodynamic noise assumes an equal proportion during landing and takeoffs. Most of the aerodynamic noise during landing and take-offs can be associated to the landing gear, the geometry of which can be modelled as a cavity. Figure 1 shows the various components of noise sources during the landing or takeoff of aircrafts. Typical values of perceived noise, due to various components, during take off and landing is shown in f gure 2.

A similar phenomenon can also be seen in other conf gurations such as weapon bays, joints between high speed train bogies, car body openings. This brings to interest the study of cavity f ows, particularly when in search of quieter aircrafts as envisaged in the report European aeronautics: a vision for 2020 by EC (2001) .

A typical cavity f ow conf guration is as shown in f gure 3. The physics of the cavity can be explained by the formation of the shear layer at the upstream cavity edge. As the shear layer propagates it breaks down due to the Kelvin-Helmholtz mechanism resulting in a membrane like oscillation. The shear layer impinges the downstream edge of the cavity and splits, resulting in the formation of vortical structure close to the downstream edge, and is of the size of the depth of the cavity. This results in the formation of acoustic waves which propagates into the upstream, causing the far-f eld noise. The cavity can be classif ed based upon the f ow mechanism it generates, as an open cavity or a closed

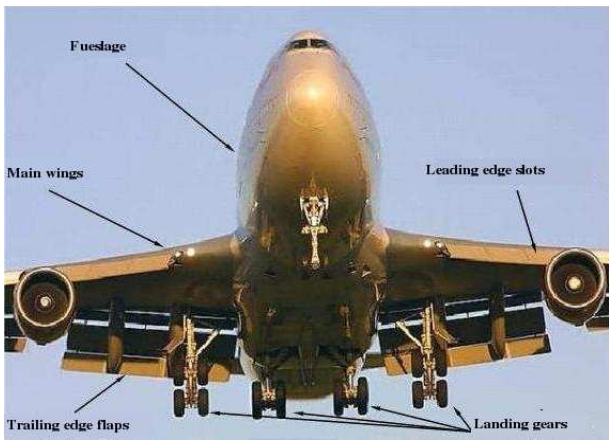

Figure 1 - *Typical airframe cavities. (Picture courtesy Ben Pritchard, airliners.com)*

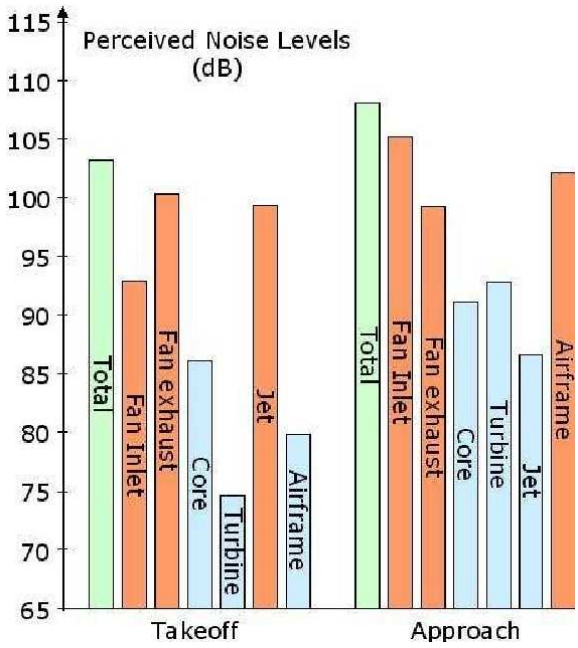

Figure 2 - *Aircraft noise sources, during approach and takeoff Owens (1979).*

cavity. Open cavities are characterised by the shear layer which attaches near the downstream corner, whereas closed cavities are characterised by the shear layer attachment at the bottom of the cavity and separation downstream. The basic difference can be summarised in f gure 4. Open cavities are further divided into deep cavities and shallow cavities based on the aspect ratio $\frac{L}{D}$. Deep cavities are charecterized by an aspect ratio $\frac{L}{D} < 1$, and shallow cavities by aspect ratio $\frac{L}{D} > 1$. Many of the airframe structures shown in f gure 1 can be treated as a shallow open cavity. The main interest of this work is then to study these f ows and to reduce the noise due to the acoustics.

There has also been numerous attempt to reduce the noise emitted from a cavity, by many heuristic

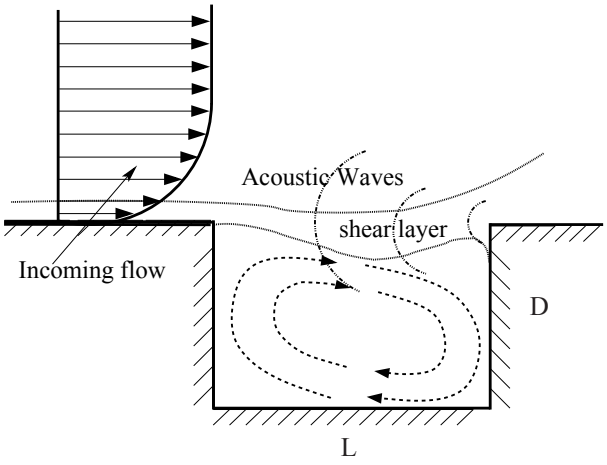

Figure 3 - *A typical cavity flow.*

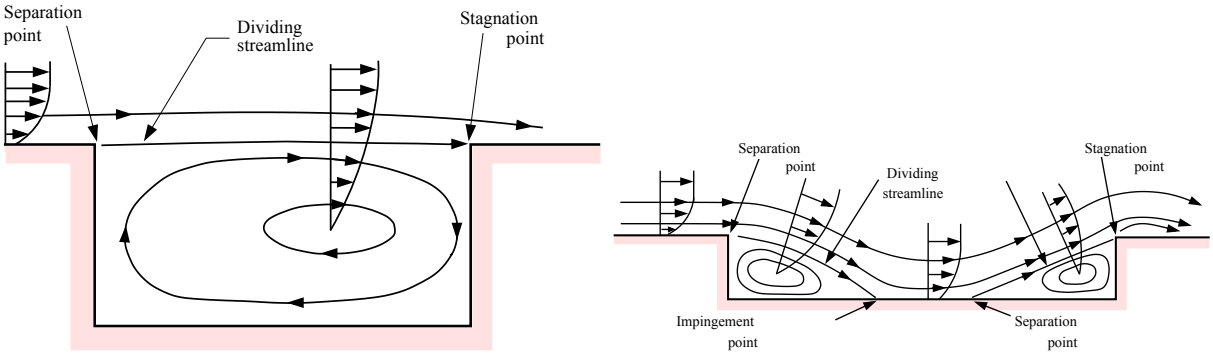

(a) Open cavities. (b) Closed cavities.

Figure 4 - *Schematic representation of open and closed cavities.*

means such as modifying the geometry by means of castellations, spoilers at the upstream edge of the cavity, so as to change the turbulent scales and hence reduce acoustic emissions. Use of synthetic jets delays the re-attachment of the shear layer and has been used in many experiments. With the advent of high performance computing as well as advanced experimental techniques such as the Particle Image Velocimetry (PIV), Laser Doppler Velocimetry (LDV) deep insights into the physics of cavity flows can be explored, with an aim to reduce the noise.

The traditional approaches like Direct Numerical Simulation (DNS) involve fully resolving the equations governing the flow dynamics *i.e.* the Navier-Stokes' equations down to the finest scale. Although this approach seems attractive it has inherent difficulties like the computational resources. An approach to reduce the computational time is the utilisation of Large Eddy Simulation (LES) where the major structures governing the flow (large eddies as they are called) are resolved and the finer scales are modelled. This approach also poses difficulties, particularly when used as an iterative tool for flow control, due to their high dimensional nature. The next proposition to reduce the dimensionality of the problem is by restricting our interest to the "most essential structures" which governs

the dynamics. The basic observation of fluid flow as a cascading phenomenon gives us the hint of this "essential" structures in terms of the energy, to obtain a low dimensional space. The reduced order model is then constructed as a projection of the high dimensional dynamics onto this lower dimensional subspace as summarised in figure 5.

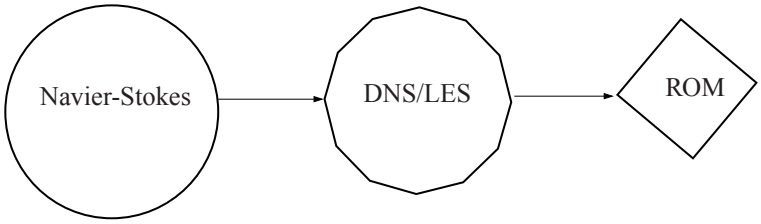

Figure 5 - *Philosophy of reduced order modelling.*

The aim of this thesis is to construct reduced order models for the cavity flows. The basic idea is to retain the most essential features of the flow called Proper Orthogonal Decomposition POD modes, which contain the maximum amount of information about the flow dynamics. By performing a DNS of the compressible Navier-Stokes equations to compute the flow of a large cavity, the POD modes are extracted. The Reduce Order Model (ROM) is then obtained by projecting the governing equation of fluid flow i,e the Navier Stokes equations on the subspace spanned the POD modes. This results in one having to solve a system of Ordinary Differential Equations (ODE) rather than the complicated system of Partial Differential Equations (PDE) and hence the name reduced order modelling. The well developed control theory is applied on this system of ODE's to obtain the noise reduction. Apart from being used in-lieu of the high fidelity model for control studies, the reduced order model obtained can also be used as a predictive tool to save computational resources. The overall strategy of using a reduced order model (ROM) can be summarised as shown in the figure 6.

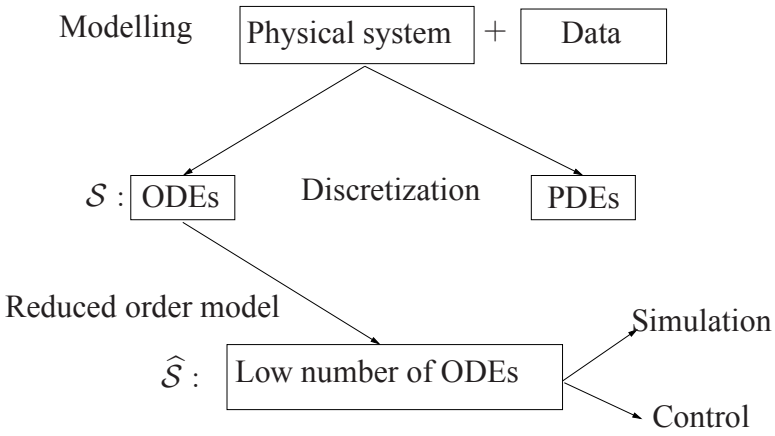

Figure 6 - *A Schematic representation of Reduced Order Modelling.*

Flow past an open cavity has been studied using ROM by Rowley *et al.* (2003) and Gloerfelt (2008) but without any application to flow control. More recently, ROM for controlled configurations has

been proposed by Kasnakoğlu (2007). In Samimy *et al.* (2007) the ROM for flows issued from an experiment has been used to design a controller. The major hurdle in using the ROM for control applications is the accuracy of the model in predicting the dynamics of the system even for short periods. Also difficulty arises when the control parameters are changed as in a real time simulation. Various numerical strategies termed as calibration techniques has been developed in the recent past to treat this problem as found in Cordier *et al.* (2009). The major contribution of this thesis is then to complete the full development as applied to cavities, like building up the ROM, including the effect of control, calibrating the model and finally performing control studies.

The outcome of the interest in reducing the cavity noise has resulted in the frame work of Aero-TraNet (Aerodynamic Training Network) projected which was a collaboration of 4 academic partners in Europe. The academic partners which included University of Leicester (U.K.), the Università degli Studi Roma Tre (Rome, Italy), Politecnico di Torino (Turin, Italy) and Institut de Mécanique des Fluides de Toulouse (Toulouse, France) were interested in various aspect of the cavity flow, like, numerical, experimental and flow control. This thesis was done in collaboration with LEA Poitiers, P. Comte for the DNS and L. Cordier for reduced order modelling. The thesis can be summarized as follows.

Organisation of the thesis

In chapter 1 we give a brief description of the numerical tool, namely the DNS used in this study and present some validation results. In chapter 2 the basic tools from control theory are introduced.

Chapter 3 concerns the basic theory of the technique of POD based ROM. The various techniques to include the effect of actuation in the ROM are summarized, with an application to the cavity flow.

In Chapter 4 the various definitions of errors between the calibrated dynamics and the original temporal dynamics are introduced and the different methods of calibration summarized are applied to the cavity flows. The methods are compared for accuracy. The calibration of the ROM is performed using a Tikhonov based regularization to obtain an accurate representation of the dynamics. We also present an improvement of the technique by introducing various type of weight matrix used in the definition of error. In the first method, we use a sensitivity analysis of the ROM, to determine the weights of the relevant terms which needs to be calibrated. The second approach is to use the energy content of the POD representation in forming the weight matrix to represent the errors.

In Chapter 5 a feedback control law based on the estimation of the observer dynamics has been presented. The observer matrix is constructed using a linear stochastic estimation. A sensititivity study of the actuated dynamics has been performed to determine the relevant terms in the linearisation of the model. Finally an Linear Quadratic Gaussian (LQG) controller is designed to obtain an optimal solution, which is introduced in the Direct Numerical Simulation to obtain a decrease in spectra of the cavity acoustic mode.

Chapter 1

Description and validation of the numerical tool

Description et validation de l'outil numérique

Dans cette partie, les outils numériques utilisés pour les études de modèle réduit et du contrôle sont décrits. Le jet synthétique est introduit pour contrôler les instabilités de cavité. L'écoulement de cavité est largement étudiée dans la littérature. Il présente des instabilités auto-entretenues qui sont difficiles à prédire numériquement (sensibilité aux différents paramètres numériques). La cavité est aussi le siège d'intéractions aéroacoustiques qui nécessitent un schéma numérique d'ordre supérieur et peu dissipatif pour capter les ondes acoustiques. Le code NIGLO utilisé est développé par Pierre Comte de l'Université de Poitiers. Il est capable de résoudre les équations de Navier Stokes compressibles en instationnaire et en tridimensionnel. La discrétisation différences finies de quatrième ordre est faite sous forme conservative.

Paramètres de non-dimensionalisation

Le code résout les équations sous forme adimensionnelle. L'adimensionalisation dépend fortement des échelles caractéristiques pour rendre les variables adimensionnelles. La forme adimensionnelle des équations de Navier-Stokes incorpore trois nombres adimensionnel, les nombres de Reynolds, de Mach et de Prandtl.

Equations du mouvement en coordonnées cartésiennes

Les équations de Navier Stokes compressibles sont écrites sous forme conservatives. Il s'agit des équations de continuité, de conservation de la quantité de mouvement et de l'énergie. Le tenseur des contraintes de cisaillement est exprimé sous l'hypothèse de Newton-Stokes et le flux thermique est donné à l'aide de la loi de Fourier. La viscosité en fonction de la température est exprimée avec la loi de en puissance.

Avancement en temps

Le schéma temporel utilisé est un schéma explicite aux différences finies utilisant la procédure prédicteur-correcteur. Une différenciation décentrée conservative est utilisée pour les deux pas temporels du schéma en alternant la direction de discrétisation entre le pas prédicteur et correcteur. Il en résulte globalement un schéma spatial centré de quatrième ordre pour les termes d'advection et de second ordre pour ceux de la diffusion. La discrétisation temporelle est du second ordre.

Conditions aux limites

Pour les parois, la condition d'adhérence est appliquée. La forme simplifiée de l'équation dynamique reliant la pression et le tenseur de cisaillement est aussi utilisée. Pour l'état thermodynamique on définit soit une paroi adiabatique ou soit une paroi isotherme.

Conditions aux limites non-réféchissantes

Pour éviter toute réflexion sur les limites du domaine de calcul, deux types de conditions peuvent être adoptées: des conditions physiques dictées par le problème continu initial ou des conditions numériques nécessaires à la méthode discrète pour compléter l'ensemble des conditions physiques. Les conditions aux limites basées sur les caractéristiques (NSCBC) de Poinsot & Lele (1992) est une méthode pour spécifier à la fois les conditions physiques et numériques pour les équations d'Euler et pour celles de Navier Stokes. La méthode NSCBC est basée sur une analyse monodimensionnelle locale en non-visqueux (LODI) des ondes traversant les limites du domaine. Les amplitudes des ondes caractéristiques associées à chaque vitesse caractéristique sont données (équations 1.19 à 1.21). On distingue les conditions aux limites non-réféchissantespour une entrée subsonique (équations 1.22 à 1.27) de celles pour une sortie subsonique (équations 1.28 et 1.29).

Validation du code numérique pour le cas de la cavité

On présente les résultats pour une cavité de rapport d'aspect $L/D = 2$. L'écoulement est initialisé par une couche limite laminaire pour avoir une épaisseur $\delta/D = 0.28$ au coin amont de la cavité. Le nombre de Reynolds basé sur la profondeur de la cavité est de 1500 et le nombre de Mach est de 0.6.Le domaine de calcul a une longueur de $14D$ et une hauteur de $7D$ (figure 1.1). Le tableau 1.1 donne la taille des différents maillages utilisés. Le maillage choisi est donné sur la figure 1.2 et correspond au maillage M. La figure 1.4 montre les niveaux de pression sonore (SPL) pour le champ acoustique au-dessus de la cavité et le spectre de vitesse normal en un point de la couche cisaillée. Le niveau de pression sonore maximal est de 170 dB qui est inférieur à celui obtenu par Rowley et al. (2002) (180 db). Ceci peut s'expliquer par la différence de précision des schémas (4^{eme} ici et 6^{eme} pour eux). Les niveaux SPL sont cependant en accord avec les résultats expérimentaux de Krishnamurthi (1956) (168 dB). Le spectre montre la valeur typique correspondant au second mode de Rossiter (avec deux tourbillons en moyenne entre les deux coins de la cavité). Les oscillations auto-entretenues sont quasi-périodiques, avec un spectre présentant une fréquence dominante.

Introduction au contrôle

Le contrôle de la cavité résonante est réalisé à l'aide d'un jet synthétique en modifiant la condition au limite convenablement. Le contrôle par jet synthétique a été réalisé auparavant numériquement et expérimentalement. L'objectif du contôle est de dévier la couche cisaillée pour qu'elle n'impacte pas sur le coin aval et éviter le phénomène du retour (feedback). Comme on peut le voir sur la figure 1.6, sous l'effet du jet, la couche cisaillée peut impacter totalement, partiellement ou pas du tout. Plusieurs positions ont été testées avant le coin amont pour améliorer l'efficacité. Ceci peut être fait en mesurant la sensibilité de l'écoulement au coin amont. Il a été montrée que c'est le point le plus sensible aux perturbations externes. Le forçage est typiquement de la forme $A\sin(\omega t)$ et l'actionneur est introduit juste avant le coin de cavité ($x \in [-0.15; -0.05]$ et $y = 0$). Le spectre de vitesse pour un forçage de la forme $A\sin(wt)$ (figure 1.7) conduistant à la diminution du mode de Rossiter. Il y a une redistribution de l'énergie sur d'autres pics. L'actionnement est cependant non optimal. Un des objectifs de ce travail est de déterminer la fréquence et l'amplitude optimales en utilisant le contrôle dans le le modèle d'ordre réduit.

Conclusion

Dans ce chapitre nous utilisées introduit l'outil numérique, les équations, la discrétisation et les conditions aux limites utilisé. Le code a été validé sur le cas de la cavité. L'introduction du contrôle avec un jet synthétique placé avant le coin amont est décrite. On note la diminution du mode de Rossiter et la distribution de l'énergie sur d'autres pics. Les outils pour réaliser un contrôle optimal seront décrits dans la suite.

1.1 Introduction

In this chapter the basic numerical tool used in this work is described. We perform a DNS resolving of a 2D cavity f ow. Regarding the introduction of actuation a synthetic jet is introduced at the upstream boundary to control the instabilities. There has been a large body of literature on physics of the cavity f ow as can be found in Rowley *et al.* (2002), Larchevêque *et al.* (2004), Bres & Colonius (2008), Rowley & Williams (2006). Flows with self sustained oscillations are diff cult to model as they are very sensitive to the disturbances, due to shear layer amplif cation. Even a small error in the numerical discretisation at the cavity leading edge can result in a large amplif cation of the errors downstream of the cavity. Problems can also arise due to the artif cial ref ections at the computational boundary, and may sometimes be indistinguishable from the physical disturbances, causing the appearance of non-physical frequencies. Also in the case of cavity f ows the feedback mechanism is acoustic and of many orders smaller than the hydrodynamic disturbances, which necessitates the utilisation of a high order, low-dissipative numerical method to resolve them. The code NIGLO used in this study is capable of solving three dimensional unsteady compressible Navier-Stokes equations on multi-block curvilinear grid. The discretisation is through a fourth order f nite difference scheme for the advective f uxes and second order scheme for the diffusive f uxes. The temporal discretisation is second order accurate. The code was initially developed by Professor Pierre Comte at the University of Poitiers.

1.2 Non-dimensionalisation parameters

Non-dimensionalising the f ow-f eld parameters removes the necessity of converting from one system to another within the code. The process of non-dimensionalisation depends on the choice of the parameter for the problem. In the code all the parameters of the simulation are non-dimensionalised by the reference values, which are the characteristics of the f ow namely the Reynolds number, Mach number & Prandtl number. The Reynolds number is used to quantify the convective effects to the viscous effects, whereas Mach number gives the ratio between the reference velocity and the speed of the sound, f nally the Prandtl number gives the ratio between the heat transfer by viscous diffusion and heat transfer by thermal conduction.

$$x^*=\frac{x}{L_0} \quad y^*=\frac{y}{L_0} \quad z^*=\frac{z}{L_0} \quad u^*=\frac{u}{U_0} \quad v^*=\frac{v}{U_0}$$

$$w^*=\frac{w}{L_0} \quad P^*=\frac{P}{P_0} \quad \rho^*=\frac{\rho}{\rho_0} \quad T^*=\frac{T}{T_0} \quad t^*=\frac{U_0 t}{L_0}$$

Where all the quantities with $(\star)$ are the non-dimensionalised scales used in the code, and values with (0) are reference values of the f ow-f eld. In the following we use only non dimensional variables without $*$

1.3 Governing equations in cartesian coordinate system

The fully compressible Navier-Stokes equation in a conservative form can be written for the non dimensionalised variables as

$$\frac{\partial U}{\partial t} - \text{div}\mathcal{F} = 0 \tag{1.1}$$

with $\mathcal{F} = (E, F, G)$ and $U = (\rho, \rho u, \rho v, \rho w, \rho e)$.
In Cartesian coordinates we have,

$$\frac{\partial U}{\partial t} + \frac{\partial E}{\partial x} + \frac{\partial F}{\partial y} + \frac{\partial G}{\partial z} = 0 \tag{1.2}$$

where E, F, G are the non-dimensionalised f uxes def ned by:

$$E = \begin{bmatrix} -\rho u \\ -\rho u^2 - \dfrac{1}{\gamma M^2}p + \dfrac{\mu}{Re}\tau_{xx} \\ -\rho uv + \dfrac{\mu}{Re}\tau_{xy} \\ -\rho uw + \dfrac{\mu}{Re}\tau_{xz} \\ -u(\rho e + p) + \gamma M^2 \dfrac{\mu}{Re}(u\tau_{xx} + v\tau_{xy} + w\tau_{xz}) + \dfrac{\gamma}{\gamma - 1}\dfrac{\mu}{RePr}q_x \end{bmatrix}$$

$$F = \begin{bmatrix} -\rho v \\ -\rho uv - \dfrac{1}{\gamma M^2}p + \dfrac{\mu}{Re}\tau_{xy} \\ -\rho v^2 - \dfrac{1}{\gamma M^2}p + \dfrac{\mu}{Re}\tau_{yy} \\ -\rho uw + \dfrac{\mu}{Re}\tau_{yz} \\ -v(\rho e + P) + \gamma M^2 \dfrac{\mu}{Re}(u\tau_{xy} + v\tau_{yy} + w\tau_{yz}) + \dfrac{\gamma}{\gamma - 1}\dfrac{\mu}{RePr}q_y \end{bmatrix}$$

$$G = \begin{bmatrix} -\rho w \\ -\rho uw - \dfrac{1}{\gamma M^2}p + \dfrac{\mu}{Re}\tau_{xz} \\ -\rho vw + \dfrac{\mu}{Re}\tau_{yy} \\ -\rho w^2 - \dfrac{1}{\gamma M^2}p + \dfrac{\mu}{Re}\tau_{zz} \\ -w(\rho e + p) + \gamma M^2 \dfrac{\mu}{Re}(u\tau_{xz} + v\tau_{yz} + w\tau_{zz}) + \dfrac{\gamma}{\gamma - 1}\dfrac{\mu}{RePr}q_z \end{bmatrix}$$

The Reynolds number is based on the characteristic length L_0 of the cavity, and velocity U_0, which represents the characteristics of the f ow can be def ned by:

$$Re = \frac{\rho_0 U_0 L_0}{\mu_0} \tag{1.3}$$

With μ_0 is the dynamic viscosity calculated at the same point of reference chosen for the velocity U_0 and for the density ρ_0. In the same manner, the Mach number based on a reference temperature T_0

$$M = \frac{U_0}{\sqrt{R\gamma T_0}} \tag{1.4}$$

The Prandtl number which corresponds to the ratio of the kinematic viscosity and thermal diffusivities:

$$Pr = \frac{\mu_0 C_p}{\lambda_0} \tag{1.5}$$

The total energy E is given by the equation of state as:

$$\rho E = \frac{1}{\gamma - 1} p + \frac{\gamma M^2}{2} \rho (u^2 + v^2 + w^2) \tag{1.6}$$

With the Stokes hypothesis the viscous stress tensor is proportional to the trace free part of the strain rate tensor.

$$\tau_{ij} = \left(\frac{\partial u_i}{\partial x_j} + \frac{\partial u_j}{\partial x_i} - \frac{2}{3} \frac{\partial u_l}{\partial x_l} \delta_{ij} \right) \tag{1.7}$$

With the above non-dimensionalisation, the Fourier law reads as

$$q_i = -k \frac{\partial T}{\partial x_i} \tag{1.8}$$

For taking into account the variation of dynamic viscosity with temperature a power law has been used and is given by

$$\mu(T) = \left\{ \mu(T_0) \left(\frac{T}{T_0} \right)^{0.7} \right. \tag{1.9}$$

1.4 Time advancement

The time advancement scheme employed in NIGLO is an explicit finite difference scheme of predictor-corrector type as proposed by Gottlieb & Turkel (1975). Conservative decentered differencing is utilised for two steps of time advancement scheme which alters the discretisation between the predictor and corrector steps, resulting in a globally centered scheme which is 4^{th} order for the advection term and 2^{nd} order for the diffusion term in space respectively. The discretisation is given by

Predictor step:

$$U_i^{n+1/2} = U_i^n + \begin{pmatrix} \frac{\Delta t}{\Delta x}[-\frac{7}{6}E_i^n + \frac{8}{6}E_{i+1}^n - \frac{1}{6}E_{i+2}^n] \\ \frac{\Delta t}{\Delta y}[-\frac{7}{6}F_i^n + \frac{8}{6}F_{i+1}^n - \frac{1}{6}F_{i+2}^n] \\ \frac{\Delta t}{\Delta z}[-\frac{7}{6}G_i^n + \frac{8}{6}G_{i+1}^n - \frac{1}{6}G_{i+2}^n] \end{pmatrix} \tag{1.10}$$

Corrector step:

$$U_i^{n+1} = \frac{1}{2}(U_i^{n+1/2} + U_i^n) + \begin{pmatrix} \frac{\Delta t}{\Delta x}[\frac{7}{12}E_i^{n+1/2} + \frac{8}{12}E_{i+1}^{n+1/2} - \frac{1}{12}E_{i+2}^{n+1/2}] \\ \frac{\Delta t}{\Delta y}[\frac{7}{12}F_i^{n+1/2} + \frac{8}{12}F_{i+1}^{n+1/2} - \frac{1}{12}F_{i+2}^{n+1/2}] \\ \frac{\Delta t}{\Delta z}[-\frac{7}{6}G_i^{n+1/2} + \frac{8}{12}G_{i+1}^{n+1/2} - \frac{1}{12}G_{i+2}^{n+1/2}] \end{pmatrix} \tag{1.11}$$

The predictor-corrector scheme described above is valid for uniform mesh. In our case when we use mesh ref nement to resolve the boundary layer, corners of cavity the mesh spacing is not constant. In that case we use a transformation of the physical variables into a new coordinates of constant length and perform the discretisation. The derivatives are then transformed back onto the physical coordinates by the inverse transform.

1.5 Boundary conditions

1.5.1 Wall boundary condition

No slip condition at the wall is applied, so that all the velocity components at the wall are zero *i.e.*

$$\begin{aligned} u_{\text{wall}} &= 0 \\ v_{\text{wall}} &= 0 \\ w_{\text{wall}} &= 0 \end{aligned} \tag{1.12}$$

The conservation of momentum equation is reduced to the following form

$$-\frac{1}{\gamma M^2}\frac{\partial p}{\partial x_n} + (\frac{\mu}{Re})(\frac{\partial \tau_{ij}}{\partial x_j}) = 0 \tag{1.13}$$

It only remains to determine the thermodynamic state at the wall, which is chosen as isothermal for the case of the cavity f ow.

1.5.2 Non-ref ective boundary conditions

The accuracy of unsteady f ow calculations relies on accurate treatment of boundary conditions. Due to the limit of computational resource, usually only a limited computational domain is considered for an unsteady f ow calculations. This means that we have to ”cut off” the domain that is not of our primary interest. However, the cut boundaries may cause artif cial wave ref ections which may include both physical and numerical waves. Such waves may bounce back and forth within the computational domain and may seriously contaminate the solutions.

Two types of conditions have to be provided to solve numerically the fully compressible Euler or Navier-Stokes equations

- Physical conditions which are the boundary conditions dictated by the original non-discretised problem.
- Soft conditions which are numerical conditions required by the discrete method to complete the set of physical conditions.

As described in Poinsot & Lele (1992), the Navier-Stokes characteristic boundary condition (NSCBC) specifies both the physical and soft boundary conditions for Euler and for Navier-Stokes equations. In this method physical conditions are specified according to the well-posedness of Navier-Stokes equation.

Viscous condition for Navier-Stokes are added to the inviscid Euler equations to obtain the right number of boundary conditions for Navier-Stokes. The viscous conditions are used only to compute the viscous terms in the conservation equations at the boundary and, therefore are not strictly enforced. The method relaxes smoothly to the Euler boundary condition when the viscosity goes to zero.

Soft conditions are constructed without any extrapolation. The NSCBC method is based on a local one dimensional inviscid (termed LODI) analysis of the waves crossing the boundary. The amplitude variation of the waves entering the domain are estimated from an analysis of the local one dimensional inviscid equations. To explain further consider the quasi-linear form of the Euler equation

$$\frac{\partial V}{\partial t} + A\frac{\partial V}{\partial x} + B\frac{\partial V}{\partial y} + C\frac{\partial V}{\partial z} = 0 \tag{1.14}$$

Which can also be written in the following compact form:

$$\frac{\partial V}{\partial t} + (\vec{A}.\vec{\nabla})V = 0 \tag{1.15}$$

Where $V = (u, v, w, T, p)^t$ is the vector of primitive variables and the matrices A, B, C are defined as:

$$A = \begin{bmatrix} u & \rho & 0 & 0 & 0 \\ 0 & u & 0 & 0 & 1/\rho \\ 0 & 0 & u & 0 & 0 \\ 0 & 0 & 0 & u & 0 \\ 0 & \gamma p & 0 & 0 & u \end{bmatrix} B = \begin{bmatrix} v & 0 & \rho & 0 & 0 \\ 0 & v & 0 & 0 & 0 \\ 0 & 0 & v & 0 & 1/\rho \\ 0 & 0 & 0 & v & 0 \\ 0 & 0 & \gamma p & 0 & v \end{bmatrix} C = \begin{bmatrix} w & 0 & 0 & \rho & 0 \\ 0 & w & 0 & 0 & 0 \\ 0 & 0 & w & 0 & 0 \\ 0 & 0 & 0 & w & 1/\rho \\ 0 & 0 & 0 & \gamma p & w \end{bmatrix}$$

In our case , we are interested in the propagation of the vector V normal to the boundary. So we introduce the matrix E_n such that

$$E_n = An_x + Bn_y + Cn_z \tag{1.16}$$

or

$$E_n = \vec{A}.\vec{n} \tag{1.17}$$

where $n = (n_x, n_y, n_z)^t$ is the unit normal. The matrix of the eigenvalues obtained by diagonalizing E_n is

$$\lambda_n = L_n E_n L^{-1} n = \text{diag}(\lambda_1, \lambda_2, \lambda_3, \lambda_4, \lambda_5) = \text{diag}(u_1 - c, u_1, u_1, u_1, u_1 + c) \tag{1.18}$$

Here c is the speed of sound. The amplitudes of the characteristics waves $L_i's$ associated with each characteristic velocity are given by:

$$\begin{aligned} L_1 &= \lambda_1(\frac{\partial p}{\partial x_1} - \rho c \frac{\partial u_1}{\partial x_1}) \\ L_2 &= \lambda_2(c^2 \frac{\partial \rho}{\partial x_1} - \frac{\partial p}{\partial x_1}) \\ L_3 &= \lambda_3 \frac{\partial u_2}{\partial x_1} \\ L_4 &= \lambda_4 \frac{\partial u_3}{\partial x_1} \\ L_5 &= \lambda_5(\frac{\partial p}{\partial x_1} + \rho c \frac{\partial u_1}{\partial x_1}) \end{aligned} \tag{1.19}$$

The LODI system can be cast in many different forms depending on the choice of variables. In terms of the primitive variable, this system can be written as

$$\begin{aligned} \frac{\partial \rho}{\partial t} + \frac{1}{c^2}[L_2 + \frac{1}{2}(L_5 + L_1)] &= 0 \\ \frac{\partial p}{\partial t} + \frac{1}{2}(L_5 + L_1) &= 0 \\ \frac{\partial u_1}{\partial t} + \frac{1}{2\rho c}(L_5 - L_1) &= 0 \\ \frac{\partial u_2}{\partial t} + L_3 &= 0 \\ \frac{\partial u_3}{\partial t} + L_4 &= 0 \end{aligned} \tag{1.20}$$

The LODI relations are used to obtain the relations on the $L_i's$ which will be used later in the system of conservation equation. Using the LODI relation alone may also provide a simple but approximate method to derive boundary conditions. For example assuming non-ref ection at the outlet is equivalent to imposing $L_1 = 0$.

$$\frac{\partial p}{\partial t} - \rho c \frac{\partial u_1}{\partial t} = 0 \tag{1.21}$$

1.5.3 Subsonic inf ow boundary condition

For the case of inf ow we consider the case where all components of velocity u_1, u_2, and u_3 as well as the temperature T are imposed. At the inlet u_1 is imposed, the LODI relation suggest the following

expression for L_5:

$$L_5 = L_1 - 2\rho c \frac{\partial U}{\partial t} \tag{1.22}$$

$$L_2 = \frac{1}{2}(\gamma - 1)(L_5 + L_1) + \frac{\rho c^2}{T}\frac{dT}{dt} \tag{1.23}$$

Also we have

$$L_3 = -\frac{\partial V}{\partial t} \tag{1.24}$$

and

$$L_4 = -\frac{\partial W}{\partial t} \tag{1.25}$$

The density can now be obtained by using the equation

$$\frac{\partial \rho}{\partial t} + d_1 = 0 \tag{1.26}$$

Where d_1 is given by

$$d_1 = \frac{1}{c^2}[L_2 + \frac{1}{2}(\gamma - 1)(L_5 + L_1] \tag{1.27}$$

In this case L_1 is computed using the interior points from (1.19).

1.5.4 Subsonic non-ref ecting outf ow boundary condition

For subsonic f ow at exit, the eigenvalue $\lambda_1 = u - c$ is negative and the disturbance propagates into the domain from outside. L_2 to L_5 can be still calculated from the interior points. However, L_1 corresponding to the eigenvalue of $u - c$ must be treated differently. The conventional method to provide a well posed boundary condition is to impose $p = p_\infty$ at the outf ow boundary.

This treatment however will create acoustic wave ref ections, which may be diffused and eventually disappear at the steady state. In case of unsteady f ows, the wave ref ection may contaminate the f ow solutions. To avoid wave ref ections, the following soft boundary condition as suggested by Poinsot & Lele (1992) is used.

$$L_1 = K(p - p_\infty) \tag{1.28}$$

where K is a constant and is determined by

$$K = \sigma(1 - M^2)c/L \tag{1.29}$$

M is the maximum Mach number in the f ow, L is a characteristic size of the domain, and σ is a constant. The preffered range for constant σ is $0.2 - 0.5$. When $\sigma = 0$ (1.29) imposes the amplitude of ref ected waves to 0 as suggested by Thompson (1987) and termed as "perfectly non-ref ecting". In this study we choose the value of $\sigma = 0.25$.

1.6 Modelling cavity f ows using NIGLO

In this section we present the results of validation for the cavity of L_e/D ratio of 2. The f ow is initialised by a laminar boundary layer so as to have a thickness of $\delta/D = 0.28$ at the leading edge of the cavity. The Reynolds number of the f ow based on the cavity depth is 1500 and the f ow Mach number is 0.6 as in Rowley *et al.* (2002). The representative f ow in our case is laminar due to the restriction of computational resources for a real time turbulent simulations. Also it is worthwhile to use scale down the problem to laminar regions to test the basic developments. The computational domain consists of $14D$ in the stream-wise direction and $7D$ in the vertical direction. The cavity f ow conf guration is as shown in f gure 1.1. For the mesh a double hyperbolic tangent distribution is used in both the stream-wise and vertical directions, with a stretch ratio of 5%. The inf uence of mesh

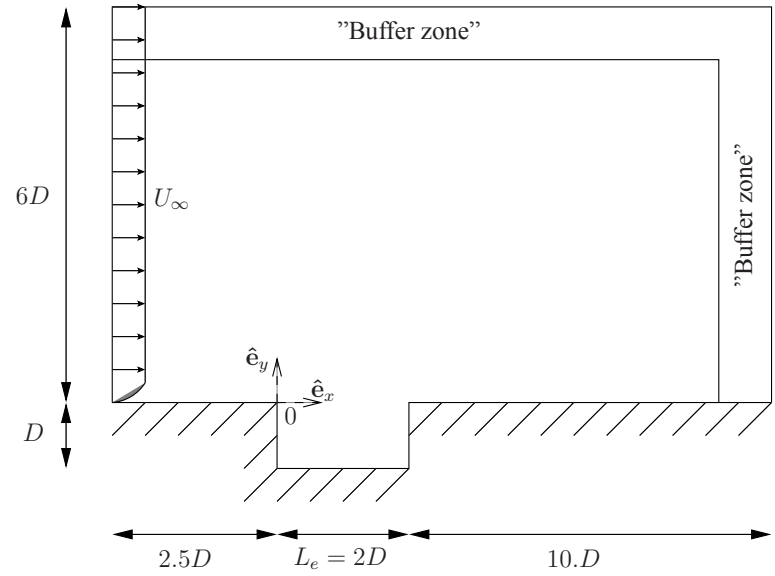

Figure 1.1 - *Schematic diagram of cavity configuration and computational domain.*

resolution on numerical results is measured by performing a mesh convergence studies to obtain grid independent results. The different mesh sizes used in the studies is given in table 1.1. The typical mesh used in this study is shown in f gure 1.2 and corresponds to mesh M.

Figure 1.3 shows the instantaneous contours of vorticity, the size of the recirculation zone being the same order as the depth. Figure 1.4(a) shows the overall sound pressure level (SPL) for the acoustic f eld above the cavity. The maximum SPL is about 170 dB at a point near the downstream edge.

This is lower than the value reported in Rowley *et al.* (2002) where a value of 180 dB is reported. This may be due to the artifact of the numerical scheme used in computation which is 4^{th} order accurate in the present study whereas it is 6^{th} order accurate in the case of Rowley *et al.* (2002). The SPL levels is however is in agreement with the experimental results of Krishnamurthi (1956) where a typical value of around 168 dB is reported.

Mesh Type	Block 1	Block 2 (cavity)	CFL
Coarse (C)	185×80	60×40	0.75
Medium (M)	260×80	102×80	0.6
Fine (F)	335×108	120×100	0.6

Table 1.1 - *Mesh sizes used in computation.*

The spectra corresponding to the normal component of velocity at a point in the shear layer is shown in Figure 1.4(b) and shows a single frequency. The value of Strouhal number is $St_2 = \frac{f_2 L}{U_\infty} = 0.72$ in good agreement with the value of 0.74 determined by the Rossiter's formula Delprat (2006)

$$St = \frac{(n - 0.25)}{(M + 1/0.57)} \quad \text{for} \quad n = 2$$

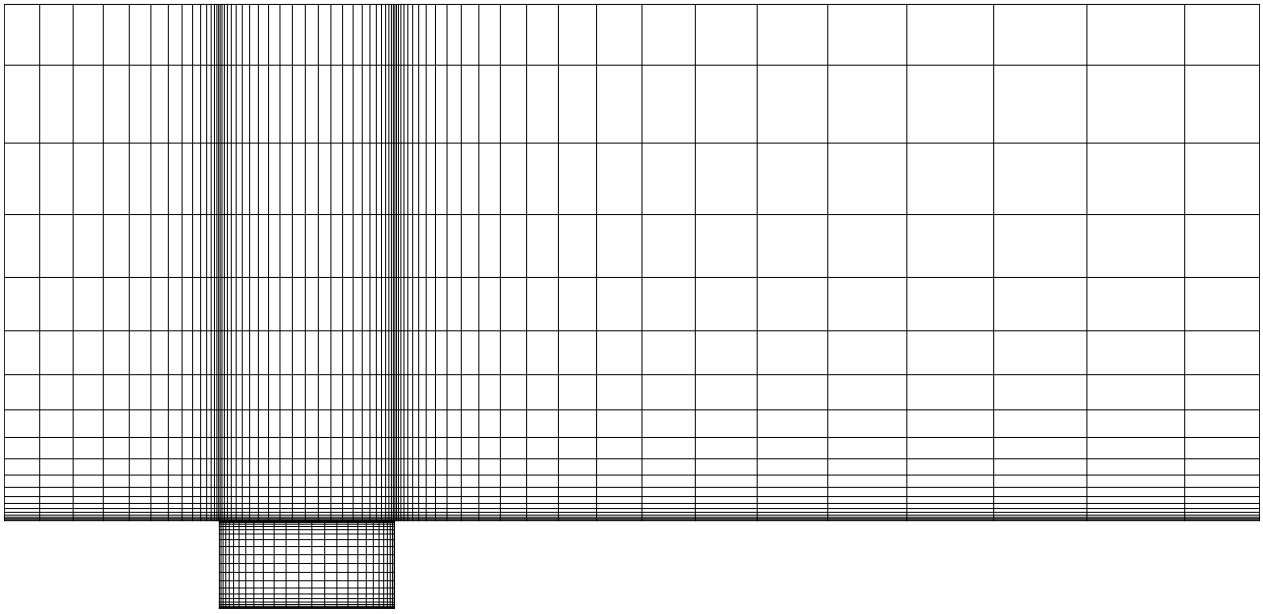

Figure 1.2 - *Typical mesh used in cavity corresponding to M in table 1.1. One in every fourth cell is plotted.*

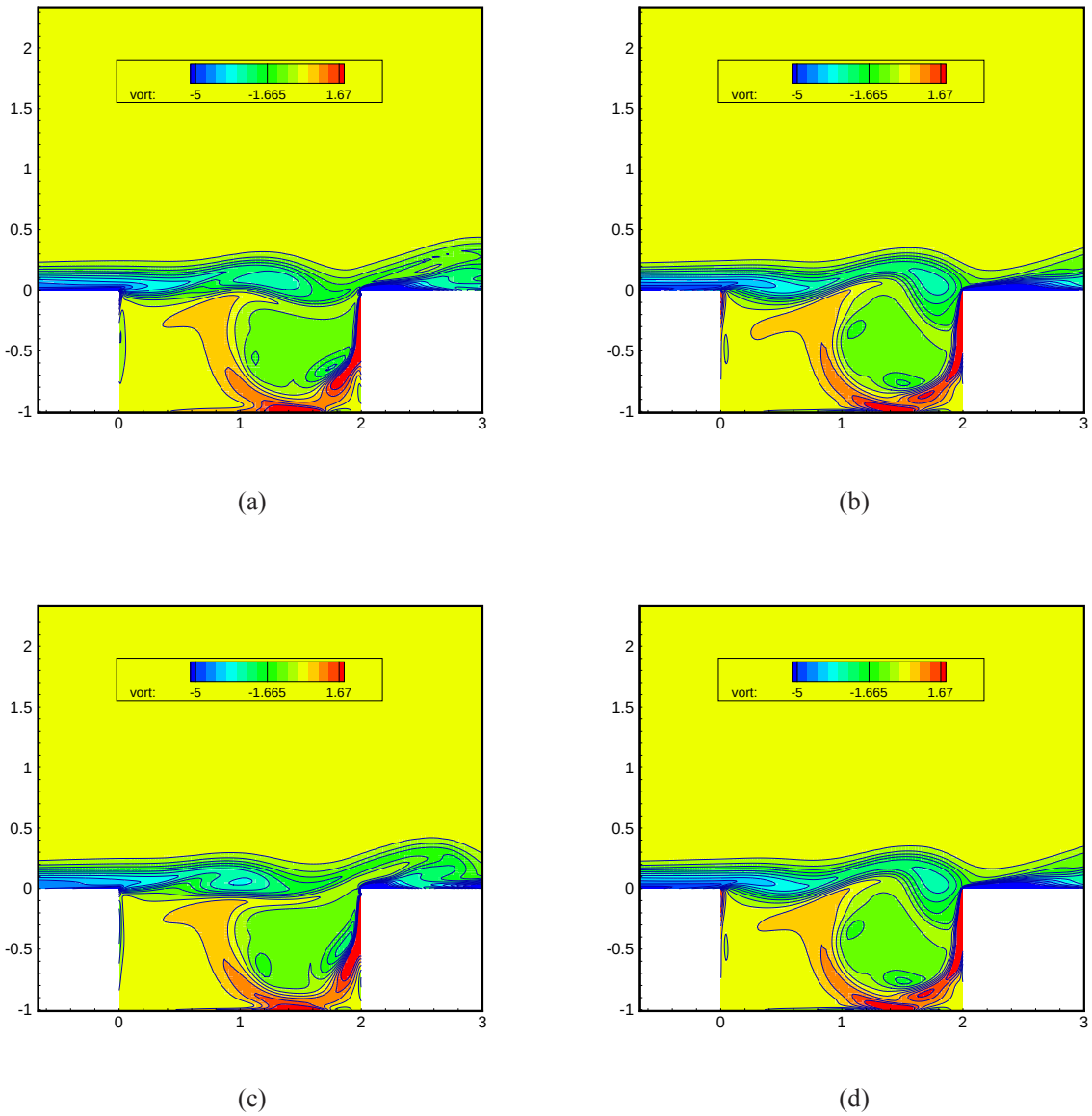

Figure 1.3 - *Instantaneous snapshots of vorticity.* 15 *contours in the range* $\frac{\omega D}{U} \in [-5, 1.67]$ *are plotted. Only a small portion of the computational domain near the cavity is shown.*

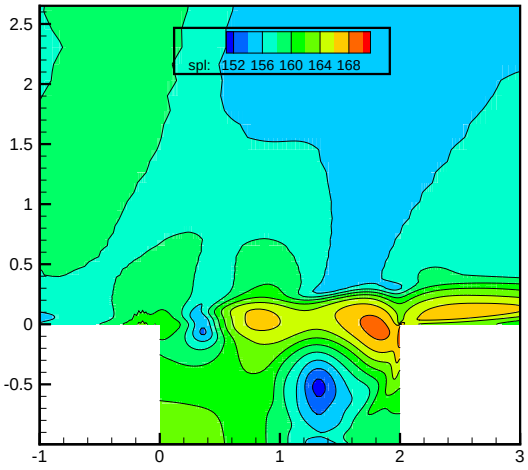

(a) SPL

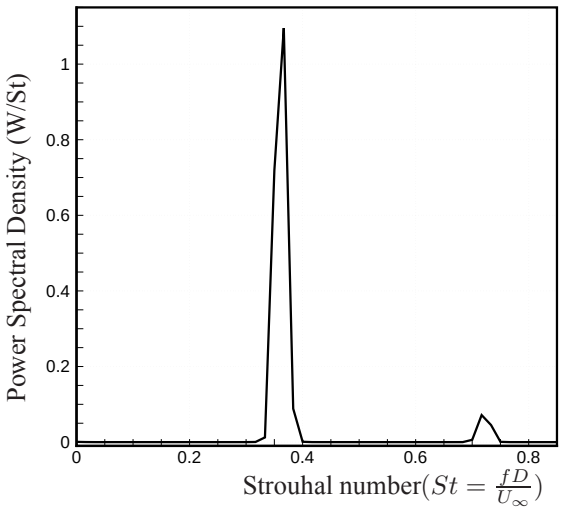

(b) Spectra

Figure 1.4 - *SPL and spectra of the normal component of velocity at* $y = 0$ *and* $x = 1.8D$ *in the shear layer.*

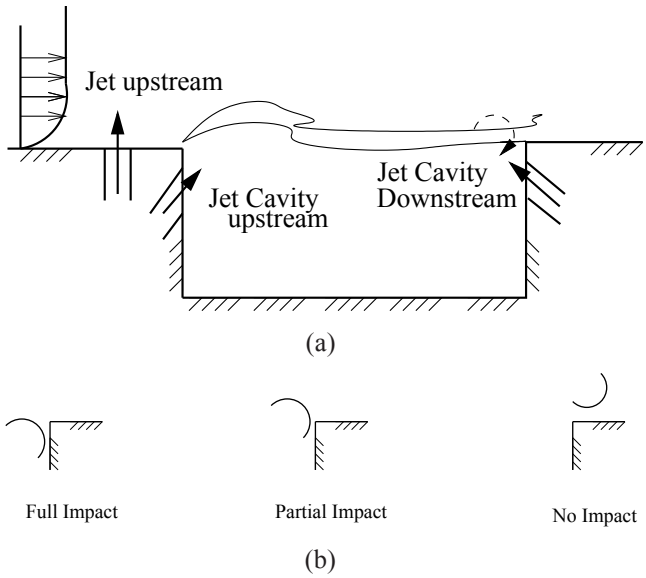

Figure 1.5 - *Schematic representation of the action of jet and its effect on the impingement of the shear layer.*

1.7 Introduction of control

The control of the cavity is achieved by means of a synthetic jet, which is achieved by modifying the boundary condition in a suitable way. The introduction of control by means of the synthetic jet has been previously performed by Shutian *et al.* (2007) for the case of f ow separation around an airfoil, Kestens (1999) and Samimy *et al.* (2007) for the case of the cavity. for the experimental control of cavity.

The basic physics behind the control of cavity resonance is to def ect the shear layer from imping-ing on the downstream edge of the cavity thereby arresting the feedback mechanism. As a result of the jet the shear layer can impinge on the downstream edge either fully, partially or can just pass over without any impingement as shown in f gure 1.5. Different positions of the jet has been tried, and the position just before the upstream edge of the cavity proves to be more effective. This can be explained by measuring the sensitivity of the f ow, where the upstream edge is more sensitive to external f ow disturbances as shown in Moret-Gabarro (2009). The forcing is typically of the form $A\sin(\omega t)$, and the actuation is introduced just before the leading edge of the cavity ($x \in [-0.15; -0.05]$ and $y = 0$), the length of actuation is dependent on cost factors, such as the cost of the actuator in case of exper-iments or the computational cost in case of numerical simulation. The snapshots of the stream wise component of velocity is shown in f gure 1.6, showing the case of no impact and partial impact of the shear layer on the trailing edge.

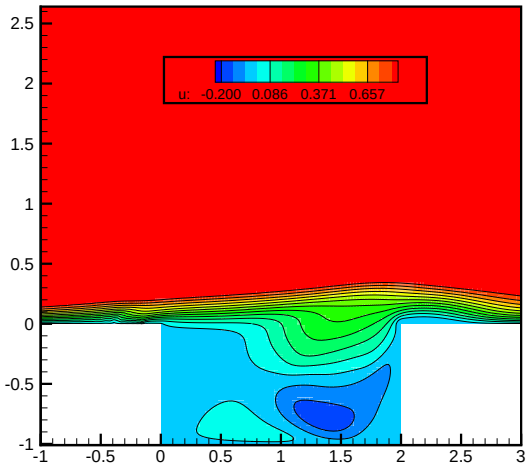

(a) No impact of shear layer on the downstream edge.

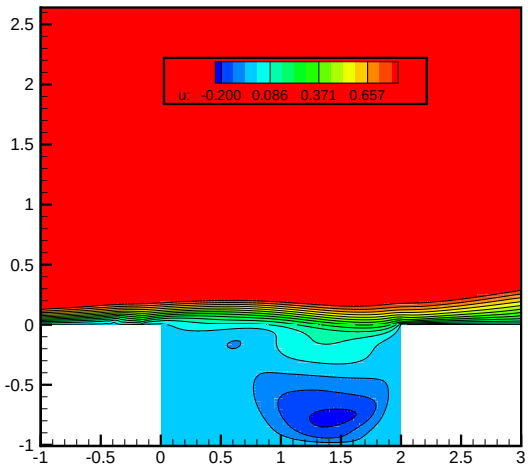

(b) Partial impact of the shear layer on the downstream edge.

Figure 1.6 - *Instantaneous snapshots of the stream wise component of velocity depicting the effect of actuation. The forcing is introduced at* $x \in [-0.15; -0.05]$ *and* $y = 0$ *and is of the form* $0.2\sin(0.4t)$.

The spectra for a typical forcing of the form $A\sin(\omega t)$ is shown in the f gure 1.7, Here the peak

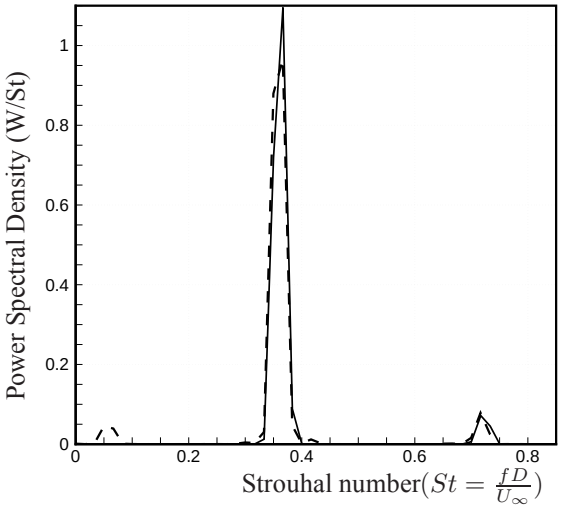

Figure 1.7 - *Spectra at $y = 0$ and $x = 1.8D$ in the shear layer for the normal component of velocity for the actuated flow (dashed line). The forcing is of the form $0.2\sin(0.4t)$. The spectra is compared for flow without any actuation (solid line).*

corresponding to the Rossiter mode is reduced. One of the objects of the current work is to determine the optimal forcing frequency and amplitude by utilising a reduced order model and check its effect by introducing it in the DNS code.

1.8 Conclusion

In this chapter we have introduced the basic numerical tool used in this study with respect to the governing equations, numerical discretisation and the various boundary conditions used. The code has been validated for the cavity f ow conf guration and will be used through in this study. Introduction of control by means of a synthetic jet at the upstream edge of the cavity, where the f ow is more sensitive to perturbations is performed. The associated spectra shows a decrease at the peak Rossiter mode followed by the appearance of new peaks suggesting the need for optimal criteria for injection. Various tools to perform the optimal control using ROM will be developed in the subsequent chapters.

Chapter 2

Basic tools from control theory

Introduction

Ce chapitre présente brièvement les différentes théories du contrôle actif Bewley & Agarwal (1996), Bewley & Liu (1998),Kim & Bewley (2007),Bagheri et al. *(2009*b*) qui ont trouvé des applications en mécanique des fluides lors de ces 15 dernières années, et qui sont utilisées en partie dans ce travail. On qualifie en premier lieu le type de contrôle en fonction de la loi de contrôle et de son action. On parle de contrôle en boucle ouverte (open loop) lorsque la loi de contrôle est déterminée optimalement pour stabiliser un système initialement instable. La loi n'est pas modifiable au cours du processus de contrôle. A l'opposé, dans le contrôle en boucle fermée (close-loop), une loi de retour (feedback) lie le contrôle à l'état réel et réactualisé du système, assurant une stabilisation plus efficace.*

Avant de chercher une loi de contrôle, on doit aussi regarder les aspects de contrôlabilité (ou commandabilité) et d'observabilité. La contrôlabilité qualifie la capacité du système à atteindre un état souhaité à partir d'une certaine loi de contrôle et d'une bonne condition initiale. La stabilisabilité, associée à la contrôlabilité, assure qu'il existe une loi de retour capable de stabiliser le système. Cela revient à dire que les modes non commandables sont tous stables. Enfin l'observabilité, qui mathématiquement est une notion duale à la notion de contrôlabilité, indique que l'observation des entrées et sorties du système, pendant un intervalle de temps fini, permet de retrouver l'état initial et donc l'état complet.

Contrôle des écoulements en boucle ouvert et optimisation sous contrainte

Un problème de contrôle est bien posé si on peut clairement définir :

- *la variable d'état du système ϕ.*
- *la variable de contrôle c.*

- *une fonctionnelle coût à minimiser $\mathcal{J}(\phi, c)$, associée à la recherche d'une réduction de traînée ou de bruit, par example.*
- *des contraintes $F(\phi, c) = 0$, qui sont les équations d'état avec les conditions aux limites ou initiales éventuellement.*

Pour minimiser la fonctionnelle coût, on introduit une fonctionnelle Lagrangienne qui, à la fonctionnelle coût, ajoute les contraintes multipliées scalairement par des multiplicateurs de Lagrange ξ, qui sont en réalité des variables d'un problème adjoint restant à définir. La minimisation de la fonctionnelle Lagrangienne se fait en calculant les dérivées de Fréchet par rapport à une variation de l'état ϕ, qu'on annule par la suite. Une fois les gradients de la fonctionnelle calculés, on utilise une méthode itérative pour aboutir au contrôle optimal, solution de notre problème. Le calcul des gradients peut aussi être effectué en appliquant la méthode des sensibilités. Il s'agit alors de dériver les contraintes par rapport à la variable de contrôle pour aboutir à la résolution directe d'un système où les dérivées sont les variables principales. Finalement, une discussion sur les intérêts et les inconvénients entre les deux approches conclut cette section :

- *différentiation puis discrétisation : en différentiant le système et ses contraintes, on obtient les gradients continus. Ensuite on discrétise l'ensemble du problème pour obtenir la solution numérique.*
- *discrétisation puis différentiation : on discrétise l'ensemble du problème (contrainte, fonctionnelle), puis on cherche les gradients des grandeurs discrètes par différentiation des équations discrètes.*

Contrôle en boucle fermée

Dans cette partie est développée l'approche classique du contrôle optimal avec loi de retour. A partir de mesure des sorties du système, on estime l'état du système optimalement. C'est l'observation et l'estimation. Ensuite, on suppose que l'état estimé est l'état réel, et on bâtit la loi de contrôle, c'est l'étape de contrôle.

Contrôle linéaire quadratique régulier (LQR)

On considère dans un premier temps un système dans le cadre d'information complète, c'est-à-dire, qu'on peut connaître à tout instant l'état du système. Par l'approche adjointe on obtient facilement une loi de contrôle de retour (rétroaction) fonction linéairement de l'état, en minimisant une fonctionnelle basée sur l'état et le coût du contrôle. La solution est en fait obtenue en résolvant une équation de Riccati stationnaire, ce qui signifie qu'on cherche à stabiliser le système sur un horizon infini ($t \to \infty$).

Dans une second étape, sur la base des mesures en sortie, on cherche à reconstruire l'état. Pour cela on applique la théorie du filtre de Kalman-Bucy qui suppose que statistiquement le système est soumis à des bruits gaussiens qui engendrent une erreur dans les mesures. Cette erreur se traduit

par un terme source dit de retour analogue à un contrôle dans l'équation d'estimation de l'état. La minimisation de cette erreur de mesure revient à résoudre une nouvelle équation de Riccati qui permet de trouver la forme du contrôle dans l'équation d'estimation de l'état. On montre en écrivant le système complet (état réel et état estimé) que le problème de contrôle et d'estimation sont duaux.

Contrôle linéaire quadratique gaussien (LQG), $\mathcal{H}_2$)

Cette fois-ci, on considère que l'état réel du système est perturbé par des bruits gaussiens, sur les mesures et sur le contrôle. L'approche et la solution sont identiques au cas précédent. La différence majeure est dans l'introduction du bruit directement dans les équations. Une étude du système complet montre que cela empêche l'état du système de tendre vers une solution complètement stationnaire au bout d'un horizon infini, le bruit gaussien présent alimentant toujours le système.

Contrôle robuste ($\mathcal{H}_\infty$)

Le contrôle robuste est une extension du contrôle LQG. Dans cette approche, la forme du bruit est devenue aussi une inconnue du problème. Le problème d'optimisation devient un problème min max : on cherche le contrôle optimal qui va minimiser la fonctionnelle coût et le pire des bruits qui va maximiser cette même fonctionnelle. La solution est encore basée sur deux équations de Riccati, mais des matrices supplémentaires relatives à l'influence du bruit dans le contrôle et les mesures interviennent. Une brève présentation de l'utilisation du contrôle en boucle fermée conclut cette section.

2.1 Introduction

This chapter summarizes the various tools from control theory. The results from this chapter are used in this thesis, while performing the LQG control on our ROM. Also the method of adjoint as introduced in this chapter is evoked on numerous occasions, in chapters on calibration, sensitivity analysis of the ROM, linearization of the model while performing feedback. To introduce the basic ideas we closely follow the work contained in Zabczyk (1996), and Evans (1983). For the application of the control theory in f uid mechanics an exhaustive treatment can be found in Bewley & Agarwal (1996), Bewley & Liu (1998), Kim & Bewley (2007) and more recently Bagheri *et al.* (2009*b*). To begin with we introduce the various terms frequently encountered in the control theory. The starting point of control theory is the differential equation

$$\dot{x}(t) = f(x, u), \quad x(0) = x_0 \in \mathbb{R}^n \tag{2.1}$$

with the right-hand side depending on a parameter u from a set $\mathcal{U} \subset \mathbb{R}^m$ called as the set of control parameters. An important question in the theory of differential equations is the continuous dependence of solutions on parameters and has been answered under appropriate conditions. In control theory we pose questions of different type, and depending on the nature of the control two def nitions of control can be found: *open loop* and *closed loop*. An *open loop* control is basically an arbitrary function $u(:) : [0, +\infty) \longrightarrow \mathcal{U}$ for which the equation

$$\dot{x}(t) = f(x(t), u(t)), \quad t \geq 0, x(0) = x_0 \tag{2.2}$$

has a well def ned solution. A *closed loop* control is a mapping $k : \mathbb{R}^n \longrightarrow \mathcal{U}$ which may depend of time $t \geq 0$, such that the equation

$$\dot{x}(t) = f(x(t), k(x(t))), \quad t \geq 0, x(0) = x_0 \tag{2.3}$$

has a well def ned solution. The mapping $k(.)$ is called *feedback*. Control are also called the *inputs* of the system and the corresponding solutions of (2.2) or (2.3) are called the *outputs* of the system.

Controllability

A state $z \in \mathbb{R}^n$ is said to be *reachable* from x in time T, if there exists an open loop control $u(.)$ such that, for the output $x(.)$, $x(0) = x_0, x(T) = z$. If the state z is reachable from an arbitrary state x in time T, then the system (2.1) is controllable. In many cases we require transferring an arbitrary state into the given one, in particular the origin. The effective characterisation of controllable systems is a partially solved problem in control theory.

Stabilizability

An important issue is that of stabilizability. If for some $\bar{x} \in \mathbb{R}^n$ and $\bar{u} \in \mathcal{U}$, $f(\bar{x}, \bar{u}) = 0$. A function $k : \mathbb{R}^n \longrightarrow \mathcal{U}$ such that $k(\bar{x}) = \bar{u}$ is called a *stabilizing feedback* if $\bar{x}$ is a stable equilibrium for the

system.

$$\dot{x}(t) = f(x(t), k(x(t))), \quad t \geq 0, x(0) = x_0$$

There exist many methods to determine weather a given equilibrium state is a stable one.

Observability

In many practical situations one observes not the state $x(t)$ but its function $h(x(t)), t \geq 0$. It is therefore necessary to consider the pair of equations

$$\dot{x} = f(x, u), \quad x(0) = x_0 \tag{2.4}$$

$$y = h(x) \tag{2.5}$$

equation (2.5) is called an observation equation. The system is (2.4)-(2.5) is said to be *observable* if, knowing a control $u(.)$ and an observation $y(.)$, on a given interval $[0, T]$, one can determine uniquely the initial condition x.

Optimality

In control theory besides the above questions of structural character one also asks optimality questions. In the time optimal problem we seek a control which transfers a state x onto z in a minimal time T. In other problems the time T is f xed and one seeks a control $u(.)$ which minimises the integral

$$\mathcal{J}(x, u) = \int_0^T P(x(t), u(t))dt + Q(x(t))$$

where P and Q are given functions. The methods of control theory can be broadly classif ed based on the right hand side of the system (2.4) being linear or non-linear where we describe the control as linear or non-linear. In case of non-linear control problems subjected to constraints the method of Lagrange multipliers is well known as described in Gunzburger (1997a), Gunzburger (1997b), Gunzburger (1997c). The method is described in the next section and is largely inspired from Gunzburger (1997a).

2.2 Open loop control and constrained optimisation

Most of the f ow control or optimisation problem can be set in an abstract setting for which we def ne the following

1. *state variables* ϕ: which are described by the governing equations, such as velocity, pressure, temperatures etc.

2. The *control* c which is usually introduced as an external source, such as mass inf ux, heating on the boundary.

3. *cost functional*: $\mathcal{J}(\phi, c)$ which is the desired objective we want to achieve by the application of control such as minimisation of the exit energy, reduction in noise, drag, etc.

4. The *constraint* $F(\phi, c) = 0$ is the f ow equations or any side constraint to be satisf ed such as the initial or boundary condition.

The constrained optimisation problem is then to f nd controls c and states ϕ such that $\mathcal{J}(\phi, c)$ is minimised (or maximised), subject to the constraint $F(\phi, c) = 0$. In many cases the functional to be minimised do not explicitly depend on the control parameters, resulting in ill-posed problems Gunzburger (1997c). This may force one to restrict the size of the control, which can be done two-fold

1. Limit the size of the control so that one looks for optimal control within a bounded set, e.g., one could look for optimal controls such that under some suitable norm

$$\|c\| \leq M$$

2. To penalize the objective functional with some norm of the control so that the new functional becomes

$$\mathcal{J}(\phi, c) = \varepsilon(\phi) + \ell^2 \|c\|^2 \tag{2.6}$$

The parameter ℓ is chosen empirically. The smaller the value of ℓ the more the control available to make the f rst term small which is presumable the goal of the optimisation. This strategy is easier to implement than the earlier one which results in variational inequalities.

In the method of Lagrange multipliers to enforce constraints we introduce an adjoint or co-state variable ξ to def ne a new objective functional

$$\mathcal{L}(\phi, c, \xi) = \mathcal{J}(\phi, c) - \langle F(\phi, c), \xi \rangle \tag{2.7}$$

where $\langle . \rangle$ denotes an appropriate inner product which depends on the setting of the problem. The constrained optimisation problem can be stated as f nding

To find controls c, states ϕ and co-states ξ such that $\mathcal{L}(\phi, c, \xi)$ is stationary. The above def nition of the functional (2.7) ensures that each argument is independent of the other contrary to the original problem in which the argument had to satisfy $F(\phi, c) = 0$. The Lagrangian functional $\mathcal{L}$ admits an extremum at the stationary points of $\mathcal{L}$ which is obtained by setting the f rst variation of $\mathcal{L}$ with respect to each variable $\delta\mathcal{L} = 0$ *i.e.*

$$\delta\mathcal{L} = \frac{\partial \mathcal{L}}{\partial \phi}\delta\phi + \frac{\partial \mathcal{L}}{\partial c}\delta c + \frac{\partial \mathcal{L}}{\partial \xi}\delta\xi = 0 \tag{2.8}$$

We suppose that the variables ϕ, c, ξ are independent [1] and the Fréchet derivative [2] with respect to each variable is identically equal to 0 with respect to each variables ϕ, c, and ξ. *i.e.*

$$\frac{\partial \mathcal{L}}{\partial \phi}\delta\phi = \frac{\partial \mathcal{L}}{\partial c}\delta c = \frac{\partial \mathcal{L}}{\partial \xi}\delta\xi = 0$$

The expressions above represents a necessary and suff cient conditions for the determination of an extremum in case the functional is convex and gives a local extremum of the functional. We do not consider the global optimisation methods as they are too expensive in f uid dynamic computation, and is still an active area of research as found in the works of Mohammadi (2007), Mohammadi & Pironneau (2004). The local optimisation methods may be stuck in a local extremum, which mat not be of interest. Also the presence of many local extrema may seriously affect the performance of the algorithm. Global optimisation method such as genetic algorithms is still less utilised in the f eld of f uid dynamic optimisation as the number of parameters is limited applications, as can be found in Quagliarella & Vicini (1997), Obayashi (1997), Makinen *et al.* (1999). Setting the f rst variation of $\mathcal{L}$ with respect to the Lagrange multiplier ξ equal to zero gives

$$\begin{aligned}\frac{\partial \mathcal{L}}{\partial \xi}\delta\xi &= \lim_{\epsilon \longrightarrow 0} \frac{\mathcal{L}(\phi, c, \xi + \epsilon\delta\xi) - \mathcal{L}(\phi, c, \xi)}{\epsilon} = 0 \\ &= \lim_{\epsilon \longrightarrow 0} \frac{-\langle F(\phi, c), \xi + \epsilon\delta\xi\rangle + \langle F(\phi, c), \xi\rangle}{\epsilon} = 0\end{aligned}$$

Where the variation $\delta\xi$ is arbitrary. On simplif cation we obtain

$$\langle F(\phi, c), \delta\xi\rangle = 0$$

or

$$F(\phi, c) = 0 \tag{2.9}$$

which is nothing but the equation of state, which is the constraint of the optimisation problem. Setting the f rst variation of $\mathcal{L}$ with respect to the state ϕ in the direction $\delta\phi$ yields

$$\begin{aligned}\frac{\partial \mathcal{L}}{\partial \phi}\delta\phi &= \lim_{\epsilon \longrightarrow 0} \frac{\mathcal{L}(\phi + \epsilon\delta\phi, c, \xi) - \mathcal{L}(\phi, c, \xi)}{\epsilon} = 0 \\ &= \lim_{\epsilon \longrightarrow 0} \left[\frac{\mathcal{J}(\phi + \epsilon\delta\phi, c) - \mathcal{J}(\phi, c)}{\epsilon} - \frac{\langle F(\phi + \epsilon\delta\phi, c), \xi\rangle - \langle F(\phi, c), \xi\rangle}{\epsilon}\right] = 0\end{aligned}$$

[1] Rigorously speaking this is not a fully correct assumption as the control and the state variables, c, ϕ are related by the equation of state $F(\phi, c) = 0$.

[2] The Fréchet derivative of $\mathcal{L}$ at the point x_0 in the direction δx is given by

$$\lim_{\epsilon \longrightarrow 0} \frac{\mathcal{L}(x_0 + \epsilon\delta x) - \mathcal{L}(x_0)}{\epsilon}$$

We consider the Taylor series expansion upto order $O(\epsilon)$, the above relation becomes

$$\lim_{\epsilon \longrightarrow 0} \left(\frac{\partial \mathcal{J}}{\partial \phi} \delta\phi - \langle \frac{\partial F}{\partial \phi} \delta\phi, \xi \rangle + O(\epsilon) \right)$$

On further simplif cation

$$\frac{\partial \mathcal{J}}{\partial \phi} \delta\phi - \langle \frac{\partial F}{\partial \phi} \delta\phi, \xi \rangle = 0$$

The f rst term can be written in terms of the inner product as

$$\langle \frac{\partial \mathcal{J}}{\partial \phi} \delta\phi, 1 \rangle - \langle \frac{\partial F}{\partial \phi} \delta\phi, \xi \rangle = 0$$

On using the def nition of the adjoint denoted by $(.)^*$:

$$\langle \delta\phi, \left(\frac{\partial \mathcal{J}}{\partial \phi} \right)^* \rangle - \langle \delta\phi, \left(\frac{\partial F}{\partial \phi} \right)^* \xi \rangle = 0$$

Since the variation $\delta\phi$ is arbitrary we obtain the adjoint or co-state equations

$$\left(\frac{\partial F}{\partial \phi} \right)^* \xi = \left(\frac{\partial \mathcal{J}}{\partial \phi} \right)^* \tag{2.10}$$

Note that the adjoint equations are linear in the adjoint variables ξ. In fact the adjoint of the state equations are linearised about the state. Finally setting the variation of the $\mathcal{L}$ with respect to the control c in the direction δc yields

$$\begin{aligned} \frac{\partial \mathcal{L}}{\partial c} \delta c &= \lim_{\epsilon \longrightarrow 0} \frac{\mathcal{L}(\phi, c + \epsilon\delta c, \xi) - \mathcal{L}(\phi, c, \xi)}{\epsilon} = 0 \\ &= \lim_{\epsilon \longrightarrow 0} \left[\frac{\mathcal{J}(\phi, c + \epsilon\delta c) - \mathcal{J}(\phi, c)}{\epsilon} - \frac{\langle F(\phi, c + \epsilon\delta c), \xi \rangle - \langle F(\phi, c), \xi \rangle}{\epsilon} \right] = 0 \end{aligned}$$

As previously, we consider the Taylor series expansion upto order $O(\epsilon)$ to obtain

$$\frac{\partial \mathcal{J}}{\partial c} \delta c - \langle \frac{\partial F}{\partial c} \delta c, \xi \rangle = 0$$

On introducing the inner product for the f rst term

$$\langle \frac{\partial \mathcal{J}}{\partial c} \delta c, 1 \rangle - \langle \frac{\partial F}{\partial c} \delta c, \xi \rangle = 0$$

again introducing the adjoint operator we have

$$\langle \delta c, \left(\frac{\partial \mathcal{J}}{\partial c} \right)^* \rangle - \langle \delta c, \left(\frac{\partial F}{\partial c} \right)^* \xi \rangle = 0$$

Finally the optimality condition is given as

$$\left(\frac{\partial F}{\partial c}\right)^{*} \xi = \left(\frac{\partial \mathcal{J}}{\partial c}\right)^{*} = \ell^2 c \tag{2.11}$$

System (2.9)-(2.11), also called as the Euler-Lagrange equations are a system of coupled partial differential equations whose solution yields the optimal control c, the optimal state ϕ and the optimal co-state ξ. The coupled system is more complicated than the original system and computationally expensive to obtain the solution directly (also called "The one shot method"), especially in the case of computational f uid dynamics where the number of degrees of freedom can go upto the order of 10^7. One therefore resorts to an iterative method in which one iterates between different equations, the algorithm for which can be summarized as below.

1. for $n = 0$ initialise the guess value for the control $c^{(0)}$.
2. Solve $F(\phi^{(n)}, c^{(n)})$ (2.4) to obtain the state $\phi^{(n)}$
3. Determine the adjoint state $\xi^{(n)}$ by resolving equation (2.10) as

$$\left(\frac{\partial F}{\partial \phi}\right)^{*(n)} \xi^{(n)} = \left(\frac{\partial \mathcal{J}}{\partial \phi}\right)^{*(n)}$$

4. The new control $c^{(n+1)}$ is obtained by solving the optimality condition (2.11) to obtain the gradient

$$\left(\frac{\partial \mathcal{J}}{\partial c}\right)^{*(n)} = \left(\frac{\partial F}{\partial c}\right)^{*(n)} \xi$$

5. The new value of the control is obtained as

$$c^{(n+1)} = c^{(n)} + s^{(n)} \left(\frac{\partial \mathcal{J}}{\partial c}\right)^{*(n)}$$

   where $s^{(n)}$ is the step length of descent obtained from any descent algorithm.

6. iterate the above step till a convergence criteria.is satisf ed

We remark that the above iterative algorithm is equivalent to the method of steepest descent for the unconstrained functional $\mathcal{J}(\phi(c), c)$ where $\phi(c)$ is the state corresponding to the control c. One important component of the optimisation problem is the determination of the gradient in step 4, which can be obtained by different methods as will be explained in the next section. Since the main aspect is the calculation of the state variables, we wish to keep the number of computation small and the principle of model reduction is one such strategy.

2.2.1 Functional gradients through sensitivities

To determine the functional gradient in step 3 of the algorithm, we use the chain rule to obtain

$$\frac{d\mathcal{J}(\phi,c)}{dc} = \frac{\partial\mathcal{J}(\phi,c)}{\partial\phi}\frac{d\phi}{dc} + \frac{\partial\mathcal{J}(\phi,c)}{\partial c} \tag{2.12}$$

Since the functional $\mathcal{J}$ depends explicitly on ϕ and c, the terms $\frac{\partial\mathcal{J}}{\partial\phi}$ and $\frac{\partial\mathcal{J}}{dc}$ can be determined easily. Since the state variable ϕ depends implicitly on the control parameter c it is more subtle to determine the sensibility $\frac{d\phi}{dc}$. A simple idea is to use a f nite difference approximation given by

$$\frac{d\phi}{dc}\,|_{c^n} \approx \frac{\phi(c^n)-\phi(\tilde{c})}{c^n-\tilde{c}} \tag{2.13}$$

where $\tilde{c}$ is a value in the neighborhood of c^n and $\phi(\tilde{c})$ is a solution of the state equation at $\tilde{c}$ *i.e.* $F(\phi(\tilde{c}),\tilde{c})=0$. This is a costly solution as it is required to solve an additional nonlinear state equation for each sensitivities and is prone to inaccuracies. A better method to determine the sensitivities is to differentiate the constraint equation $F(\phi,c)=0$ again by chain rule to obtain a linear system for sensitivities as

$$dF = \frac{\partial F}{\partial\phi}d\phi + \frac{\partial F}{\partial c}dc = 0 \tag{2.14}$$

therefore

$$\left(\frac{\partial F}{\partial\phi}|_{c^n}\right)\frac{d\phi}{dc}|_{c^n} = -\frac{\partial F}{\partial c}|_{c^n} \tag{2.15}$$

The major disadvantage of this method is to resolve a linear system with the optimal parameters. The terms $\frac{\partial F}{\partial\phi}|_{c^n}$ and $\frac{\partial F}{\partial c}|_{c^n}$ can be determined at the beginning of the iteration just after the resolution of the state.

2.2.2 Functional gradients using adjoint equations

One can also use the adjoint equations to determine the gradients of the functional. To demonstrate we write the adjoint equation (2.10) for the sake of convenience as

$$\left(\frac{\partial F}{\partial\phi}\right)^{*}\xi = \left(\frac{\partial\mathcal{J}}{\partial\phi}\right)^{*}$$

which is equivalent to the equation

$$\xi^{*}\frac{\partial F}{\partial\phi} = \frac{\partial\mathcal{J}}{\partial\phi} \tag{2.16}$$

Substituting this in equation (2.12) we obtain

$$\frac{d\mathcal{J}(\phi,c)}{dc} = \xi^{*}\frac{\partial F(\phi,c)}{\partial c}\frac{d\phi}{dc} + \frac{\partial\mathcal{J}(\phi,c)}{\partial c} \tag{2.17}$$

Finally on using 2.15

$$\frac{d\mathcal{J}(\phi^n, c^n)}{dc} = -(\xi^n)^* \frac{\partial F}{\partial c}|_{c^n} + \frac{\partial \mathcal{J}}{\partial c}|_{c^n} \tag{2.18}$$

The advantage of this method is that to determine the sensibilities, we need to resolve the adjoint system once independent of the number of optimal parameters. Also the adjoint of the optimality condition (2.11) is valid for non zero values of the gradient of the cost functional $\frac{d\mathcal{J}}{dc}$. When the optimality condition is satisf ed we have $\frac{d\mathcal{J}}{dc} = 0$. For problems with many design parameters this approach is much cheaper than using sensitivities. However sensitivities are useful in their own right as they help in determining how a variation in a parameter affect the f ow.

2.2.3 Differentiation then Discretisation

Sensitivities can be determined in two ways. One can differentiate the continuous f ow system at the partial differential equation (PDE) level to obtain a system of equations for sensitivities and then discretise the continuous sensitivity system. Alternatively one can also discretise the continuous f ow equations and then differentiate to obtain the sensitivities of the discrete system. It is also worthwhile to note that the differentiation and discretisation process do not commute and yields a different approximation to the sensitivities. The difference between the two approach can be summarized in f gure 2.1. In the following section we give a brief discussion between the two approaches.

2.2.4 Discretisation-Differentiation

This approach consists of discreting the equation of state and then differentiating the discrete expression to obtain the gradients. The main advantage of this method is the sensitivities of the optimisation problem are obtained exactly. Contrary to the case of discretisation-differentiation approach there is no need of calculating new solutions of the discretised equations. This method requires a choice of parameter in the code and returns a new code which computes the approximate parameters and exact sensitivities without any user intervention. Although this method has gained some popularity in f eld like shape optimisation it has been very less utilised for f uid dynamic problems Hinze & Slawing (2003) is one such work. The overhead cost of this operation is very large as it requires more CPU time than the differentiate-discreisation approach.

2.2.5 Differentiation-Discretisation

In this approach the continuous state system is differentiated with respect to the parameters to yield a continuous system of equations for sensitivities of the exact solution with respect to the parameter. The sensitivities then might be descretized with respect to the given parameter to obtain an approximation for the exact sensitivities. Although the approach is cost effective, the diff culty lies in approximating the sensitivities as they are not the exact derivatives of anything. This leads to inconsistent gradients of functional *i.e.* the approximate gradient is not the true gradient of anything. Also in applications where inherent discontinuities in the solution are present such as shocks the approach

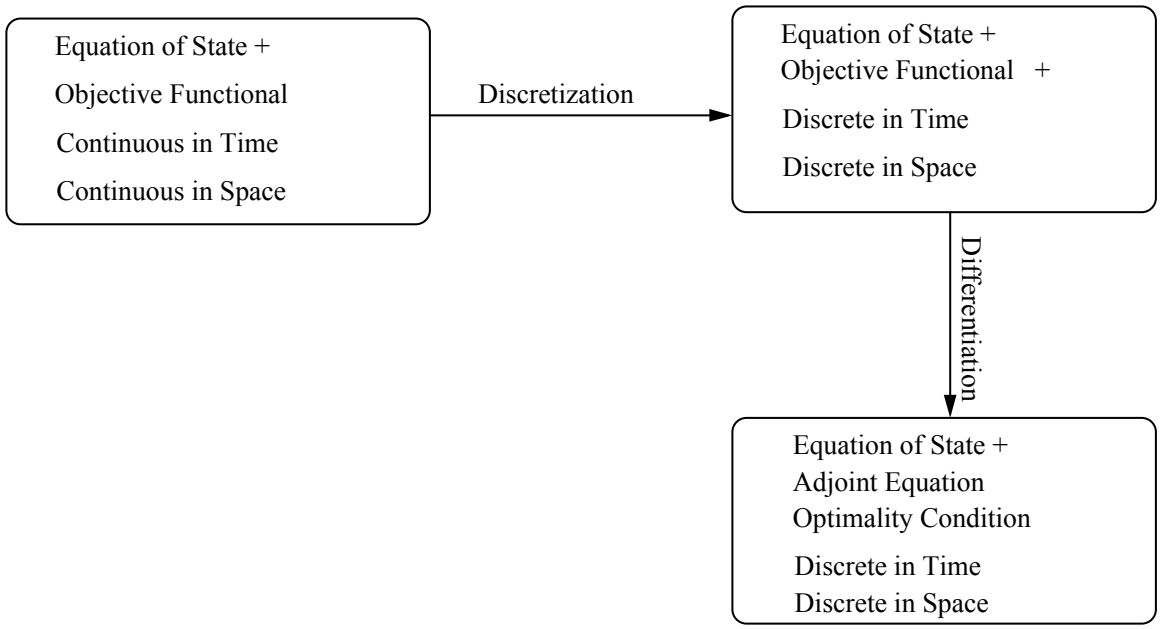

(a) Differentiation then discretisation

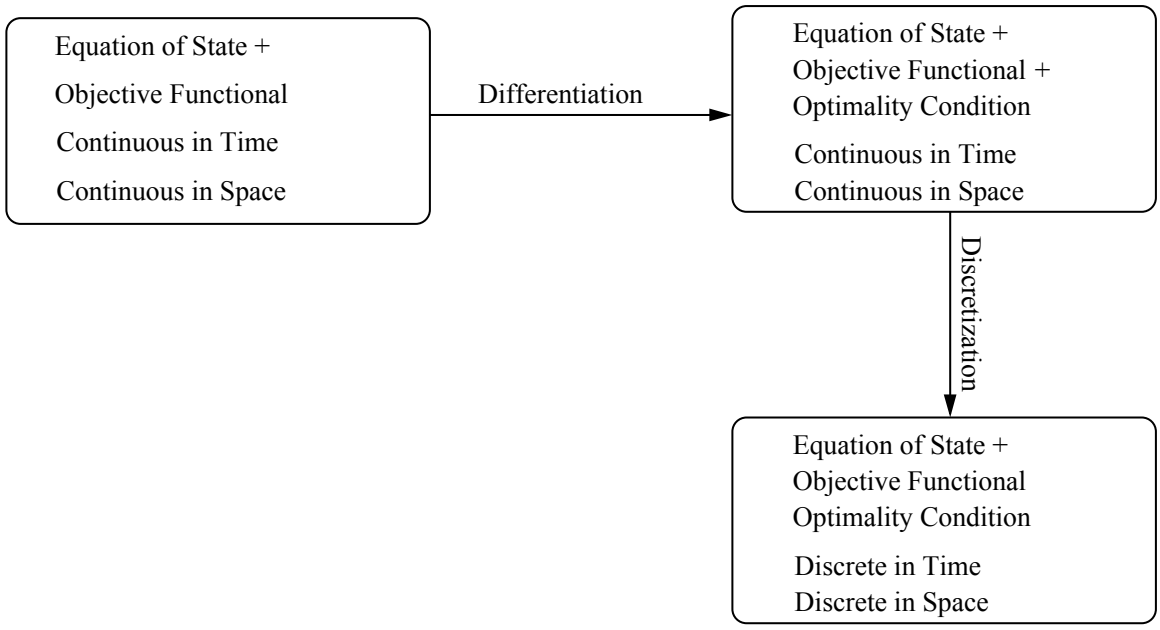

(b) Discretisation then differentiation

Figure 2.1 - *Schematic representation of the different approaches of resolution of the optimal system. Discussion of the commutativity between the discretisation and differentiation operator.*

need not be feasible as the weak solution of the shock namely the Rankine-Hugoniot condition need to be considered as a constraint Castro *et al.* (2008), Bardos & Pironneau (2003). In literature we do

f nd a large application of this method in the f uid dynamic context notably in Bewley & Liu (1998), Walther *et al.* (2001), Spagnoli & Airiau (2008), Shrif. (2008),Marquet *et al.* (2008) and will be used for the later developments in the context of reduced order modelling. An interesting study of comparison of the comparison of the various adjoint techniques is found in Noack & Walther (2007) where the difference between the discrete adjoint and continuous adjoint are compared.

2.3 Feedback control

In this section we demonstrate the principles of a feedback control. The control on the physical system can be applied by computing the effect of control in advance such that the desired state of the physical system is achieved. This strategy is known as open-loop control. However when there are disturbances in the physical system, due to the presence of uncertainties open-loop control fails to give the desired effect. Closed-loop control or feedback control is based on the concept that one is able to monitor the model by means of output measurements and establishes a connection between the measurements and the input of the system. Figure 2.2 illustrates the concept of a feedback control. Here P is the plant that describes our model and is usually given by a dynamical system of the form

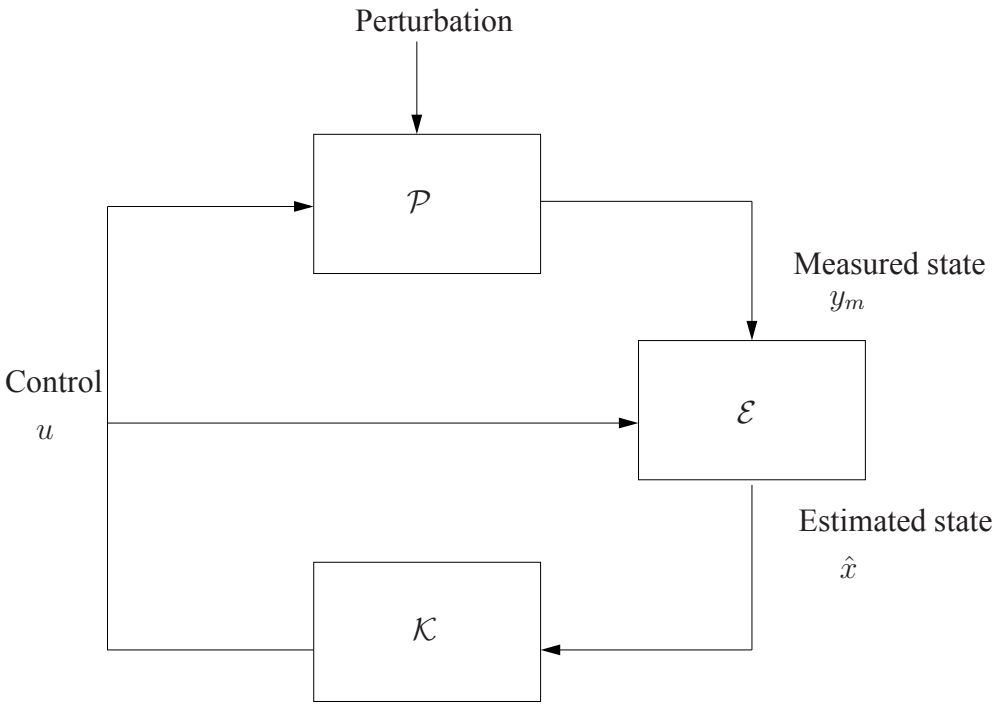

Figure 2.2 - *Block diagram of control with estimation*

$$\dot{x} = Ax + Bu \tag{2.19a}$$
$$y_m = Cx + Du \tag{2.19b}$$

Where the matrix A also known as the state matrix determines the evolution of the state x, the control u is applied to the system to drive the state towards zero, the control is based on measurements y_m. The matrices B, C, D are mainly problem dependent and depends on the way the control is applied (weather a boundary control or an internal forcing) and the way the measurements are made. In many cases the state is an internal variable and cannot be observed. Instead a few noisy measurements $\hat{y}_m$ are made, and used to estimate the state $\hat{x}$, which is then fed to the controller to determine the control u which is then applied back to the plant to drive the state towards zero. The estimation problem can be stated more precisely as follows

$$\dot{\hat{x}} = A\hat{x} + Bu - \hat{u} \tag{2.20a}$$
$$\hat{y}_m = C\hat{x} + Du \tag{2.20b}$$
$$\hat{u} = \mathcal{L}(y_m - \hat{y}_m) \tag{2.20c}$$

Where $\hat{u}$ can be interpreted as forcing applied to the plant $\mathcal{P}$ and $\hat{y_m}$ denotes the measurement associated with the state $\hat{x}$. Once the state $\hat{x}$ has been determined using the estimator $\mathcal{E}$ the control can be determined as

$$u = -\mathcal{K}(\hat{x}) \tag{2.21}$$

The problem now lies in determining the operators $\mathcal{L}$, $\mathcal{K}$ such that the term $\hat{u}$ forces the state variable $\hat{x}$ toward the actual state x and the control u drives the state x towards zero. The equivalent criteria for determining the controllability and Observability for a finite dimensional system is discussed in appendix A. We present the methods in section §2.4, and section §2.5 the different strategies of determining the control, based on the solution of the Ricatti equation. Based on the functional space in which the optimisation problem is solved the control can be classified as $\mathcal{H}_2$ and $\mathcal{H}_\infty$ which will be discussed in the next section. For details one can refer Lewis & Syrmos (1995), Bewley & Agarwal (1996), Zhou *et al.* (1996), Kim & Bewley (2007).

2.4 $\mathcal{H}_2$ control theory

2.4.1 Linear Quadratic Regulator LQR control

One considers a linear system continuous, invariant in time of the form.

$$\dot{x} = Ax + Bu \tag{2.22a}$$
$$u = -K_{LQR}x \tag{2.22b}$$

with x representing the state, u representing the control law, the second equation represents the feedback law. We assume that there is no external disturbances and we are able to measure the full state. The LQR consists is to find a control law that stabilises the system (2.22), and minimises the cost functional given by

$$\mathcal{J}_{LQR} = \frac{1}{2}\int_0^\infty \left(x^T Q x + u^T R u\right) dt \tag{2.23}$$

where the weight matrices Q, R are assumed positive def nite. The control is found out in knowing the full information in that the state of the system at the input and output is known in advance for all time. As in the previous section we introduce the Lagrange multipliers ξ to def ne the augmented functional

$$\mathcal{L} = \int_0^\infty (\frac{1}{2}x^T Q x + \frac{1}{2}u^T R u - \xi^T[\dot{x} - Ax - Bu])dt \tag{2.24}$$

Variation of the above functional gives

$$\delta\mathcal{L} = \left[-\xi^T \delta x\right]_0^\infty + \int_0^\infty (\{x^T Q + \xi^T A + \dot{\xi}^T\}\delta x + \{u^T R + \xi^T B\}\delta u)dt \tag{2.25}$$

The minimisation is achieved if

$$\begin{aligned} \dot{\xi} &= -A^T\xi - Qx & (2.26)\\ u &= -R^{-1}B^T\xi & (2.27)\\ \left[-\xi^T\delta x\right]_0^\infty &= 0 & (2.28) \end{aligned}$$

We assume a linear relation between the state and the adjoint variable as

$$\xi = X(t)x \tag{2.29}$$

where X is any positive def nite matrix. The feedback law (2.27) becomes

$$K_{LQR} = R^{-1}B^T X \tag{2.30}$$

On using (2.22) and (2.29), equation (2.26) becomes

$$X\dot{x} + \dot{X}x = -(A^T X + Q)x = \dot{X}x + X(Ax + Bu) = \dot{X}x + X(Ax + B[-R^{-1}B^T Xx])$$

This equation is verif ed for some value of x, if X is the solution of Riccati equation given

$$-\dot{X} = A^T X + XA + Q - XBR^{-1}B^T X \tag{2.31}$$

In general the inf nite time horizon problem is solved by taking the term $\dot{X} = 0$ in (2.31)

2.4.2 Lyapunov equation and minimum of the functional $\mathcal{J}_{LQR}$

The functional $\mathcal{J}_{LQR}$ being a scalar can be written using the feedback law as

$$\begin{aligned} \mathcal{J}_{LQR} &= \text{Trace}\left[\int_0^\infty (\frac{1}{2}x^T Q x + \frac{1}{2}u^T R u)dt\right] = \frac{\text{Trace}}{2}\left[\int_0^\infty (x^T(Q + K_{LQR}^T R K_{LQR})x)dt\right]\\ &= \frac{\text{Trace}}{2}\left[(Q + K_{LQR}^T R K_{LQR})L\right] \end{aligned} \tag{2.32}$$

Where the matrix $L = \int_0^\infty xx^T dt$. The equation of state can be now written as

$$\dot{x} = A_f x \quad \text{with} \quad A_f = A - BK_{LQR}$$

The solution of the above equation can be characterised as

$$x(t) = \exp(A_f t)x_0$$

We now recall a result from the Lyapunov theory which states that the above system is asymptotically stable if

$$A_f L + LA_f^T = -x_0 x_0^T$$

It can be shown that using the equation of state and the Riccati equation $XA_f + A_f^T X = -(Q + K_{LQR}^T RK_{LQR})$, the minimum of the functional is given as

$$\mathcal{J}_{min} = \frac{\text{Trace}}{2}\left[(Q + K_{LQR}^T RK_{LQR})L\right] = -\frac{\text{Trace}}{2}\left[(XA_f + A_f^T X)\right]$$

where $\mathcal{J} = \mathcal{J}_{LQR}$ for notational convenience. On observing that Trace(AB) = Trace(BA) and Trace$(A + B)$ = Trace(A) + Trace(B) the minimum can be written as

$$\mathcal{J}_{min} = \frac{1}{2}x_0^T X x_0 \tag{2.33}$$

A typical LQR plant model can be summarized as shown in the f gure 2.3

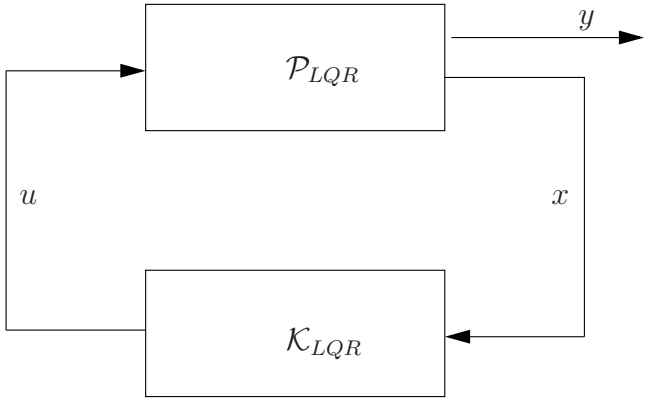

Figure 2.3 - *Typical block diagram of an LQR control*

2.4.3 Estimation and the Kalman-Bucy Filter (KBF)

In real time systems it is often natural to encounter external disturbances that enter into the system and hence the state is not precisely known. For example when acoustic measurements of f ow are

made using a microphone one can expect the presence of the instrument noise affecting the measurement. This leads us to the estimation problem in which the state (a part of it) needs to estimated before designing the control. The Kalman-Bucy Filter (KBF) is a well known tool for the estimation problem. The external disturbances for the state w_1 and the measurements w_2 is assumed to be uncorrelated white Gaussian process with zero mean and the covariance matrix defined by $E[w_1^* w_1] = I$, $E[w_2^* w_2] = I$, where $E[.]$ is any expectation operator. We define the square root of the covariance of the disturbance to the state equation and measurements by G_1, G_2 respectively. The system $\mathcal{P}$ can be written as

$$\dot{x} = Ax + G_1 w_1 + B_2 u \tag{2.34a}$$
$$y_m = Cx + G_2 w_2 + Du \tag{2.34b}$$

The objective of the Kalman Bucy Filter is to estimate the state x as accurately as possible based on the measurements y_m. In other words the KBF tries to minimise the estimation error e_x defined by

$$e_x = x - \hat{x} \tag{2.35}$$

where the state $\hat{x}$ is determined using a filter. The cost functional can be written as

$$\mathcal{J}_{KBF} = E[\|\chi_e\|^2]$$

where $\chi_e \equiv e_x$ for the sake of notation, and E is any expectation operator [3]. For the sake of generalisation in latter sections we introduce the following notations, assuming G_2 nonsingular. The disturbance vector can be defined as

$$w = \begin{pmatrix} w_1 \\ w_2 \end{pmatrix}$$

we also define

$$B_1 \equiv (G_1, 0) \qquad C_2 \equiv G_2^{-1} C \qquad D_{21} \equiv (0, I)$$

On using a simple change of variable the observation vectors y, $\hat{y}$ is defined as

$$y \equiv G_2^{-1}(y_m - Du) \quad \hat{y} \equiv G_2^{-1}(\hat{y}_m - Du)$$

With the change of variable (2.34) and (2.20) can be written as

$$y = C_2 x + D_{21} w \tag{2.36a}$$
$$\hat{y} = C_2 \hat{x} \tag{2.36b}$$

[3] The definition of the functional by means of an integral on $t \in [0, \infty]$ is not convenient due to the problem of convergence, the expectation being the suitable measure.

It is also appropriate to def ne the output estimation error $e_y \equiv y - \hat{y}$. The equations for the state estimation error and output estimation error can be written by the def nition of errors e_x, e_y and equations (2.20), (2.36) as

$$\dot{e}_x = Ae_x + B_1 w + \hat{u} \tag{2.37a}$$
$$\chi_e = e_x \tag{2.37b}$$
$$e_y = C_2 e_x + D_{21} w \tag{2.37c}$$

The Kalman-Bucy estimator matrix $\mathcal{L}_{KBF}$ is estimated such that the control $\hat{u}$, forces the state variable of the estimation error $\hat{e}_x$ towards the minimisation of $\mathcal{J}_{KBF}(\chi_e)$ in the presence of disturbances w. The above facts can be written in a shorthand form as shown in table. Where $\mathcal{P}_{KBF}$ represents the

$$\mathcal{P}_{KBF} = \begin{array}{c|ccc} & e_x & w & \hat{u} \\ \hline \dot{e}_x & A & B_1 & I \\ \chi_e & I & 0 & 0 \\ e_y & C_2 & D_{21} & 0 \end{array}$$

plant and $\mathcal{L}_{KBF}$ represents the f lter gain. We introduce the Hamiltonian as

$$H_{KBF} = \begin{pmatrix} A^T & -C^T C \\ -B_1 B_1^T & -A \end{pmatrix}$$

The Ricatti equation associated with H_{KBF} can be written as

$$AY^T + YA^T - Y(C_2^T C_2)Y + (B_1 B_1^T) = 0 \tag{2.38}$$

also denoted by $Y = \mathrm{Ric}(H_{KBF})$. Note that the gain obtained from the KBF is the dual of the gain obtained from the LQR control described in (2.31). The feedback operator L can be written as

$$L = -YC_2^T \tag{2.39}$$

and the Kalman-Bucy f lter $\mathcal{L}_{KBF}$ given by

$$\hat{u} = Le_y = -YC_2^T e_y \tag{2.40}$$

The estimator $\hat{y}$ is given by the equation

$$\dot{\hat{y}} = A\hat{x} + B_2 u - L(y - C_2\hat{x}) \tag{2.41}$$

and minimises $E(\|e_x\|^2)$ for a system with Gaussian disturbances. The block diagram of the KBF can be summarized as shown in f gure 2.4.3

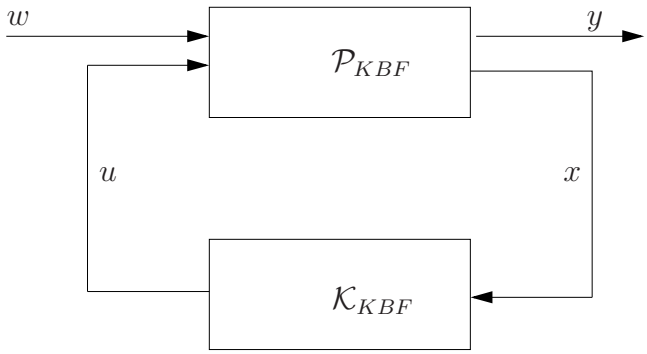

Figure 2.4 - *Block diagram of Kalman Filter.*

2.4.4 Linear Quadratic Gaussian LQG control

We combine the results obtained from LQR for the control and the KBF for the estimation part to obtain a system $\mathcal{P}_{LQG}$ subjected to Gaussian disturbances. The cost functional for minimisation can be written as

$$\mathcal{J}_{LQG} = E\left[\|x\|^2 + \ell^2 u^2\right] \tag{2.42}$$

Note that $Q = I$ and $R = \ell^2$ in the def nition of (2.23), $\|.\|$ represents the euclidian norm or the L_2 norm. The functional (2.42) can be written in a form similar to that of the Kalman-Bucy f lter by introducing the transformation variable

$$\chi = \begin{pmatrix} Q^{1/2}x/\ell \\ u \end{pmatrix}$$

to obtain the new functional of minimisation as

$$\mathcal{J}_{LQG} = E[\|\chi\|^2] \tag{2.43}$$

The term LQG comes from the fact that the plant being linear, the cost functional being quadratic, and the external disturbances being Gaussian. Using the same way the plant (2.34) can be written as

$$\dot{x} = Ax + B_1 w + B_2 u \tag{2.44a}$$
$$\chi = C_1 x + D_{12} u \tag{2.44b}$$
$$y = C_2 x + D_{21} w \tag{2.44c}$$

where

$$C_1 = \begin{pmatrix} Q^{1/2}/\ell \\ 0 \end{pmatrix} \qquad D_{12} = \begin{pmatrix} 0 \\ I \end{pmatrix}$$

An $\mathcal{H}_2$ controller relates the measurements y and the control u such that when applied to the plant controls the evolution of the state x so as to minimise the cost functional $\mathcal{J}_{LQG}(\chi)$. We state a result

as found in Lewis & Syrmos (1995), in that the $\mathcal{H}_2$ controller which minimises $\mathcal{J}_{LQG}$ can be found as a combination of optimal controller and the Kalman-Bucy f lter. The estimator is given by the equation

$$u = -K\hat{x} \tag{2.45a}$$
$$\dot{\hat{x}} = A\hat{x} + B_2 u - L(y - C_2\hat{x}) \tag{2.45b}$$

Where

$$K = -B_2^T X \qquad X = \text{Ric}\begin{pmatrix} A & -B_2 B_2^T \\ -C_1^T C_1 & -A^T \end{pmatrix} \tag{2.46a}$$

$$L = -Y^T C_2^T \qquad Y = \text{Ric}\begin{pmatrix} A^T & -C_2 C_2^T \\ -B_1 B_1^T & -A \end{pmatrix} \tag{2.46b}$$

One observes the separation structure of the solution in that the computation of the control gain K_2 does not depend on the external disturbances which are taken care of by the terms B_1 and C_2. Similarly the estimation gain L does not depend on the cost functional which are taken care of by the term C_1 or the way the state is measured as accounted for by B_2, thus resulting in a decoupling of the problem for control and estimation, which is usually reffered to as the principle of separation.

2.5 $\mathcal{H}_\infty$ control: robust control

The formulation of the $\mathcal{H}_\infty$ is similar to the $\mathcal{H}_2$ controller, only difference is that one considers the worst disturbance which destabilises the system, rather than a Gaussian disturbance. The governing equation are similar to the system of equation (2.44) and can be written as

$$\dot{x} = Ax + B_1 w + B_2 u \tag{2.47a}$$
$$\chi = C_1 x + D_{12} u \tag{2.47b}$$
$$y = C_2 x + D_{21} w \tag{2.47c}$$

in that one replaces the Gaussian disturbance w with the worst case disturbance w which destabilises the system. One considers the transfer function $\mathcal{T}_{\chi w}$ of the perturbation w which is obtained by solving the estimator problem for the feedback law χ. In an $\mathcal{H}_\infty$ control one tries to bound the ∞ norm of the transfer function to be less than a chosen value γ *i.e.* $\|\mathcal{T}_{\chi w}\|_\infty < \gamma$, where γ is a constant and $\|.\|_\infty$ is the inf nity norm of the transfer function and as def ned in Zhou *et al.* (1996)

$$\|T_{\chi w}\|_\infty = \sup_\omega \sigma_{\max}(T_{\chi w})(j\omega) \tag{2.48}$$

where σ_{max} corresponds to the largest singular value. The objective functional for minimisation can be written as

$$\mathcal{J}_\infty = E[x^T Q x + \ell^2 u^T u - \gamma^2 w^T w]$$

and the control u is chosen to minimise $\mathcal{J}_\infty$, while simultaneously finding the maximal external disturbance κ which destabilises the system. Thus the $\mathcal{H}_\infty$ control is termed as a min-max problem. As in the previous section the covariance matrices G_1 and G_2 which characterises the system disturbances and the measurement disturbances are assumed to be known. As described in Lewis & Syrmos (1995) the $\mathcal{H}_\infty$ controller minimises $\mathcal{J}_\infty$ for the worst possible disturbance κ and is given by

$$u = -K_\infty \hat{x} \tag{2.49a}$$
$$\dot{\hat{x}} = A\hat{x} + B_2 u - L_\infty(y - C_2\hat{x}) \tag{2.49b}$$

where the controller feedback K_∞ and the estimator feedback L_∞ are given by

$$K_\infty = -B_2^T X_\infty \qquad X_\infty = \text{Ric}\begin{pmatrix} A & \gamma^{-2}B_1B_1^T - B_2B_2^T \\ -C_1^TC_1 & -A^T \end{pmatrix} \tag{2.50a}$$

$$L_\infty = -Y_\infty C_2^T \qquad Y_\infty = \text{Ric}\begin{pmatrix} A^T & \gamma^{-2}C_1C_1^T - C_2C_2^T \\ -B_1B_1^T & -A \end{pmatrix} \tag{2.50b}$$

The case of a LQG controller of $\mathcal{H}_2$ theory is obtained as a limit of $\gamma \longrightarrow \infty$. Also the terms $\gamma^{-2}B_1B_1^T - B_2B_2^T$ and $\gamma^{-2}C_1C_1^T - C_2C_2^T$ need not be necessarily negative definite, so a solution of the Ricatti equation exist for sufficiently large values of γ. The smallest value of $\gamma = \gamma_0$ for which the solution exist is determined numerically. For $\gamma > \gamma_0$ the controller is termed as suboptimal. Also another important thing is that contrary to the $\mathcal{H}_2$ formulation the control and state estimation are coupled in the $\mathcal{H}_\infty$ formulation, as the computation of state feedback gain K_∞ depends on the covariance of state disturbances which are handled by the term B_1, and the estimator gain L_∞, depending on the weights of the cost functional which are accounted for in C_1. In comparison the $\mathcal{H}_\infty$ controller performs better than the $\mathcal{H}_2$ in terms of the stability.

Regarding the application of feedback control an extensive survey has been provided in Kim & Bewley (2007). Estimation based feedback control for spatially developing flows has been studied by Chevalier *et al.* (2007). Optimal and Robust control of channel flow in the presence of normal magnetic fields has been studied by Debbagh *et al.* (2007). Application of feedback control to cavity flows using reduced order modelling has been performed by Samimy *et al.* (2007). Recent developments includes the work of Bagheri *et al.* (2009*a*) who propose the use of balanced modes to obtain a reduction in the dimensionality of the full Navier Stokes equation and then design a feedback controller. Extension of the control design to the case of a spatially developing flows has been studied by Bagheri *et al.* (2009*b*) for the case of the linear complex Ginzburg-Landau equations. The use of global modes to perform control studies for the case of cavity flow has been studied by Barbagallo *et al.* (2009). Feedback control for the flow around a bluff body has been studied by Pastoor *et al.* (2008), and more recently Weller *et al.* (2009*a*). Ahuja & Rowley (2009) have studied the flow past a flat plate by constructing a reduced order model for the stable reduced order space of the Navier-Stokes equation which is determined using global unstable eigenmodes, and then designing an LQG control to stabilise the flow. Application of robust control has been

studied by Zuccher *et al.* (2004) for boundary layers and Gavarini *et al.* (2005) for the case of pipe flows. Application of feedback control to the linearised Navier-Stokes equation by solving a low dimensional Ricatti equation, which corresponds to the dimension of the unstable subspace is found in the work of Raymond & Thevenet (2009). This approach is similar in principle to model reduction in terms of the reduction in the dimensionality of the Ricatti equation being solved, but is different in that we seek a control for the high fidelity system. Other work include the application of the feedback control to study the flow around the flat plate, around a stationary state, in the presence of perturbations which has implications in turbulence control as in Buchot & Raymond (2009*a*), Buchot & Raymond (2009*b*).

2.6 Conclusions

To conclude this chapter is basically a glossary introduction to the various terms in the control literature which will be frequently used in this thesis. Control of a dynamical system can be basically classified as open loop or closed loop depending on the output observation of the response. The constrained optimisation technique based on the method of Lagrange multipliers has been described. The determination of functional gradients is accomplished through a sensitivity based approach and an adjoint based approach. The adjoint based method of determining the gradients can be further classified as discretise-differentiate, differentiate-discretise based on the order in which the differentiation is applied, the two approaches are not commutative.

The closed loop control also known as the feedback control has been discussed. Closed loop control is basically used when there are disturbances in the physical system, due to the presence of uncertainties and when open-loop control fails to give the desired effect. It is based on the concept of being able to monitor the model by means of output measurements and establishes a connection between the measurements and the input of the system. This involves the solution of an estimation problem. Based on the functional space setting in which the control is determined the feedback control can be classified as an $\mathcal{H}_2$ or a $\mathcal{H}_\infty$ problem. The $\mathcal{H}_2$ is based on minimising a quadratic functional and can be further classified as an LQR or an LQG feedback control. In LQR control we assume that the external disturbances do not influence the plant dynamics and the states are estimated accurately. In the presence of external Gaussian noise the control is termed as an LQG. LQG control is equivalent to coupling of a LQR problem and a Kalman filter for estimation. The principle of separation ensures that the plant dynamics and observer dynamics are uncoupled. The $\mathcal{H}_\infty$ is similar to the $\mathcal{H}_2$ controller, only difference being that one considers the worst disturbance which destabilises the system, rather than a Gaussian disturbance. This results in the solution of a min-max problem in which one tries to find a control which minimises the cost functional subjected to the maximisation of the external disturbance. Also the principle of separation is no longer valid as in case of $\mathcal{H}_\infty$ control. In terms of the stability the $\mathcal{H}_\infty$ controller performs better than the $\mathcal{H}_2$ controller.

Chapter 3

Proper Orthogonal Decomposition (POD) based Reduced Order Modelling (ROM)

Décompposition orthogonale aux valeurs propres (POD) basée sur modèle d'ordre réduit (ROM)

Introduction

La modélisation des structures cohérentes constitue un des aspects les plus excitant des simulations des écoulements instationnaires. Ces structures qui maintiennent leur individualité pendant l'évolution de l'écoulement présentent un défi pour les chercheurs du domaine aérodynamique. La description des écoulements passe par la résolution des équations de Navie–Stokes. La résolution d'un tel système pour décrire finement les propriétés de l'écoulement peut ne pas être possible dans ces types d'écoulements à cause du coût prohibitif demandé. Une façon de contourner cette difficulté est d'adopter les modèles d'ordre réduit basés sur le principe de la décomposition orthogonale aux valeurs propres (POD). Le ROM basé sur le projections de Galerkin est introduit dans le cas d'écoulements compressibles. Son extension pour inclure l'effet d'actionnement est discutée suivie par l'application au cas d'écoulement de cavité.

Approche modèle d'ordre réduit

La réduction du modèle sur une base autre que la POD peut être réalisée. La présentation générale de la réduction du modèle est simplement donnée à travers les équations 3.1 à 3.5. Les propriétés que doit vérifier l'espace réduit sont également données. Dans le cas présent la projection de Galerkin est utilisée.

Etat de l'art sur la POD

La POD employée pour déterminer la base optimale de reconstruction de données est bien connue depuis 1943. Elle a été utilisée pour des objectifs autres que l'identification des structures cohérentes:

traitement d'image, analyse des signaux, compression de données, etc ... Pour la dynamique des fluides, la POD a été introduite par Lumley (1987) pour analyser les écoulements turbulents. Une revue détaillée de la POD peut être trouvée dans (Holmes et al. (1996), Delville et al. (1999). La POD comme moyen d'identification des structures a été largement utilisée par Fiedler (1998) pour les jets et sillages, Delville et al. (1998) pour les couches cisaillées turbulentes et pour le post-traitement des données en référence de phase obtenues par PIV Perrin et al. (2007)). Les propriétés mathématiques et l'estimation d'erreur ont été étudiées. L'application au cas de la cavité a été proposée par Rowley et al. (2003) et Gloerfelt (2008).

Application de la POD dans le contrôle des écoulements et la turbulence

L'utilisation de la POD comme moyen pour le contrôle des écoulements turbulents a été faite la première fois par Aubry et al. (1988). Ukeiley et al. (2001) l'ont utilisée pour analyser les structures de grandes échelles dans une couche de mélange turbulente. Les modèles d'ordre réduit pour le contrôle ont été traités par Ukeiley et al. (2001). Les principes généraux du contôle optimal utilisant la modélisation d'ordre réduit des équations de Navier–Stokes a été l'oeuvre de Ravindran (2000a), Ravindran (2000b). Le contrôle d'écoulements utilisant les régions de confiance a été employé par Fahl (2000). Bergmann & Cordier (2008) ont réalisé le contrôle optimal du sillage d'un cylindre circulaire en utilisant une région de confiance. Luchtenburg et al. (2009) l'a fait pour une configuration portante. Une extension pour inclure les effets des actionneurs a été étudiée par Kasnakoğlu (2007), Weller et al. (2009b). Le contrôle du bruit émis par l'écoulement de cavité basé sur les mesures expérimentales peut être consulté dans Samimy et al. (2007).

La décomposition orthogonale aux valeurs propres

La Décomposition Orthogonale aux valeurs Propres ou Proper Orthogonal Decomposition (POD) est une technique efficace d'analyse de données, qui permet d'approximer un système de dimension élevée par un autre de dimension nettement plus faible. Essentiellement, cette méthode est linéaire et consiste à déterminer une base de modes propres orthogonaux représentatifs par définition des réalisations les plus probables.

La décomposition orthogonale propre suivant Holmes et al. (1996), est une technique pour extraire les structures cohérentes de données numériques d'un écoulement pour le représenter dans le contexte d'une dimension finie plus pratique pour une simulation numérique. Cette section présente les idées générales et les propriétés de la POD en s'inspirant de Cordier & Bergmann (2002) et de Chatarjee (2000).

Le principe fondamental de toute approximation théorique est d'extraire une base satisfaisant une contrainte donnée, par exemple une relation d'optimalité pour l'énergie. Comme l'a proposée Lumley (1967) une structure cohérente est une fonction déterministe qui est bien corrélée avec les réalisations $u(\mathbf{X})$. L'approximation pour u dans un espace adapté est donnée par l'équation 3.6. Le choix de la base orthogonale de projection est obtenu par la minimisation de l'erreur exprimée par l'équation 3.7. L'optimisation sous contrainte est donnée par l'équation 3.8. Cette équation qui est une maximisation peut être traitée comme un problème aux valeurs propres pour lequel un opérateur

de corrélation est fournie (R). La relation donnant les valeurs propres est donnée par l'équation 3.9. Cette équation peut également être obtenue par une autre méthode Cordier & Bergmann (2002).

Les propriétés de la POD sont résumées ainsi :

1. *L'existence de la solution est assurée par l'équation 3.13*
2. *Les valeurs propres sont réelles et positives*
3. *Les fonctions propres (Φ^n) forment une base orhogonale (équation 3.14) et elles peuvent être orthonormales*
4. *Les coefficients temporels a^n peuvent être obtenus par l'équation 3.15*
5. *Le tenseur de corrélation en deux points peut être décomposé en série convergente (équation 3.16)*
6. *Les coefficients doivent vérifier l'équation 3.17*
7. *Le théorème de Mercers et l'orthonormalité des fonctions propres conduisent à l'équation 3.18*

Dans la réduction de modèle utilisant la POD, la condition d'optimalité énergétique suggère l'existence d'un petit nombre de modes POD nécesssaire pour décrire efficacement les données. L'erreur de troncature est définie par l'équation 3.21. Le cas de dimension finie est d'un grand intérêt pour le traitement de données expérimentales ou numériques. Le problème d'approximation est de trouver une base de fonctions orthonormales résolvant le problème de minimisation (équation 3.23).

Pour faciliter la résolution de ce problème, l'ensemble des données est rangé dans une matrice (équation 3.24). Les modes sont donnés par l'équation (3.25) et l'approximation de toute réalisation est donnée par l'équation 3.28. La décompositttion aux valeurs singulières de toute matrice est donnée par l'équation 3.30. Le calcul direct des valeurs singulières et vecteurs singuliers associés est souvent fastidieux, et il est préférable de les déterminer par la résolution de problèmes aux valeurs propres équivalents.

A toute matrice A de dimension $M \times N_t$, il est possible d'associer une application linéaire qui envoie tout vecteur de ϵ_{Nt}, espace vectoriel de dimension N_t, dans ϵ_M, espace vectoriel de dimension M. Soit la sphère unité dans ϵ_{Nt} i.e. l'ensemble des vecteurs de longueur unité, multiplier ces vecteurs par la matrice A donne de nouveaux vecteurs qui définissent une ellipsoïde de dimension r dans l'espace ϵ_M où r est le nombre de valeurs non singulières de A. Les valeurs singulières σ_1,σ_2, ..., σ_r correspondent aux longueurs respectives des axes principaux de cette ellipsoïde (figure 3.1). Intuitivement donc, les valeurs singulières caractérisent le facteur de déformation que va subir chacun des vecteurs initiaux par action de A. Par ailleurs, puisque la matrice V est orthogonale, l'équation 3.30 s'écrit encore $AV = U\Sigma$. Les directions de ces axes principaux sont donc données par les colonnes de U et les antécédents de ces mêmes axes par les colonnes de V.

Une seconde interprétation geométrique peut être donnée à la décomposition en valeurs singulières (SVD). Pour cela, nous considérons la matrice A comme la liste des coordonnées de M

points notés P_1, P_2,... , P_M dans un espace vectoriel de dimension N_t. Chaque point P_k est representé sur la figure 3.2. Quel que soit $k \leq N_t$, nous cherchons un sous-espace de dimension k tel que la distance quadratique moyenne de l'ensemble de ces points à ce sous-espace soit minimisée, en d'autres termes nous cherchons le vecteur Φ_k tel que $\sum_{i=1}^{M} |P_i H_i|^2$ soit minimisée. Cette procédure peut être geométriquement interprétée comme une rotation de l'espace des phases, du système de coordonnées initiales à un nouveau système de coordonnées dont les axes orthogonaux coïncident avec les axes d'inertie des données. Cette formulation de la SVD correspond à la manière utilisée généralement dans la litérature pour introduire l'Analyse en Composantes Principales Joliffe (1986).

Il existe une méthode de calcul des valeurs singuliéres σ_i et des vecteurs singuliers gauches et droites d'une matrice rectangulaire A quelconque. Cette méthode est basée sur la résolution des problèmes aux valeurs propres associés à des matrices carrées $A^T\ A$ et $A\ A^T$. Par comparaison des deux expressions de $A^T\ A$, on trouve la matricea des valeurs propres $\Sigma^2 = \Lambda$ et celle des vecteurs propres $W = V$. En d'autres termes, $\sigma_i = \sqrt{\lambda_i}$ et (V,Λ) représente la décomposition aux valeurs propres de la matrice $A^T A$. Cette méthode de calcul est bien plus légère que le calcul direct de la SVD de A. Dans le contexte de la POD, on m'apelle méthode des snapshots.

L'approximation du rang minimum de A s'obtient en utilisant l'équation 3.31. On a ainsi une relation entre le rang k de l'approximation X de A et la valeur singulière d'ordre $(k+1)$ de A. Par conséquent, si les valeurs singulières décroissent suffisamment rapidement alors nous pouvons espérer déterminer une approximation de A possédant un rang très faible.

*Dans le cas de dimension infinie basée sur l'opérateur de la moyenne choisie, il existe deux approches au problème aux valeurs propres, la méthode directes comme introduite par Lumley (1967) et la méthode de snapshots comme décrite par Sirovich (1987b). Dans l'approche directe, la moyenne est temporelle et elle est évaluée à l'aide d'une moyenne d'ensemble en invoquant des hypothèses de stationnarité et d'ergodicité. La variable **X** est assimilé à la variable spatiale $x = (x, y, z)$ définie sur tout le domaine spatial Ω. L'équation intégrale de Fredholm à résoudre est donnée par 3.32.*

la POD est une généralisation de l'analyse de Fourier aux directions inhomogènes comme montré dans Cordier & Bergmann (2002). Une manière d'éviter d'être face à un problème aux valeurs propres de grande taille, consiste à décomposer les directions de l'écoulement en directions homogènes , pour lesquelles on appliquera la transformation de Fourier, et en directions inhomogènes pour lesquelles, on appliquera la POD. Cette approche est généralement utilisée dans les études expérimentales Delville et al. (1999), Ukeiley et al. (2001) afin de simplifier la résolution numérique du problème POD. Si le nombre de réalisations nécessaires pour décrire l'ecoulement est égale à $N_t \leq M$, on peut économiser beaucoup de temps de calcul, même si le problème aux valeurs propres peut être résolu de manière précise, en résolvant uniquement un problème de taille N_t. C'est la base de la méthode des snapshots

*La méthode des snapshots, introduite par Sirovich (1987b), est exactement symétrique de la POD classique. L'opérateur de moyenne correspond alors à une moyenne spatiale évaluée sur tout le domaine Ω et la variable **X** est assimilée a t. Le problème aux valeurs propres est directement déduit de l'équation 3.33 et les modes temporels sont déduits des modes POD spatiaux (équation 3.34). Dans le cas de dimension finie, on peut écrire la matrice "snapshot" comme donnée par 3.35. Les*

modes temporels sont une combinaison linéaire des échantillons (snapshots) (équation 3.36). Les modes spatiaux sont donnés par l'équation 3.39.

L'utilisation de la méthode des snapshots repose sur l'hypothèse d'ergodicité , ainsi la génération de snapshots dépend largement de la compréhension physique de l'utilisateur et peut être différente avec le problème. L'extrapolation des fonctions POD aux différentes géométries et au paramétres du contrôle peut être difficile et a été mentionnée dans le passé par Bergmann et al. (2009). Une récente étude de la sensibilié des coefficients de la POD à un paramétre donné a été réalisée par Hay et al. (2009) dans laquelle la base POD est utilisée avec la sensibilité pour augmenter la taille de l'attracteur du modèle de dimension réduite. L'échantillonage des données donne une erreur numérique qui affecte la POD Rathinam & Petzold (2003). Bui-Thanh et al. (2008) utilisent le facteur de sensibilité de la POD comme une mesure de la sensibilité relative de la projection par rapport à l'erreur d'échantillonage. En conclusion la snapshot POD reste fortement dépendante de la fonctionalité recherchée par l'utilisateur et a besion d'être affinée pour que la POD soit applicable à des problèmes plus généraux d'optimisation.

La ROM dans la litérature

Aubry et al. (1988) sont les premiers à l'utiliser la réduction de modéle pour étudier les structures cohérentes. De nombreuses autres applications, toujours pour des écoulements incompressibles ont alors vu le jour. L'application au fluide compressible reste limitée (Rowley et al. (2003), Gloerfelt (2008), Bourget et al. (2007)). La réduction de modéle sur la base POD et de projectionde Galerkin a été étendue au contrôle des écoulements en fluide incompressible e t commence à l'être pour le cas compressible (Samimy et al. (2007),Kasnakoğlu (2007)). Le principe de la projection de Galerkin est présenté à la section 3.10 (équations 3.44 à 3.52). L'application du modèle réduit au cas incompressible est donné au paragraphe 3.11 (équations 3.53 à 3.60).

Cas compressible

Dans le cas d'écoulement compressible, les variables cinématiques et thermodynamiques sont couplées. Le tenseur des corrélations contient des termes liés aux variables cinématiques et thermodynamiques. Rowley et al. (2003) a cherché un produit scalaire pour les variables d'écoulement isentropique qui donne un sens énergétique. Ce produit a été largement utilisé Gloerfelt (2008).

Le modèle d'ordre réduit isentropique est donné dans le cas déquations sans dimension. Cette adimensionalisation fait apparaitre explicitement le nombre de Reynolds et le nombre de Mach (équation 3.61). Après projection de Galerkin du modèle isentropique, le modèle d'ordre réduit obtenu est donné par l'équation 3.64.

Extension au cas du contrôle

Dans ce paragraphe on prend en compte dans le modèle d'ordre réduit l'effet d'un actionnement. Nous recherchons un modèle dynamique où l'introduction de l'actionnement est très simple. L'idée repose sur la méthode de séparation de Kasnakoğlu et al. (2008) qui consiste à diviser le domaine

d'écoulement en sous-domaines comprenant ceux sans contrôle et ceux où opère le contrôle. Le produit scalaire est ainsi redéfini pour tenir compte de cette subdivision. La procédure conduit à un systéme d'équations différentielles simples (équation 3.65) avec l'actionnement (γ) et le mode spatial (ψ). Les propriétés que doivent vérifier l'action sont données. On doit imposer une condition d'optimalité de sorte que l'énergie non capturée par équation 3.66 soit minimale. Ces conditions peuvent être systématiquement obtenues en respectant le théorème de Kasnakoğlu (2007) comme explicité en annexe E.

Le modèle d'ordre réduit pour le cas contrôlé est explicité par les équations 3.67 à 3.72. Une notation polynômiale qui peut simplifier le modèle est donnée à travers les équations 3.73 à 3.77. Il est trivial d'étendre la précédente procédure pour inclure le contrôle à entrées multiples. Le détail de la procédure est donné a travers les équations 3.78 à 3.82.

Application à l'écoulement de cavité

On applique la POD aux configurations de cavité traitées dans le chapitre 1. $98,5\%$ de l'énergie est contenue dans les quatre premières valeurs propres (figure 3.4). L'évolution des six premiers coefficients temporels de la POD est donnée sur la figure 3.5. La vorticité et la dilatation des six premiers modes sont présentées sur les figures 3.6 et 3.7. Les modes apparaissent par paire présentant des valeurs propres distinctes mais avec une même topologie pour leur mode. La dilatation est liée à la propagation des ondes sonores. Pour les modes POD supérieurs, la dilation montre clairement l'angle de propagation de l'onde sonore, suggérant son utilisation si l'on veut appliquer des modèles d'ordes réduits pour les phénomènes acoustiques. La figure 3.8 montre la capture de l'effet de l'actionnement. La figure 3.9 donne la différence entre les cas avec et sans contrôle. L'erreur de projection moyenne présentée sur la figure 3.10 montre que les erreurs sont faibles pour les modes les plus énergétiques. L'évolution temporelle et le portrait des phases sont donnés respectivement sur les figures 3.11 et 3.12.

Conclusion

Dans ce chapitre nous avons exposé les principes de base de la décomposition orthogonale propre. Nous avons également donné certaines propriétés qui rendent facile le choix du modèle réduit des écoulements, principalement l'optimalité de la représentation relative à toute base orthonormale. Le choix des produits scalaires pour les cas d´coulements incompressibles et compressibles a été discuté. Nous allons maintenant passer à l'utilisation des modes POD pour former des modèles réduits pratiques pour modéliser la dynamique de modèle de haute fidélité et diférentes procédures pour introduire les effets du contrôle dans notre modèle d'ordre réduit, en vue de l'application de la théorie du contrôle. Son extension pour tenir compte d'effet d'actions multiples a été discuté. Les résultats du modèle réduit montrent une divergence par rapport aux résultats obtenus par la POD. Ceci a motivé d'envisager sa stabilisation, ce qui fait l'objet du chapitre suivant.

3.1 Introduction

In this chapter we present the principles of model reduction based on the principles of Proper Orthogonal Decomposition (POD). In this method one decomposes the flow field into energy ranked coherent and is one such technique which has been used widely for flow control applications. The POD bases is then used to form the Reduced Order Model by the projection of the governing equations on the POD bases. The theory of POD and the various properties that make them useful choice for ROM in case of fluid dynamics are discussed. The ROM based on the Galerkin projections is introduced for the case of compressible flows. The extension of the ROM to include the effect of actuation is discussed, followed by an application to the cavity flow case.

3.2 Reduced order modelling an overview

Model reduction on bases other than the one obtained from POD can be performed. A general approach to ROM in case of linear finite dimensional systems is presented in section, to motivate the general ideas. To present the general idea of model reduction one considers a physical system of the form

$$\mathcal{S} : \begin{cases} \dot{a}(t) = f(t, a(t), \gamma(t)), \\ b(t) = g(t, a(t), \gamma(t)), \end{cases} \tag{3.1}$$

The RHS can be considered as any evolutionary model representing the dynamics, for example the Navier-Stokes equations. Although the ideas are easily extended to infinite dimension we present them for a finite dimensional case which is just considering the usual approach of numerically resolving the equations by means of discretisation in n space dimension. $a \in \mathbb{R}^n$ represents the state variables, $\gamma \in \mathbb{R}^m$ represents the inputs or the control applied to the flow, and $b \in \mathbb{R}^p$ represents the output of observables. To apply the general principles of linear control theory, the RHS of (3.1) can be linearised to obtain a state-space form given by

$$\mathcal{S}_{LTI} : \begin{cases} E\,\dot{a}(t) = A\,a(t) + B\gamma(t), \\ b(t) = C\,a(t) + D\gamma(t). \end{cases} \tag{3.2}$$

where $E \in \mathbb{R}^{n\times n}$, $A \in \mathbb{R}^{n\times n}$, $B \in \mathbb{R}^{n\times m}$, $C \in \mathbb{R}^{p\times n}$ and $D \in \mathbb{R}^{p\times m}$. E need not necessarily be invertible. The dimension of the model usually corresponds to the dimension of the spatial discretisation which can be very large, hence the principle of model reduction seeks a subspace V of dimension $r \ll n$. The non-linear reduced order model can be written as

$$\widehat{\mathcal{S}} : \begin{cases} \dot{\hat{a}}(t) = \hat{f}(t, \hat{a}(t), \gamma(t)), & \text{where} \quad \hat{a} \in \mathbb{R}^r \quad \text{with} \quad r \ll n \\ \hat{b}(t) = \hat{g}(t, \hat{a}(t), \gamma(t)), & \text{and} \quad \hat{b} \in \mathbb{R}^p. \end{cases} \tag{3.3}$$

and the corresponding linear time invariant (LTI) model can be written as

$$\widehat{\mathcal{S}}_{LTI} : \begin{cases} \hat{E}\,\dot{\hat{a}}(t) = \hat{A}\,\hat{a}(t) + \hat{B}\,\gamma(t) \\ \hat{b}(t) = \hat{C}\,\hat{a}(t) + \hat{D}\,\gamma(t). \end{cases} \tag{3.4}$$

The reduced subspace has to have the following desirable properties when used as an approximation to the high fidelity model (3.1)

1. $\|b - \hat{b}\| < \epsilon \times \|\gamma\| \quad \forall \gamma$ where ϵ is the tolerance
2. The approximated need to preserve the stability and be passive (no additional generation of energy) of the high fidelity model $\mathcal{S}$.
3. The reduced model must be numerically stable and be efficient.
4. Possible automatic generation of models

To present the idea of projection, from now on we just consider the linear model $\widehat{\mathcal{S}}$, we seek biorthogonal matrices V and W of size $\mathbb{R}^{n\times r}$ such that $W^T Q V = I_r$ where $Q \in \mathbb{R}^{n\times n}$ is a weight matrix. The Reduced Order Model is obtained by a projection of the state variable a on the matrix V such that $a = V\ \hat{a}$ and $\hat{b} \simeq b$. One defines the residue $\mathcal{R}$ to measure the accuracy of the projection, $a \simeq V\ \hat{a}$ as

$$\begin{aligned} \mathcal{R} &= E\ V\ \dot{\hat{a}}(t) - A\ V\hat{a}(t) - B\ \gamma(t) \\ \hat{b}(t) &= C\ V\ \hat{a}(t) + D\ \gamma(t). \end{aligned} \tag{3.5}$$

The Petrov-Galerkin projection is obtained by requiring the residue orthogonal to the approximated space, *i.e.* $W^T\ Q\,\mathcal{R} = 0_r$. The projection matrices of the system $\hat{\mathcal{S}}_{LTI}$ can now be obtained after a simple calculation as

$$\hat{A} = W^T\ Q\ A\ V \qquad \hat{B} = W^T\ Q\ B$$
$$\hat{C} = C\ V \qquad \hat{D} = D$$
$$\hat{E} = W^T\ Q\ E\ V$$

The well known Galerkin projection is obtained by taking $V \equiv W$. Several projection methods exist for the linear system (3.2). Example are the Krylov subspace method of the controllability matrix which relies on the identification of the moments of transfer function as in Gugercin & Antoulas (2004), projection on the dominant modes of controllability and Observability matrix as in Moore (1981), Rowley (2005), projection of global stability modes as in Barbagallo *et al.* (2008), POD based projection method on the subspace determined from the snapshots as in Sirovich (1987*b*) in which the flow fields are decomposed into energy ranked coherent structures, which is the method used in this study. We now proceed to introduced the general theory of POD.

3.2.1 Historical background of POD

The POD technique to determine the optimal basis for the reconstruction of a data set has been well known since Kosambi (1943), Karhunen (1946), Loève (1945) although they were used for different purposes other than coherent structure identification like image processing, Sirovich (1987*a*), Sirovich (1987*b*) signal analysis Algazi & Sarkinson (1969), data compression, Andrews *et al.* (1967). The POD was first introduced in the context of fluid dynamics by Lumley (1987) in the study of turbulent flows. Since then there has been a rapid increase in the application of the POD technique, and good reviews can be found in Holmes *et al.* (1996), Delville *et al.* (1999)

and Gordeyev (1999). The POD technique as a means of structure identification has been widely used by Fiedler (1998) for identification of jets and wakes, Delville *et al.* (1998) to study turbulent shear flows, for data obtained from particle image velocimetry Perrin *et al.* (2007). The mathematical properties and error estimate of the POD approach along with the Galerkin projection is found in the works of Volkwein (1999). For the other systems of conservation laws one can consult Lucia & Beran (2003) for hyperbolic systems with shocks, Cizmas *et al.* (2003) for systems with species conservation. Application to cavity flows but without control can be found in Rowley *et al.* (2003), Gloerfelt (2008).

3.2.2 Application of POD in control and turbulence

In the context of using POD for the control of turbulent flows Ukeiley *et al.* (2001) have used POD to study large scale structures in turbulent mixing layers. Reduced order modelling based control of fluid flow problems have been studied by Hinze (2000). The general principles of optimal control using reduced order modelling of Navier-Stokes equations has been described in Ravindran (2000a), Ravindran (2000b). Flow control using trust regions has been employed by Fahl (2000). Optimal control of the wake flows behind a circular cylinder using a trust region frame work has been studied by Bergmann & Cordier (2008) , for high lift configuration by Luchtenburg *et al.* (2009). An extension to include the effect of actuation has been studied by Kasnakoğlu (2007), Weller *et al.* (2009*b*). Control of cavity flows based on experimental measurements and its application to perform a model based control of cavity flows can be found in Samimy *et al.* (2007).

Extrapolation of the POD functions to different geometry or control parameters has been addressed by Bergmann *et al.* (2009). A recent study on the sensitivity of POD coefficients to given parameter has been performed by Hay *et al.* (2009) in which the POD basis is enriched using a sensitivity analysis. Usually the sampled data have inherent numerical error which affect the model reduction procedure, and has been investigated by Rathinam & Petzold (2003). A greedy algorithm to estimate the sampling space in an efficient way has been proposed by Bui-Thanh *et al.* (2008), who introduce the POD sensitivity factor as a measure of the relative sensitivity of the projection.

3.3 Proper Orthogonal Decomposition

We introduce the the Proper Orthogonal Decomposition following Holmes *et al.* (1996), as technique of extracting the coherent structures from the numerical flow data in the context of an infinite dimensional setting. The context of the finite dimensional case, which is used for more practical purpose of numerical simulation will be discussed as a particular case. To present the general for the case of POD ideas we closely follow Chatarjee (2000) and Cordier & Bergmann (2002).

General Principles

The fundamental principle in any approximation theory is to extract a bases satisfying a given constraint, for example an optimality relation for the energy, projection error etc. Consider the example

of a spatio temporal realisations $u(X) \in H(\Omega \times [0,T])$ where H is a Hilbert space (usually of L^2 integrable functions, other choices are possible) and $\Omega \subset \mathbb{R}^3$ represent spatial domain and $T > 0$ is the time. As given by Lumley (1967) a coherent structure is a deterministic function which is best correlated on an average with the realisations $u(X)$. If we define the usual inner product on the space of L^2 integrable functions as $\langle \phi, \psi \rangle = \int_\Omega \phi(X)\psi(X)dX$ such that $\phi, \psi \in L^2$, we seek an approximation for u in a suitable subspace.

$$u(X) \approx \sum_{i=1}^{\infty} \langle u, \phi_i(X) \rangle \, \phi_i(X) \tag{3.6}$$

We wish to chose an orthogonal basis $\phi_i \in H(\Omega)$ which minimises the average projection error given by

$$\langle \| \, u - \sum_{i=1}^{\infty} (u, \phi_i(X)) \, \phi_i(X) \, \|^2 \rangle_A \tag{3.7}$$

where $\langle . \rangle_A$ is any averaging operator applied over the family of realisations and $\| \ . \ \|$ is the norm induced by the inner product on $H(\Omega)$.

We also desire the basis $\phi_i(X)$ be orthogonal *i.e.* $\langle \phi_i, \phi_i \rangle = \| \ \phi(X) \ \|^2 = 1$ which casts (3.7) as a constrained optimisation problem Berkooz *et al.* (1993) given by

$$\max_{\psi \in L^2(\Omega)} \frac{\langle | \ (u, \psi) \ |^2 \rangle_A}{\| \ \psi \ \|^2} = \frac{\langle | \ (u, \phi) \ |^2 \rangle_A}{\| \ \phi \ \|^2} \tag{3.8}$$

such that

$$\langle \phi, \phi \rangle = \| \ \phi \ \|^2 = 1$$

The above maximisation problem (3.8) can be re-casted as an eigen value problem for which we define the correlation operator $\mathcal{R} : L^2(\Omega) \longrightarrow L^2(\Omega)$ as

$$\mathcal{R}\phi(X) = \int_X R(X', X)\phi(X')dX'$$

where $R(X, X') = \langle u(X) \otimes u(X') \rangle$ then an easy calculation shows that the operator $\tilde{R} : H(\Omega) \longrightarrow H(\Omega)$, defined by $\tilde{R}\phi(X) = \langle \mathcal{R}\phi, \phi \rangle$ is positive semidefinite, *i.e.*

$$\begin{aligned}
\langle \mathcal{R}\phi, \phi \rangle &= \left\langle \int_X \langle u(X) \otimes u(X') \rangle \phi(X')dX', \phi(X') \right\rangle_A \\
&= \int_X \int_X \left\langle u(X) \otimes u(X') \right\rangle \phi(X')dX', \phi(X)dX \\
&= \left\langle \int_X u(X).\phi(X)dX, \int_{X'} u(X').\phi(X')dX' \right\rangle \\
&= \langle | \ (u, \phi) \ |^2 \rangle_A \geq 0
\end{aligned}$$

Also the operator $\tilde{R}$ can be shown to be symmetric *i.e.*

$$\left\langle \tilde{R}\phi, \psi \right\rangle = \left\langle \phi, \tilde{R}\psi \right\rangle, \forall \phi, \psi \in L^2(\Omega)$$

$\tilde{R}$ is thus a linear, self adjoint operator on $L^2(\Omega)$ and as a consequence of spectral theory Riesz & Nagy (1955), and is given by the largest eigenvalue of the problem

$$\tilde{R}\phi = \lambda\phi \tag{3.9}$$

The above equation can be also obtained by a variational principle of the original problem, for which (3.8) can be recasted as a maximisation problem of finding a ϕ which maximises λ where

$$\lambda = \frac{\langle \mid (u,\phi) \mid^2 \rangle_A}{\parallel \phi \parallel^2} = \frac{\langle \mathcal{R}\phi, \phi \rangle}{\langle \phi, \phi \rangle} \tag{3.10}$$

and verifies for all $\phi \in H(\Omega)$:

$$\frac{dF(\epsilon)}{d\epsilon} = 0$$

where

$$\begin{aligned} F^{'}(\epsilon) &= \frac{d}{d\epsilon}\frac{\langle \mathcal{R}\left(\phi+\epsilon\psi\right), \left(\phi+\epsilon\psi\right)\rangle}{\langle \left(\phi+\epsilon\psi\right), \left(\phi+\epsilon\psi\right)\rangle} \mid_{\epsilon=0} \\ &= \frac{d}{d\epsilon}\frac{\langle \mathcal{R}\phi,\phi\rangle + \epsilon\langle \mathcal{R}\phi,\psi\rangle + \epsilon\langle \phi,\mathcal{R}\psi\rangle + \epsilon^2\langle \mathcal{R}\phi,\psi\rangle}{\langle \phi,\phi\rangle + \epsilon\langle \phi,\psi\rangle + \epsilon\langle \phi,\psi\rangle + \epsilon^2\langle \phi,\psi\rangle} \mid_{\epsilon=0} \qquad (3.11) \\ &= \frac{\left\langle \tilde{R}\phi,\psi \right\rangle \|\phi\|^2 - \left\langle \tilde{R}\phi,\phi \right\rangle \langle \phi,\psi\rangle}{\|\phi\|^4} \qquad (3.12) \end{aligned}$$

which is satisfied for any ψ if

$$\tilde{R}\phi = \lambda\phi$$

showing the equivalence with (3.9). We now proceed discuss some properties of POD that make them an useful tool in the low order modelling of fluid flows.

3.4 Properties of POD

1. For a bounded domain X, Hilbert-Schmidt theory assures a denumerable infinity of solutions of equation (3.9), which implies the existence of discrete solutions satisfying

$$\int_X R(X^{'},X)\phi_n(X^{'})dX^{'} = \lambda_n\phi_n(X) \tag{3.13}$$

where λ_n and $\phi_n(X)$ denote the POD eigenvalues and eigenfunctions of order $1,2,3,\ldots,\infty$ Each eigenfunctions is a solutions of the optimisation problem subject to the constraint of being orthogonal to all the previously determined eigenfunctions. They can also be chosen orthonormal.

2. $\tilde{R}$ being self-adjoint and positive the eigen values are real and positive

$$\lambda_1 \geq \lambda_2 \geq \ldots \lambda_\infty \geq 0$$

and the corresponding series converges *i.e.*

$$\sum_{n=1}^{\infty} \lambda_n < \infty$$

3. The eigenfunctions ϕ_n forms a complete orthogonal set, which implies that every member of the snapshot (except on a set of measure zero) can be reconstructed as

$$u(X) = \sum_{n=1}^{\infty} a_n \phi_n(X) \tag{3.14}$$

4. The eigen functions ϕ_n can be chosen mutually orthonormal *i.e.*

$$\langle \phi_m, \phi_n \rangle = \delta_{mn}$$

where δ_{mn} is the Kronecker symbol. with this the coefficients a_n can be calculated by a projection of u onto ϕ given by

$$a_n = \langle u, \phi \rangle = \int_X u(X)\phi_n(X)dX \tag{3.15}$$

5. The two-point correlation tensor $\mathcal{R}$ can be decomposed as a uniformly convergent series as:

$$\mathcal{R}_{ij}(X, X') = \sum_{n=1}^{\infty} \lambda_n \phi_{ni}(X)\phi_{nj}(X') \tag{3.16}$$

This result is also known as Mercers theorem, see Courant & Hilbert (1953).

6. By the Orthogonality of the eigenfunctions ϕ and the decomposition of the correlation tensor as given above in (3.16) the coefficients a_n can be shown to be mutually uncorrelated with their mean square values being the eigenvalues themselves

$$\langle a_n a_m \rangle = \delta_{mn}\lambda_n \tag{3.17}$$

$$\begin{aligned} \mathcal{R}_{ij}(X, X') &= \left\langle \sum_{n=1}^{\infty} a_n \phi_{ni}(X) \sum_{m=1}^{\infty} a_m \phi_{mj}(X') \right\rangle \\ &= \sum_{n=1}^{\infty}\sum_{m=1}^{\infty} \langle a_n a_m \rangle \phi_{ni}(X)\phi_{mj}(X') \end{aligned}$$

also from (3.16) we have that:

$$\mathcal{R}_{ij}(X, X') = \sum_{n=1}^{\infty} \lambda_n \phi_{ni}(X)\phi_{nj}(X')$$

and using the ortho-normality of ϕ we have that $\langle a_n a_m \rangle = \delta_{mn}\lambda_n$

7. It can be shown from the Mercers theorem and the ortho-normality of ϕ_n that:

$$\int_X \mathcal{R}_{ij}(X, X^{'})dX = \sum_{n=1}^{\infty} \lambda_n = \langle a_i^2 \rangle = 2E \tag{3.18}$$

where E corresponds to the total turbulent kinetic energy over the whole domain Ω, *i.e.* every structure in the representation contributes independently to the total kinetic energy, the amplitude λ_n measures the relative importance of these structures with respect to the energy. We now discuss the optimality of the POD bases in representing the total kinetic energy of the approximation with respect to any other orthonormal bases. Let $\{\phi_1(X), \phi_2(X), \ldots, \phi_\infty(X)\}$ denote the orthonormal set given by the POD bases, with corresponding eigenvalues $\lambda_1, \lambda_2, \ldots, \lambda_\infty$, with the representation of $u(X)$ given by

$$u(X) = \sum_{n=1}^{\infty} a_n \phi_{ni}(X)$$

Let $\psi_n(X), n = 1, 2, \ldots, \infty$ be another set of orthonormal bases with the representation of $u(X)$ given by

$$u(X) = \sum_{n=1}^{\infty} b_n \psi_{ni}(X)$$

with $\langle b_n b_n \rangle$ representing the average kinetic energy in the n^{th} mode, we have, see Holmes *et al.* (1996)

$$\sum_{n=1}^{N} \langle a_n a_n \rangle = \sum_{n=1}^{N} \lambda_n \geq \sum_{n=1}^{N} \langle b_n b_n \rangle \tag{3.19}$$

This follows when we notice that the correlation tensor $\mathcal{R}_{ij}$ can be expressed in terms of ψ_n, $n = 1, \ldots, \infty$ as:

$$\mathcal{R}_{ij} = \sum_{n=1}^{\infty} \sum_{n=1}^{\infty} \langle b_n b_m \rangle \psi_{ni} \psi_{nj}$$

which can be written in a matrix form as

$$\mathcal{R} = \begin{bmatrix} \langle b_1 b_1 \rangle & \langle b_1 b_2 \rangle & \langle b_1 b_3 \rangle & \ldots \\ \langle b_2 b_1 \rangle & \langle b_2 b_2 \rangle & \ldots & \ldots \\ \langle b_3 b_1 \rangle & \ldots & \ldots & \ldots \\ \vdots & \vdots & \vdots & \vdots \end{bmatrix} \tag{3.20}$$

The result of Temam (1988) on linear operators which states that the sum of first N dimensional eigenvalues of a self-adjoint operator is greater than or equal to its trace in any of its N dimensional projection gives:

$$\sum_{n=1}^{N} \lambda_n \geq Tr(\mathcal{R}) = \sum_{n=1}^{N} \langle b_n b_m \rangle$$

which proves that among all decompositions, the POD contains the maximum possible kinetic energy on an average.

Model reduction using POD

The energy optimality condition (3.19) suggests that only a very small number of POD modes, say N_{pod}, may be necessary to efficiently describe the data $u(X)$. The error of representation using the M modes is given by

$$\begin{aligned} \epsilon(M) &= \langle \| u(X) - \sum_{n=1}^{M} (u(X), \phi_n(X))\, \phi_n(X) \|^2 \rangle_A \\ &= \| \sum_{n=M+1}^{N_{\text{pod}}} \langle u(X), \phi_n(X) \rangle\, \phi_n(X) \|^2 \end{aligned} \tag{3.21}$$

The quantity $\epsilon(M)$ denotes the accumulated squared error of representation, due to the neglected POD basis elements that corresponds to small eigenvalues. We also define another quantity namely the Relative Information Content (RIC):

$$RIC(N_{\text{pod}}) = \frac{\sum_{i=1}^{N_{\text{pod}}} \lambda_i}{\sum_{i=1}^{M} \lambda_i} \tag{3.22}$$

which measures the average ensemble energy captured by the first N_{pod} modes of the representation. Usually the number of modes in the truncation is chosen so as to capture a certain percentage of reconstruction of our data set (say 99%). This criteria is largely used in the literature to define the truncated bases. The choice of the truncated bases using the definition of (3.22) is one such definition. Other definitions which uses a linear correlation between the flow and the observable termed as "least-order model" has been proposed by Jordan *et al.* (2007). In other words the effect of the lower modes which corresponds to the slow evolution of the mean flow may be necessary to represent the relevant dynamics of the system as in many physical systems. Example of such a case arises while studying the acoustics, like the cavity flow.

3.5 Finite dimensional case

The finite dimensional case is more relevant in problems of practical interest, like data issued from experiment or even a numerical simulation as the number discretisation points is finite. The approximation problem (3.6) is to find a set of orthonormal functions $\{\phi_k\}_{k=1}^{M}$ solving the minimisation problem

$$\min \sum_{i=1}^{N_t} \| u(\mathbf{x}, t_i) - \sum_{k=1}^{M} \langle u(\mathbf{x}, t_i), \phi_k(\mathbf{x}) \phi_k(\mathbf{x}) \rangle \|^2 \tag{3.23}$$

N_t is the number of realisations also called as snapshots, which are issued from the experimental or numerical simulations at given intervals. Here $\|.\|_2$ is the norm induced by the L^2 inner product. Also note that for any $\mathbf{x} \in \mathbb{R}^M$, we have $\|\mathbf{x}\|_2 = \sqrt{\mathbf{x}^T\, \mathbf{x}}$. The data set $\mathcal{U} = \{u(\mathbf{x}, t_1), \ldots, u(\mathbf{x}, t_{N_t})\}$, can

be arranged as an $M \times N_t$ matrix given by

$$\mathcal{U} = \begin{pmatrix} u(x_1,t_1) & u(x_1,t_2) & \dots u(x_1,t_{N_t}) \\ u(x_2,t_1) & u(x_2,t_2) & \dots u(x_2,t_{N_t}) \\ \vdots & \vdots & \vdots \\ u(x_M,t_1) & u(x_M,t_2) & \dots u(x_M,t_{N_t}) \end{pmatrix} \in \mathbb{R}^{M \times N_t} \tag{3.24}$$

The product $\mathcal{M}$ norm between two spatial mode ϕ and ψ can be defined as

$$\langle \phi, \psi \rangle = \phi^t \mathcal{M} \psi \tag{3.25}$$

where $\mathcal{M}$ is the weighted mass matrix of integration. We can employ a Cholesky decomposition for the matrix $\mathcal{M} = \mathcal{M}^{\frac{1}{2}} \mathcal{M}^{\frac{1}{2}^T}$, the weighted norm (3.25) can be related to the usual Euclidean norm as

$$\|u\|_{\mathcal{M}} = \langle u, u \rangle_{\mathcal{M}}^{\frac{1}{2}} = \|(\mathcal{M}^{\frac{1}{2}})^T u\|_2$$

the correlation tensor in the finite dimensional case can be written as

$$C = \frac{1}{N_t} \mathcal{U}^T \mathcal{U} \text{ where } C_{ij} = \frac{1}{N_t} \sum_{i=1}^{N_t} u(\mathbf{x}, t_i) u(\mathbf{x}, t_j) \tag{3.26}$$

The POD are modes given by the solution of the discrete eigenvalue problem:

$$C\mathcal{M}\phi = \lambda \phi \tag{3.27}$$

where ϕ stands for the matrix of the POD modes $\{\phi_{i=1}^{N_t}\}$. The matrix $\tilde{C} = C\mathcal{M}$ is symmetric positive definite. As a consequence of the spectral theorem it has a set of real eigenvalues, and is completely diagonisable with respect to the POD modes except on the null space of the operator $\tilde{C}$. The approximation of any realisation u with respect to the first N_{pod} modes is given by the relation

$$u(\mathbf{x}, t_i) \approx \sum_{j=1}^{N_{\text{pod}}} a_j^i \phi_j \text{ with } a_j^i = u_i^T \mathcal{M} \phi_j \tag{3.28}$$

the orthogonality relations for the POD modes ϕ_i and the coefficients a_j satisfy

$$\phi_i^T \mathcal{M} \phi_j = \delta_{ij} \text{ and } \frac{1}{N_t} \sum_{k=1}^{N_t} a_i^k a_j^k = \lambda_i \delta_{ij} \tag{3.29}$$

At this stage we would like to remark that the POD procedure explained above was extensively developed in the context of modelling coherent structures that arise while modelling turbulent flows as demonstrated in Lumley (1967). In the general context of the finite dimensional setting it is worthwhile to mention that the procedure described above to determine the POD modes, can be linked to the Singular Value Decomposition (SVD) of the snapshot matrix $\mathcal{U}$. To illustrate this connection we introduce the SVD and its connection to POD in the next section.

3.6 Singular Value Decomposition (SVD)

Let A be a complex matrix of dimension $M \times N_t$. The Singular Value Decomposition (SVD) of A is given by the the factorisation

$$A = U\Sigma V^T \tag{3.30}$$

where [1] U and V are unitary matrices of dimension $M \times M$ and $N_t \times N_t$ respectively, *i.e.* $UU^T = I_M$ and $VV^T = I_{N_t}$, $\Sigma = diag(\sigma_1, \sigma_2, \ldots, \sigma_r)$ with $\sigma_1 \geq \sigma_2 \geq \ldots \sigma_r \geq 0$ where $r = \min(M, N_t)$ and is called the singular values of A, the first r columns of $V = (v_i)_{i=1}^{N_t}$ the right singular vectors, the first r columns of $U = (u_i)_{i=1}^{M}$ the left singular vectors and i the index of the singular value also called as the singular value number. The rank of A is the number of nonzero singular value of its SVD. The SVD has a nice geometric interpretations as will be made clear in the next section.

3.6.1 Geometric interpretations of SVD

Any matrix A of dimension $M \times N_t$ can be interpreted as the action of a linear operator on the bases of the linear space say ε_{N_t} of dimension N_t onto the bases of the M dimensional subspace ε_M. The illustration is shown in figure 3.1 by the action of A on the unit sphere of ε_{N_t} to produce an r dimensional ellipsoid in ε_M where r denotes the rank of A. The singular values $\sigma_1, \sigma_2, \ldots, \sigma_r$ are the lengths of the principal radii of the ellipsoid. One can conceive of the singular values as the extent of deformation of the unit sphere produced by the matrix A. Moreover since the matrix V is unitary we can rearrange equation (3.30) as $AV = U\Sigma$, which implies that the directions of the principal radii are given by the columns of U and the pre-images by columns of V. A second geometric interpretation of

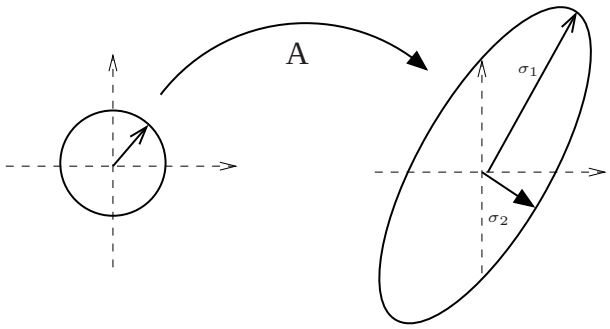

Figure 3.1 - *Geometric interpretation of the SVD of matrix A.*

SVD, which emerges from the Principal Component Analysis (PCA), when we view the the columns of the matrix A as a set of M points $P_1, P_2, \ldots, P_M$, in an N_t dimensional space as shown in the figure 3.2 then for any $k \leq N_t$, the PCA seeks a subspace such that the projection of the points P_i onto the line of the position vector ϕ_1 given by $\sum_{i=1}^{M} |P_i H_i|^2$ is minimised. The problem of minimising the projection norm is equivalent to the constrained optimisation problem (3.8) and the process can be interpreted as a change of bases such the axes of inertia coincide. When SVD is used for data analysis,

[1] here V^T denotes the adjoint matrix of V given by the conjugate transpose of V

usually the mean value is subtracted from each column which means a shift of the center of mass of the data cloud onto the origin of the coordinate system see Joliffe (1986)

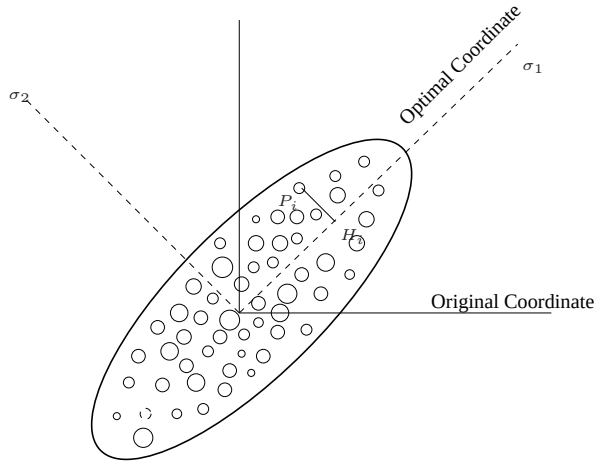

Figure 3.2 - *Geometric interpretation of the SVD of matrix A: as change of inertial coordinate*

3.6.2 Connection between the SVD and eigenvalue problems

There is relation between the SVD and eigenvalue problem. Let $A = U\Sigma V^T$ be the singular value decomposition of $A \in \mathbb{R}^{M\times N_t}$. Then $A^TA = V\Sigma U^TU\Sigma V^T = V\Sigma^2V^T$ where Σ^2 is a diagonal matrix. Also note that since A^TA is a hermitian matrix, its eigenvalue decomposition is given by $A^TA = W\Lambda W^{-1} = W\Lambda W^T$. On comparing the two expressions, we conclude that $\Sigma^2 = \Lambda$ *i.e.* $\sigma_i = \sqrt{\lambda}$ and $W = V$, where λ denotes the singular values of A^TA. The pair (V, Λ) is called the eigenvector-eigenvalue decomposition of $A^TA \in \mathbb{R}^{N_t\times N_t}$. Similarly one can obtain the eigenvector-eigenvalue decomposition (U, Λ) of $AA^T \in \mathbb{R}^{M\times M}$ as $AA^T = U\Sigma V^TV\Sigma U^T = U\Sigma^2U^T = W\Lambda W^T$. We note that if the number of snapshots N_t is much lesser than the number of data points as it happens in the case of a Direct Numerical Simulation (DNS) of fluid flows, it is more practical to solve the eigenvalue-eigenvector problem corresponding to A^TA. On the other hand as it is experienced in case of experimental situations the number of data points M is lesser than the snapshot set N_t. The eigenvector-eigenvalue problem of AA^T is then more feasible. This gives rise to two approaches to POD the classical and the snapshot method which will be described in the next section. Before we move on to the discuss the difference between the two methods, a quick reference to the work of Higham (1989) which gives an estimate of error of the low dimensional approximation given by POD and the decrease in the magnitude of singular values is worth mentioning. If $A \in \mathbb{R}^{M\times N_t}$, and if the matrix $X \in \mathbb{R}^{M\times N_t}$ with $\text{rank}(X) = k \leq \text{rank}(A)$ is such that the appropriate norm of the error $E = A - X$ is minimised then the Eckhart-Young theorem which states that:

$$\min_{\text{rank}(X)\leq k}\|A - X\|_F = \|A - A_k\|_F = \sqrt{\sum_{i=k+1}^{r}\sigma_i^2(\text{A})} \tag{3.31}$$

where F denotes the usual matrix Frobenius norm. The above expression gives a relation between the rank k of the approximant, and the $(k+1)^{\text{th}}$ largest singular value of A. It also expresses the fact that the quality of the approximant is related to the rate of decrease of eigenvalues, *i.e.* if the eigenvalues decrease rapidly we can hope to capture the given data with lesser number of singular values.

3.7 Direct and snapshot method

We have seen in the previous section that based on the choice of the correlation matrix AA^T or A^TA we have different dimensions of the eigen value problem, the choice of course depends on the size of the data set. In case of the infinite dimensional case based on the choice of the averaging operator $\langle . \rangle$, we choose in equation (3.19), we have different approaches to the eigenvalue problem reffered to as the direct method as originated by Lumley (1967) or the method of snapshot as described by Sirovich (1987*b*). In the case of the direct method the average operator $\langle . \rangle$ is temporal:

$$\langle . \rangle_A = \frac{1}{T} \int_T .dt$$

and is evaluated as an ensemble average, based on the assumption of ergodicity and stationarity. On the other hand variable X is assimilated to the spatial variables $\mathbf{x}$ defined over Ω. The corresponding eigenvalue (3.9) follows from replacing the domain of integration X by Ω and the variable X by $\mathbf{x}$. The integral Fredholm equation (3.13) is given

$$\int_\Omega \sum_{j=1}^{N_{\text{pod}}} R_{ij}(\mathbf{x}, \mathbf{x}') \phi_{nj}(\mathbf{x}) d\mathbf{x} = \lambda_n \phi_{ni}(\mathbf{x}) \tag{3.32}$$

where $R_{ij}(\mathbf{x}, \mathbf{x}')$ is the two point spatial correlation tensor defined by

$$R_{ij}(\mathbf{x}, \mathbf{x}') = \frac{1}{T} \int_T u_i(\mathbf{x}, t) u_j(\mathbf{x}', t) dt = \sum_{n=1}^{N_{\text{pod}}} \lambda_n \phi_{ni}(\mathbf{x}) \phi_{nj}(\mathbf{x})$$

where T is the period of time over which the signal $u(\mathbf{x})$ is sampled and N_{pod} represents the number of POD modes. Also the eigenfunctions determined in this case is spatial.

3.7.1 On the application of the classical eigenvalue problem:

Given M number of spatial points and we assume that we sample n_c component of our vector $u(\mathbf{x})$, we have the size of POD problem as $N_{\text{pod}} = M \times n_c$. In case of a numerical simulation like DNS in which the average number of points even in case of $2D$ simulation is of the order of $10^4 - 10^5$ and is of order $10^6 - 10^7$ in case of a $3D$ simulation, the size of the eigenvalue problem becomes huge. It is also the case with experimental measurement like the Particle Image Velocimetry where a large spatial data is sampled in a short period of time. The solution of the POD problem demands a

huge storage of memory and even with a numerical library like ARPACK [2] the numerical precision is difficult. The POD can be viewed as the generalization of the harmonic decomposition to the inhomogeneous direction as demonstrated in Cordier & Bergmann (2002). This method has been exploited by Delville *et al.* (1999), Ukeiley *et al.* (2001), on data obtained from experiments, by decomposing the flow field into homogenous and inhomogeneous component, thereby reducing the size of the POD problem. If the number of ensemble members $N_t \ll M$ then even though the eigenvalue problem can be accurately solved, time can be saved by solving a problem of size N_t, which gives rise to the method of snapshots as described in the next section.

3.7.2 Snapshot POD

In snapshot method as illustrated by Sirovich (1987*b*), the average operator $\langle . \rangle$ is evaluated as a space average over the domain Ω of interest:

$$\langle . \rangle_A = \int_\Omega . d\mathbf{x}$$

and the variable X is assimilated in time. The corresponding eigenvalue problem is immediately deduced as

$$\int_T C(t,t')a_n(t')dt' = \lambda_n a_n(t) \tag{3.33}$$

where $C(t,t')$ is the two point spatial correlation tensor defines as:

$$C(t,t') = \frac{1}{T}\int_\Omega u(\mathbf{x},t)u(\mathbf{x},t')d\mathbf{x} = \frac{1}{T}\sum_{n=1}^{N_{\text{pod}}} a_n(t)a_n(t')$$

once the temporal modes $a_n(t)$ are determined the spatial POD modes are determined as

$$\phi_i(\mathbf{x}) = \frac{1}{\lambda_i T}\int_0^T u(\mathbf{x},t)a_i(t)dt \ \text{ for } \ \lambda_i > 0 \tag{3.34}$$

In the case of finite dimension we can write the snapshot matrix as

$$Q = \begin{bmatrix} u(x_1,t_1) & u(x_1,t_2) & \dots & u(x_1,t_{N_t}) \\ u(x_2,t_1) & u(x_2,t_2) & \dots & u(x_{N_x},t_{N_t}) \\ \vdots & \vdots & \vdots & \vdots \\ u(x_{N_x},t_1) & u(x_{N_x},t_2) & \dots & u(x_{N_x},t_{N_t}) \end{bmatrix} \tag{3.35}$$

where N_x is the dimension of the spatial variables, and N_t is the number of snapshots. we notice that the temporal modes ϕ can be expressed as a linear combination of the snapshot $u(\mathbf{x},t_k)$ as

$$\phi(\mathbf{x}) = \sum_{i=1}^{N_t} a(t_k)u(\mathbf{x},t_k) \tag{3.36}$$

[2] http://www.caam.rice.edu/software/ARPACK

where the coefficients $a(t_k)$ are determined so that ϕ obtained from (3.36) solves the maximisation problem (3.8). Written for convenience the point correlation tensor $C(t,t') = C_t$ is given as

$$C_(t) = \frac{1}{N_t} Q^T M Q \tag{3.37}$$

where M is the mass matrix for spatial integration, the discrete eigenvalue problem becomes

$$C_t a_i = \lambda_i a_i \text{ with } \frac{1}{N_t} a_i^T a_j = \lambda_i \delta_{ij} \tag{3.38}$$

the spatial modes are determined as

$$\phi_i = \frac{1}{\lambda_i N_t} Q a_i \tag{3.39}$$

In this method we assume that snapshots are linearly independent. The choice between the direct method and the snapshot depends on the pertinent method we use to study the system. In case of the numerical simulation where the spatial resolution is of high order as also in the case of the particle image velocimetry, with a moderate time history, *i.e.*, $N_t \ll N_x$, the snapshot method greatly reduces the size of the problem and is widely utilised, for a well converged value of the temporal correlation tensor $C(t,t')$. On the other hand experimental approaches like Laser Doppler Velocimetry which gives a good temporal resolution and a moderate spatial resolution, *i.e.*, $N_x \ll N_t$, the spatial correlation tensor $R(\mathbf{x},\mathbf{x}')$ is well converged and the direct method is preferred. Before we move on to the next section to discuss the various choice of inner product, we would like to mention an important property of the spatial POD modes. As demonstrated in equation (3.39) the spatial modes is a linear combination of the snapshots and hence all the properties of the snapshot carry over to the spatial POD modes. This is a useful property in incompressible flows, in that, if the snapshots field is solenoidal, then the spatial modes are also solenoidal :

$$\nabla.u = 0 \Longrightarrow \nabla.\phi_i = 0 \ \ \forall i = 1, \ldots, N_{\text{pod}}$$

If the snapshot satisfy homogenous Dirichlet boundary condition the spatial POD modes also satisfies the homogenous boundary condition. This property has been utilised when performing control studies using POD by Bergmann & Cordier (2005), where the snapshots where generated for a value of actuation satisfying a suitable homogenous boundary condition.

3.8 Choice of inner product

The Hilbert space of functions $H(\Omega,[0,T])$ is usually assumed to be L^2 with the standard inner product, which guarantees a finite kinetic energy of the system [3]. It is also worthwhile looking into other definitions of inner product based on the underlying physics of the problem we are modelling. We summarise a few definitions of inner products used in literature

[3] Note the $L^2\Omega$ consists of functions $f(x)$ such that $\int_\Omega |f(x)|^2 dx < \infty$

3.8.1 L^2 inner product

The Hilbert space $L^2(\Omega)$ is the most naturally encountered in the study of incompressible fluids. the norm arising from the inner product naturally giving rise to kinetic energy of the fluid occupying Ω. For a vector valued field $\mathbf{u}$ having components u, v, w, the $L^2(\Omega)$ inner product and the corresponding norm is defined by:

$$\langle u, v\rangle = \int_\Omega (u_1u_2 + v_1v_2 + w_1w_2)d\Omega; \quad \|u\|^2 = \langle u, u\rangle \tag{3.40}$$

The energy aspect of the L^2 inner product makes it a most natural choice in the application of POD in fluid mechanics.

3.8.2 H^1 inner product

The $H^1(\Omega)$ is the Sobolev space of $L^2(\Omega)$ functions and their first derivative. Iollo *et al.* (1998) demonstrated the instability of the Galerkin model developed by the $L^2(\Omega)$ inner product for the Euler equations of gas dynamics. For the system of incompressible flow Iollo (1997), demonstrates the improvement of the numerical result by the use of Sobolev inner product defined by

$$\langle u, v\rangle_{H^1(\Omega)} = \int_\Omega u\, v d\Omega + \epsilon \int_\Omega \nabla u\, \nabla v d\Omega \tag{3.41}$$

where ϵ is a user defined numerical parameter.

3.8.3 Compressible inner product

For the case of compressible flows, the velocity variables are dynamically coupled with the thermodynamic variables. The inner product which defined the correlation tensor adds the flow variables and the thermodynamic variables. A question arises when we add two variables of different dimensions to make sense when we use the usual L^2 inner product. The scalar inner product can be computed for each variable as has been used by Rowley (2002). For vector valued variables one choice could be to non-dimensionalise the variables, but then the sense of non-dimensionalisation on the optimality of the projections poses a problem. Rowley (2002) seeks an inner product, for the isentropic flow variables which makes an intuitive sense in terms of the energy. This inner product has been used widely to study cold isentropic flows at low Mach numbers by Rowley *et al.* (2003), Gloerfelt (2008), for which the equations of Navier-Stokes can be simplified by replacing the variables the state variables by the speed of sound. For a vector variable $q = (u, v, c)$, where u and v are flow variables and c the local speed of sound. The inner product is defined by.

$$\langle q_1, q_2\rangle = \int_\Omega \left(u_1u_2 + v_1v_2 + \frac{2\alpha}{\gamma - 1}c_1c_2\right) d\Omega \tag{3.42}$$

where γ is the ratio of specific heats and α is a parameter to be chosen. If $\alpha = 1$ it corresponds to the integration of the stagnation enthalpy. This inner product has been used in this thesis. Another inner

product suggested by Bourget *et al.* (2007) for a vector variables v, with d components v_i is given by

$$\left\langle v^1, v^2 \right\rangle = \sum_{i=1}^{d} \int_{\Omega} \frac{v_i^1 v_i^2}{\sigma_i^2 + \epsilon} d\Omega \tag{3.43}$$

where σ_i^2 is the temporal statistical invariance of v_i and is defined as

$$\sigma_i^2(\mathbf{x}) = \frac{1}{T} \int_0^T (v_i(\mathbf{x}, t) - \overline{v_i(\mathbf{x})})^2 dt$$

where $\overline{v_i(\mathbf{x})}$ is the temporal average over the span of the snapshots. ϵ is a small positive constant. This method has been successfully applied to study the buffeting phenomenon of the unsteady transonic flow around airfoil.

Having discussed the basic theory of POD, we now move on to the utilisation of the POD modes to form reduced-order models which are useful to model the dynamics of the high fidelity model. Various procedures to introduce the effect of control on our reduced-order model are discussed.

3.9 ROM in literature

The earliest application of ROM to study the near wall coherent structures has been studied by Aubry *et al.* (1988). Boundary layer transition of shear flows has been studied using ROM by Rempfer (1996), Rempfer (2000). Mixing layers has been studied by Rajaee *et al.* (1994), Ukeiley *et al.* (2001), wake flows by Ma & Karniadikis (2002), Noack *et al.* (2003), Galetti *et al.* (2004). Turbulent channel flows using a minimal flow unit can be found in Smith *et al.* (2005) and using a squire coordinate in Juttijudata *et al.* (2005). Bifurcation and stability of the high fidelity model for lid driven cavity flows has been performed by Cazemier *et al.* (1998). Reduced-order model to study the scale transfers of a turbulent separated flows can be found in Couplet *et al.* (2003).

All the references above represents the application of the ROM for incompressible flows. Application to compressible flows has been limited and one can find applications in Rowley *et al.* (2003) where a simplified isentropic model has been applied to study the self sustained instabilities of a $2D$ cavity in conjunction with a high fidelity DNS solver. $3D$ cavity simulations with reduced order modelling has been performed by Gloerfelt (2008). An approach to extend the ROM to full equations of compressible flows has been given by Vigo (1998) by recasting the Navier-Stokes equations in terms of the specific volume. Hyperbolic systems with shocks has been studied using ROM by Lucia & Beran (2003) and transonic flows around airfoils by Bourget *et al.* (2007).

Utilising ROM to perform control has been studied for the incompressible case by Ravindran (1999), where the general principles of POD based optimal control has been discussed. Influence of control on the ROM of wall bounded turbulent shear flows has been studied by Graham *et al.* (1999a), Graham *et al.* (1999b). Bergmann & Cordier (2005), have used the ROM to perform optimal control of wake flows. Luchtenburg *et al.* (2009) to study high lift configurations with actuation. Feedback control laws using the ROM has been performed by Weller *et al.* (2009*b*).

In the compressible regime reference can be made to Samimy *et al.* (2007), Kasnakoğlu (2007) for the extension of the ROM to controlled configuration. The ROM can be built on bases other than the one obtained from POD. Example of which can be found in Burkardt *et al.* (2006) where the bases is obtained by minimising the tesslation energy. In the next few sections, we discuss the general principles of the POD based Galerkin projection for the reduced order modelling. After giving an overview of the ROM for incompressible case, we introduce the compressible case of the isentropic model which is used in this thesis. The method of introducing the effect of actuation into the ROM will be further discussed with an application to the compressible cavity flow.

3.10 Galerkin projection, principles

Consider a dynamical system which evolves on a Hilbert space H. The form of the dynamical system can be written in a canonical way as

$$\dot{u} = \mathcal{X}(u) \tag{3.44}$$

where $u(t) \in H$ and $\mathcal{X}$ is any differential operator on H. For example, consider a partial differential equation governed by the variable $u(\mathbf{x}, t)$, defined on some domain $\Omega \times [0, T]$, where $\Omega \in \mathbb{R}^n$ represents the spatial domain of evolution, over a period $[0, T]$. Given a finite dimensional subspace S of H, the Galerkin projection specifies a dynamical system which evolves on S and approximates the original equation (3.44) in some approximate sense. This approximate dynamical system is obtained by an orthogonal projection of the vector field $\mathcal{X}(u)$ onto the subspace S and is denoted by a operator $\mathcal{X}_s$ giving rise to a new dynamical system

$$\dot{r} = \mathcal{X}_s(r) \tag{3.45}$$

Where r is the projection variable. Galerkin projection specifies this vector field as

$$\mathcal{X}_s(r) = \mathbb{P}\mathcal{X}(r) \tag{3.46}$$

where $\mathbb{P}_s : H \rightarrow S$ denotes the projection map. From projection theorem, Robinson (2007), this approximation minimises the error $\|\mathcal{X}_s(r) - \mathcal{X}(r)\|$ if

$$\langle \mathcal{X}_s(r) - \mathcal{X}(r), w_k \rangle = 0 \tag{3.47}$$

for any set of bases functions $w_k \in S$. This gives a hint of choosing the basis functions for the subspace S as the POD modes. Writing $r(t)$ in terms of the coordinates $a_k(t)$ of the POD bases we have

$$r(t) = \sum_{k=1}^{n} a_k(t)\phi_k \tag{3.48}$$

On using (3.47) and the orthogonality of the POD modes we obtain a system of ODE's as

$$\dot{a}_k(t) = \langle \mathcal{X}(r(t)), \phi_k \rangle, k = 1, \cdots, n \tag{3.49}$$

For many types of equations, the ODE's given by (3.49) can be computed analytically in terms of the coordinates a_k. This is useful as the inner product need not be computed at each time step. The Galerkin procedure as described can also be easily extended to affine spaces, *i.e.* given a linear space S and an element $b \in H$ the affine subspace $S_b := \{b + v | v \in S\}$. In this case the expansion (3.48) takes the form

$$r(t) = b + \sum_{k=1}^{n} a_k(t)\phi_k \tag{3.50}$$

Usually in the application of POD to fluid flow simulations the element b is chosen to be the mean of the snapshots, denoted by $\bar{u}$. It is also helpful to note the projection for a quadratic operator $\mathcal{X}(u)$, as it arises in many applications of fluid mechanics *i.e*

$$\mathcal{X}(u) = L(u) + Q(u, u) \tag{3.51}$$

where $L : H \to H$ is linear and $Q : H \times H \to H$ is bilinear, the reduced order model can be obtained by the projection onto the affine subspace. Using (3.50) in (3.49) we obtain the reduced-order model as,

$$\begin{aligned}
\dot{a}_k(t) &= \langle L(r) + Q(r, r), \phi_k \rangle \\
&= \left\langle L\left(b + \sum_i a_i(t)\phi_i\right) + Q\left(b + \sum_i a_i(t)\phi_i, b + \sum_j a_j(t)\phi_j\right), \phi_k \right\rangle \\
&= C_k + \sum_i L_{ki} a_i(t) + \sum_{ij} Q_{kij} a_i(t) a_j(t)
\end{aligned}$$

where

$$\begin{aligned}
C_k &= \langle L(b) + Q(b, b), \phi_k \rangle \\
L_{ki} &= \langle L(\phi_i) + Q(b, \phi_i) + Q(\phi_i, b), \phi_k \rangle \\
Q_{kij} &= \langle Q(\phi_i, \phi_j), \phi_k \rangle
\end{aligned} \tag{3.52}$$

The coefficients are independent of time, and can be determined before integrating. We will refer to the above system when we discuss the isentropic compressible case of the cavity, for which we find a quadratic dynamics of the flow equation.

3.11 Incompressible case

We now highlight the basic principles of ROM for the incompressible case, just to highlight the differences for the compressible flows. In incompressible we assume that the velocity field $\mathbf{u} = (u, v, w)$ is divergence free *i,e* $\nabla \mathbf{u} = 0$. The Navier-Stokes equation in this case can be written as

$$\frac{D\mathbf{u}}{Dt} = -\nabla p + \nu \nabla^2 \mathbf{u} \tag{3.53}$$

ν denotes the kinematic viscosity, p the pressure, and $\frac{D}{Dt} = \frac{\partial}{\partial t} + \mathbf{u}.\nabla$ denotes the material derivative. On using the notation

$$\mathcal{N}(\mathbf{u}) = -(\mathbf{u}.\nabla)\mathbf{u} + \nu\nabla^2\mathbf{u}$$

equation (3.53) can be written as

$$\dot{\mathbf{u}} = \mathcal{N}(\mathbf{u}) - \nabla p \tag{3.54}$$

We use the POD expansion for the velocity $\mathbf{u}$ as:

$$\mathbf{u}(\mathbf{x}, t) = \bar{\mathbf{u}} + \sum_{k=1}^{n} a_k(t)\phi_k(\mathbf{x}) \tag{3.55}$$

where our Hilbert space is $L^2(\Omega)^3$ with the usual inner-product given by

$$\langle \mathbf{u}, \mathbf{v} \rangle = \int_\Omega \mathbf{u}(\mathbf{x})\mathbf{v}(\mathbf{x})d\Omega \tag{3.56}$$

On using the expansion (3.55) in (3.53) and using the definition of inner-product (3.56) we have the reduced-order model of incompressible equation as

$$\dot{a}_k = \langle \mathcal{N}(\mathbf{u}), \phi_k \rangle - \langle \nabla p, \phi_k \rangle \tag{3.57}$$

The second term can be written after integration by parts and using Green's theorem

$$\langle \nabla p, \phi_k \rangle = \langle p, \nabla\phi_k \rangle - [p\phi_k] \tag{3.58}$$

where $[p\phi_k] = \int_{\partial\Gamma} p.\phi_k \mathbf{n} d\Gamma$ denotes the surface integral with $\mathbf{n}$ denoting the normal to the boundary. The first term on the right hand side of equation (3.58) is zero due to the divergence criteria and if the velocity is zero along the boundaries the second term also vanishes. Thus we have the reduced order model of the incompressible case as

$$\dot{a}_k = \langle \mathcal{N}(\mathbf{u}), \phi_k \rangle = C_k + \sum_i L_{ki} a_i(t) + \sum_{ij} Q_{kij} a_i(t) a_j(t)$$

with the initial conditions

$$a_k(0) = \langle \mathbf{u} - \bar{\mathbf{u}}, \phi_k \rangle \tag{3.59}$$

The coefficients of the ODE given by (3.59) are written as,

$$\begin{aligned} C_k &= -\langle (\bar{\mathbf{u}}.\nabla)\bar{\mathbf{u}}, \phi_k \rangle - \nu\langle (\nabla \otimes \phi_k)^T, \nabla \otimes \bar{\mathbf{u}} \rangle + \nu[(\nabla \otimes \bar{\mathbf{u}})\phi_k] \\ L_{ki} &= -\langle (\bar{\mathbf{u}}.\nabla)\phi_i, \phi_k \rangle - \langle (\phi_i.\nabla)\bar{\mathbf{u}}, \phi_k \rangle - \nu\langle \nabla\phi_i, \phi_k \rangle + \nu[(\nabla\phi_j)\phi_k] \\ Q_{kij} &= -\langle (\phi_i.\nabla)\phi_j, \phi_k \rangle \end{aligned} \tag{3.60}$$

Note in this study we have assumed that the boundaries as a wall, and hence we neglect the pressure terms. In case the boundaries are treated as artificial boundaries, by considering only a limited portion of the domain of the whole flow, the pressure terms represent a significant contribution as shown by Noack *et al.* (2005). Also one more feature is that the mean field is assumed to be constant, but Aubry *et al.* (1988) considers a slow variation of the mean field with time and try to model the mean in terms of the fluctuation, which gives rises to cubic terms in the ROM, corresponding to the Reynolds stress. One challenge is to extend the development to the compressible case.

3.12 Compressible case

We now move on to the case of compressible flow. The main feature which distinguishes from the incompressible case is the velocity variables which are dynamically coupled with the thermodynamic variables. A question which arises due to this coupling is the formulation of the governing equations which in some cases can be simplified to the formulation of the quadratic dynamics as discussed in §3.10. As suggested by Rowley *et al.* (2003) using the isentropic formulation which is valid for cold-flows at low mach number one simplify the formulation to the quadratic case. Vigo (1998) suggests the use of specific volume to simplify the dynamics. Choice of inner product is also one issue and has been discussed in detail in §3.8. The coupled equations can be treated as a scalar in each variable or as a vector variable. Rowley (2002) has shown the distinct advantage of using a vector formulation, in which the stability of the attractor at the origin is preserved. In this work we mainly discuss the vector formulations which are used to build the ROM of the cavity flows.

Isentropic reduced order model

Scaling the velocities u, v by the free stream velocity U_∞, the local sound speed c by the ambient sound speed c_∞, the lengths by the cavity depth D, and time by D/U_∞, the equations are given by

$$\begin{aligned} u_t + uu_x + vu_y + \frac{1}{M^2}\frac{2}{\gamma-1}cc_x &= \frac{1}{Re}(u_{xx}+u_{yy}) \\ v_t + uv_x + vv_y + \frac{1}{M^2}\frac{2}{\gamma-1}cc_y &= \frac{1}{Re}(v_{xx}+v_{yy}) \\ c_t + uc_x + vc_y + \frac{\gamma-1}{2}c(u_x+v_y) &= 0 \end{aligned}$$

where $M = U_\infty/c_\infty$ is the Mach number and $Re = U_\infty D/\nu$ is the Reynolds number. The non-dimensionalisation is useful in that the Mach number which appears explicitly in the Galerkin projections, helps to investigate the parametric dependence of the reduced order model. There has also been studies of rescaling the cavity length by the momentum thickness to investigate its effect. Denoting $q = (u, v, c)$ the vector of flow variables, the above equations can be re-casted to obtain a quadratic form as

$$\dot{\mathbf{q}} = \frac{1}{Re}\mathbf{L}(q) + \frac{1}{M^2}\mathbf{Q_1}(q,q) + \mathbf{Q_2}(q,q) \qquad \text{with} \tag{3.61}$$

$$\mathbf{L}(q) = \begin{bmatrix} u_{xx}+u_{yy} \\ v_{xx}+v_{yy} \\ 0 \end{bmatrix}, \quad \mathbf{Q_1}(q^1,q^2) = -\tfrac{2}{\gamma-1}\begin{bmatrix} c^1c^2_x \\ c^1c^2_y \\ 0 \end{bmatrix}$$

$$\mathbf{Q_2}(q^1,q^2) = -\begin{bmatrix} u^1u^2_x + v^1u^2_y \\ u^1v^2_x + v^1v^2_y \\ u^1c^2_x + v^1c^2_y + \frac{\gamma-1}{2}c^1(u^2_x+v^2_y) \end{bmatrix} \tag{3.62}$$

To obtain the reduced order model by means of a Galerkin projection we define an inner product on the state space as explained in equation (3.42).

$$\left\langle q^1, q^2 \right\rangle_\Omega = \int_\Omega (u^1 u^2 + v^1 v^2 + \frac{2\alpha}{\gamma - 1} c^1 c^2)\, d\Omega$$

where α is a constant and γ is the ratio of specific heats. In this work we choose the value of $\alpha = 1$, which gives the definition of stagnation enthalpy while calculating the norm. We use the expansion of the vector variable q as

$$q(\mathbf{x}, t) = \overline{q}(\mathbf{x}) + \sum_{k=1}^{n} a_k(t)\phi_{\mathbf{k}}(\mathbf{x}) \tag{3.63}$$

where $\bar{q}$ denote the mean of the snapshot for the vector variable. On using (3.63) and the definition of the inner product given above to perform the Galerkin projection onto the first $n \ll N_{POD}$ spatial eigenfunctions, we obtain after some manipulation, the Reduced Order Model given by

$$\begin{aligned} \dot{a}_k^R(t) &= \frac{1}{Re} C_k^1 + \frac{1}{M^2} C_k^2 + C_k^3 + \sum_{i=1}^{n} \left(\frac{1}{Re} L_{ki}^1 + \frac{1}{M^2} L_{ki}^2 + L_{ki}^3 \right) a_i^R(t) \\ &+ \sum_{i,j=1}^{n} \left(\frac{1}{M^2} Q_{kij}^1 + Q_{kij}^2 \right) a_i^R(t) a_j^R(t) \\ &= C_k + \sum_{i=1}^{n} L_{ki} a_i^R(t) + \sum_{i,j=1}^{n} Q_{kij} a_i^R(t) a_j^R(t) = f_k(C_k, \mathbf{L}_k, \mathbf{Q}_k, \mathbf{a}^R(t)) \end{aligned} \tag{3.64}$$

where f_k is a polynomial of degree 2 in $\mathbf{a}^R$ and where the coefficients are given by

$$\begin{array}{lll} C_k^1 = \langle \phi_k, \mathbf{L}(\overline{q}) \rangle_\Omega & L_{ki}^1 = \langle \phi_k, \mathbf{L}(\phi_i) \rangle_\Omega & Q_{kij}^1 = \langle \phi_k, \mathbf{Q_1}(\phi_i, \phi_j) \rangle_\Omega \\ C_k^2 = \langle \phi_k, \mathbf{Q_1}(\overline{q}, \overline{q}) \rangle_\Omega & L_{ki}^2 = \langle \phi_k, \mathbf{Q_1}(\overline{q}, \phi_i) + \mathbf{Q_1}(\phi_i, \overline{q}) \rangle_\Omega & Q_{kij}^2 = \langle \phi_k, \mathbf{Q_2}(\phi_i, \phi_j) \rangle_\Omega \\ C_k^3 = \langle \phi_k, \mathbf{Q_2}(\overline{q}, \overline{q}) \rangle_\Omega & L_{ki}^3 = \langle \phi_k, \mathbf{Q_2}(\overline{q}, \phi_i) + \mathbf{Q_2}(\phi_i, \overline{q}) \rangle_\Omega & \end{array}$$

As already mentioned instead of the isentropic equations one can as well use the full Navier-Stokes equations which leads to cubic terms in the ROM. The use of specific volume defined as $\varsigma = \frac{1}{\rho}$ which preserves the quadratic nature of the dynamical system both these methods have been discussed in Appendix B and C

3.13 Extension to actuated case

Having discussed the ROM for the un-actuated case we now move on to introduce the effect of actuation on our ROM. The advantage of the reduced order models can be fully exploited when they are capable of being used in control studies, also we would like to have a dynamical system where the actuation effect is naturally embedded. There has been recent attempts to take care of the introduction of actuation by Bergmann & Cordier (2005),Weller *et al.* (2009*b*) for a feedback control where snapshots from the controlled case are augmented with the un-actuated modes (baseline flow as

usually called) to obtain a global representation for the controlled case. The regions where the control is introduced is explicitly identified while performing the projections, these methods are referred to as input separation methods as found in Kasnakoğlu *et al.* (2008). To explain further the flow domain Ω into two sub-regions, such that $\Omega = \Omega_{ac} + \Omega_{unac}$ where Ω_{ac}, Ω_{unac} represents the actuated and the un-actuated part of the domain respectively. The inner product for the corresponding domains is defined as $\langle ., . \rangle = \langle ., . \rangle_{\Omega_{ac}} + \langle ., . \rangle_{\Omega_{unac}}$, with the corresponding boundary condition imposed for Ω_{ac}. This procedure yields an autonomous system of ODE's of the form, (on using the summation convention)

$$\dot{a}_k = C_k + L_{ki} a_i + Q_{kij} a_i a_j + h_{1k}\gamma + h_{2ki} a_i \gamma + h_{3k}\gamma^2 \tag{3.65}$$

where γ is the actuation signal. This methods suffers the disadvantage in that one must be able to explicitly identify the control regions, while taking care to reproduce the un-actuated dynamics when the actuation value tends to zero. Also the information of the input actuation is hidden in the model. Another procedure of introducing actuation is to identify the system coefficients based on a stochastic estimation technique, to give a ROM of the form (3.65). More details of the method can be found in Caraballo *et al.* (2008), an explanation of which can be found in Appendix D. This involves determining additional POD actuation modes combined with a stochastic estimation. One would then look for an alternative separation methods *i.e.* look for an expansion of the form

$$q(\mathbf{x}, t) = \overline{q}(\mathbf{x}) + \sum_{k=1}^{n} a_k(t)\phi_k(\mathbf{x}) + \gamma(t)\psi(\mathbf{x}) \tag{3.66}$$

where γ is the actuation and ψ is the spatial actuated coefficient and which would satisfy the following condition

1. The actuation effect should be explicitly available in our ROM and should be able to reproduce the un-actuated dynamics in case the value of actuation tends to zero.

2. Most of the actuated dynamics in the space spanned by the un-actuated POD modes are well captured by the un-actuated POD modes and hence the completion of the full actuated dynamics is obtained by an extension of the bases. This condition is an additional constraint to condition 1 in that we require a constraint on the dimension of our actuation by specifying that the base-line modes capture most of the dynamics and is the crux of the whole problem.

3. We further strengthen this condition by imposing an optimality condition in that the energy not captured by (3.66) is minimal.

Figure 3.3 summaries the above condition to give a basis extension problem. The conditions can be systematically algorithmized as below followed by the theorem due to Kasnakoğlu (2007) as found in appendix E.

Algorithm 1:

1. To start with, let the actuated snapshot sets be denoted as $\{q_k^{ac}, \gamma_k\}_{k=1}^{m}$, where $\gamma_k = \gamma(t_k)$ is the value of the actuation, $q_k^{ac} = q^{ac}(\mathbf{x}, t_k)$ and m is the number of actuated snapshots

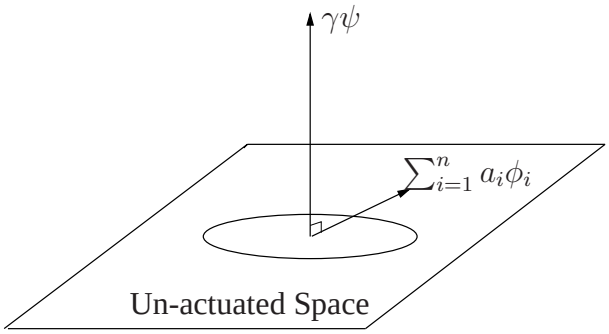

Figure 3.3 - *Diagrammatic representation of the actuated expansion, the un-actuated subspace must be able to capture most of the dynamics and the actuated space is the completion of our subspace in an optimal way to include the actuation effect.*

2. We subtract the mean $\overline{q}$ of the un-actuated base flow from the snapshot set. We define a new set of realisations by an innovation operator defined by

$$\tilde{q_k} = q_k^{ac} - P_{\mathcal{S}} q_k^{ac} = q_k^{ac} - \sum_{i=1}^{n} \langle q_k^{ac}, \phi_i \rangle \, \phi_i$$

   to take care of the part of the actuated mode which can be captured by the un-actuated subspace.

3. We then wish to construct an orthogonal subspace to the un-actuated space to capture the effect of actuation. This is done by solving an L_2 minimisation problem for the functional given by

$$\mathcal{J}(\psi) = E\left[\|\tilde{q_k} - \gamma_k \psi\|^2\right]$$

   where E is any averaging operator.

4. The solution of the above minimisation problem for the actuated mode ψ is given by

$$\psi = \frac{E[\gamma_k \tilde{q_k}]}{E[\gamma_k^2]}$$

5. The expansion for the flow field can now be written for the actuated case as

$$q_k^{ac}(\mathbf{x}, t) = \overline{q}^{ac}(\mathbf{x}) + \sum_{k=1}^{n} a_k^{ac}(t)\phi_k(\mathbf{x}) + \gamma(t)\psi(\mathbf{x})$$

3.13.1 Reduced order model for the actuated case

Let $V = \overline{q} + \text{span}\{\phi_1, \ldots, \phi_n, \psi^*\}$. Consider the dynamical system that evolves on $\mathbf{X}$ given by

$$\dot{r} = \mathcal{X}(r) \tag{3.67}$$

The reduced order dynamical system that approximates (3.67) can be obtained by a Galerkin projection as

$$\mathcal{X}_V(r) = \mathbb{P}_V \mathcal{X}(r) \tag{3.68}$$

and is optimal in the sense that it minimises $\|\mathcal{X}_V(r) - \mathcal{X}(r)\|$. since $\mathcal{X}_V(r) - \mathcal{X}(r) \perp V$ we have

$$\langle \mathcal{X}_V(r) - \mathcal{X}(r), \phi_k \rangle = 0, k = 1, \ldots, n \tag{3.69}$$

substituting $r = \overline{q} + a_k\phi_k + \gamma\psi^*$ in (3.69) one can write

$$\begin{aligned}
\langle \dot{a_k}\phi_k + \dot{\gamma}\psi^* - \mathcal{X}(r), \phi_k \rangle &= 0 \\
\dot{a_k}\langle \phi_k, \phi_k \rangle + \dot{\gamma}\langle \psi^*, \phi_k \rangle - \langle \mathcal{X}(r), \phi_k \rangle &= 0 \\
\dot{a_k}\langle \phi_k, \phi_k \rangle - \langle \mathcal{X}(r), \phi_k \rangle &= 0 \\
\dot{a_k} = \langle \mathcal{X}(r), \phi_k \rangle &
\end{aligned} \tag{3.70}$$

As in the un-actuated case, we now derive the reduced-order model for the special case of the quadratic dynamics as

$$\mathcal{X}(q) = L(q) + Q(q, q) \tag{3.71}$$

substituting (3.71) in (3.70) gives

$$\begin{aligned}
\dot{a_k} &= \langle \mathcal{X}(r), \phi_k \rangle \\
&= \langle L(\overline{q} + a_i\phi_i + \gamma\psi^*) + Q(\overline{q} + a_i\phi_i + \gamma\psi^*, \overline{q} + a_i\phi_i + \gamma\psi^*) \rangle \\
&= \langle L(\overline{q}), \phi_k \rangle + \langle L(\phi_i), \phi_k \rangle a_i + \langle L(\psi^*), \phi_k \rangle \gamma + \langle Q(\overline{q}, \overline{q}), \phi_k \rangle \\
&+ \langle Q(\overline{q}, \phi_j), \phi_k \rangle a_j + \langle Q(\overline{q}, \psi^*), \phi_k \rangle \gamma + \langle Q(\phi_i, \overline{q}), \phi_k \rangle a_i + \langle Q(\phi_i, \phi_j), \phi_k \rangle a_i a_j \\
&+ \langle Q(\phi_i, \psi^*), \phi_k \rangle a_i \gamma + \langle Q(\psi^*, \overline{q}), \phi_k \rangle \gamma + \langle Q(\psi^*, \phi_i), \psi^* \rangle a_i \gamma + \langle Q(\psi^*, \psi^*), \phi_k \rangle \gamma^2 \\
&= C_k + L_{kj}a_j + Q_{kij}a_i a_j + h_{1k}\gamma + h_{2ki}a_i\gamma + h_{3k}\gamma^2
\end{aligned} \tag{3.72}$$

where

$$
\begin{aligned}
C_k &= \langle L(\overline{q}), \phi_k \rangle + \langle Q(\overline{q}, \overline{q}), \phi_k \rangle \\
L_{kj} &= \langle L(\phi_j), \phi_k \rangle + \langle Q(\overline{q}, \phi_j), \phi_k \rangle + \langle Q(\phi_j, \overline{q}), \phi_k \rangle \\
h_{1k} &= \langle L(\psi^*), \phi_k \rangle + \langle Q(\overline{q}, \psi^*), \phi_k \rangle + \langle Q(\psi^*, \overline{q}), \phi_k \rangle \\
Q_{kij} &= \langle Q(\phi_i, \phi_j), \phi_k \rangle \\
h_{2ki} &= \langle Q(\phi_i, \psi^*), \phi_k \rangle + \langle Q(\psi^*, \phi_i), \psi^* \rangle \\
h_{3k} &= \langle Q(\psi^*, \psi^*), \phi_k \rangle
\end{aligned}
$$

3.13.2 A polynomial notation for the reduced-order model

We give a notation for the ROM (3.72) which will be helpful in simplifying the model, if we note that the ROM is nothing but a polynomial of degree 2 in the unknown variable $\mathbf{a}^R = \{a_1, \ldots, a_n\}$. Equation (3.72) can be written by separating the actuated and the un-actuated parts in a compact notation as

$$\dot{a_k}^R = f_k(\mathbf{y_k}, \mathbf{a}^R(t)) + g_k(\mathbf{z_k}, \mathbf{a}^R(t), \gamma) \tag{3.73}$$

where

$$f_k(\mathbf{y_k}, \mathbf{a}^R(t)) = C_k + L_{kj} a_j(t) + Q_{kij} a_i(t) a_j(t) \tag{3.74}$$

$$g_k(\mathbf{z_k}, \mathbf{a}^R(t), \gamma) = h_{1k}\gamma(t) + h_{2ki} a_i(t)\gamma(t) + h_{3k}\gamma(t)^2 \tag{3.75}$$

with $j = 1, \ldots, n$ and $i = 1, \ldots, j$ the coefficients $\mathbf{y}_k$ and $\mathbf{z}_k$ in (3.73) denote the unknown coefficients for the actuated and the un-actuated part respectively and is given by

$$\mathbf{y_k} = \begin{pmatrix} C_k \\ L_{k1} \\ \vdots \\ L_{kn} \\ Q_{k11} \\ \vdots \\ Q_{knn} \end{pmatrix} \in \mathbb{R}^{N_{y_k}} \quad \text{and} \quad \mathbf{z_k} = \begin{pmatrix} h_k \\ h_{21k} \\ \vdots \\ h_{2nk} \\ h_{3k} \end{pmatrix} \in \mathbb{R}^{N_{z_k}}$$

To reduce the size of $\mathbf{y}_k$ we use the properties of symmetry of the quadratic terms Q_{ijk} by noting that $Q_{ijk} = 1/2(Q_{ijk} + Q_{ikj})$ and hence the size of vector $y_k = N_{y_k} = 1 + n + \frac{n(n+1)}{2}$ and $N_{z_k} = 2 + n$.

The unknown coefficients of the ROM can be written in a vectorial notation as

$$\mathbf{m}(t) = \begin{pmatrix} 1 \\ a_1(t) \\ \vdots \\ a_n(t) \\ a_1(t)a_1(t) \\ \vdots \\ a_n(t)a_n(t) \end{pmatrix} \in \mathbb{R}^{N_{y_k}} \quad \text{and} \quad \mathbf{n}(t) = \begin{pmatrix} \gamma(t) \\ \gamma(t)a_1(t) \\ \vdots \\ \gamma(t)a_n(t) \\ \gamma^2(t) \end{pmatrix} \in \mathbb{R}^{N_{z_k}}$$

with this notation (3.74) and (3.75) can be written as

$$\begin{aligned} f_k(\mathbf{y}_k, \mathbf{a}^R(t)) &= \mathbf{m}(t).\mathbf{y}_k \\ g_k(\mathbf{z_k}, \mathbf{a}^R(t), \gamma) &= \mathbf{n}(t).\mathbf{z}_k \end{aligned} \tag{3.76}$$

Equation (3.76) can be further written in a vector notation to give the final form of the ROM as [1]

$$\dot{\mathbf{a}}^{\mathbf{R}} = \mathbf{f}(\mathbf{y}, \mathbf{a}^{\mathbf{R}}) + \mathbf{g}(\mathbf{z}, \mathbf{a}^{\mathbf{R}}, \gamma) \tag{3.77}$$

where for the uncontrolled contribution we have:

$$\mathbf{f} = \begin{pmatrix} f_1 \\ \vdots \\ f_N \end{pmatrix} \in \mathbb{R}^n \quad \text{and} \quad \mathbf{y} = \begin{pmatrix} y_1 \\ \vdots \\ y_N \end{pmatrix} \in \mathbb{R}^{N_y} \quad \text{with} \quad N_y = nN_{y_k}$$

and for the controlled contribution:

$$\mathbf{g} = \begin{pmatrix} g_1 \\ \vdots \\ g_N \end{pmatrix} \in \mathbb{R}^n \quad \text{and} \quad \mathbf{z} = \begin{pmatrix} z_1 \\ \vdots \\ z_N \end{pmatrix} \in \mathbb{R}^{N_z} \quad \text{with} \quad N_z = nN_{z_k}$$

3.13.3 Extension to multiple modes

In the case of multiple inputs, it is trivial to extend the above procedure to include multiple control inputs for example assume we have determined $\{\psi_j\}_{j=1}^M$ actuation modes corresponding to $\{\gamma_j(t)\}_{j=1}^M$ inputs. We have an expansion of the form,

$$q^{ac}(\mathbf{x}, t) = \overline{q}^{ac}(\mathbf{x}) + \sum_{i=1}^{n} a_i^{ac}(t)\phi_{\mathbf{i}}(\mathbf{x}) + \sum_{j=1}^{M} \gamma_j(t)\psi_{\mathbf{j}}(\mathbf{x}) \tag{3.78}$$

[1] Computationally $\mathbf{f}$ can be computed at any time instant t as a product of a block diagonal matrix M where each block is equal to m^T multiplied by the vector $\mathbf{y}$. Similarly $\mathbf{g}$ can be obtained as the product of a block diagonal matrix Q where each block is equal to n^T multiplied by the vector $\mathbf{z}$.

and the corresponding Galerkin model is obtained just by a summation over the corresponding inputs as

$$\dot{a_k} = C_k + L_{kj}a_j + Q_{kij}a_i a_j + h_{1ki}\gamma_i + h_{2kij}a_i\gamma_j + h_{3kij}\gamma_i\gamma_j \tag{3.79}$$

It is also possible to include the effect of the derivatives of the input as in many cases the derivatives will be known. For example assuming that the derivative of the input $\dot{\gamma}(t)$ is available, the algorithm can be summarized as follows.

Algorithm 2:

1. To start with, let the actuated snapshot sets be denoted as $\{q_k^{ac}, \gamma_k, \dot{\gamma_k}\}_{k=1}^m$, where $\gamma_k = \gamma(t_k)$ is the value of the actuation, $\dot{\gamma_k} = \dot{\gamma}(t_k)$ is the derivative of the input,$q_k^{ac} = q^{ac}(\mathbf{x}, t_k)$ and m is the number of actuated snapshots.

2. We subtract the mean $\overline{q}$ of the un-actuated base flow from the snapshot set. We define a new set of realisations using an innovation operator given by

$$\tilde{q_k} = q_k^{ac} - P_{\mathcal{S}}q_k^{ac} = q_k^{ac} - \sum_{i=1}^{n} \langle q_k^{ac}, \phi_{\mathbf{i}} \rangle \, \phi_{\mathbf{i}}$$

3. We then wish to construct an orthogonal subspace to the un-actuated space to capture the effect of actuation. This is done by solving an L_2 minimisation problem for the functional given by

$$\mathcal{J}(\psi) = E\left[\|\tilde{q_k} - \gamma_k\psi\|^2\right]$$

   where E is any averaging operator, to obtain an actuation mode ψ_1 for input.

4. Define $\breve{q}_k = q_k^{ac} - P_{S_1}q_k^{ac}$ where $S_1 = \text{span}\{\phi_1, \ldots, \phi_N, \psi_1\}$. In general $\|\psi_1\| \neq 1$ and hence while projecting on the actuation mode we define the projection operator of the form

$$P_{\psi_1}q_k = \|\psi_1\|^{-1}\langle q_k, \psi_1\rangle\psi_1$$

5. To include the effect of the derivative of the actuation, we follow the same procedure as above with $\breve{q}$ replacing $\tilde{q}$ to solve a minimisation problem for the functional given by

$$\mathcal{J}(\psi) = E\left[\|\breve{q}_k - \gamma_k\psi_1\|^2\right]$$

   to obtain an actuation mode for the derivative given by ψ_2.

6. The expansion for the flow field can now be written for the actuated case as

$$q^{ac}(\mathbf{x}, t) = \overline{q}^{ac}(\mathbf{x}) + \sum_{i=1}^{n} a_i^{ac}(t)\phi_i(\mathbf{x}) + \gamma(t)\psi_{\mathbf{1}}(\mathbf{x}) + \dot{\gamma}(t)\psi_2(\mathbf{x}) \tag{3.80}$$

As mentioned before the above procedure can be easily extended to include the derivatives of multiple inputs in which case the expansion for the flow field is given by

$$q^{ac}(\mathbf{x},t) = \overline{q}^{ac}(\mathbf{x}) + \sum_{i=1}^{n} a_i^{ac}(t)\phi_i(\mathbf{x}) + \sum_{j=1}^{M} \gamma_j(t)\psi_{1j}(\mathbf{x}) + \sum_{j=1}^{M} \dot{\gamma_j}(t)\psi_{2j}(\mathbf{x}) \tag{3.81}$$

The Galerkin model for the multiple control inputs with its derivative can be written in the form

$$\begin{aligned} \dot{a_k} &= C_k + L_{kj}a_j + Q_{kij}a_i a_j + h_{1ki}\gamma_i + h_{2kij}a_i\gamma_j + h_{3kij}\gamma_i\gamma_j \\ &+ g_{1ki}\dot{\gamma_i} + g_{2kij}a_i\dot{\gamma_j} + g_{3kij}\dot{\gamma_i}\dot{\gamma_j} + g_{4kij}\gamma_i\dot{\gamma_j} \end{aligned} \tag{3.82}$$

3.14 Application to cavity flows

We present results for the cavity flow configuration described in chapter 1. The DNS is performed and snapshots are taken once the flow has stabilised for a non-dimensional time of 80. 56 snapshots are uniformly sampled which corresponds to about 1 periods of the flow oscillation (2.8 in non dimensional time) corresponding to the first Rossiter mode. Figure 3.4 demonstrates a degenerate eigen spectrum showing eigenvalues which occur in pairs. Also the first 4 eigenmodes capture around 98.5% of the total fluctuation energy as shown by the Relative Information Content (RIC), and the first 6 modes capture 99.99% of the total energy. In this work we construct the ROM keeping 6 modes from the POD representation. The POD temporal coefficients in figure 3.5 shows that the modes occurring in pair have a phase shift of $\frac{\pi}{2}$. The representation of the first 6 spatial POD modes for the vorticity and dilatation is shown in 3.6, and 3.7. The dilatation represents the directivity of sound and is given by the equation

$$\Theta = \frac{\partial u}{\partial x} + \frac{\partial v}{\partial y}$$

Although the spatial modes occur in pairs and their values are distinct, the representation is topologically equivalent. The vorticity and dilatation has been determined using a 6^{th} order accurate compact scheme. The wiggles in the representation are mainly the artifact of the numerical scheme used in the DNS computation. We suspect that using a higher order compact scheme may improve the result. There is also a strong evidence of the effect of discretisation when we compute the dilatation modes which are mainly acoustic, and very sensitive to numerical discretisation. The vorticity modes mainly represent the hydrodynamic component and the dilatation the acoustic phenomenon. The two vorticity modes occur in pair with a phase shift of $\pi/2$ as can be seen in the representation of the temporal coefficient in figure 3.5. The dilatation being a high frequency phenomenon, is clearly depicted for the higher POD modes where the angle of the wave propagation at 135^o is distinctly visible. Cavity flows represent a distinct coupling between these two phenomenon in which the high frequency acoustic components feedback into the low frequency hydrodynamic component, resulting in self sustained oscillations. Hence to have a faithful behaviour of the ROM it is necessary to consider the prominent acoustic modes represented by the high frequency POD coefficients.

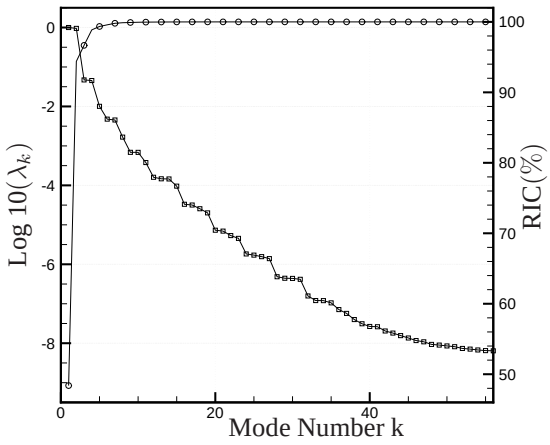

Figure 3.4 - *eigen spectra and Relative Information Content (RIC)*

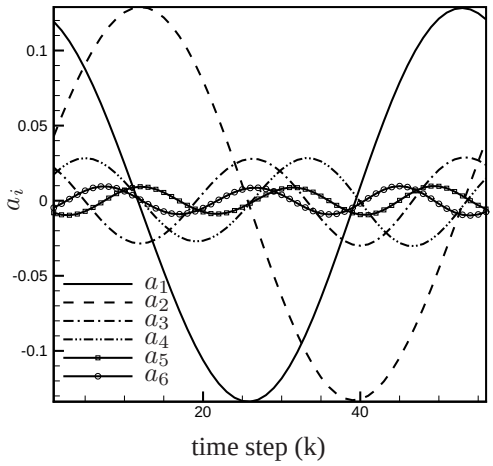

Figure 3.5 - *first 6 POD temporal coefficients*

Regarding ROM snapshots are obtained from the DNS by introducing an actuation of the form $A\sin(\omega t)$ just before the leading edge of the cavity ($x \in [-0.15; -0.05]$ and $y = 0$) where the flow is more sensitive to actuation. The spatial modes as shown in 3.8 exhibit a local behaviour capturing the effect of actuation which is the salient feature of the L_2 optimisation method introduced in the preceeding sections. Since the actuated subspace is orthogonal to the un-actuated subspace we have from (3.66), the actuated temporal modes a_i^{ac} given by:

$$a_i^{ac}(t) = \langle \phi_i, q^{ac} - \overline{q}^{ac} - \gamma(t)\psi \rangle_\Omega$$

Here we make the assumption that the average of the mean flow in un-actuated and actuated cases are equal, ($\overline{q}^{ac} = \overline{q}$), since the value of actuation introduced is small. The term $\delta\overline{q}^{ac} := q^{ac} - \overline{q}^{ac}$ can now be interpreted as a translation of the reduced order subspace. We also introduce, an error to take care of the difference in the average values while performing the Galerkin projections as

$$\varepsilon_i = \frac{\langle \delta\overline{q}^{ac}, \phi_i \rangle}{\langle \phi_i, \overline{q}^{ac} \rangle} \tag{3.83}$$

Also since the actuated mode is orthogonal to the un-actuated subspace *i.e.* $\psi \perp \phi$ the term $a_i^{ac}(t) \longrightarrow 0$. This is an essential point as the temporal dynamics of our model is mainly represented by the un-actuated subspace, the actuated mode represents the completion of the basis to include the effect of actuation. The difference in average values δq^{ac} for the stream-wise and normal component of velocity is shown in figure 3.9, and the value of the error in the projection ε_i in figure 3.10, showing a small errors for the most energetic modes. We are unable to explain the behaviour of the error at the certain higher modes which seem pretty large. The time traces and the phase portrait of the first 6 modes of the Galerkin model is shown in figure 3.11 and 3.12. The Galerkin model compares well with the POD coefficients for the initial time and shows a divergence as time progresses. Also the

deviation from the expected behaviour is large in the case of higher modes. One of the reason for the divergence can be attributed to the truncation of the terms in our Galerkin model, but increasing the number of modes does not improve the results, as shown by Rempfer (1996) even the full order system can converge to a wrong attractor. This brings in the problem of calibration of the ROM *i.e.*, to correctly determine the coefficients of the ROM so as to reproduce the POD dynamics. The reasons for the divergence of our ROM model as well as the various techniques of calibration will be discussed in the next chapter.

3.15 Conclusion

In this chapter, we have discussed the basic principles of the Proper Orthogonal Decomposition. We have also given some of the properties of POD that make them an useful choice in the model reduction of fluid flows. Choice of inner-products for both in-compressible and compressible case has been discussed.

The principles of a ROM based on a Galerkin projection has been discussed. A comparison between the incompressible and compressible case has been presented. To model the cavity flows we construct the ROM of the isentropic Navier-Stokes equations. Extension of the model to include the effect of actuation, is by means of constructing an actuated mode based on solving an L_2 optimisation problem, and the corresponding ROM presented. The extension of the ROM to include the effect of multiple actuation as well as the derivative of the actuation has been discussed. Results of the ROM shows a divergence from the predicted dynamics obtained from the POD, which motivates the next chapter on the stabilisation of the ROM.

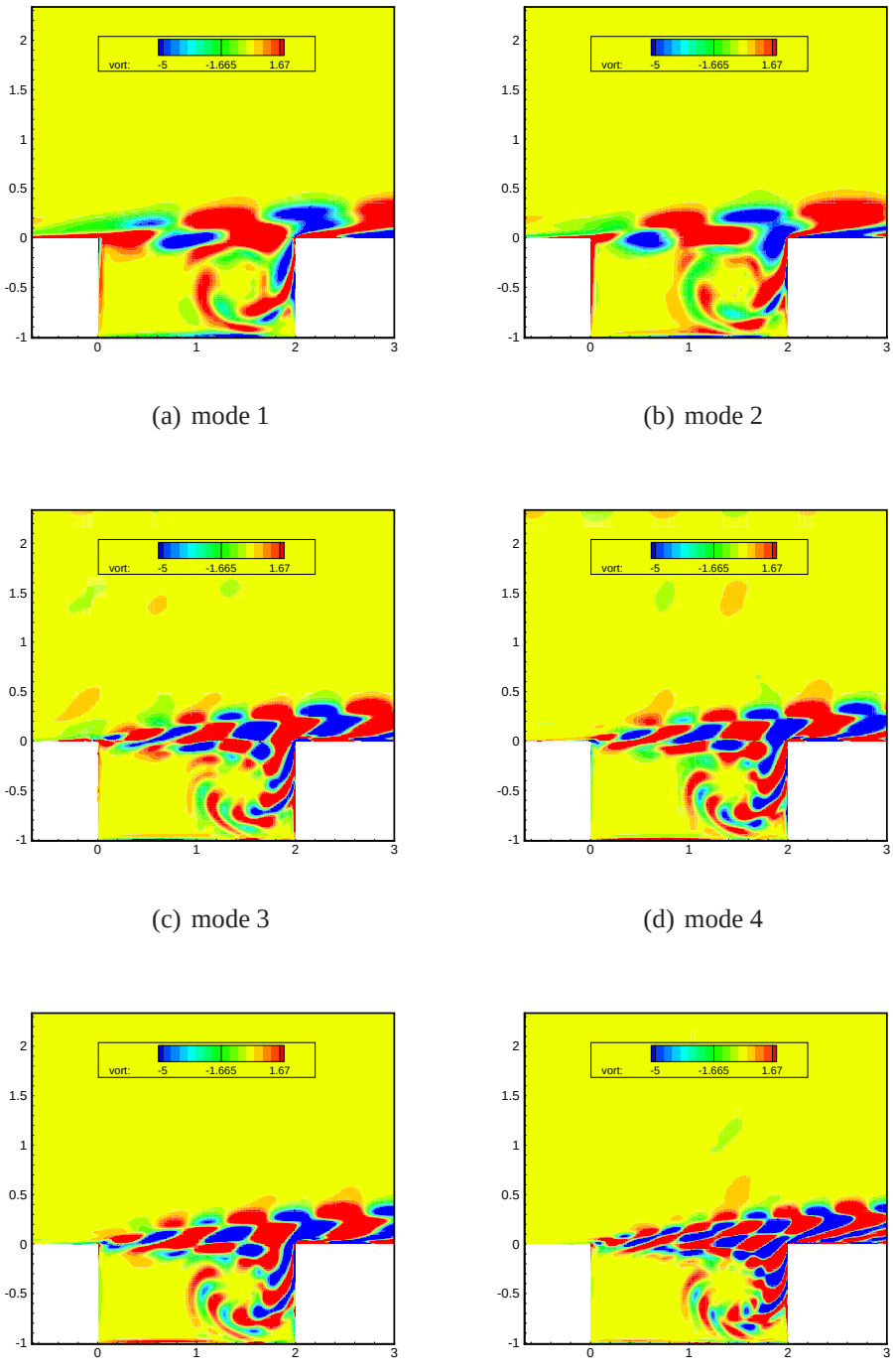

(a) mode 1 (b) mode 2

(c) mode 3 (d) mode 4

(e) mode 5 (f) mode 6

Figure 3.6 - *Vorticity contours of the first* 6 *POD modes.* 15 *contours in the range* $[-5, 1.67]$ *are plotted. We note that the cascade of the energy in the POD representation in terms of the size of the eddies represented. The vorticity being a hydrodynamic phenomenon represents the low frequency dynamics of the flow.*

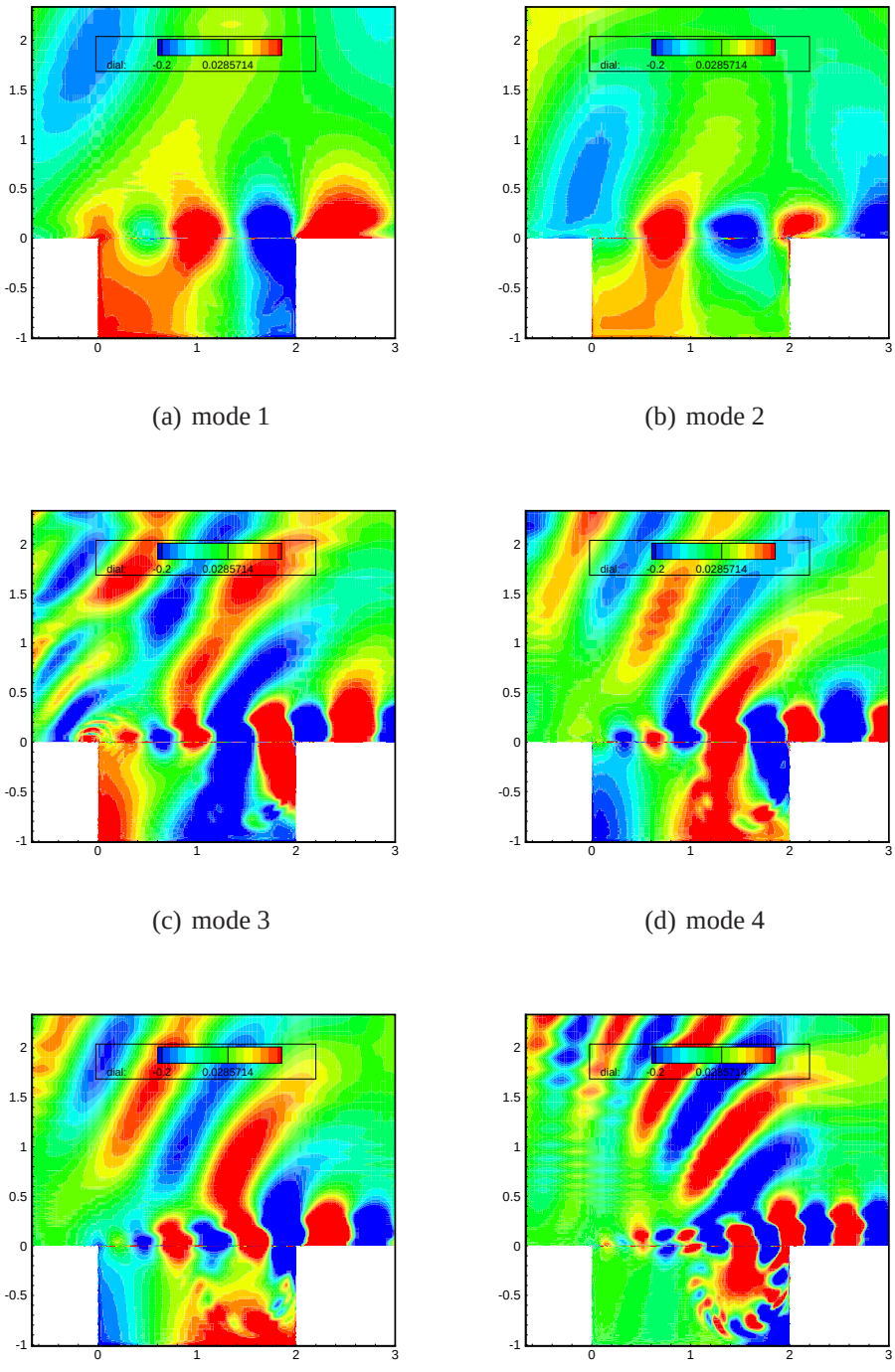

(a) mode 1 (b) mode 2

(c) mode 3 (d) mode 4

(e) mode 5 (f) mode 6

Figure 3.7 - *Dilatation contours of the first* 6 *POD modes.* 15 *contours in the range* $[-0.2, 0.2]$ *are plotted. Dilatation mainly represent the acoustic phenomenon which occurs at high frequency and we can see the dilatation more prominent in the higher modes, where the angle of wave propagation is clearly visible.*

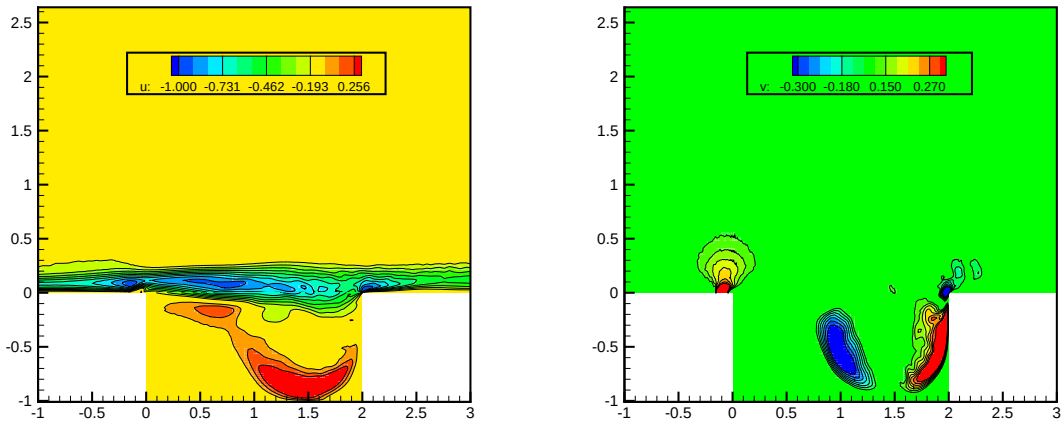

(a) u (b) v

Figure 3.8 - *u and v velocity components of the actuation mode ψ corresponding to an actuation defined by $v_{wall} = 0.2\ \sin(0.4t)$. The plot shows a local behaviour capturing the effect of actuation.*

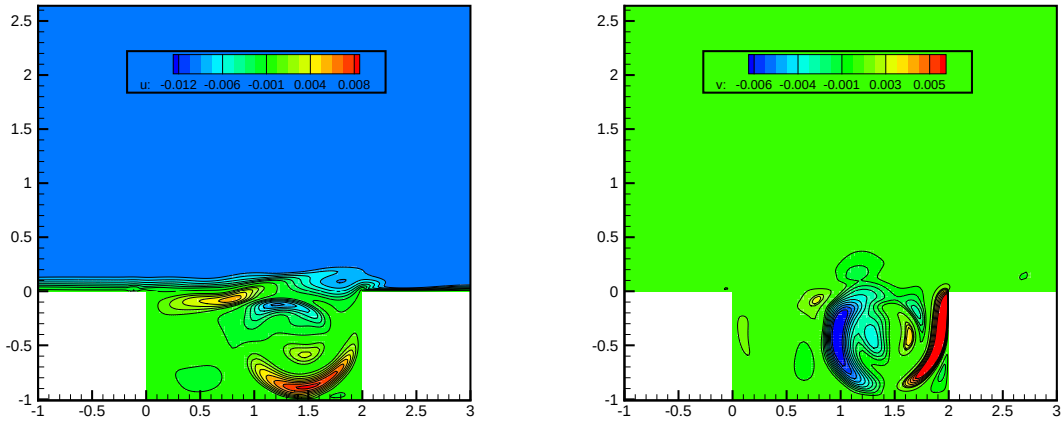

(a) u (b) v

Figure 3.9 - *u and v of the difference in the average value $\delta\overline{q}^{ac}$ between the actuated and the un-actuated case. The average of the mean flow in un-actuated and actuated cases are equal, ($\overline{q}^{ac} = \overline{q}$), since the value of actuation introduced is small.*

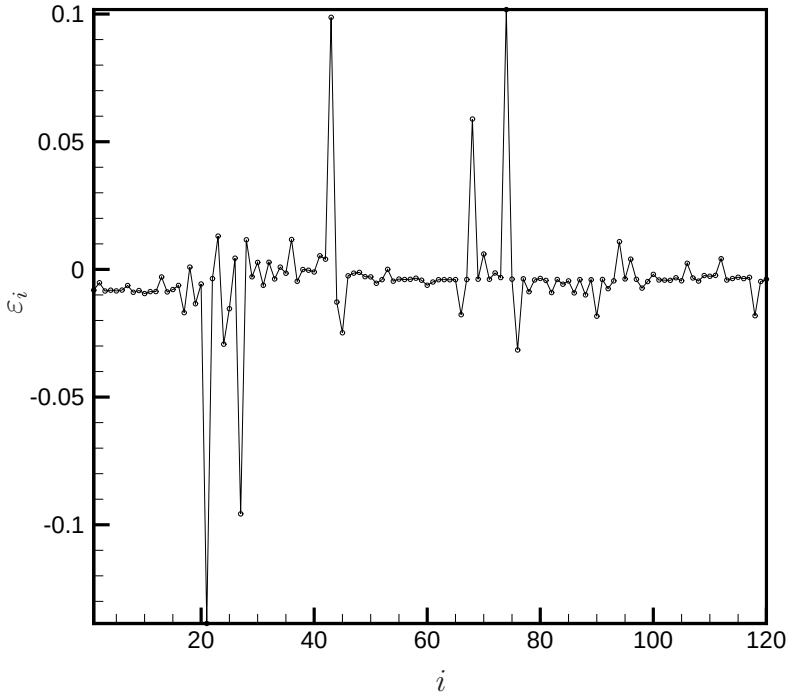

Figure 3.10 - *Average projection error ε_i and shows a small errors for the most energetic modes.*

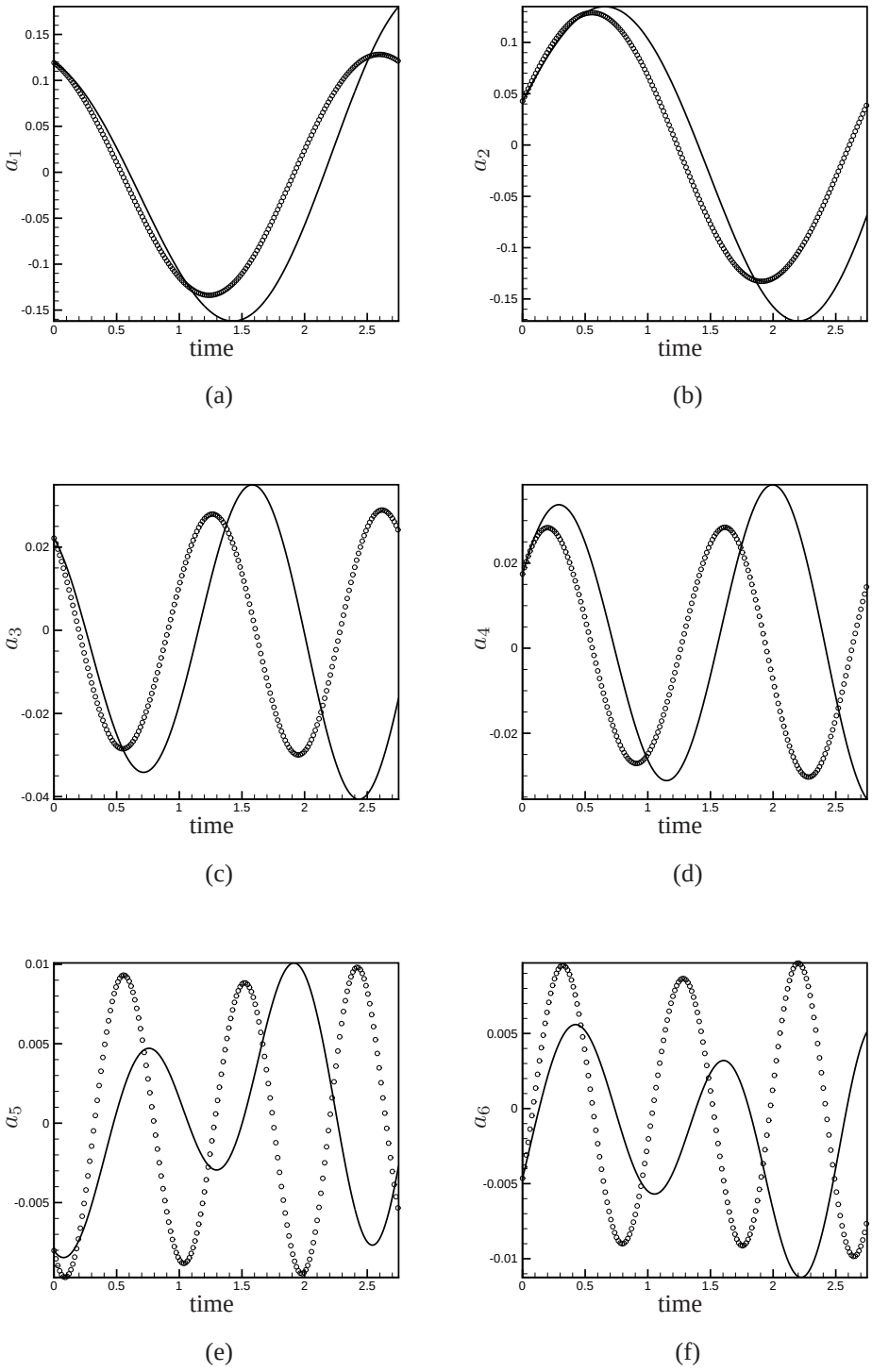

Figure 3.11 - *Temporal comparison of the first* 6 *modes, with the POD coefficients:ROM prediction(solid line), reference POD dynamics (o). The Galerkin model compares well with the POD coefficients for the initial time and shows a divergence as time progresses.*

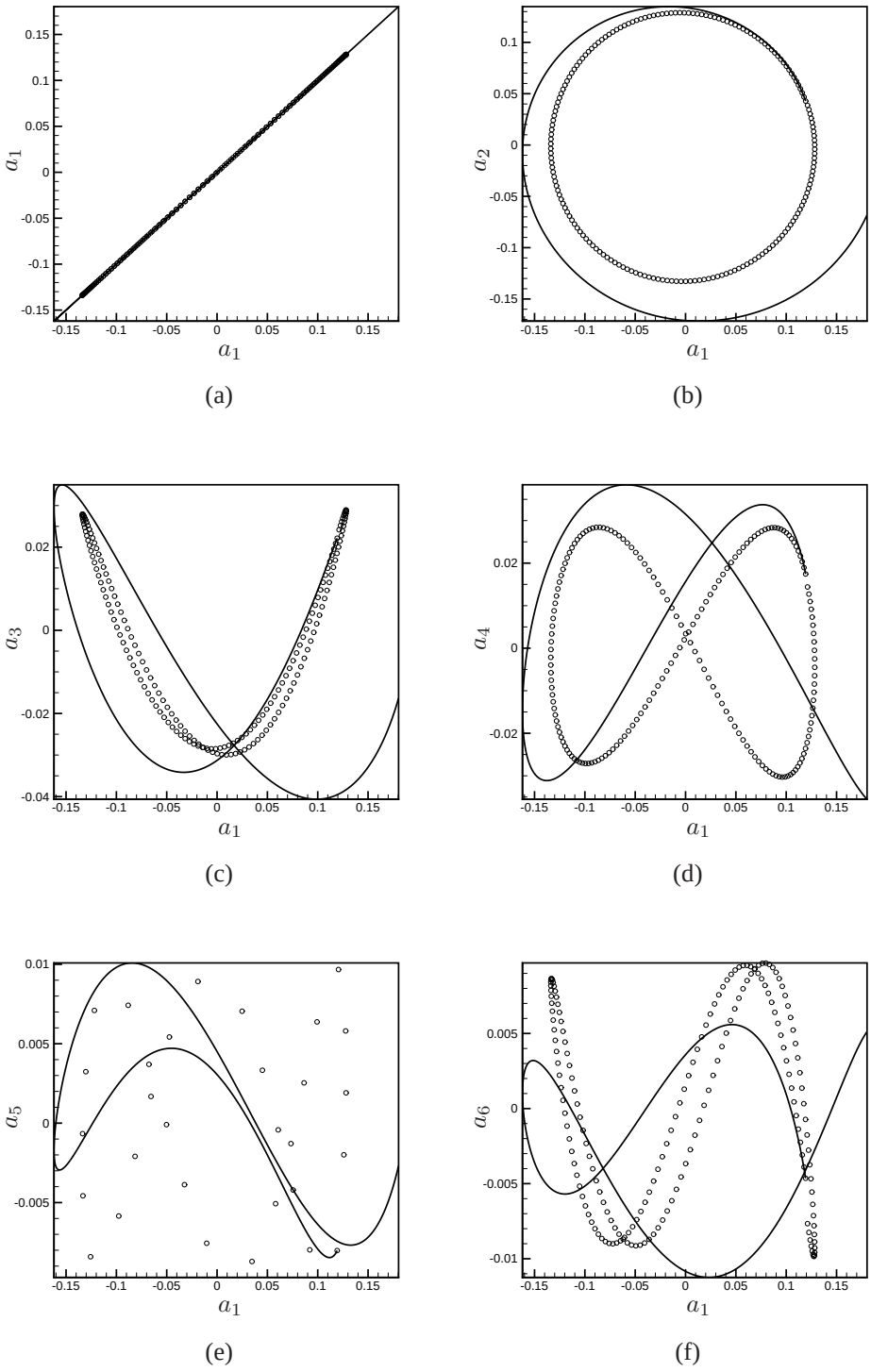

Figure 3.12 - *Phase portrait comparison of the first* 6 *modes, with the POD coefficients:ROM prediction(solid line), reference POD dynamics (o). The Galerkin model compares well with the POD coefficients for the initial time and shows a divergence as time progresses.*

Chapter 4

Integration and calibration of ROM

Introduction

Ce chapitre concerne essentiellement les différentes techniques de calibration utiliser pour stabiliser le modèles d'ordre réduit. Il est souvent difficile de représenter avec suffisament de précision, même sur un temps court la dynamique du système initial, ce qui interdit l'utilisation des modèles d'ordre réduits pour des études de sensibilité, d'optimisation et de contrôle optimal. L'idée principale de la calibration est d'identifier les coefficients du modèle POD Galerkin (ROM) de sorte que sa dynamique propres coïncide avec la dynamique temporelle de la POD issue des simulations numériques directes et qui est connue à l'avance. Les raisons de la mauvaise précision du modèle ROM peut être attribuée à la troncature des bases POD où les échelles dissipatives incluses dans les modes POD d'ordres élevés ne sont pas prises en compte. C'est un problème analogue à celui rencontré en Simulation de Grandes Echelles (LES) où la dissipation des petites échelles est manquante. Même si tous les modes de la projection de Galerkin sont pris en compte, on peut aboutir à un mauvais attracteur à cause des instabilités structurales comme celles observées par Rempfer (2000),Noack et al. (2003). Les techniques de calibration peuvent être classées en deux catégories, la première consiste à traiter le problème de calibration comme un problème de fermeture de la turbulence. La seconde considère un problème d'identification de coefficients, ce qui revient à une problème d'optimisation ou de contrôle optimal. Couplet et al. (2005) donne une vue générale des différentes erreurs qui apparaissent dans le ROM et propose une technique de calibration basée sur la minimisation d'une fonctionnelle linéaire de l'erreur. Récemment une amélioration des propositions de Couplet et al. (2005) a été présentée dans Cordier et al. (2009). Nous proposons une amélioration supplémentaire de cette technique en introduisant différents types de matrice de pondération dans la définition de l'erreur. Dans la première méthode les poids sont déterminés à partir d'une analyse de sensibilité de l'énergie. Dans la seconde approche les poids sont définies à partir du contenu énergétique de la représentation en ROM.

Définition des erreurs

L'actionnement dans le systèmes ROM est déterminé par une procédure d'optimisation L_2 se retrouve principalement restreint de à un mode spatial. Par conséquent il est suffisant de présenter les principales idées sur la calibration associée Les dynamiques temporelles aux cas sans actionnement. Les erreurs pour une identification polynômiale du modèle d'ordre réduit (ROM) peuvent être essentiellement classées en:

1. *La calibration d'état, où les coefficient du modèle ROM sont identifiés pour représenter avec précision l'état temporel du ROM en accord avec les coefficient temporels de la POD du système original.*

2. *La calibration d'écoulement, où les coefficients sont identifiés pour représenter les champs de vecteurs de l'integration temporelle du ROM en accord avec les champs de vecteurs obtenus par la POD.*

Trois erreurs peuvent être définies par les équations 4.2, 4.4 et 4.6. Une fois l'erreur choisi, l'identification polynômiale est obtenue par minimisation des fonctionnelles coût basées sur cette erreur comme données par les équations 4.3, 4.5, 4.7. Dans la fonctionnelles coût tous les modes sont donnés de poids égaux. La minimisation des fonctionnelles 4.5, 4.7 conduit à la résolution d'un système linéaire puisque les erreurs (équations 4.4 et 4.6) sont des fonctions affines des coefficients polynômiaux.

Méthode de calibration de Couplet

La méthode de Couplet et al. (2005) introduit la minimisation de fonctionnelles basées sur la combinaison linèaire convexe des termes qui représentent l'erreur normalisée et une mesure de la variation des coefficients du modèle par rapport aux valeurs obtenues par la POD. Cependant, Il s'avère que le système linéaire est mal conditionné et diverge après un temps court comme on peut le voir sur la figure 4.1. Pour résoudre cela on régularise la fonction coût. Cependant le choix du paramétre de régularisation dépend de l'utilisateur. Pour y remédier Cordier et al. (2009) utilisent la méthode de régularisation de Tikhonov pour mieux conditionner le problème.

Approche pondérée de régularisation de Tikhonov

Dans ce travail une nouvelle méthode de calibration basée sur l'amélioration de la méthode de Cordier et al. (2009) est utilisée en introduisant des poids convenables dans la définition de l'erreur dans la fonctionnelle coût, en donnant ainsi une importance aux modes qui le sont. Deux voies pour définir les poids sont proposées:

1. *Dans , nous considérons que le plus intéressant est dans la modélisation de l'effet des structures énergétiques et ainsi les spectres propres servent comme une mesure de l'importance des modes. C'est le choix le plus naturel pour la définition des poids dans l'erreur.*

2. *Dans , l'erreur est basée sur une sensibilité globale de la foncionnelle coût.*

Les deux matrices poids comme représentées sur la figure 4.10 sont similaires, étant donné que les poids sont basés sur l'utilisation d'un critère énergétique.

Application aux écoulements de cavité

La méthode de régularisation pondérée basée sur la sensibilité globale a été appliquée au cas de lécoulement de cavité. La méthode reproduit les dynamiques temporelles de la POD comme on peut le voir sur les figures 4.11 et 4.12. La méthode a été comparée avec d'autres techniques de calibration comme on peut le constater dans 4.4 et sur la figure 4.13. La régularisation pondérée de Tikhonov surpasse les autres techniques de calibration en termes d'erreurs normalisées et d'erreurs modales. La principale force de cette régularisation réside dans le fait que les paramétres de régularisation sont déterminés sans aucune intervention de l'utilisateur. Finalement nous vérifions l'adéquation du modèle de calibration pour de longues périodes d'intgration temporelle comme on peut le voir sur la figure 4.14. Ainsi le modèle prédit les dynamiques pour à peu près 4 *périodes d'oscillation de l'écoulement, mais diverge rapidement quand on intègre au-delà. Ceci est dû au fait que les modes négligés (tronqués) ne sont pas pris en compte et le problème de fermeture reste ouvert, même en déterminant correctement les coefficients. Nous devons donc calibrer sur plus de périodes si nous souhaitons utiliser le modèle pour des études de contrôle.*

4.1 Introduction

As demonstrated in the previous chapter it is often diff cult to represent with suff cient accuracy even the short time dynamics of the original system which bars the utility of the Reduced Order Model for applications in sensitivity studies, optimisation and optimal control. Methods in the literature that pertain to improving the accuracy of the Reduced Order Model is termed as calibration The main idea of calibration is to identify the coeff cients of the POD Galerkin model so as to match the temporal dynamics of the POD which are known in advance. This strategy is usually called as a system identif cation or black-box model in control literature when the dynamical system is determined with respect to an identif able dynamics of the process. The reasons for the inaccurate behaviour of the ROM can be attributed to the truncation of the POD bases. An analogous problem occurs in the Large Eddy Simulation (LES) of f ows where there is lack of dissipation, due to truncation of the smaller scales. Even including all the modes in Galerkin projection may still lead to the wrong attractor due to structural instability as has been demonstrated in Rempfer (2000),Noack *et al.* (2003) . Other problems may arise due to the contribution of pressure at the boundaries of the domain, which is usually neglected Noack *et al.* (2005). The stability properties of the compressible POD-Galerkin approximation has been studied by Iollo *et al.* (2000) and shows that just the stability of the numerical scheme is not suff cient for the stability of the ROM and a suitable numerical stabilisation is required. Consecutively a Sobolev inner product has been def ned for the norm to improve the accuracy of the ROM. The calibration techniques can be broadly classif ed into two categories,

1. To treat the problem of calibration similar to the closure problem of turbulence

2. As a process of system identif cation for the coeff cients, leading to an optimisation problem.

Regarding the calibration techniques for the ROM, based on treating them as a closure problem, the earliest attempt is due to Aubry *et al.* (1988). In this work inter-modal transfer of energy between the truncated POD modes and the resolved POD modes by means of an artif cial viscosity are modeled. Podvin (2001) proposes a connection between the closure problems encountered in the large eddy simulation of turbulence and the truncation terms of the ROM where one has to model the missing terms. An approach to model the inter-modal transfers by means of artif cial viscosity assuming the conservation of the average kinetic energy in the ROM can be found in Cazemier *et al.* (1998). A spectral vanishing viscosity method has been proposed by Karamanos & Karniadakis (2000), which was initially developed for LES to improve the long term integration of the ROM. The time dependent modal eddy viscosity can be found as a solution of an optimisation as given in Bergmann & Cordier (2005), for the stabilisation of ROM for wake f ows.

Regarding the problem of calibration, based on an optimisation procedure, most of the calibration techniques tries to identify the system coeff cients, so as to minimise the error between the POD temporal dynamics and that predicted by the ROM. The methods mainly relay on the def nition of the error leading to an optimisation problem, which can be solved iteratively as found in Galetti *et al.* (2004). Couplet *et al.* (2005) gives a general frame work of the various error which arises in the ROM and proposes a calibration technique based on minimising a linear functional of error. Stabilisation of the ROM by means of a polynomial identif cation of the ROM independent of the physical system can

be found in Perret *et al.* (2006). A method called as "Intrinsic stabilisation" has been proposed by Kalb & Deanne (2007) which takes into account the instantaneous error with respect to the reference dynamics, and is obtained by replacing the original ROM, with another ROM with the polynomial coeff cients obtained from the temporal POD dynamics. Recently an improvement of the above ideas of Couplet *et al.* (2005) has been presented in Cordier *et al.* (2009).

In this work we evaluate different methods of calibration based on the solution of the optimisation problem. We begin by introducing various def nitions of errors, between the calibrated dynamics and the original temporal dynamics. The optimisation problem of minimising the error leads to a solution of a linear system, in case the errors are aff ne functions of the predicted dynamics. The linear system is ill conditioned and needs to be regularised. Cordier *et al.* (2009) have used the method of Tikhonov regularization to solve the ill-conditioned problem. We present a further improvement of this technique by introducing the various type of weight matrix used in the def nition of error. The f rst method is by performing a sensitivity analysis of the ROM with respect to a given cost functional, to determine the weights of the relevant dynamics of calibration. The second method is by using the energy content of the representation in forming the weight matrix to be used in calibration.

4.2 Definition of errors

4.2.1 State calibration method with nonlinear constraints

We start with the polynomial form of the ROM explained in the previous chapter, which we restate as

$$\dot{\mathbf{a}}^R = \mathbf{f}(\mathbf{y}, \mathbf{a}^R) + \mathbf{g}(\mathbf{z}, \mathbf{a}^R, \gamma) \tag{4.1}$$

As previously shown, the temporal dynamics obtained by adding the actuation mode, determined by an L_2 optimisation procedure is mainly restricted to the un-actuated space, it is suff cient to present the main ideas for the case of $\mathbf{g} = 0$. The objective of the POD based model (4.1) is to accurately represent the dynamics of the POD temporal modes $\mathbf{a}^P$, and the problem of calibration is to identify the coeff cients $\mathbf{y}$ such that this representation is possible. One then naturally seeks to minimise the error

$$\mathbf{e}^1(\mathbf{y}, t) = \mathbf{a}^P(t) - \mathbf{a}^R(t) \tag{4.2}$$

with the constraints

$$\mathcal{P}_\mathcal{C} \begin{cases} \dot{\mathbf{a}}^R(t) = f(\mathbf{y}, \mathbf{a}^R(t)) \\ \mathbf{a}^R(0) = \mathbf{a}^P(0) \end{cases}$$

$\mathbf{e}^1 \in \mathbb{R}^N$ is time dependent and we seek to minimise

$$\mathcal{I}^1(\mathbf{y}) = \left\langle \|\mathbf{e}^1(\mathbf{y}, t)\|^2_\Lambda \right\rangle_{T_0} \tag{4.3}$$

where $\langle . \rangle_{T_0}$ is a time averaging operator over $[0, T_0]$, for N_t equally spaced elements on $[0, T_0]$ we have

$$\langle f(t) \rangle_{T_0} = \frac{1}{N_t} \sum_{i=1}^{N_t} f(t_i) \quad \text{with} \quad t_i = (i-1)\Delta t \quad \text{and} \quad \Delta t = \frac{T_0}{N_t - 1}$$

$\|.\|_\Lambda$ is a norm on $\mathbb{R}^N$. For any positive def nite matrix $\Lambda \in \mathbb{R}^{N\times N}$ the norm of any vector $\mathbf{e} \in \mathbb{R}^N$ is given by

$$\|\mathbf{e}\|_\Lambda^2 = \mathbf{e}^T \Lambda \mathbf{e}$$

The matrix Λ acts as a weight function giving importance to the specif c POD modes, when $\Lambda = I_N$ it means that all the POD modes have the same importance in terms of the error. Later in this chapter we shall describe a method to utilise this weight matrix to def ne the relative importance of the error with respect to the POD mode. Minimisation of $\mathcal{I}^1$ under the constraints $\mathcal{P}_\mathcal{C}$ leads to a non-linear constrained optimisation problem of minimising

$$\mathcal{I}^1(\mathbf{y}) = \frac{1}{N_t}\sum_{k=1}^{N_t}\sum_{i=1}^{N}(a_i^P(t_k) - a_i^R(t_k))^2$$

The optimisation problem can be solved iteratively as in Bergmann & Cordier (2005) to f nd the optimal eddy viscosity or using a single shot constrained optimisation problem with a pseudo-spectral discretisation of the variables as found in Galetti *et al.* (2004)

4.2.2 State calibration method

Couplet *et al.* (2005) have argued that the method based on the $\mathcal{I}^1$ formulation does not have a unique solution and also there are problems of convergence when the well known gradient methods are used to f nd the minimum. As a result the nonlinear constraint is suppressed in the def nition of $\mathbf{e}^1$. By integrating the POD ROM the error $\mathbf{e}^1$ can be written as

$$\mathbf{e}^1(\mathbf{y},t) = \mathbf{a}^P(t) - \mathbf{a}^P(0) - \int_0^t \mathbf{f}(\mathbf{y},\mathbf{a}^R(\tau))d\tau$$

The nonlinear constraint is suppressed by replacing $\mathbf{a}^R$ with $\mathbf{a}^P$. We have a new def nition of the error $\mathbf{e}^2$ def ned as

$$\mathbf{e}^2(\mathbf{y},t) = \mathbf{a}^P(t) - \mathbf{a}^P(0) - \int_0^t \mathbf{f}(\mathbf{y},\mathbf{a}^P(\tau))d\tau \tag{4.4}$$

Minimisation of the error def ned by $\mathcal{I}^2(\mathbf{y}) = \langle\|\mathbf{e}^2(\mathbf{y},t)\|_\Lambda^2\rangle_{T_0}$ has been used more recently by Bourget *et al.* (2007) to determine the constant and linear coeff cients, for the study of transonic f ows around airfoils. All the modes have equivalent weights leading to the minimisation of the error def ned by

$$\mathcal{I}^2(\mathbf{y}) = \frac{1}{N_t}\sum_{k=1}^{N_t}\sum_{i=1}^{N}\left(a_i^P(t_k) - a_i^P(0) - \int_0^t f_i(\mathbf{y},\mathbf{a}^P(\tau))d\tau\right)^2 \tag{4.5}$$

4.2.3 Flow calibration method

A third criterion of error is obtained by taking the temporal derivative of the $\mathbf{e}^1$ criterion.

$$\frac{d}{dt}\mathbf{e}^1(\mathbf{y},t) = \dot{\mathbf{a}}^P(t) - \mathbf{f}(\mathbf{y},\mathbf{a}^R(t))$$

the error is given by replacing $\mathbf{a}^R(t)$ with $\mathbf{a}^P(t)$ in order to suppress the nonlinear constraint, to obtain the def nition of error given by

$$\mathbf{e}^3(\mathbf{y},t) = \dot{\mathbf{a}}^P(t) - \mathbf{f}(\mathbf{y},\mathbf{a}^P(t)) \tag{4.6}$$

The corresponding minimisation can be def ned for the error def ned by $\mathcal{I}^3(\mathbf{y}) = \langle \|\mathbf{e}^3(\mathbf{y},t)\|^2_\Lambda \rangle_{T_0}$. In this method we impose that the temporal POD eigen functions are the solutions of the f ow, given by $\mathbf{f}$. This method as described in Couplet *et al.* (2005) has been applied to experimental data obtained from PIV measurements by Perret *et al.* (2006). If we assume an identity matrix for Λ giving equal weights to all the modes. We have the minimisation problem for the functional def ned by

$$\mathcal{I}^3(\mathbf{y}) = \frac{1}{N_t}\sum_{k=1}^{N_t}\sum_{i=1}^{N}\left(\dot{a}_i^P(t_k) - f_i(\mathbf{y},\mathbf{a}^P(\tau))d\tau\right)^2 \tag{4.7}$$

4.2.4 Affine function of error

For $i = 2$ and 3, we have $\mathbf{e}^i$ an aff ne function with respect to $\mathbf{y} \in \mathbb{R}^{N_y}$, *i.e.* we def ne

$$\begin{array}{rcl} \mathbf{e}^i(.,t) & : & \mathbb{R}^{N_y} \longrightarrow \mathbb{R}^N \\ & & \mathbf{y} \longrightarrow E^i(t)\mathbf{y} + \mathbf{e}^i(0,t) \quad \text{with} \quad E^i(t) \in \mathbb{R}^{N\times N_y} \end{array}$$

where for $i = 2$

$$E^2(t)\mathbf{y} = -\int_0^t f(\mathbf{y},\mathbf{a}^P(\tau))d\tau \quad \text{and} \quad \mathbf{e}^2(0,t) = \mathbf{a}^P(t) - \mathbf{a}^P(0)$$

and for $i = 3$

$$E^3(t)\mathbf{y} = -\mathbf{f}(\mathbf{y},\mathbf{a}^P(t)) \quad \text{and} \quad \mathbf{e}^3(0,t) = \dot{\mathbf{a}}^P(t)$$

Assuming a symmetric Λ, we have for $i = 2, 3$

$$\begin{array}{rcl} \mathcal{I}^{(i)}(\mathbf{y}) = \left\langle \|\mathbf{e}^i(\mathbf{y},t)\|^2_\Lambda \right\rangle_{T_0} & = & \mathbf{y}^T\langle E^{(i)}(t)^T\Lambda E^{(i)}(t)\rangle_{T_0}\mathbf{y} + 2\langle \mathbf{e}^{(i)}(0,t)^T\Lambda E^{(i)}(t)\rangle_{T_0}\mathbf{y} \\ & + & \langle \mathbf{e}^{(i)}(0,t)^T\Lambda \mathbf{e}^{(i)}(0,t)\rangle_{T_0} \\ & = & \mathbf{y}^T A^{(i)}\mathbf{y} - 2{b^{(i)}}^T\mathbf{y} + c^{(i)} \end{array}$$

where

$$\begin{array}{rcl} A^{(i)} & = & \langle E^{(i)}(t)^T\Lambda E^{(i)}(t)\rangle_{T_0} \in \mathbb{R}^{N_y\times N_y} \\ b^{(i)} & = & -\langle E^{(i)}(t)^T\Lambda \mathbf{e}^{(i)}(0,t)\rangle_{T_0} \in \mathbb{R}^{N_y} \\ c^{(i)} & = & \langle \mathbf{e}^{(i)}(0,t)^T\Lambda \mathbf{e}^{(i)}(0,t)\rangle_{T_0} \in \mathbb{R} \end{array}$$

If Λ is symmetric then so is $A^{(i)}$ by def nition and minimising the quadratic function $\mathcal{I}^{(i)}$ reduces to solving the linear system:

$$A^{(i)}\mathbf{y} = b^{(i)}$$

4.3 Calibration method of Couplet

As mentioned in Couplet *et al.* (2005), the general idea is to determine the coeff cients $\mathbf{y}_\alpha^{(\mathbf{i})}$, as a solution to an optimisation problem which minimises the cost functional given by

$$\mathcal{J}_\alpha^{(i)}(\mathbf{y}) = (1-\alpha)\varepsilon^{(i)}(\mathbf{y}) + \alpha\mathcal{D}(\mathbf{y}) \quad \text{for} \quad i = 2,3 \tag{4.8}$$

$\alpha \in [0,1]$ is a regularising parameter. $\varepsilon^{(i)}(\mathbf{y})$ measures the normalised error between the actual temporal data $\mathbf{a}^P(t)$ and that predicted by the model $\mathbf{a}^R(t)$. $\mathcal{D}$ is a measure of the difference between the coeff cients of the model $\mathbf{y}$ and coeff cients obtained from the Galerkin projection $\mathbf{y}^{GP}$. $\varepsilon^{(i)}$ and $\mathcal{D}$ are def ned as

$$\varepsilon^{(i)}(\mathbf{y}) = \frac{\langle \|\mathbf{e}^{(i)}(\mathbf{y},t)\|_\Lambda^2 \rangle_{T_0}}{\langle \|\mathbf{e}^{(i)}(\mathbf{y}^{GP},t)\|_\Lambda^2 \rangle_{T_0}} = \frac{\mathcal{I}^{(i)}(\mathbf{y})}{\mathcal{I}^{(i)}(\mathbf{y}^{GP})} \tag{4.9}$$

and

$$\mathcal{D}(\mathbf{y}) = \frac{\|\mathbf{y}-\mathbf{y}^{GP}\|_\Pi^2}{\|\mathbf{y}^{GP}\|_\Pi^2} \tag{4.10}$$

where $\|.\|_\Pi$ is a semi-norm on the polynomial vector space and for any $\mathbf{y} \in \mathbb{R}^{N_y}$ is def ned as

$$\|\mathbf{y}\|_\Pi^2 = \mathbf{y}^T\Pi\mathbf{y} \tag{4.11}$$

where $\Pi \in \mathbb{R}^{N_y \times N_y}$ is a non-negative symmetric matrix. For $\Pi = I_{N_y}$ it means that all the coeff cients are given equal importance in the calibration. A partial calibration for different values of I_{N_y} is possible as reported by Couplet *et al.* (2005). The functional in (4.8) can be written as

$$\mathcal{J}_\alpha^i(\mathbf{y}) = \chi_A^\alpha \underbrace{\mathcal{I}^{(i)}(\mathbf{y})}_{f_1(\mathbf{y})} + \chi_\Pi^\alpha \underbrace{\|\mathbf{y}-\mathbf{y}^{GP}\|_\Pi^2}_{f_2(\mathbf{y})} \tag{4.12}$$

where

$$\chi_A^\alpha = \frac{1-\alpha}{\mathcal{I}^{(i)}(\mathbf{y}^{GP})} \quad \text{and} \quad \chi_\Pi^\alpha = \frac{\alpha}{\|\mathbf{y}^{GP}\|_\Pi^2}$$

As demonstrated in section §4.2.4 when Λ is symmetric we have $f_1(\mathbf{y}) = \mathbf{y}^T A^{(i)}\mathbf{y} - 2b^{(i)^T}\mathbf{y} + c^{(i)}$. Similarly for a symmetric Π it can be shown that $f_2(\mathbf{y}) = \mathbf{y}^T\Pi\mathbf{y} - 2\mathbf{y}^{GP^T}\Pi\mathbf{y} + \mathbf{y}^{GP^T}\Pi\mathbf{y}^{GP}$. For the quadratic functions, f_1 and f_2 one obtains the gradient as

$$\nabla f_1(\mathbf{y}) = 2\left(A^{(i)}\mathbf{y} - b^{(i)}\right) \quad \text{and} \quad \nabla f_2(\mathbf{y}) = 2\Pi\left(\mathbf{y}-\mathbf{y}^{GP}\right) \tag{4.13}$$

Minimisation of the functional $\mathcal{J}_\alpha^{(i)}$ is obtained at $\mathbf{y}_\alpha^{(i)}$ where $\nabla\mathcal{J}_\alpha^{(i)}(\mathbf{y}_\alpha^{(i)}) = 0$ and is equivalent to solving the system of linear equations for $\mathbf{y}_\alpha^{(i)}$ given by

$$A_\alpha^{(i)}\mathbf{y}_\alpha^{(i)} = b_\alpha^{(i)} \tag{4.14}$$

with

$$\begin{aligned} A_\alpha^{(i)} &= \chi_A^\alpha A_\alpha^{(i)} + \chi_\Pi^\alpha \Pi \\ b_\alpha^{(i)} &= \chi_A^\alpha b^{(i)} + \chi_\Pi^\alpha \Pi \mathbf{y}^{GP} \end{aligned}$$

The parameter α is user dependent and needs to be f xed. The question on its optimality remains open.

4.4 Application to cavity flow

4.4.1 Introduction

The method described in the preceding section has been applied to the cavity f ow. The normalised errors $\varepsilon^{(i)}$ and the cost of calibration is reported in table 4.1. The constrained optimisation problem is solved for the minimisation of the error $\mathcal{I}^{(1)}$. For the case of minimisation of $\mathcal{I}^{(3)}$ different parameters are experimented for the determination of the linear, constant and eddy viscosity term. Also the results are compared with the intrinsic calibration method. The most effective method of calibration is obtained by minimising $\mathcal{I}^{(1)}$ subjected to the constraint $\mathcal{P}_C$, for any criterion $\varepsilon^{(i)}$. The normalised error decreases as the number of terms in the calibration increases as seen from the minimisation of $\mathcal{I}^3$. There is a similar trend when one notices that the criterion $\varepsilon^{(2)}$ is more stringent as the corresponding error is greater for most of the cases. For the corresponding costs of calibration represented by $\sqrt{\mathcal{D}(\mathbf{y})}$, it is found that minimising $\mathcal{I}^{(1)}$ under the constraint $\mathcal{P}_C$, the cost is around 27% as compared to 22% of minimising $\mathcal{I}^{(3)}$ for both the constant and the linear terms. The cost of the calibration evaluated only based on the values of $\mathcal{D}(\mathbf{y})$ is not a real measure of the cost as there are many criteria for the utility of the POD ROM. The cost of the calibration can be treated as twofold namely:

1. CPU time and memory cost

2. Numerical implementation of the method

Couplet *et al.* (2005) argues out that for methods based on the identif cation of parameters, the cost corresponds to the numerical implementation of the calibration and not to the variation of parameters. As argued out in Cordier *et al.* (2009) the benef t of an accurate model out-weighs the cost, especially when used to perform control studies, as one always prefers a correct prediction for the variation of the controlled dynamics.

The intrinsic stabilisation method as demonstrated in Table 4.1 is less accurate in terms of the normalised errors. Since the constrained optimisation problem $\mathcal{I}^{(1)}$ and the minimisation of $\mathcal{I}^{(3)}$ compares well in terms of the error, we have tried to determine all the coeff cients of $\mathcal{I}^{(3)}$ and as seen in the f gure 4.1, the POD ROM diverges even for a very short period of numerical integration. This is due to the ill-conditioning of the corresponding matrix $A_0^{(3)}$ as will explained in the next section.

Method	Control terms	$\sqrt{\mathcal{E}^{(1)}(\mathbf{y})}$	$\sqrt{\mathcal{E}^{(2)}(\mathbf{y})}$	$\sqrt{\mathcal{E}^{(3)}(\mathbf{y})}$	$\sqrt{\mathcal{D}(\mathbf{y})}$
Minimisation of $\mathcal{I}^{(3)}$	L	$2.87 \cdot 10^{-2}$	$3.33 \cdot 10^{-1}$	$7.9 \cdot 10^{-2}$	$3.15 \cdot 10^{-1}$
Minimisation of $\mathcal{I}^{(3)}$	L and C	$3.61 \cdot 10^{-3}$	$3.35 \cdot 10^{-1}$	$2.4 \cdot 10^{-2}$	$2.24 \cdot 10^{-1}$
Minimisation of $\mathcal{I}^{(3)}$	V	$8.3 \cdot 10^{-1}$	$8.22 \cdot 10^{-1}$	$9.3 \cdot 10^{-1}$	$1.00 \cdot 10^{-1}$
Minimisation of $\mathcal{I}^{(1)}$ under constraint $\mathcal{P}_C$	C and L	$1.62 \cdot 10^{-2}$	$3.5 \cdot 10^{-1}$	$1.86 \cdot 10^{-1}$	$2.68 \cdot 10^{-1}$
Intrinsic Stabilisation	C and L	$7.91 \cdot 10^{-2}$	$1.67 \cdot 10^{-1}$	$2.2 \cdot 10^{-1}$	$2.6 \cdot 10^{-1}$

Table 4.1 - *Normalised error $\varepsilon^{(i)}$ and cost of calibration $\mathcal{D}$. 1. Comparison between the results by minimising $\mathcal{I}^{(3)}$ with identifying the Linear term (L), Constant and Linear term (L and C), Eddy viscosity terms (V). 2. Minimising $\mathcal{I}^{(1)}$ with constraint $\mathcal{P}_C$. 3. Intrinsic Stabilisation.*

4.4.2 Minimisation of $\mathcal{J}_\alpha^{(2)}$ and $\mathcal{J}_\alpha^{(3)}$

The calibration by minimisation of $\mathcal{J}_\alpha^{(2)}$ and $\mathcal{J}_\alpha^{(3)}$ as described in §4.3 is performed. The difficulty of the method is the choice of the regularising parameter α. Figure 4.2 represents the evolutions of the normalised error and the calibration for the two functionals $\mathcal{J}_\alpha^{(i)}$ as the parameter α is varied ($\alpha \in \{0.05, 0.1, \cdots, 1\}$). From figure 4.2 we observe that the errors vary rapidly as the parameter $\alpha \to 1$. To observe the behaviour of the error close to 1, Couplet *et al.* (2005) introduces a new scaling by a parameter δ which is in a monotonic bijection with α on $[0, 1]$, and defined by

$$\alpha = \frac{\delta}{\zeta^{(i)}(1-\delta)+\delta} \quad \text{with} \quad \zeta^{(i)} = \frac{\mathcal{I}^{(i)}(\mathbf{y}^{GP})}{\mathcal{I}^{(i)}(0)}$$

The variation of the new parameter δ with respect to α is shown in figure 4.3. The cost functional (4.8) with respect to the parameter δ becomes

$$\tilde{\mathcal{J}}_\delta^{(i)}(\mathbf{y}) = [\zeta(1-\delta)+\delta]\mathcal{J}_\alpha^{(i)}(\mathbf{y}) \tag{4.15}$$

We can see in figure 4.2 that only $\varepsilon^{(2)}(\mathbf{y}_\alpha^{(2)})$, $\varepsilon^{(3)}(\mathbf{y}_\alpha^{(3)})$, $\mathcal{D}(\mathbf{y}_\alpha^{(2)})$, $\mathcal{D}(\mathbf{y}_\alpha^{(3)})$ are monotone functions of α. This has a significance when we consider that the optimal solution $\mathbf{y}_\alpha$ of (4.8) satisfies a sub-optimality criteria given by:

$$(1-\alpha)\varepsilon^{(i)}(\mathbf{y}_\alpha) + \alpha\mathcal{D}(\mathbf{y}_\alpha) \leq (1-\alpha)\varepsilon^{(i)}(\mathbf{y}) + \alpha\mathcal{D}(\mathbf{y})$$

For any given polynomial $\mathbf{y}$, we expect a monotone behaviour of the error with respect to the optimal solution satisfying the above condition. Numerically as $\alpha \to 0$, the trend is to decrease the normalised error (also interpreted as an increase in the cost of the calibration) and hence the result is a better calibrated model. However it is difficult in practice to utilise the results of the curve 4.2 to determine the value of α so as to have a balance between the reduction of the normalised error and the cost of calibration. As already mentioned the cost of calibration is not very relevant when seeking an accurate model. One may then be tempted to minimise the normalised error by setting $\alpha = 0$. This results in an ill-conditioning of the matrix $A_\alpha^{(2)}$ and $A_\alpha^{(3)}$ as $\alpha \to 0$ as demonstrated in 4.4. This leaves us

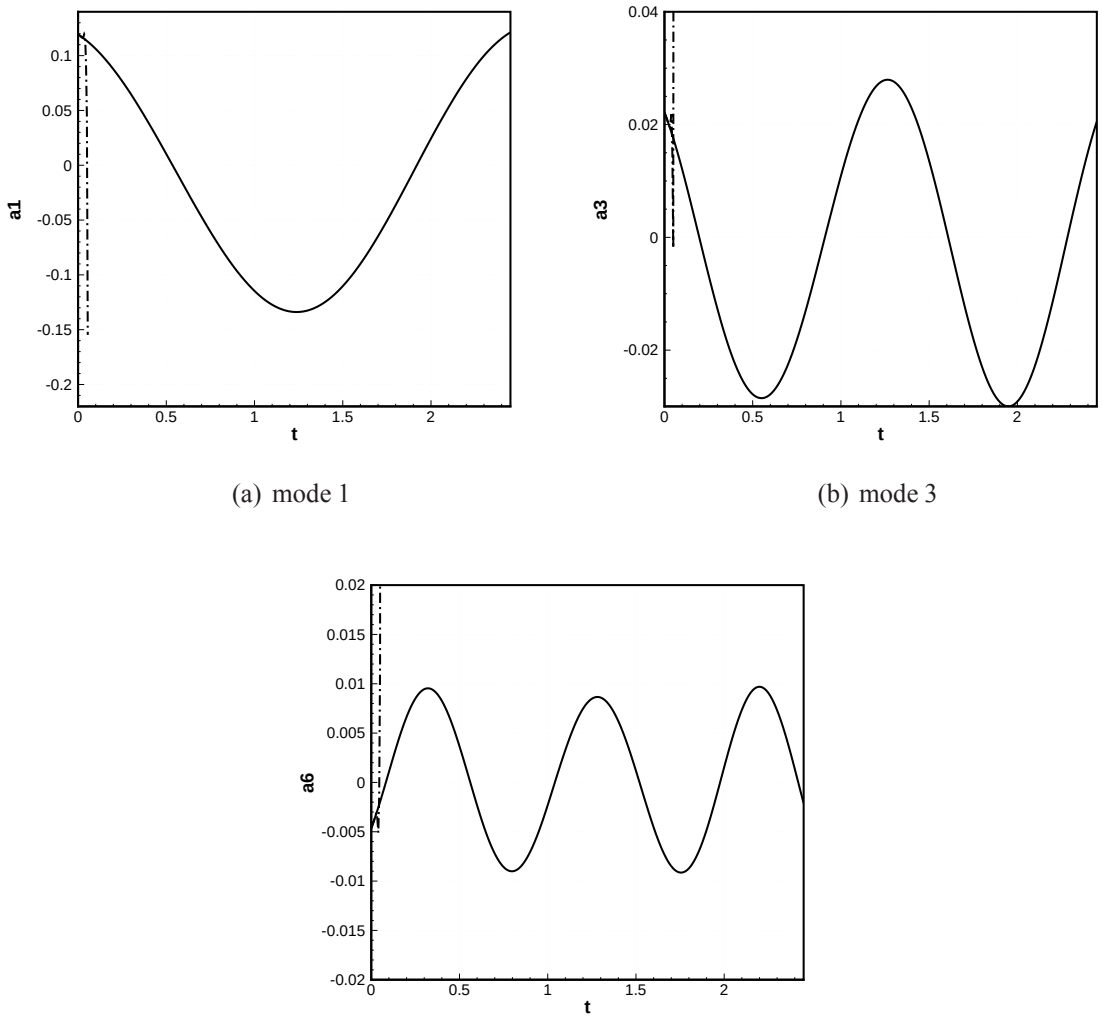

(a) mode 1

(b) mode 3

(c) mode 6

Figure 4.1 - *Comparison between the temporal evolutions of the projected (black line) POD and the POD ROM (dashed line).The POD ROM is calibrated using the $\mathcal{I}^{(3)}$ minimisation for all coefficients. The linear system is not regularised* i.e. *the value of $\alpha = 0$.*

with no choice other than to regularise the cost functional, but then the choice of the parameter is arbitrary. We therefore propose in the next section a method to solve the ill-conditioned system (4.14) corresponding to $\alpha = 0$ by another method of regularization, due to Tikhonov, Hansen (1994), which corresponds directly to the minimisation of $\mathcal{I}^{(3)}$.

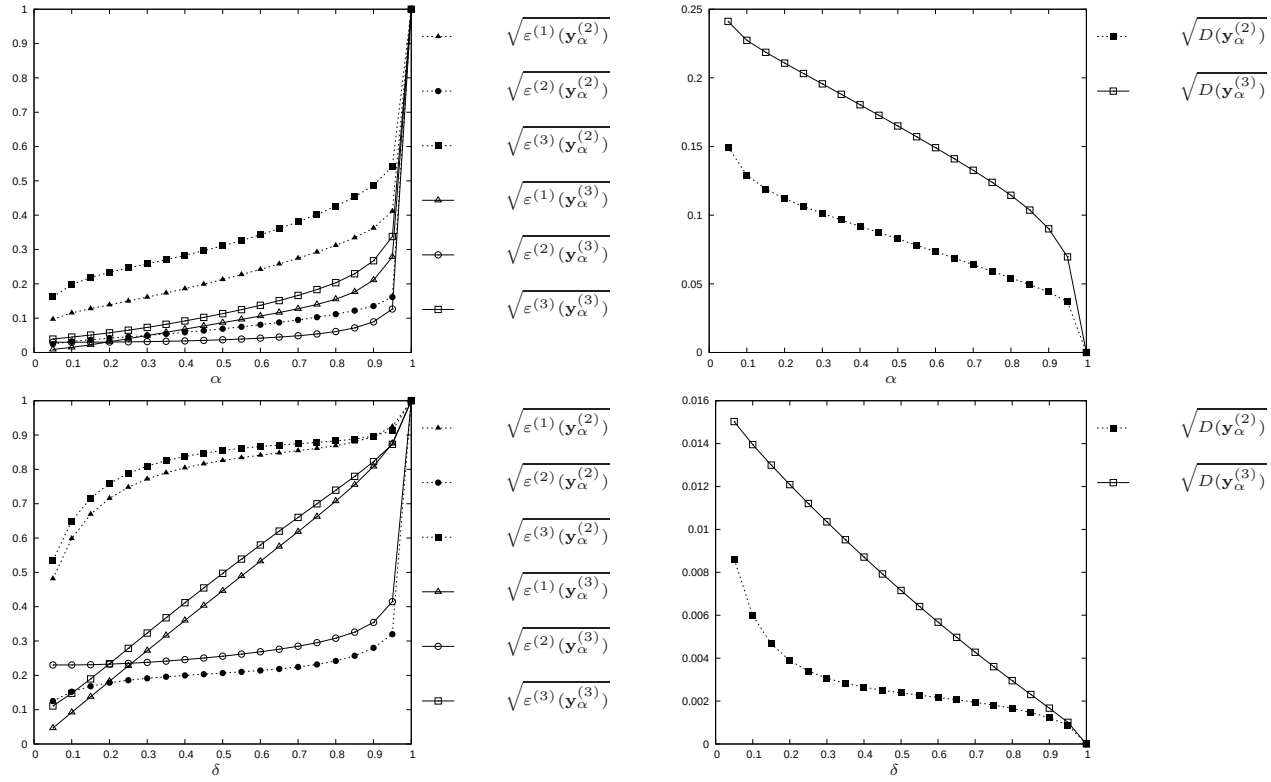

Figure 4.2 - *Normalised errors $\varepsilon^{(i)}$ and costs of calibration $\mathcal{D}$ from the minimisation of $\mathcal{J}_\alpha^{(2)}$ and $\mathcal{J}_\alpha^{(3)}$, for α varying in $[0.05, 0.1, \cdots, 1]$ (top) and δ varying in $[0.05, 0.1, \cdots, 1]$ (bottom) .*

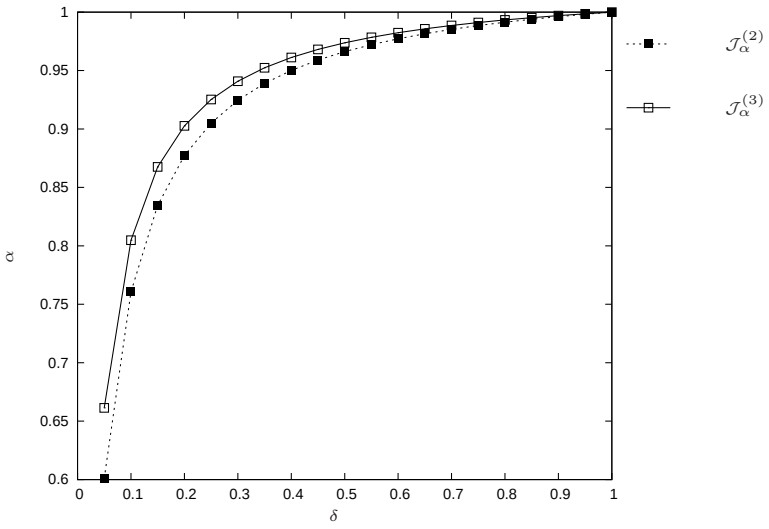

Figure 4.3 - *Evolution of α with respect to δ*

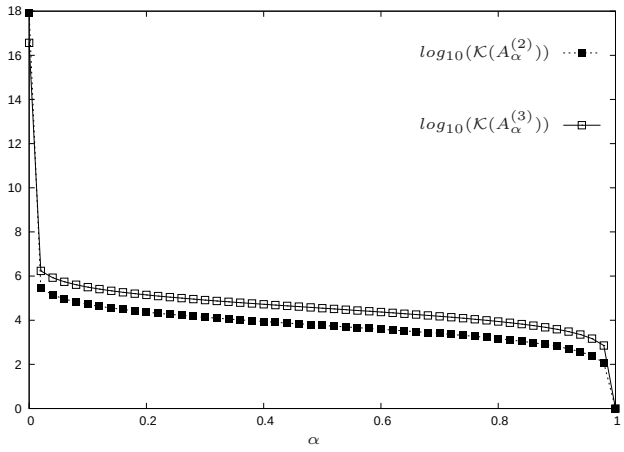

(a)

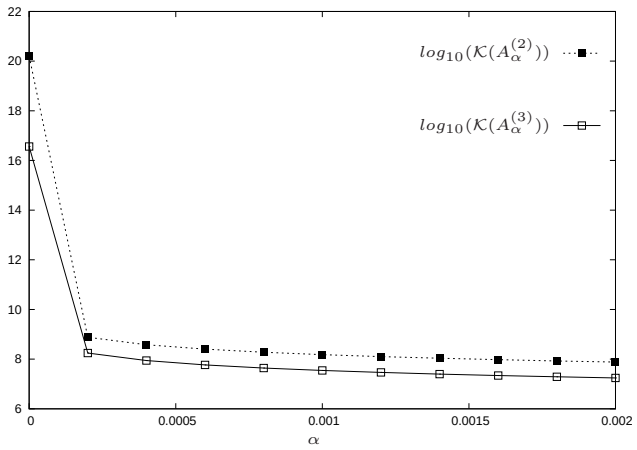

(b)

Figure 4.4 - *Condition numbers* $\mathcal{K}(A_\alpha^{(i)})(i = 2, 3)$ *obtained during the minimisations of* $\mathcal{J}_\alpha^{(2)}$ *and* $\mathcal{J}_\alpha^{(3)}$ *with* α *varying in (a)* $[0.05, 0.1, \cdots, 1]$*, (b)* $[0.0, 0.0005, \cdots, 0.002]$

4.5 Calibration by the method of Tikhonov regularization

4.5.1 Filter factors and Picard's criteria

The minimisation of the functional $\mathcal{I}^{(3)}$ amounts to solving the linear system $A^{(3)}\mathbf{y} = b^3$. To explain the ideas we henceforth omit the superscripts and simply write the linear system as $A\mathbf{y} = b$. In practice, the right hand side may be contaminated by approximation errors related to the evaluation of the time derivatives of the POD eigenfunctions (as $\mathbf{e}^{(3)}(0, t) = \dot{\mathbf{a}}^P(t)$). To understand the inf uence of errors on the solution of the linear system we introduce the concept of a f lter factor. To do so we

note that the singular value decomposition of A given by

$$A = U\Sigma V^T = \sum_{j=1}^{N_y} u_j \sigma_j v_j^T$$

where $U = (u_1, \cdots, u_{N_y})$ and $V = (v_1, \cdots, v_{N_y})$ are orthogonal matrices containing the left and right singular vectors, given by u_j and v_j respectively and $\Sigma = \text{diag}(\sigma_1, \cdots, \sigma_{N_y})$ is a diagonal matrix of singular values of σ_j arranged in an increasing order

$$\sigma_1 \geq \cdots \sigma_{N_y}$$

Since U and V are orthonormal matrices ($UU^T = VV^T = I_{N_y}$) the solution of the linear system $\mathbf{y}$ is given as

$$\mathbf{y} = \sum_{j=1}^{N_y} \frac{1}{\sigma_j} u_j^T b v_j = \sum_{j=1}^{N_y} h_j \frac{1}{\sigma_j} u_j^T b v_j \quad \text{with} \quad h_j = 1$$

where h_j are the filter factors. Numerical difficulties arises if the coefficients $|u_j^T b|$, corresponding to the smaller singular values σ_j, do not decrease sufficiently rapidly as compared to the singular values. This behaviour is illustrated by the discrete Picard condition shown as illustrated in figure 4.5. For $j \simeq 20$, the singular value decay faster than the coefficients $|u_j^T b|$. As a result the solution obtained, oscillates around zero, and appears random. Figure 4.6 depicts the solution without any regularization. To fix this, the filter factor h_j is modified so as to behave as a low-pass filter defined as:

$$h_j = \begin{cases} 1 & \text{if} \quad j \geq 20 \\ 0 & \text{if} \quad j > 20 \end{cases} \tag{4.16}$$

For the case of cavity flows the temporal dynamics are simple as can be seen from the abrupt fall of the singular value for $j \simeq 20$. In case of more complex dynamics as encountered in turbulent flows, the singular values increase sufficiently and hence it is necessary to modify the filter factors in a more sophisticated way.

4.5.2 Tikhonov regularization

The method of Tikhonov regularization for solving ill-conditioned system has been well known as in Hansen (1994). The idea is to seek a regularised solution $\mathbf{y}_p$ as the minimiser of the following weighted functional:

$$\phi_\rho(\mathbf{y}) = \|A\mathbf{y} - b\|_2^2 + \rho \|L(\mathbf{y} - \mathbf{y}_0)\|_2^2$$

The first term corresponds to the residual norm, and the second to a side constraint imposed on the solution. ρ is a regularization parameter and L represents the discrete approximation matrix of a differential operator. The matrix is typically the identity matrix of order N_y (derivative of order zero) or a banded matrix dimension $(N_y - d) \times N_y$ of order d. In particular $d = \{0, 1, 2\}$ and the approximation is termed as zeroth, first and second order respectively. Hereafter, these operators will be denoted by $L = I$ $(d = 0)$, $L = \text{FOD}$ $(d = 1)$ and $L = \text{SOD}$ $(d = 2)$. The regularization above can be intuitively thought of as a balance satisfying the criterion:

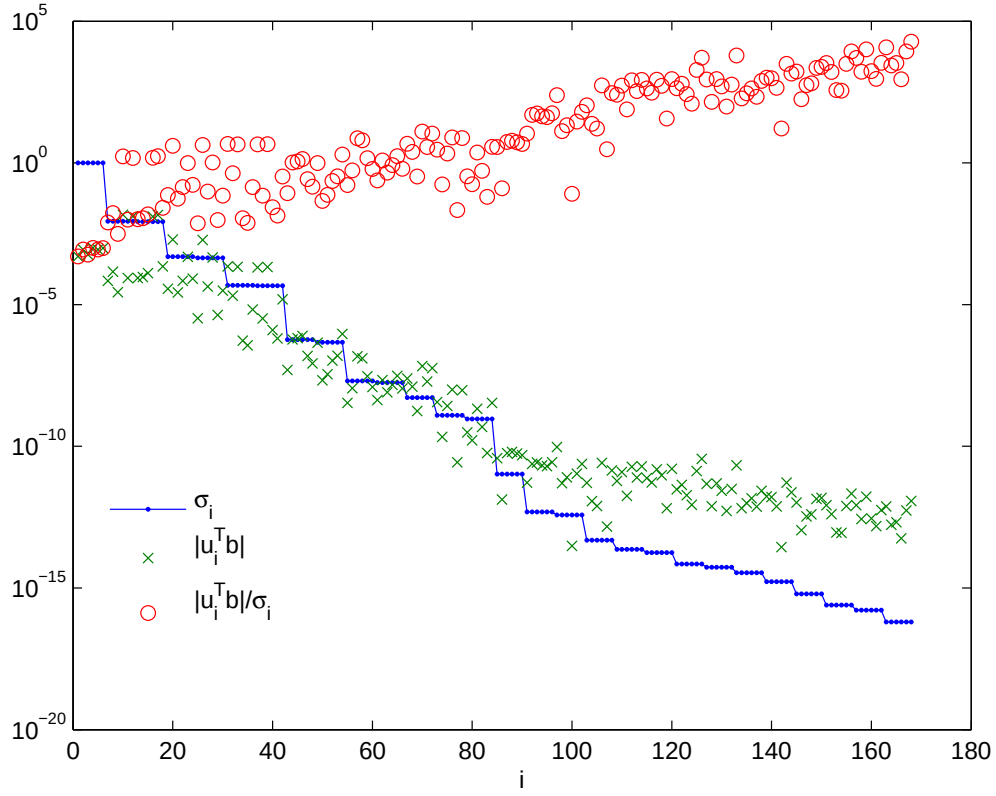

Figure 4.5 - *Discrete Picard visualisation, corresponding to the minimisation of* $\mathcal{I}^{(3)}$ *with determination of all coefficients* i.e. *constant, linear, quadratic, the Tikhonov regularization is applied for* ($L = 0$,$\mathbf{y_0} = 0$).

1. $\mathbf{y}_\rho$ should be determined so as to give a small residue $A\mathbf{y}_\rho - b$.
2. $L(\mathbf{y}_\rho - \mathbf{y}_0)$ should be small with respect to the 2-norm.

The f lter factors h_j introduced in the previous section can be reintroduced here. For the case of $\mathbf{y}_0 = 0$, the regularised solution $\mathbf{y}_\rho$ can be written as follows:

$$\mathbf{y}_\rho = \sum_{j=1}^{N_y} h_j \frac{1}{\sigma_j} u_j^T b v_j \quad \text{with} \quad h_j = \frac{\sigma_j^2}{\sigma_j^2 + \rho} \quad \text{if} \quad L = I_{N_y}$$

and

$$\mathbf{y}_\rho = \sum_{j=1}^{N_y - d} h_j \frac{1}{\sigma_j} u_j^T b x_j + \sum_{j=N_y-d+1}^{N_y} u_j^T b x_j \quad \text{with} \quad h_j = \frac{\gamma_j^2}{\gamma_j^2 + \rho} \quad \text{if} \quad L \neq I_{N_y}$$

$\gamma_j (j = 1, \cdots, N_y - d)$ are the the generalised singular values of (A, L), (see appendix D for details) and x_j the j^{th} column of $X \in \mathbb{R}^{N_y \times N_y}$. The regularization parameter ρ is computed using the L-curve

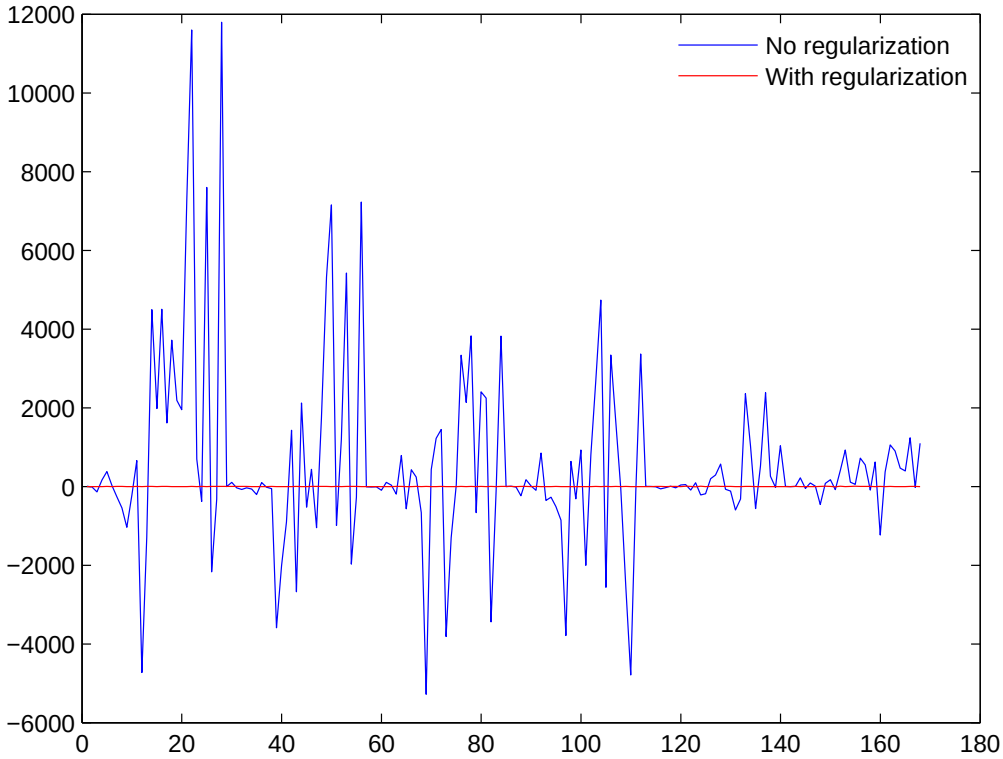

Figure 4.6 - *Comparison between solutions obtained with and without regularization, for the minimisation of* $\mathcal{I}^{(3)}$ *with determination of all coefficients* i.e. *constant, linear, quadratic, the Tikhonov regularization is applied for (*$L = 0$,$\mathbf{y_0} = 0$*).* $N = 6$, $N_y = 168$.

method implemented in the ”regularization tools” package of Hansen (1994). The L-curve method is based on f nding the inf exion point of the curve representing the semi-norm of the regularised solution $L\|\mathbf{y}_\rho\|_2$, versus the corresponding residual norm $\|A^{(3)}\mathbf{y}_\rho - b^{(3)}\|_2$. The inf exion point represents the compromise between the minimisation of the norm of the residual (horizontal axis) and the semi-norm of the solution (vertical axis) and is based on the maximisation of the curvature of the L-curve. The temporal evolution after calibration is shown in f gure 4.8. This brings a immediate consequence in the modal energy distribution associated to the calibrated model. The model energy E_i is def ned as

$$2E_i = \langle a_i, a_i \rangle = \lambda_i \quad \text{for} \quad i = 1 \dots n \tag{4.17}$$

Figure 4.9 shows that the calibrated model is in perfect agreement with the POD energy distribution. As already stated before the temporal dynamics of the cavity is relatively simple, and the decrease of the eigen value is rapid. The calibration proposed may fail in more complicated case (although it has not been tried so far in the literature as far as our knowledge). A recent development of Noack *et al.* (2008), called ”Finite Time Thermodynamics” (FTT), which unif es the weakly non-

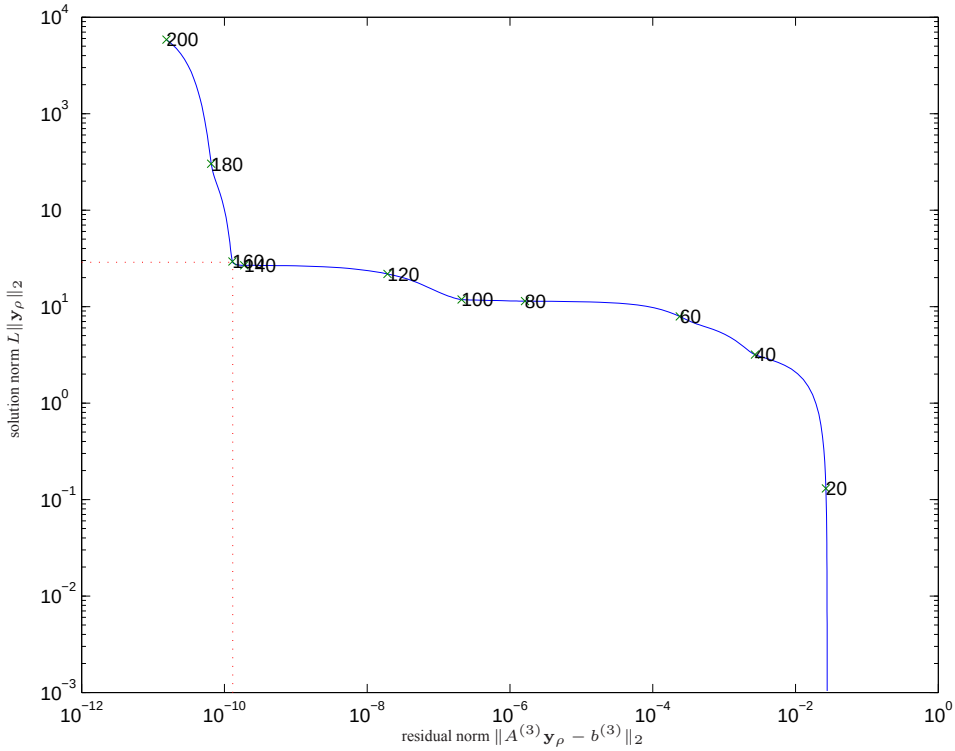

Figure 4.7 - *L curve corresponding to the minimisation of $\mathcal{I}^{(3)}$, with determination of all coefficients* i.e. *constant, linear, quadratic, the Tikhonov regularization is applied for ($L = 0$,$\mathbf{y_0} = 0$). The inflexion of L-curve is at $\rho = 3.88 \cdot 10^{-12}$.*

linear stability theory and the statistical physics limit of turbulence theory, resulting in parameter-free Galerkin model is worth exploring. In the next section an improvement of the method where the f ow sensitivity is used as measure while def ning the corresponding errors is described.

4.5.3 A weighted approach to Tikhonov regularization

We have the error def ned for the minimisation of the functional $\mathcal{I}^{(i)}$ as

$$\mathcal{I}^{(i)}(\mathbf{y}) = \left\langle \|\mathbf{e}^i(\mathbf{y}, t)\|^2_\Lambda \right\rangle_{T_0}$$

The matrix Λ is chosen as Identity, for the cases we have discussed so far, which means that we give equal weights to all the modes in the def nition of calibration. However as already mentioned this matrix can be chosen in suitable way so as to include the effect of mode selection in the def nition. Two ways of def ning the weights can be proposed:

1. We consider that the main interest is in modelling the effect of the energetic structures and hence the eigen spectra themselves serve as a measure of the relative importance of the modes, which is the most natural choice of the weights for the def nition of error.

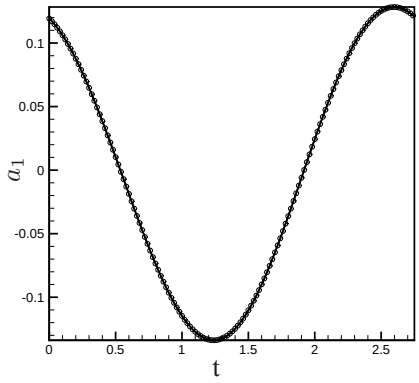

(a) mode 1

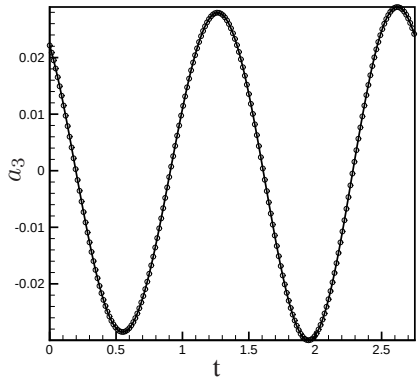

(b) mode 3

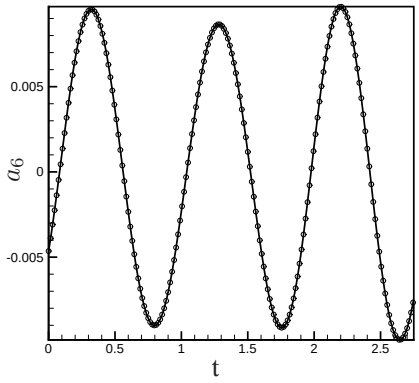

(c) mode 6

Figure 4.8 - *Comparison between the temporal evolutions of the projected □ (POD) and the predicted ■ POD ROM.The POD ROM is calibrated using the $\mathcal{I}^{(3)}$ minimisation for all coefficients. The Tikhonov regularization is applied for ($L = 0$,$\mathbf{y_0} = 0$).*

2. The error can be based on an overall sensitivity of the model with respect to a cost functional.

The weight matrix Λ for the def nition of error for the case (1) can be simply written as a diagonal matrix:

$$\Lambda_{ii} = \frac{\sigma_i}{\max \sigma_i} \quad \text{for} \quad i = \{1, \cdots, N\}$$

For the case (2) we consider the state equations

$$\dot{\mathbf{a}}^R = \mathbf{f}(\mathbf{y}, \mathbf{a}^R) \tag{4.18}$$

Variation of any convex cost functional $\mathcal{J}$ with respect to the state variables $\mathbf{a}^R = \{a_i^R\}_{i=1}^N$ gives the adjoint equation of (4.18) as

$$\dot{\xi}^R = \mathbf{g}(\mathbf{y}, \mathbf{a}^R, \xi^R) \tag{4.19}$$

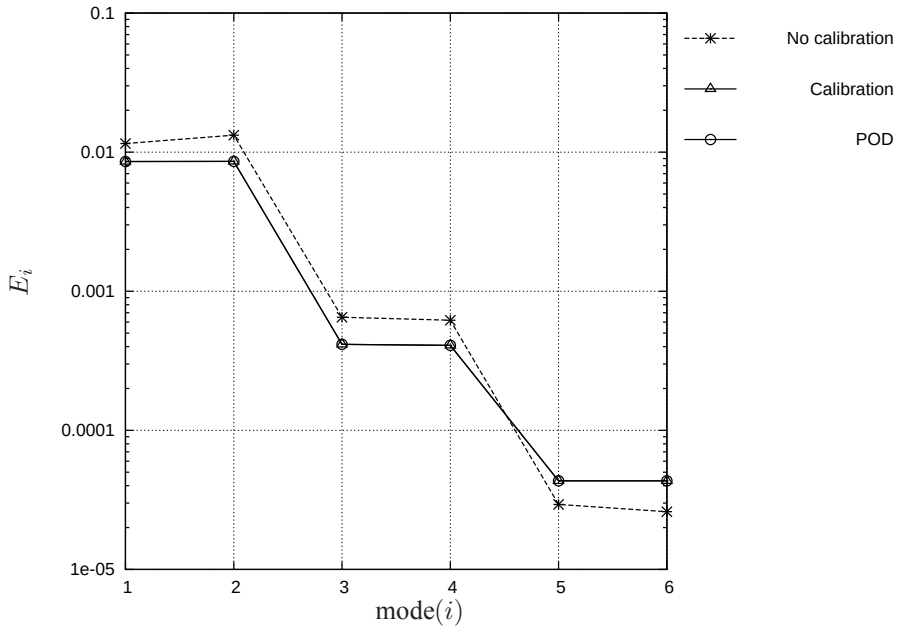

Figure 4.9 - *Comparison between the modal energetic contents obtained before and after calibration. The POD eigenvalues are plotted for reference. The POD ROM is calibrated by minimising* $\mathcal{I}^{(3)}$ *with determination of all coefficients* i.e. *constant, linear, quadratic, the Tikhonov regularization is applied for* $(L = 0, \mathbf{y_0} = 0)$.

Where $\xi^R(t) = \{\xi_i^R\}_{i=1}^N$ is the adjoint variable. The overall sensitivity of the cost functional $\mathcal{J}$ with respect to $\mathbf{a}^R$ is obtained as

$$\mathcal{S}_i = \frac{d\mathcal{J}}{d\, a_i^R} = \langle a_i^R(t) \xi_{\mathbf{i}}{}^R(t) \rangle \tag{4.20}$$

where $\langle . \rangle$ is any time averaging operator. We can then def ne the weight matrix Λ with respect to the sensitivity as

$$\Lambda_{ii} = \frac{\mathcal{S}_i}{\max \mathcal{S}_i} \quad \text{for} \quad i = \{1, \cdots, N\} \tag{4.21}$$

In this study we have taken the cost functional $\mathcal{J}$ based on the energy of the temporal modes as

$$\mathcal{J} = \frac{1}{2} \int_0^T \sum_{i=1}^{N} (a_i^R(t))^2 dt \tag{4.22}$$

where α is a positive constant. The above functional is minimised subject to the constraint (4.18), by the method of Lagrange multipliers. The adjoint state equation (4.19) is given by

$$\dot{\xi}_i = -a_i(t) - \sum_{i=1}^{N} \left(L_{ij} + \sum_{j=1}^{N} \left(Q_{jik} + Q_{jki} \right) a_k(t) \right) \xi_j(t) \tag{4.23}$$

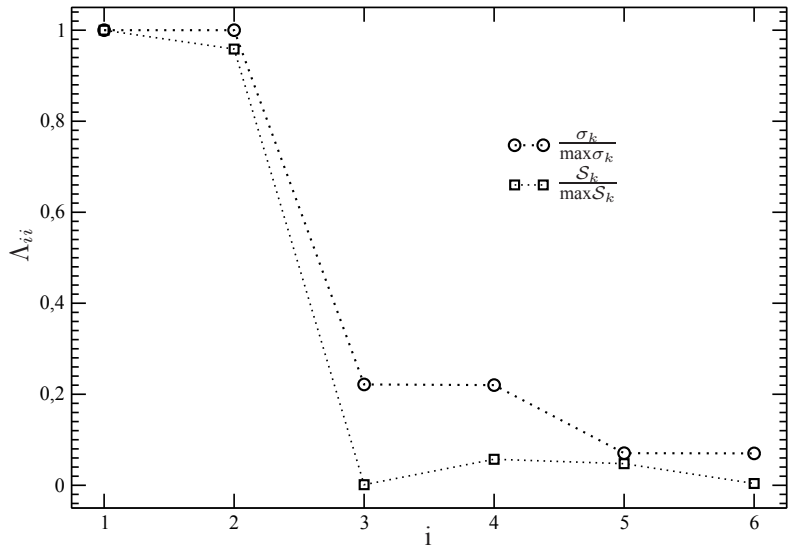

Figure 4.10 - *Comparison of the weight matrices used in definition of errors (a) Weight matrix based on the eigen spectra of the POD* i.e. $\frac{\sigma_k}{max\sigma_k}$ *(b) Weight matrix based on the sensitivity analysis for the cost functional based on energy* i.e. $\frac{\mathcal{S}_k}{max\mathcal{S}_k}$.

In f gure 4.10 a comparison of the two weight matrix is given. We note a similar behaviour between the two weights introduced as an energy based criteria is used in both cases [1]. The sensitivity based weight is different for mode 3, and this allows to speculate that in the case where the ROM is not built using the POD bases, but on a different criteria, such as the Observability as described in Jordan *et al.* (2007), the above analysis may yield a sensitivity weight for the lower modes which may be acoustically important. The temporal evolution and phase plot for the case of the sensitivity based calibration is shown in f gure 4.11 and f gure 4.12 respectively and shows a very good visual agreement with the POD dynamics.

4.5.4 Comparison of different types of Tikhonov regularization

The various type of Tikhonov regularization are compared in table 4.2 for the normalised errors and the cost of calibration, obtained for the zeroth, f rst and second order Tikhonov regularization. The error in all the cases remains the same. When comparing the cost of calibration the regularization $L = SOD; \mathbf{y}_0 = 0$ is more economical. The result is more effective than the errors obtained for the different type of calibration described in table 4.1 although the cost is an order times more, but then again to reiterate this cost is not important than the accuracy we desire. The different errors for the weighted regularization are compared in table 4.3. The errors do not differ much when compared to the classical case when all the modes are given equal weights, but then the temporal dynamics which we are treating is rather simple to conclude the advantages of the weighted Tikhonov regularization over the classical method. More complicated dynamics like turbulent f ows, acoustics,

[1] Although the sense of energy is different in two cases, it is a energy of projection in the case of POD and the energy contained of the f ow dynamics, for the sensitivity based analysis.

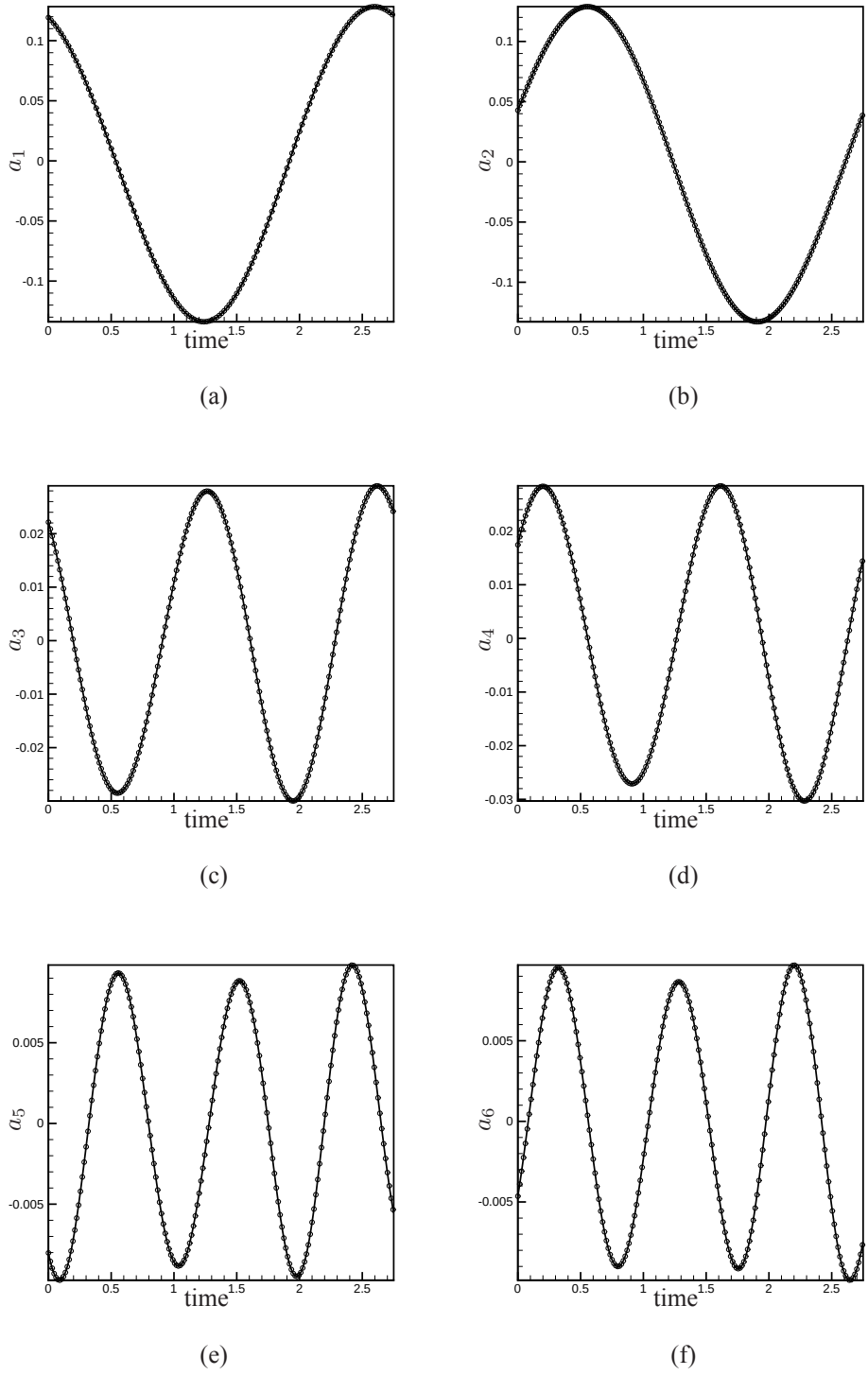

Figure 4.11 - *Temporal comparison of the first* 6 *modes, with the POD coefficients:ROM calibrated (solid line), reference POD dynamics (o). POD ROM is calibrated using the* $\mathcal{I}^{(3)}$ *minimisation for all coefficients. The Tikhonov regularization is applied for (*$L = 0$,$\mathbf{y_0} = 0$*), and the weight matrix* Λ *based on the overall sensitivity.*

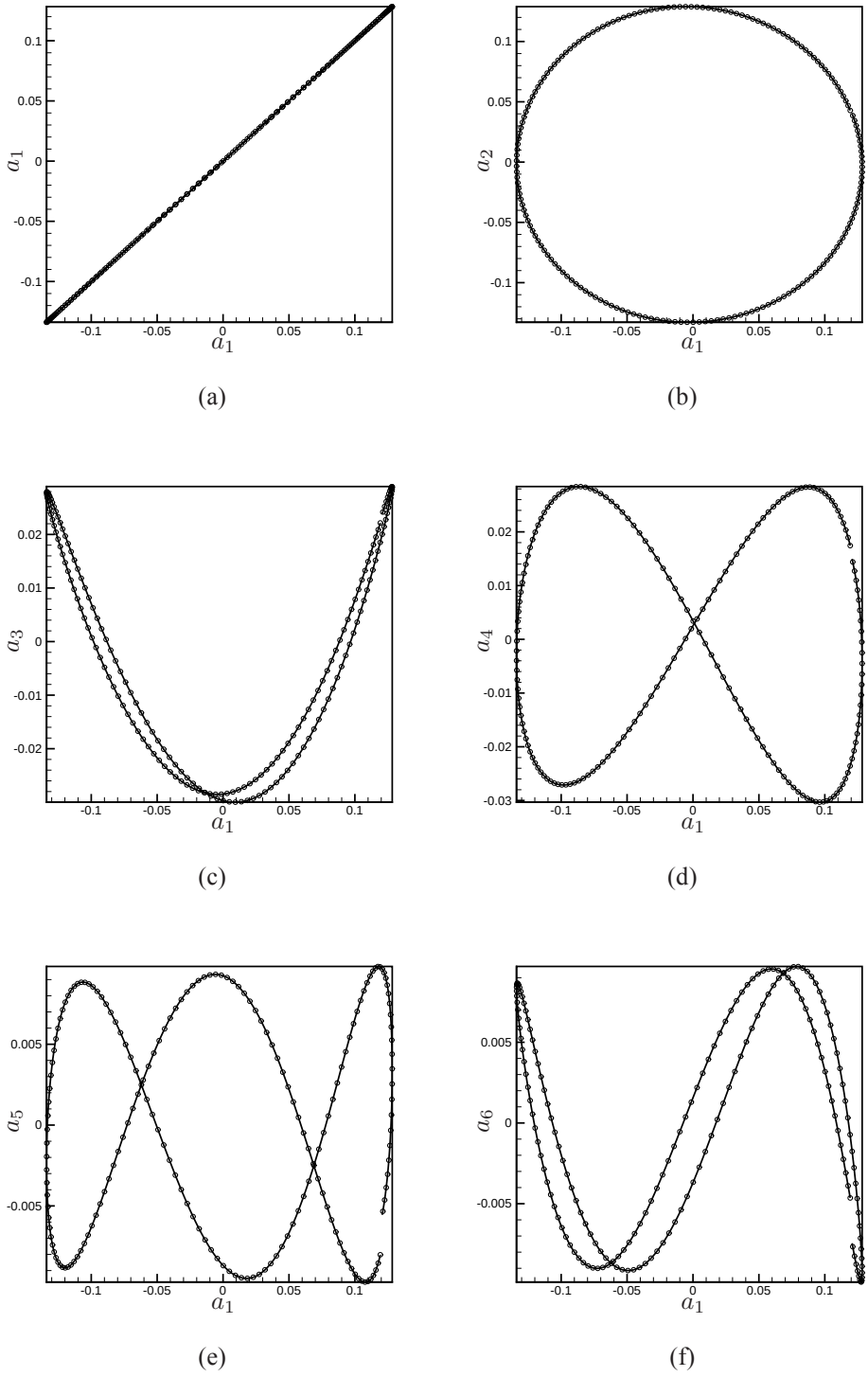

Figure 4.12 - *Phase portrait comparison of the first* 6 *modes, with the POD coefficients:ROM calibrated (solid line), reference POD dynamics (o). POD ROM is calibrated using the* $\mathcal{I}^{(3)}$ *minimisation for all coefficients. The Tikhonov regularization is applied for (*$L = 0$,$\mathbf{y_0} = 0$*), and the weight matrix* Λ *based on the overall sensitivity.*

Type of Tikhonov regularization	$\sqrt{\mathcal{E}^{(1)}(\mathbf{y})}$	$\sqrt{\mathcal{E}^{(2)}(\mathbf{y})}$	$\sqrt{\mathcal{E}^{(3)}(\mathbf{y})}$	$\sqrt{\mathcal{D}(\mathbf{y})}$
$L = I; \mathbf{y}_0 = 0$	$4.0 \cdot 10^{-4}$	$6.13 \cdot 10^{-3}$	$2.11 \cdot 10^{-2}$	2.74
$L = I; \mathbf{y}_0 = \mathbf{y}^{GP}$	$4.0 \cdot 10^{-4}$	$6.13 \cdot 10^{-3}$	$2.11 \cdot 10^{-2}$	2.72
$L = FOD; \mathbf{y}_0 = 0$	$4.0 \cdot 10^{-4}$	$6.13 \cdot 10^{-3}$	$2.11 \cdot 10^{-2}$	4.9
$L = FOD; \mathbf{y}_0 = \mathbf{y}^{GP}$	$4.0 \cdot 10^{-4}$	$6.13 \cdot 10^{-3}$	$2.11 \cdot 10^{-2}$	4.7
$L = SOD; \mathbf{y}_0 = 0$	$4.0 \cdot 10^{-4}$	$6.13 \cdot 10^{-3}$	$2.11 \cdot 10^{-2}$	1.22
$L = SOD; \mathbf{y}_0 = \mathbf{y}^{GP}$	$4.0 \cdot 10^{-4}$	$6.13 \cdot 10^{-3}$	$2.11 \cdot 10^{-2}$	6.7

Table 4.2 - *Normalised error $\varepsilon^{(i)}$ and cost of calibration $\mathcal{D}$. POD ROM is calibrated using the $\mathcal{I}^{(3)}$ minimisation for all coefficients (constant, linear, quadratic) for different type of Tikhonov regularization with the weight matrix $\Lambda = I$.*

Type of Tikhonov regularization	$\sqrt{\mathcal{E}^{(1)}(\mathbf{y})}$	$\sqrt{\mathcal{E}^{(2)}(\mathbf{y})}$	$\sqrt{\mathcal{E}^{(3)}(\mathbf{y})}$	$\sqrt{\mathcal{D}(\mathbf{y})}$
$L = I; \mathbf{y}_0 = 0$	$5.0 \cdot 10^{-4}$	$2.96 \cdot 10^{-2}$	$2.16 \cdot 10^{-2}$	2.88
$L = I; \mathbf{y}_0 = \mathbf{y}^{GP}$	$5.0 \cdot 10^{-4}$	$2.96 \cdot 10^{-2}$	$2.16 \cdot 10^{-2}$	2.84
$L = FOD; \mathbf{y}_0 = 0$	$3.49 \cdot 10^{-3}$	$2.96 \cdot 10^{-2}$	$2.16 \cdot 10^{-2}$	5.32
$L = FOD; \mathbf{y}_0 = \mathbf{y}^{GP}$	$1.53 \cdot 10^{-3}$	$2.96 \cdot 10^{-2}$	$2.16 \cdot 10^{-2}$	4.9
$L = SOD; \mathbf{y}_0 = 0$	$5.38 \cdot 10^{-4}$	$2.96 \cdot 10^{-2}$	$2.16 \cdot 10^{-2}$	7.0
$L = SOD; \mathbf{y}_0 = \mathbf{y}^{GP}$	$5.38 \cdot 10^{-4}$	$2.96 \cdot 10^{-2}$	$2.16 \cdot 10^{-2}$	6.0

Table 4.3 - *Normalised error $\varepsilon^{(i)}$ and cost of calibration $\mathcal{D}$. POD ROM is calibrated using the $\mathcal{I}^{(3)}$ minimisation for all coefficients (constant, linear, quadratic) for different type of Tikhonov regularization with the weight matrix $\Lambda_{ii} = \frac{\mathcal{S}_i}{max \mathcal{S}_i}$ obtained from the sensitivity analysis.*

which have different scales of dynamics need to be studied to establish the advantage of the method. In any case both the methods of Tikhonov regularization compare much better than the other methods.

4.6 Comparison with other calibration methods

We compare in this section the three most effective methods of calibration for the cavity f ow conf g-uration. Table 4.4 gives the normalised errors and cost of calibration obtained by minimisation of $\mathcal{I}^{(1)}$ under the constraint $\mathcal{P}_C$, minimisation of $\mathcal{J}_\alpha^{(3)}$ with $\alpha = 0.001$ and determining all the coeff cients, and application of the most effective weighted Tikhonov regularization *i.e.* for $L = I$ and $\mathbf{y}_0 = 0$. The weighted Tikhonov method is most effective when comparing the normalised errors, which is minimum than the other two methods. A further analysis can be done if we analyse the modal errors

$\mathcal{I}_i^{(j)}$ defined [2] for $i = 1, \cdots, N$ and $j = \{1, 2, 3\}$ as

$$\mathcal{I}^{(j)}(\mathbf{y}) = \sum_{i=1}^{N} \mathcal{I}_i^{(j)}(\mathbf{y})$$

The modal errors $\mathcal{I}_i^{(3)}$ are represented in figure 4.13 for the various calibration techniques presented in table 4.4. The method of weighted Tikhonov regularization is most effective for all POD modes. Minimisation of $\mathcal{J}_\alpha^{(3)}$ for $\alpha = 0.001$ compares with the weighted Tikhonov for the initial POD modes, but for higher modes the Tikhonov method clearly out performs. Both the methods of minimisation of $\mathcal{J}_\alpha^{(3)}$ and the method of weighted Tikhonov regularization are far better than the minimisation of $\mathcal{I}^{(1)}$ under the constraint $\mathcal{P}_C$ for the higher modes. The main strength of the weighted Tikhonov regularization is that the choice of the parameter ρ is determined by the L-curve without any user intervention. Also the higher modes are well calibrated which is important from an acoustic point of view.

Method of calibration	control terms	$\sqrt{\mathcal{E}^{(1)}(\mathbf{y})}$	$\sqrt{\mathcal{E}^{(2)}(\mathbf{y})}$	$\sqrt{\mathcal{E}^{(3)}(\mathbf{y})}$	$\sqrt{\mathcal{D}(\mathbf{y})}$
Minimisation of $\mathcal{I}^{(1)}$ under constraint $\mathcal{P}_C$	C and L	$1.62 \cdot 10^{-2}$	$3.5 \cdot 10^{-1}$	$1.86 \cdot 10^{-1}$	$2.68 \cdot 10^{-1}$
Minimisation of $\mathcal{J}_\alpha^{(3)}$ with $\alpha = 0.001$	C , L and Q	$1.23 \cdot 10^{-3}$	$2.97 \cdot 10^{-2}$	$2.36 \cdot 10^{-2}$	$4.0 \cdot 10^{-1}$
Minimisation of $\mathcal{I}^{(3)}$ with the weighted Tikhonov regularization ($L = I : \mathbf{y}_0 = 0$)	C, L and Q	$5.0 \cdot 10^{-4}$	$2.96 \cdot 10^{-2}$	$2.16 \cdot 10^{-2}$	2.88

Table 4.4 - *Normalised error $\varepsilon^{(i)}$ and cost of calibration. Comparison between the results obtained by: (a) minimisation of $\mathcal{I}^{(1)}$ under the constraint $\mathcal{P}_C$. (b) minimisation of $\mathcal{J}_\alpha^{(3)}$ with $\alpha = 0.001$. (c) minimisation of $\mathcal{J}_\alpha^{(3)}$ with determination of all the coefficients (constant, linear and quadratic) and application of the weighted Tikhonov regularization ($L = I$ and $\mathbf{y}_0 = 0$).*

4.7 Long time time integration of the POD ROM

Since we are dealing with periodic flow it is natural to expect that the temporal coefficients once determined is valid for a time longer than the period of snapshot acquisition. As shown by Sirisup & Karniadakis (2004) although the system is initialised with correct state the solution may drift away for a long period of integration. Figure 4.14 shows that the calibrated model predicts the dynamics for a non-dimensional time 11, which corresponds to around 4 cycle of the flow period, after which it diverges rapidly. This is different from the results where the calibrated model is shown to work for a much longer periods. The reason is that the neglected modes which contribute to the

[2] Rigorously speaking these errors can be introduced only when $\Lambda = I$ the identity matrix of size N.

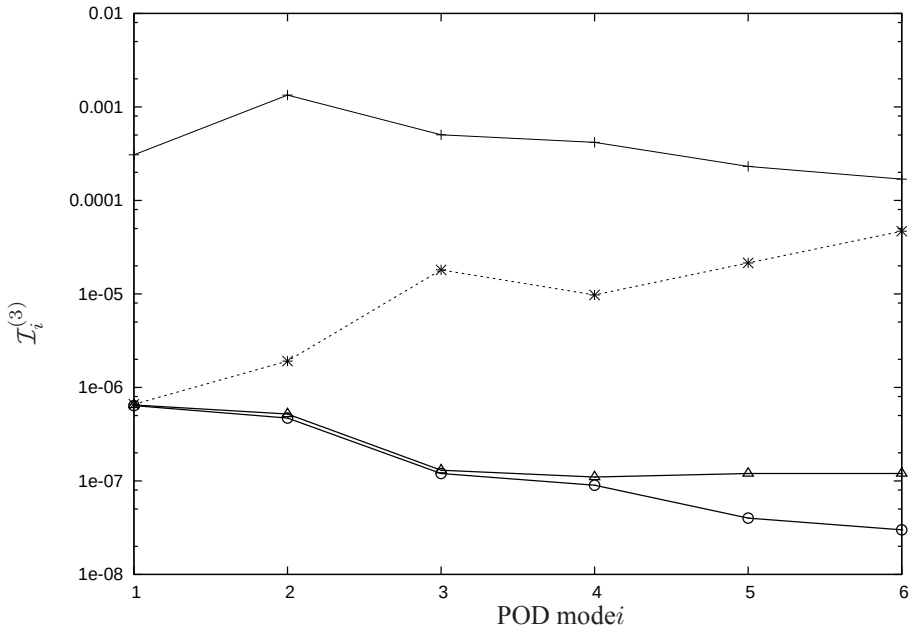

Figure 4.13 - *Modal errors $\mathcal{I}_i^{(3)}$. Comparison between the results obtained by: (a) minimisation of $\mathcal{I}^{(1)}$ under the constraint $\mathcal{P}_C$, denoted by $(\star)$. (b) minimisation of $\mathcal{J}_\alpha^{(3)}$ with $\alpha = 0.001$ denoted by $(\triangle)$. (c) minimisation of $\mathcal{J}_\alpha^{(3)}$ with determination of all the coefficients (constant, linear and quadratic) and application of the weighted Tikhonov regularization ($L = I$ and $\mathbf{y}_0 = 0$) denoted by $(\circ)$. The no calibration case is denoted by $(+)$. Note $\mathcal{I}^{(3)}(\mathbf{y}) = \sum_{i=1}^{N} \mathcal{I}_i^{(3)}(\mathbf{y})$.*

regularization of the system is not modeled during calibration. The validity of ROM for a longer time of integration is still open, where the coeff cients need to be given suitable weights to model the neglected term. While performing control since the time period where the control is determined is much larger than the period of validity of the model, it is imperative that we calibrate more than one period of the f ow as will be demonstrated in the next chapter.

4.8 Conclusion

In this chapter a unif ed framework for the different calibration methods described in the literature is given, with an application to the cavity f ow. It is found that the method based on minimisation of $\mathcal{I}^{(1)}$, under the constraint of the Cauchy problem $\mathcal{P}_C$ is more effective than the methods based on the minimisation of $\mathcal{I}^{(3)}$, or the intrinsic stabilisation method. We have then applied the method of Couplet *et al.* (2005) based on the minimisation of functional based on the convex linear combination of terms which represent the normalised error and a measure of the variation of the coeff cients of the model to their values obtained from POD. The benef t of an accurate model outweighs the cost consideration. It can be shown that adding the regularising term, improves the conditioning number of the linear system associated to the minimisation of $\mathcal{I}^{(2)}$ and $\mathcal{I}^{(3)}$. The choice of the parameter α in

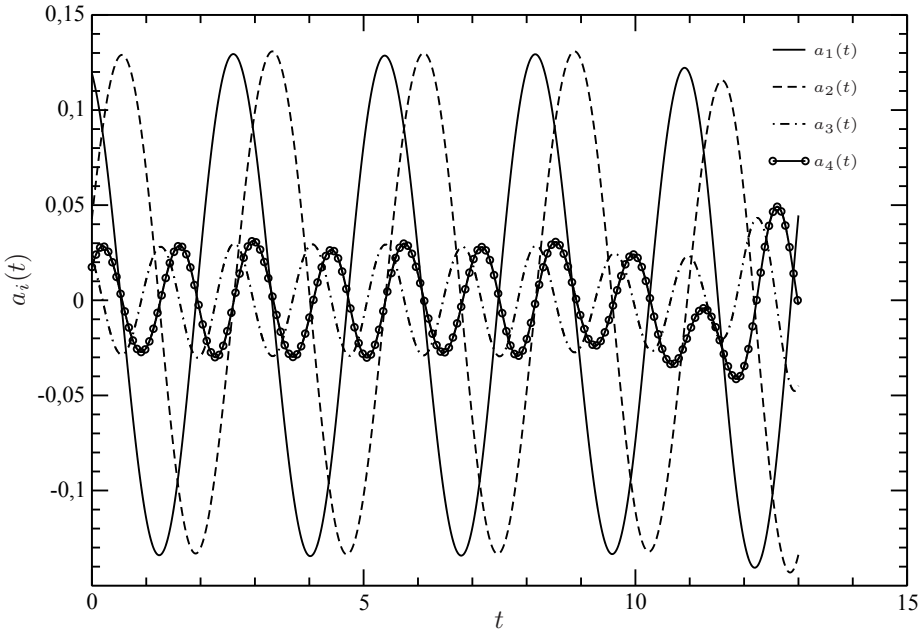

Figure 4.14 - *Evolution of first* 4 *temporal modes* $a_i(t)$ *of the POD ROM for period greater than the period of validity of the model. The model diverges after a time* 11.

the regularising term is quite tricky and is problem dependent.

The method of Tikhonov regularization for the error associated to the minimisation of $\mathcal{I}^{(3)}$ is formed. The weight matrix in the def nition of errors for the minimisation of $\mathcal{I}^{(3)}$, is chosen based on two criteria. One based on the eigen spectra and the other based on the sensitivity of the POD temporal coeff cients with respect to a energy based cost functional. We compared the errors for the two type of Tikhonov regularization and it is found that the zeroth order regularization ($L = I$) with $\mathbf{y_0} = 0$ is the most effective among all the types of Tikhonov regularization considered.

Numerical experiments demonstrates that the weighted Tikhonov regularization outperforms, in terms of the normalised errors, the minimisation of $\mathcal{I}^{(1)}$ with constraint $\mathcal{P}_C$ and the minimisation of $\mathcal{J}_\alpha^{(3)}$ with $\alpha = 0.001$. The main strength of the weighted Tikhonov regularization is that the choice of the parameter ρ is determined by the L-curve without any user intervention. Also the higher modes are well calibrated which is important from an acoustic point of view. Finally we verify the suitability of the calibrated model for longer periods of time integration. Although the model predicts the dynamics for about 4 periods of f ow oscillation, it diverges rapidly when integrated beyond. This is due to the fact that the neglected modes are not taken into consideration and the problem of closure remains open, even after correctly determining the coeff cients. We therefore required to calibrate for more periods if we have to utilise the model for control studies.

Having established all the tools of ROM, *i.e.* extension to actuated case, stabilisation of ROM, we are now proceed to utilise the above development for control studies, in the next chapter.

Chapter 5

Feedback control of cavity flows

Introduction

Dans ce chapitre est mis en oeuvre un contrôle optimal en boucle fermée du système dynamique forcé associé à la cavité. Un contrôle optimal a déjà été appliqué sur des modèles réduits, par exemple pour le cas du sillage d'un cylindre, comme dans Graham et al. (1999a), Graham et al. (1999b) et Bergmann & Cordier (2005). Parce que le contrôle modifie intrinsèquement le système dynamique il faut pouvoir prendre en compte correctement le forçage dans le modèle, comme cela est proposé par Weller et al. (2009a). Pour le contrôle en boucle fermée de l'écoulement de cavité, nous nous sommes inspirés des travaux numériques de Rowley & Juttijudata (2005) et des travaux expérimentaux de Samimy et al. (2007) qui ont obtenus des résultats mitigés. Le chapitre est découpé en deux parties, l'une consacrée à la linéarisation du système dynamique forcé, l'autre à l'application d'un contrôle linéaire quadratique gaussien et à son utilisation dans l'espace physique.

Construction du système à contrôler

Le système est décrit par la figure 5.2. Il repose sur une estimation de l'état à partir de l'observation de la pression en certains points de l'écoulement (6 au total) sur la base d'une estimation stochastique linéaire (LES) qui est obtenue très simplement par projéction sur l'espace des coefficients POD temporels et qui s'avère extrêmement précise comme la reconstruction le montre (figure 5.3), à cause de l'orthogonalité de la base POD.

Une analyse de sensibilité des coefficients du modèle réduit prenant en compte un forçage (figure 5.4) met en évidence la nécessité de linéariser le système fortement non linéaire avec soin. La linéarisation se fait autour d'un état d'équilibre calculé par une méthode de Newton.

Calcul de la loi de contrôle

La loi de contrôle en boucle fermée implique une relation linéaire (matrice gain) entre l'état du système et le contrôle lui-même. Ce gain est obtenu à partir de la résolution d'une équation de

Riccati. On peut aussi montrer que l'estimation de l'état (l'observateur) est obtenue par la résolution d'une autre équation de Riccati, en se basan sur la théorie du filtre de Kalmann-Bucy. En appliquant le principe de séparation, on simule finalement le comportement du système complet comprenant le vecteur d'état et l'erreur d'estimation. On observe que la réponse du système dépent de la condition initiale, de la forme du contrôle et des bruits extérieurs qui viennent perturber le système.

Pour l'application à l'écoulement de cavité, rappelons la procédure générale. Dans un premier temps, nous effectuons une simulation sans contrôle et par projection de Galerkin nous contruisons et calibrons une modèle réduit non forcé. Ensuite, le système réel (les équations de Navier–Stokes) sont forcées par un signal (eq. 5.26) contenant de nombreuses fréquencés (fig. 5.6). Un modèle réduit prenant en compte ce forçage est ensuite construit et sert de base pour la détermination du contrôle optimal. Le contrôle LQG permet de stabiliser le système linéarisé comme le montre le spectre des valeurs propres du système avant et après application de la loi de feedback (fig. 5.7). Il apparaît que l'approche se contente de stabiliser les valeurs propres à partie réelle positive, sans toucher à la partie imaginaire, c'est-à-dire aux fréquencés. On remarque aussi que le gain du contrôle $||K_c|| \approx 950$ *est extrêmement élevé, si on compare à l'amplitude du forçage dans le modèle complet (de l'ordre de 0.08). Il n'est donc pas réaliste. Il s'explique par le fait qu'on cherche un contrôle sur un temps infini pour le modèle réduit alors que pour le modèle complet on cherche un contrôle possible sur un temps très limité, de quelques périodes au maximun. Suivant l'approche proposée dans Samimy et al. (2007), on introduit un nouveau paramètre* α *qui donne au final l'amplitude du contrôle (fig. 5.8).* $\alpha = 0.5$ *fournit la valeur minimale pour obtenir une stabilisation du modèle réduit.*

La matrice gain de l'observateur est construite aussi à partir de la solution d'une équation de Riccati et nous trouvons (fig. 5.9) une solution stabilisant l'erreur d'estimation (si on ne prend pas en compte le bruit gaussien qui existera toujours).

Pour obtenir la forme du contrôle optimal, on simule le système augmenté constitué du système linéarisé et du système bâti à partir de l'erreur d'estimation, avec comme entrée, le forçage multi-fréquentiel utilisé plus haut. On obtient l'évolution de l'état et par conséquent du contôle par la loi de feedback. Cette fonction est donnée sur la figure 5.10, en comparaisont avec le contrôle multifréquentiel. On trouve une loi très simple qu'on approxime par un sinus (eq. 5.28) dont on détermine la phase, la fréquence et l'amplitude. La fréquence est celle de la moins stable des valeurs propres du système. Ce nouveau forçage est alors introduit dans le problème complet (la DNS), moyennant cependant une réduction de l'amplitude pour éviter la divergence numérique. La figure 5.11 présente la densité spectrale de puissance de la vitesse verticale dans un point de la couche de cisaillement, et on observe une petite réduction du pic pour le second mode de Rossiter. Par contre d'autres fréquences mal prises en compte dans le modèle sont amplifiées, ce qui est une forte limitation de notre approche.

Enfin la réponse complète du modèle réduit ainsi que l'erreur d'estimation en boucle fermée sont montrées sur les figures 5.12 et 5.13. Encore une fois on remarque que la théorie fonctionne mais que les amplitudes obtenus ne sont pas réalistes pour l'application dans les simulations numériques directes.

5.1 Introduction

In this chapter we extend the developments of the previous chapter to perform closed loop control of cavity flows. Regarding the use of ROM for optimal control studies one can refer Graham *et al.* (1999a), Graham *et al.* (1999b) and Bergmann & Cordier (2005) where the optimal control has been applied for the control of wake flows behind a cylinder. Since the ROM is designed for a particular flow condition Fahl (2000) propose a method where the model is refined during the optimisation process, to take care of the validity of the model to the variation of control parameters. This method has been applied for the optimal control of wake flows by Bergmann & Cordier (2008). Weller *et al.* (2009*b*), Weller *et al.* (2009*a*) proposes a method to include the effect of actuation in the ROM to obtain a feedback control. Control of cavity flows, using experimental data to build the ROM and its application to perform a model based control has been proposed in Rowley & Juttijudata (2005), Samimy *et al.* (2007). This chapter can be divided into two parts, in the first part we introduce the various tools necessary for the feedback design, namely the construction of the observer and linearisation of the model. The observer is constructed by a Linear Stochastic Estimation (LSE) of the state based on the observed pressure measurements. A sensitivity analysis is performed to identify the terms which are important while linearising the model. The second part consists of designing a feedback control of the LQG type. The obtained control is introduced into the DNS to obtain an overall reduction in the spectra corresponding to the second Rossiter mode of the cavity.

5.2 Tools used for the feedback design

In this section we propose a feedback law based on an observer design, obtained from the pressure measurements inside the cavity. The plant model utilised in this study is shown in the figure 5.2. Control of cavity flows, using experimental data to build the ROM has been performed by Samimy *et al.* (2007), but without any calibration of the temporal dynamics. When we cannot measure the states a we construct an observer C, usually using wall pressure sensors, and try to predict the flow field by measuring the output y. Prediction of flow field from the observed states has been studied in the past by performing a Linear Stochastic Estimation(LSE) by Adrian & Moin (1998), Ukeiley *et al.* (2001). It consist in correlating the sensor signals with flow data base information, to predict the flow feld. A higher order correlations is also possible as demonstrated in Buffoni *et al.* (2008), where a Quadratic Stochastic Estimation (QSE) is performed. The main drawback of the LSE or the QSE is that they take into account the correlations at a particular time only, without considering the time history of the previous measurements, hence they are termed as 'static' estimators. In an experimental setup this poses a problem due to the measurement noise and also on the limitations of the number of sensors that can be placed. Rowley & Juttijudata (2005) have used a dynamic estimator *i.e.* of combining the estimation with a reduced order model to take care of the time history of sensor measurements. A combination of the isentropic model with the data obtained from experiments has been studied by Samimy *et al.* (2007). The technique of LSE which is used in this work for the observer is briefly explained in the next section.

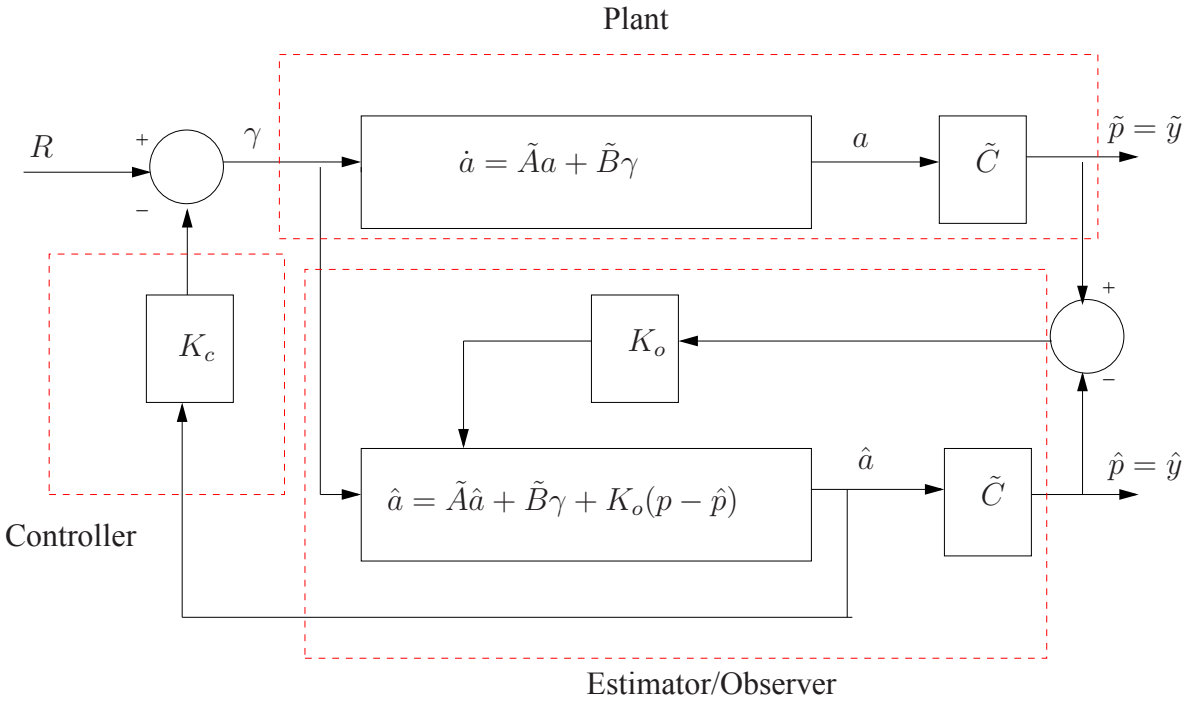

Figure 5.1 - *Plant and Observer for feedback control. $\tilde{C}$: observer, K_0: Estimator, K_c: Feedback*

5.2.1 Linear Stochastic Estimation (LSE)

The LSE technique enables us to determine the observer matrix $\tilde{C}$, as shown in f gure 5.2, given a limited number of pressure measurements obtained from sensors along the walls of the cavity. For each sensor $i \in [1 \;\; N_s]$, we can estimate the pressure $\tilde{p}_i(t)$ coeff cients by a series expansion of the discrete temporal POD coeff cients $a_j(t)$ as

$$\tilde{p}_i(t) = \sum_{j=1}^{N_s} \tilde{C}_{ij}\, a_j(t) + \sum_{j=1}^{N_s}\sum_{k=1}^{N_s} \tilde{D}_{ijk}\, a_j(t)a_k(t) + \ldots \tag{5.1}$$

The expansion can be truncated above the linear term or the quadratic term which corresponds to the LSE or QSE problem. The coeff cients $\tilde{C}_{ij}$ and $\tilde{D}_{ijk}$ are determined so as to minimise the mean square error between the estimated pressure signal $\tilde{p}_i(t)$ and the one obtained from measurement $p_i(t)$.

$$e_i = \int_0^T [\tilde{p}_i(t) - p_i(t)]^2\, dt = \langle [\tilde{p}_i(t) - p_i(t)]^2 \rangle \tag{5.2}$$

Since the number of snapshots is much larger than pressure sensors, the above system is overdetermined and the coeff cients are determined using the method of least squares by solving an overdetermined linear system given by

$$\frac{de_i}{d\tilde{C}_{ij}} = 0 \quad \text{and} \quad \frac{de_i}{d\tilde{D}_{ijk}} = 0 \tag{5.3}$$

On noting the orthogonality of the temporal modes $\langle a_j, a_k \rangle = \lambda_i \delta_{jk}$, the pressure f eld can be simply expanded in terms of the temporal modes as

$$\tilde{p}_i(t) = \sum_{i}^{N_s} \tilde{C}_{ij} a_j(t) \qquad \text{where} \qquad \tilde{C}_{ij} = \frac{\langle p_i, a_j \rangle}{\langle a_j, a_j \rangle} \tag{5.4}$$

In this study $N_s = 6$ sensors along the wall and the shear layer are used to measure the pressure as shown in f gure 5.2. It is also worthwhile mentioning that solving the system of equation given

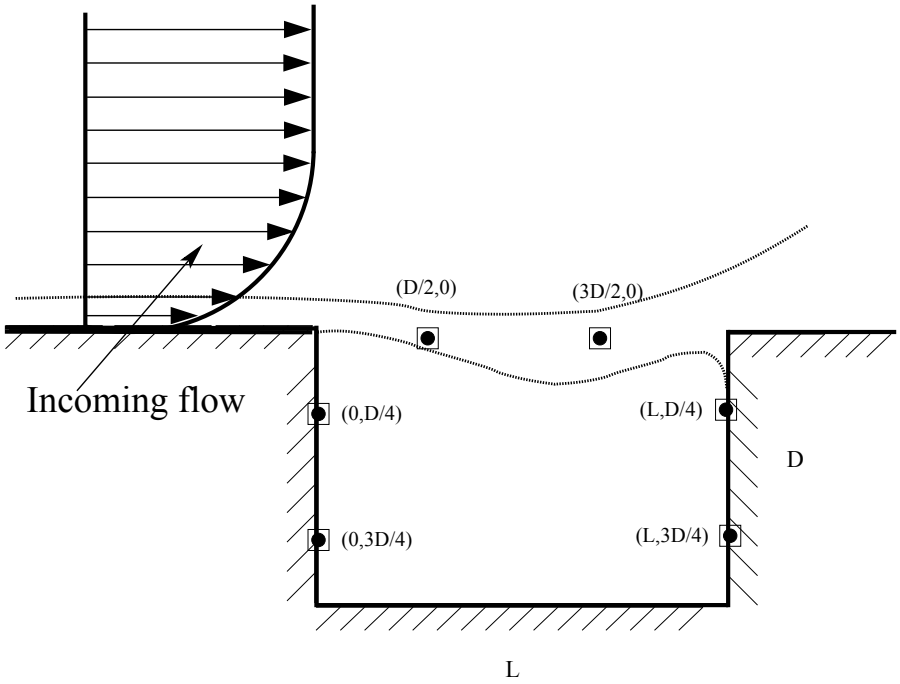

Figure 5.2 - *Location of pressure sensors for observer design*

by (5.3) leads to an ill conditioned problem. A luxury afforded by numerical simulations is that we can modify the condition number by changing the location of the pressure sensors, however for data obtained from experimental simulations where the sensor positions are f xed we can use the method of Tikhonov regularization mentioned in section §4.5.2. The observer dynamics for the construction of the pressure signals, issued from (5.4) is shown in f gure 5.3, and provides a good estimation of the wall pressure, due to the orthogonality property of the eigen modes.

5.2.2 Sensitivity analysis of the actuated terms

Sensitivity studies help in analysing the variation of a given quantity (generally given by a functional) with respect to a parameter of the model. In this study a sensitivity analysis is performed to identify

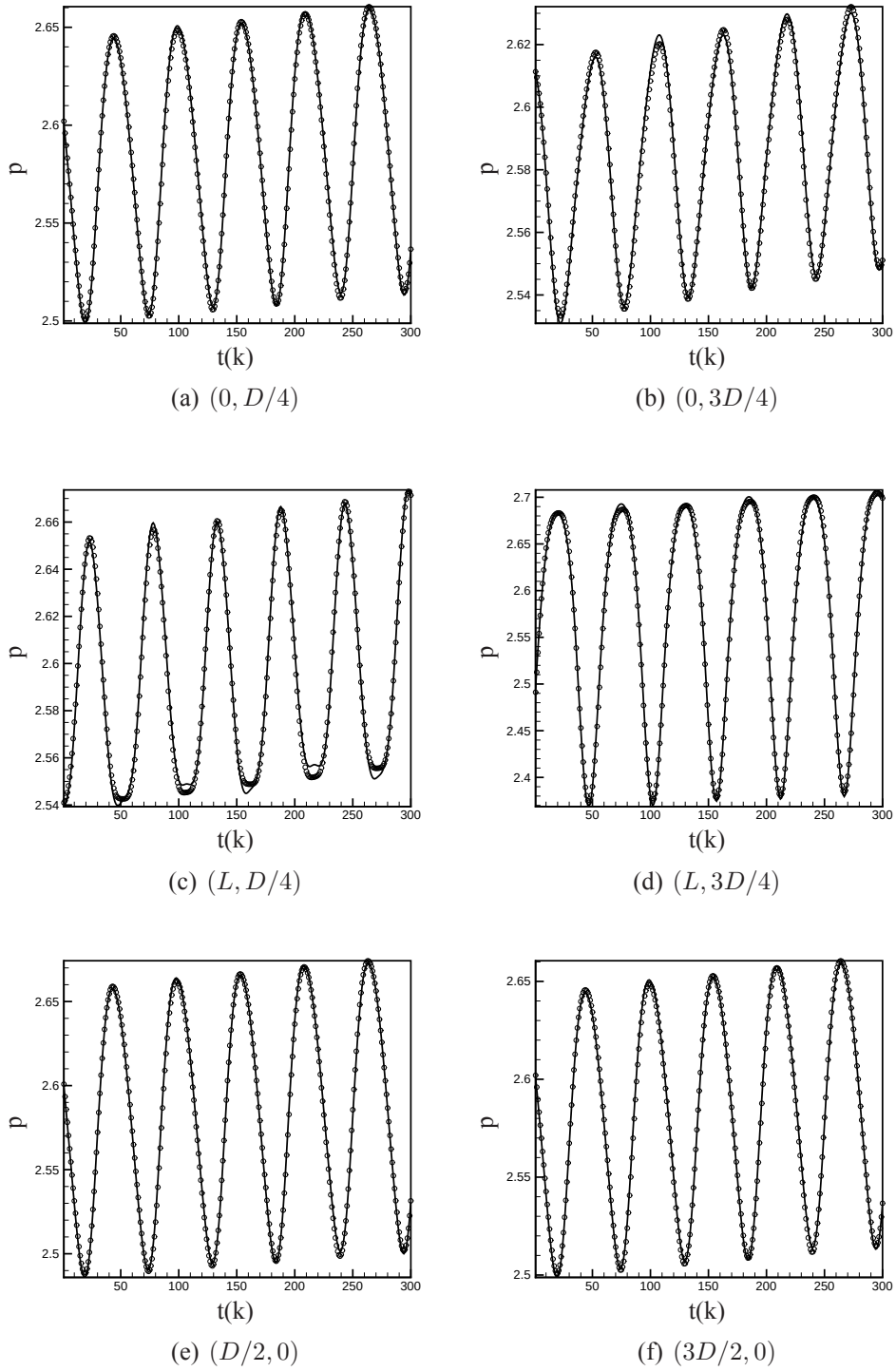

Figure 5.3 - *LSE reconstruction of the pressure signals. The pressure value from the sensor are denoted by solid line, and the coefficients obtained from LSE denoted by □. The sensors are located at positions* $(0, D/4)$, $(0, 3D/4)$, $(L, D/4)$, $(L, 3D/4)$ *along the cavity walls, and* $(D/2, 0)$, $(3D/2, 0)$ *in the shear layer.*

the terms to be neglected in the linearisation of the model. The state equation can be written as

$$\begin{aligned} \dot{a}_k &= \mathcal{N}(\mathbf{a}, \gamma(t)) \\ &= C_k + L_{jk}a_j + Q_{ijk}a_i a_j + h_{1k}\gamma + h_{2ik}a_i\gamma + h_{3k}\gamma^2 \end{aligned} \tag{5.5}$$

In the present case we seek for sensitivity with respect to the time-independent actuated coeff cients h_{1i}, h_{2ij} and h_{3i} of the model. The functional $\mathcal{J}$ is based on the energy of the modes and is given by

$$\begin{aligned} \mathcal{J}(\mathbf{a}, \gamma(t)) &= \int_0^T \int_\Omega J(\mathbf{a}, \gamma(t)) d\Omega dt \\ &= \frac{1}{2}\int_0^T \sum_{i=1}^{n} (a_i(t))^2 dt \end{aligned} \tag{5.6}$$

A variation of the augmented functional based on an adjoint vector ξ and the state equation (5.5) yields the sensitivities :

$$\frac{\partial \mathcal{J}}{\partial h_{1i}} = \langle \xi_i(t)\gamma(t) \rangle, \frac{\partial \mathcal{J}}{\partial h_{2ij}} = \langle a_j(t)\xi_i(t)\gamma(t) \rangle, \frac{\partial \mathcal{J}}{\partial h_{3i}} = \langle \xi_i(t)\gamma^2(t) \rangle \tag{5.7}$$

and

$$\frac{\partial \mathcal{J}}{\partial \gamma} = \sum_i h_{1i}\xi_i(t) + \sum_i \sum_j h_{2ij}\xi_i(t)a_j(t) + 2\sum_i h_{3i}\xi_i(t)\gamma(t)$$

where the adjoint equation is given by :

$$\dot{\xi}_i(t) = g_i(C_i, \mathbf{L_i}, \mathbf{Q_i}, \mathbf{a}(t), \xi(t)) + \sum_i h_{2ji}\xi_j(t)\gamma(t) - a_i(t) \tag{5.8}$$

Here $\langle . \rangle$ is the time averaging operator. The sensitivities are plotted in f gure 5.4 and shows that the constant term of the actuated model h_{1i} has a higher sensitivity when compared to the quadratic terms h_{3i} by an order of magnitude and hence plays an important role in linearisation. It is also important to note that the f rst two mode which drives the actuation dynamics does not contribute signif cantly to the sensitivity of the terms h_{1i} and h_{3i} as compared to h_{2ij}, this signif es that more care has to be taken while linearising these terms.

5.2.3 Linearisation of the plant

Once through the observer design, the plant (eq. (5.5)) is built by linearising the ROM around a suitable equilibrium point $\mathbf{a}_0$. Determination of the equilibrium point involves the task of solving a nonlinear algebraic matrix equation for the un-actuated case $\gamma = 0$. Equation (5.5) can be re-casted for the un-actuated part as:

$$f(a) := C + L\mathbf{a} + \begin{pmatrix} \mathbf{a}^T Q^1 \mathbf{a} \\ \vdots \\ \mathbf{a}^T Q^N \mathbf{a} \end{pmatrix} \tag{5.9}$$

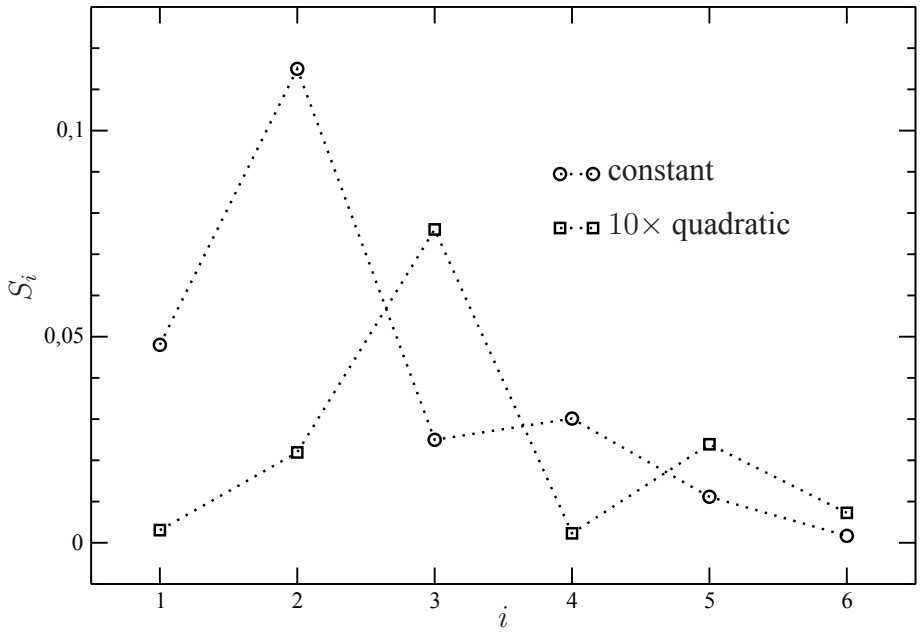

(a)

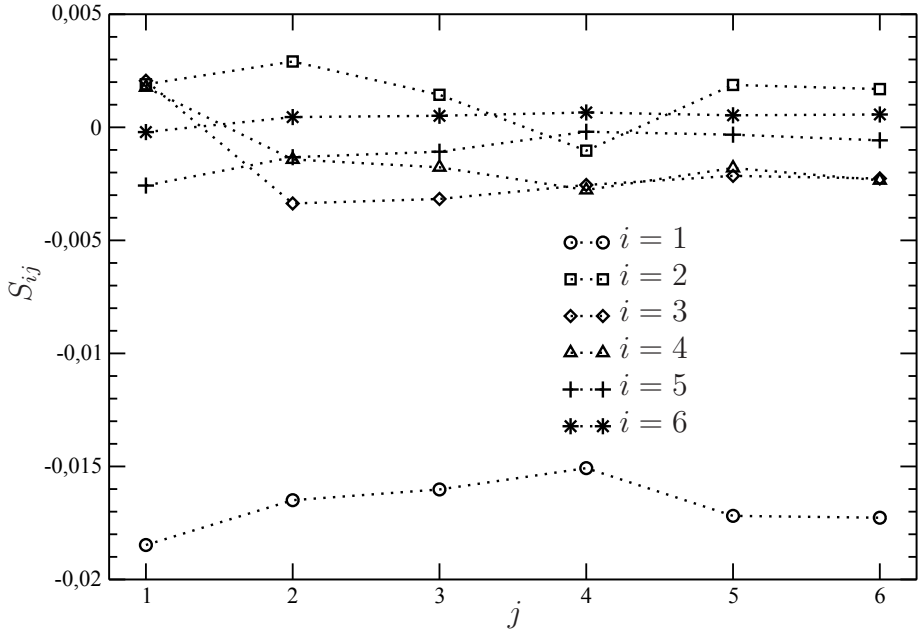

(b)

Figure 5.4 - *Sensitivity of the actuated coefficients. Constant :* $S_i = \frac{\partial \mathcal{J}}{\partial h_{1i}}$*, quadratic :*$S_i = \frac{\partial \mathcal{J}}{\partial h_{3i}}$ *(rescaled by 10), linear :* $S_{ij} = \frac{\partial \mathcal{J}}{\partial h_{2ij}}$

In this study a Newton's iterative method is used to calculate the equilibrium point $\mathbf{a}_0$ as given by the following algorithm :

$$\mathbf{a}_{k+1} = \mathbf{a}_k - J^{-1}(\mathbf{a}_k) f(\mathbf{a}_k) \tag{5.10}$$

where $J(\mathbf{a})$ is the Jacobian matrix : $J = \frac{\partial f(\mathbf{a})}{\partial \mathbf{a}}$. Also note that the solution of the Newton's method (eq. (5.10)) depends on initial conditions and is not unique. The initial value of guess, is chosen as the initial conditions of the dynamical system at $t = 0$. To linearise the plant, consider the equation (5.5) which can be recasted as

$$f(a) := C + L\mathbf{a} + \begin{pmatrix} \mathbf{a}^T Q^1 \mathbf{a} \\ \vdots \\ \mathbf{a}^T Q^N \mathbf{a} \end{pmatrix} + h_1 \gamma + \begin{pmatrix} (h^1_{21j}\gamma)^T \mathbf{a} \\ \vdots \\ (h^N_{2Nj}\gamma)^T \mathbf{a} \end{pmatrix} \tag{5.11}$$

In this system the quadratic term γ^2 is neglected. A linearisation is possible but since the mean value of $\gamma(t)$ is zero, it gives the same results as neglecting it. As the equilibrium point is unaltered in the presence of a feedback, we perform a linearisation by introducing the perturbation $\tilde{\mathbf{a}} = \mathbf{a} - \mathbf{a}_0$ to write the above system as:

$$\begin{aligned} \dot{\tilde{\mathbf{a}}} &= \dot{\mathbf{a}} = C + L(\tilde{\mathbf{a}} + \mathbf{a}_0) + \begin{pmatrix} (\tilde{\mathbf{a}} + \mathbf{a}_0)^T Q^1 (\tilde{\mathbf{a}} + \mathbf{a}_0) \\ \vdots \\ (\tilde{\mathbf{a}} + \mathbf{a}_0)^T Q^N (\tilde{\mathbf{a}} + \mathbf{a}_0) \end{pmatrix} + h_1\gamma + \begin{pmatrix} (h^1_{21j}\gamma)^T (\tilde{\mathbf{a}} + \mathbf{a}_0) \\ \vdots \\ (h^N_{2Nj}\gamma)^T (\tilde{\mathbf{a}} + \mathbf{a}_0) \end{pmatrix} \\ &= C + L\mathbf{a}_0 + \begin{pmatrix} \mathbf{a}_0^T Q^1 \mathbf{a}_0 \\ \vdots \\ \mathbf{a}_0^T Q^N \mathbf{a}_0 \end{pmatrix} + L\tilde{\mathbf{a}} + \begin{pmatrix} \tilde{\mathbf{a}}^T Q^1 \mathbf{a}_0 + \mathbf{a}_0^T Q^1 \tilde{\mathbf{a}} \\ \vdots \\ \tilde{\mathbf{a}}^T Q^N \mathbf{a}_0 + \mathbf{a}_0^T Q^N \tilde{\mathbf{a}} \end{pmatrix} + \begin{pmatrix} \tilde{\mathbf{a}}^T Q^1 \tilde{\mathbf{a}} \\ \vdots \\ \tilde{\mathbf{a}}^T Q^1 \tilde{\mathbf{a}} \end{pmatrix} \\ &+ h_1\gamma + \begin{pmatrix} (h^1_{21j}\gamma)^T \mathbf{a}_0 \\ \vdots \\ (h^N_{2Nj}\gamma)^T \mathbf{a}_0 \end{pmatrix} + \begin{pmatrix} (h^1_{21j}\gamma)^T \tilde{\mathbf{a}} \\ \vdots \\ (h^N_{2Nj}\gamma)^T \tilde{\mathbf{a}} \end{pmatrix} \end{aligned} \tag{5.12}$$

Since $\mathbf{a}_0$ is the equilibrium point of the un-actuated model it satisf es equation (5.9). The terms in (5.12) can be rearranged perturbed state $\tilde{\mathbf{a}}$ as

$$\dot{\tilde{\mathbf{a}}} = \tilde{L}\tilde{\mathbf{a}} + \begin{pmatrix} \tilde{\mathbf{a}}^T Q^1 \tilde{\mathbf{a}} \\ \vdots \\ \tilde{\mathbf{a}}^T Q^N \tilde{\mathbf{a}} \end{pmatrix} + \tilde{h}_1\gamma + \begin{pmatrix} (h^1_{21j}\gamma)^T \tilde{\mathbf{a}} \\ \vdots \\ (h^N_{2Nj}\gamma)^T \tilde{\mathbf{a}} \end{pmatrix} \tag{5.13}$$

where

$$\tilde{L} = L + \begin{pmatrix} \tilde{\mathbf{a}}_0^T (Q^1 + Q^1)^T) \\ \vdots \\ \tilde{\mathbf{a}}_0^T (Q^N + Q^N)^T) \end{pmatrix}, \tilde{h}_1 = h_1 + \begin{pmatrix} (h^1_{21j})^T \\ \vdots \\ (h^N_{2Nj})^T \end{pmatrix} \mathbf{a}_0$$

The observer model can be similarly linearised by introducing the transformation $\tilde{\mathbf{p}} = \mathbf{p} - \mathbf{p}_0$ as :

$$\tilde{\mathbf{p}} = \mathbf{p} - \mathbf{p}_0 = \tilde{C}\mathbf{a} - \tilde{C}\mathbf{a}_0 = \tilde{C}\tilde{\mathbf{a}} \tag{5.14}$$

On using a linearisation at the origin of equation (5.13), the linearised plant system can be written as

$$\begin{aligned} \dot{\tilde{\mathbf{a}}} &= \tilde{A}\tilde{\mathbf{a}} + \tilde{B}\gamma \\ \tilde{\mathbf{p}} &= \tilde{C}\tilde{\mathbf{a}} \end{aligned} \tag{5.15}$$

where $\tilde{A} = \tilde{L}$ and $\tilde{B} = \tilde{h}_1$,

5.3 Feedback design.

5.3.1 Controller

After linearising the plant, one can perform a feedback control. The full plant, control and estimator model are shown on f gure 5.2. The model for the controller is given by the equations for a LQG design as

$$\begin{aligned} \dot{\mathbf{a}} &= \tilde{A}\mathbf{a} + \tilde{B}\gamma + w_1 \\ y &= \tilde{C}\mathbf{a} + w_2 \end{aligned} \tag{5.16}$$

where for the sake of clarity we denote $a = \tilde{\mathbf{a}}$ and $y = \tilde{p}$. The controller noise w_1 and the measurement noise w_2 are assumed to be uncorrelated, zero mean, white Gaussian processes with modelled spectral densities Q_1 and Q_2 as described in 2.4.3. In this work the matrices Q_1 and Q_2 matrices are set to identity. We also introduce the noise perturbation vector $\mathbf{w} = [w_1\ w_2]$. The response of the state can be separated into three components, the natural response $\mathbf{a}_0(\tilde{A}, \mathbf{a}(0); t)$ which depends on the eigen values of the main plant matrix $\tilde{A}$ and on the initial condition $\mathbf{a}(0)$, the response to a given control $\gamma(t)$ denoted by $\mathbf{a}_\gamma(\tilde{A}, \tilde{B}, \gamma; t)$ and the response to the noise w_1 given by $\mathbf{a}_\mathbf{w}(\tilde{A}, w_1; t)$. The solution of the plant model (5.16) can be written as

$$\begin{aligned} \mathbf{a}(t) &= e^{\tilde{A}t}\mathbf{a}(0) + \int_0^t e^{\tilde{A}(t-\tau)}\,\tilde{B}\,\gamma(\tau)\,d\tau + \int_0^t e^{\tilde{A}(t-\tau)}\,w_1(\tau)\,d\tau \\ &= \mathbf{a}_0(\tilde{A}, \mathbf{a}(0); t) + \mathbf{a}_\gamma(\tilde{A}, \tilde{B}, \gamma; t) + \mathbf{a}_\mathbf{w}(\tilde{A}, w_1; t). \end{aligned} \tag{5.17}$$

Assuming a full information state, the feedback law is given by

$$\gamma = -K_c\,\mathbf{a} \tag{5.18}$$

where the matrix K_c is chosen so as to stabilise the plant and minimise the quadratic cost functional given by :

$$\mathcal{J} = \int_0^T \left(\mathbf{a}^T W \mathbf{a} + \ell^2\gamma^2\right) dt \tag{5.19}$$

where W is a weight matrix (chosen as identity in our case) and ℓ represents the cost of the control. By a simple variational approach, it can be demonstrated that the gain vector K_c is given by

$$K_c = \frac{1}{\ell^2}\tilde{B}^T X \tag{5.20}$$

where X is the solution of the steady Ricatti equation to get inf nite horizon stabilisation:

$$\tilde{A}^T X + X\tilde{A} - \frac{1}{\ell^2} X\tilde{B}\tilde{B}^T X + W = 0 \tag{5.21}$$

5.3.2 Observer

In many cases the state $\mathbf{a}$ is known only from a limited number of output measurements $\mathbf{y}$, and must be built from an observation $\hat{\mathbf{y}}$ which is an approximation of the real value of the measurement $\mathbf{y}$. Denoting $\hat{\mathbf{a}}$ the approximation of the state, the observer equations can be written as :

$$\begin{array}{rcl} \dot{\hat{\mathbf{a}}} & = & \tilde{A}\hat{\mathbf{a}} + \tilde{B}\gamma + K_o(\mathbf{y} - \hat{\mathbf{y}}) \\ \hat{\mathbf{y}} & = & \tilde{C}\hat{\mathbf{a}} \end{array} \tag{5.22}$$

The observer gain matrix K_o is obtained by solving the Ricatti equation for Y and the observer matrix $\tilde{C}$ and is given by

$$\tilde{Y}A^T + \tilde{A}Y - Y\tilde{C}^T\tilde{C}Y + Q_2 = 0 \tag{5.23}$$

As described in Bewley & Liu (1998) the observer problem is dual of the controller problem described in equation (5.21). The estimation gain K_o is obtained f nally as

$$K_o = Y\tilde{C}^T \tag{5.24}$$

5.3.3 Simulation of the full system

The full system for the controller and observer, def ned in terms of the state and the estimator error $e_{\mathbf{a}} = \mathbf{a} - \hat{\mathbf{a}}$, with the state denoted by $\mathbf{x} = [\mathbf{a},\ e_{\mathbf{a}}]$, and the observer $\tilde{\mathbf{y}} = [\mathbf{y},\ e_{\mathbf{y}}]$ can be written as :

$$\begin{array}{rcl} \dot{\mathbf{x}} & = & A_t\mathbf{x} + D_t\,\mathbf{w} \\ \dot{\tilde{\mathbf{y}}} & = & C_t\mathbf{x} \end{array} \tag{5.25}$$

$$\text{where} \quad A_t = \begin{bmatrix} \tilde{A} - \tilde{B}K_c & \tilde{B}K_c \\ (0)_{\dim\tilde{A}} & \tilde{A} - K_o\tilde{C} \end{bmatrix} \quad D_t = \begin{bmatrix} I_d & 0 \\ I_d & -K_o \end{bmatrix} \quad C_t = \begin{bmatrix} \tilde{C} & 0_{\dim\tilde{C}} \\ (0)_{\dim\tilde{C}} & \tilde{C} \end{bmatrix}$$

To get the system the feedback is applied on the observer state $\hat{\mathbf{a}}$ as $\gamma = -K_c\hat{a}$. The eigenvalue of the full matrix A_t are the same as the eigenvalue of the matrices $\tilde{A} - \tilde{B}K_c$ and $\tilde{A} - K_o\tilde{C}$. By the principle of separation as described in chapter 2 the A_t is stable, if the corresponding gain matrices K_c and K_o obtained by the solution of the Ricatti equations are stable. In the absence of any noise, the state errors goes to zero in the inf nite horizon, hence the estimation state $\hat{\mathbf{a}}$ goes to the real state $\mathbf{a}$, and in the same way, the observer error $e_{\mathbf{y}} = \mathbf{y} - \hat{\mathbf{y}} = \tilde{C}e_{\mathbf{a}}$ goes to zero. In presence of Gaussian noise $\mathbf{w}$,

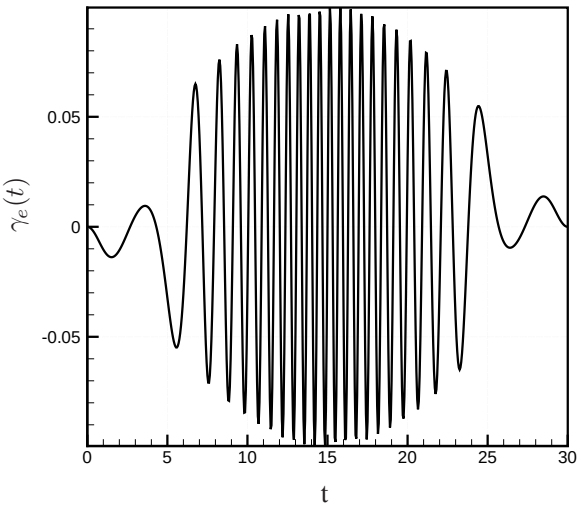

Figure 5.5 - *Chirp excitation γ_e : forcing the DNS.*

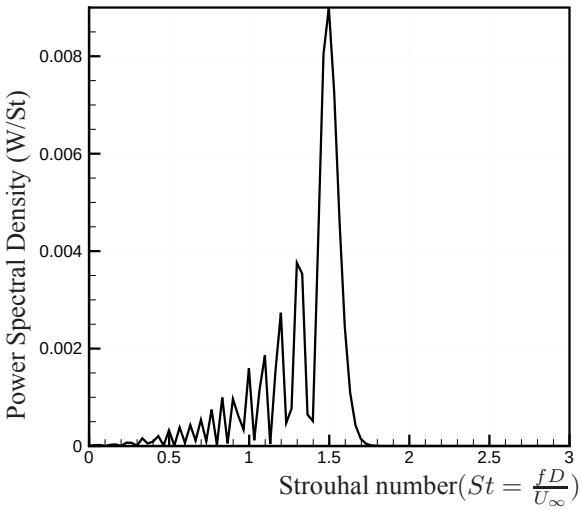

Figure 5.6 - *Spectra of the initial chirp.*

errors $e_{\mathbf{a}}$ and $e_{\mathbf{y}}$ remains under a given threshold, and are functions of the correlation matrices Q_1 and Q_2 as stated in Bagheri *et al.* (2009*b*). Following the notation of equation (5.17), the solution of the full plant model can written as :

$$\mathbf{x}(t) = \mathbf{x}_0(A_t, \mathbf{x}(0); t) + \mathbf{x}_{\mathbf{w}}(A_t, D_t\, \mathbf{w}; t).$$

where $||\mathbf{x}_0|| \to 0$ when $t \to \infty$.

5.3.4 Application to cavity

To remind of the overall procedure, a simulation without control is performed, and the un-actuated ROM model is constructed using a Galerkin projection. The model is further calibrated to avoid the divergence of solution when integrated in time. To introduce the effect of actuation, the high f delity model is forced with a chirp excitation of the form.

$$\gamma_g(t) = A_1 \sin(2\pi St_1 t) \times \sin\left(2\pi St_2 t - A_2 \sin(2\pi St_3 t)\right) \tag{5.26}$$

at the upstream corner of the cavity where $A_1 = 0.1, A_2 = 27, f_1 = 1/60, f_2 = 2/3, f_3 = 1/30$. The form of the excitation is as shown in f gure 5.5. The spectra of the chirp is represented in f gure 5.6 depicting a large spectral band in the range $0.2 - 1.5$ with a concentration around the value of 1.5. 300 snapshots are sampled, which corresponds to a time $T = 15$, *i.e.* half the period of excitation of the full chirp. The actuated mode and the plant model are constructed with the help of these realisations. The control has been design for different values of the cost $\ell \in [0.01, 5000]$, and the result was found to be independent of the value of ℓ. Finally the value of $\ell = 1$ was chosen for this study. In f gure 5.7 the eigen values of the open loop matrix $\tilde{A}$ and the closed loop matrix $\tilde{A} - \tilde{B}K_c$ are represented. The

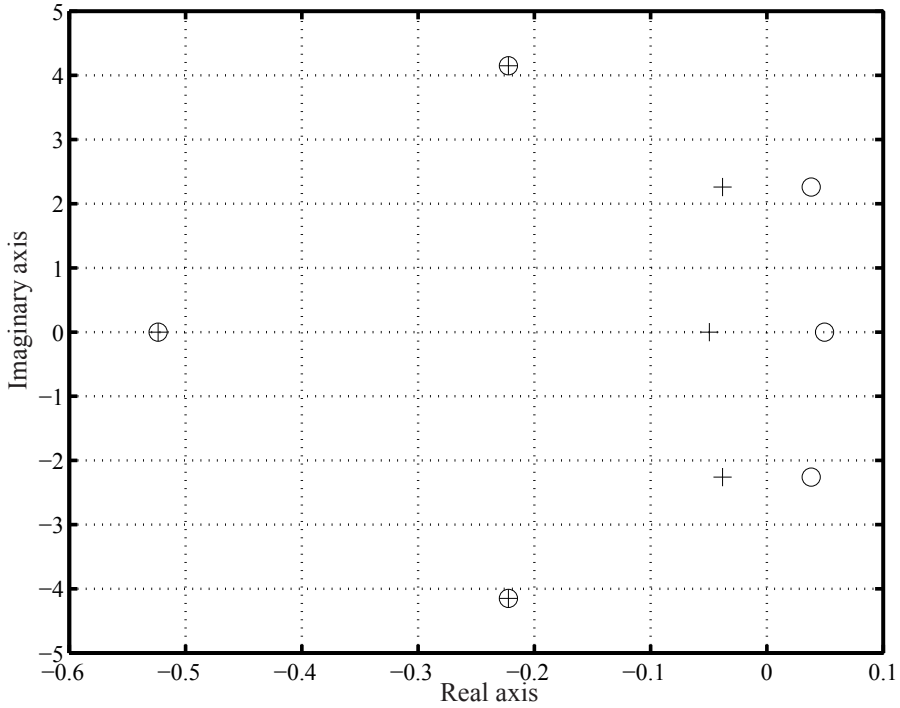

Figure 5.7 - *Eigen values of the plant: eigen values of $\tilde{A}$, (o) : eigen values of $\tilde{A} - \tilde{B}K_c$, (+).*

feedback control clearly mirrors the unstable eigenvalues, with dominant eigen values of the closed loop $\lambda_{\max} = -0.038 \pm i2.26$. For values of $\ell > 5000$, it seems numerically diff cult to use the Matlab system toolbox for the solution of the Ricatti equation, to f nd an accurate and stable eigenvalue of $\tilde{A} - \tilde{B}K_c$. The value of the feedback gain $||K_c|| \approx 950$ which seems quite large. When $\ell \to \infty$ the cost of the control goes to zero and the system can not be stabilised, as the the norm of the gain goes to zero. Similarly when ℓ is small, the eff ciency of the control increases due to the large amplitude of the control. However in practical cases the value of the control that can be fed into the actuator is limited by a range of the input signal as a large gain may damage the actuator Samimy *et al.* (2007).

To scale down the large gain, a new parameter α such that the amplitude of the control could decrease is introduced such that $\gamma_\alpha(t) = \alpha K_c$ with $\alpha \in [0, 1.1]$. In f gure 5.8 the real part of the largest eigenvalue of $\tilde{A} - \alpha\tilde{B}K_c$ is represents. The value of $\alpha = 1$ corresponds to the optimal control, while $\alpha = 0$ corresponds to the uncontrolled case. The value of $\alpha = 0.5$ corresponds to the stability limit of the controlled system, and is the result of mirroring of the unstable eigenvalues about the imaginary axis. It means that to stabilise the plant, the norm of the gain control vector should be at least equal to 475, which is quite large. The observer response is directly related to the largest eigenvalue of the matrix $\tilde{A} - K_o\tilde{C}$. For our case we found a real value of -0.45 which is suff cient to ensure the decrease of the estimation errors e_a with time. To determine the optimal control input $\gamma(t)_{opt}$, we solve the full system (5.25), and use the feedback law $\gamma(t)_{opt} = -K_c(a - e_{\mathbf{a}})$. In this work the noise $\mathbf{w} = [w_1\ w_2]$ is neglected while performing the full state simulation. The estimator eigen values are represented in f gure 5.9 and shows three eigen values which are marginally stable. The

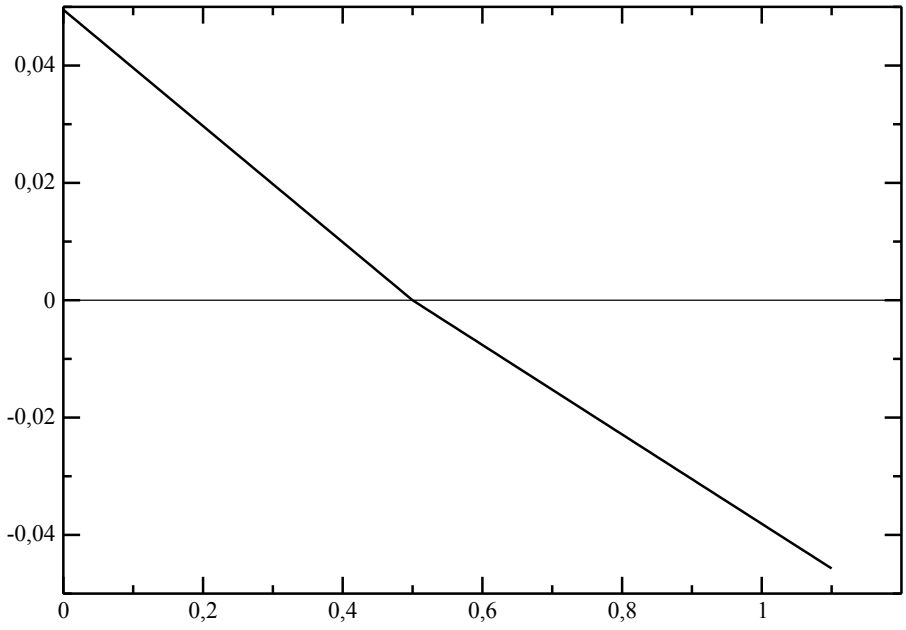

Figure 5.8 - $Re(\lambda_{\max})$ *with respect to* α

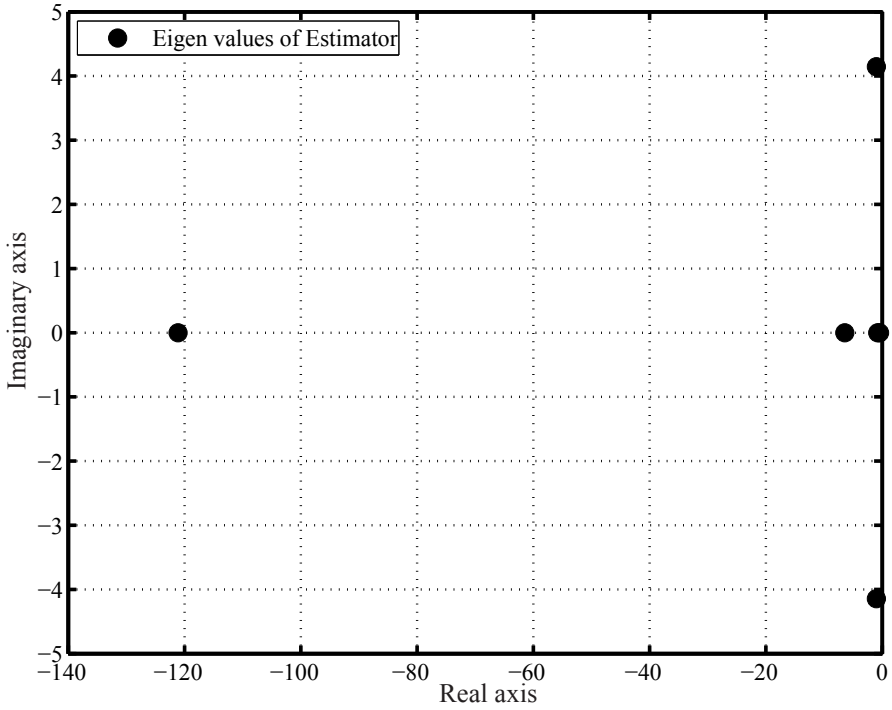

Figure 5.9 - *Estimator eigen values* $A - K_0C$

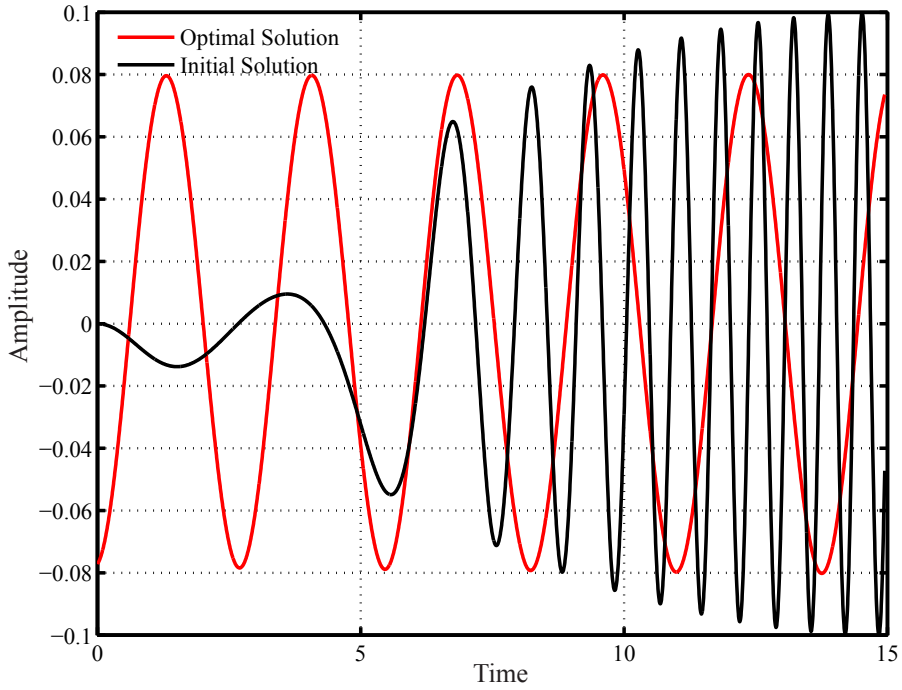

Figure 5.10 - *Comparison of the initial value and optimal value of the closed loop system.*

problem now is to determine the value of control $\gamma_{\text{DNS}}(t)$ to be introduced in the numerical simulation to stabilise the f ow or the acoustic f uctuations.

The plant model with the input $\gamma_g(t)$ is simulated. The feedback law $\gamma(t) = -K_c a_g$ obtained corresponds to the solution given by:

$$\gamma(t) = -K_c(e^{\tilde{A}\,t}a(0) + \int_0^t e^{\tilde{A}(t-\tau)}\, B\, \gamma_g(\tau)\, d\tau) \tag{5.27}$$

The new updated control is found to be of large magnitude $\max(\gamma(t)) = G_{\max} \approx 250$. The evolution of the f nal optimal control in comparison with the initial solution is as shown in f gure 5.10. A f tting approach demonstrates that $\gamma(t)$ is given by

$$\gamma(t) = G_{\max} \sin(\omega t + \varphi) \tag{5.28}$$

where $\omega = 2.27$, corresponding to a frequency $f = 0.3617$ and a phase $\varphi = -0.164$. The frequency is in good approximation to the imaginary part of the largest eigenvalue of the controlled plant (matrix $\tilde{A} - \tilde{B}K_c$). As is seen from equation (5.27), the gain vector K_c acts as a f lter and signals out the frequency which correspond to the shear layer instability of the second Rossiter mode.

To avoid numerical divergence of the numerical solution on the introduction of control, the amplitude (gain) G_0 of any control is set to a maximum value of $G_0 = 0.08$, so the updated control is of the same form as $\gamma(t)$ but with an amplitude G_0. The power spectral density for the vertical component of velocity at a point in the shear layer is compared with the simulation from the un-actuated case as

shown in figure 5.11 and shows a decrease in amplitude of the second Rossiter mode. However there is an increase in amplitude at other frequency due to the effect of actuation. The full system response

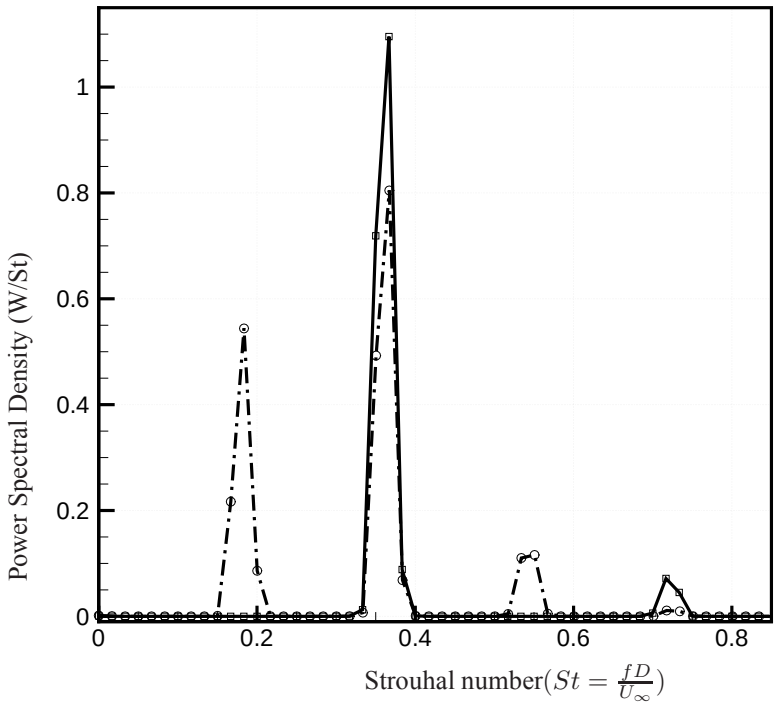

Figure 5.11 - *Comparison of Spectra of the DNS solution: Actuated (dashed line), Un-actuated (solid line).*

of the closed loop system is shown in figure 5.12 for the first two modes showing an asymptotic stability.

The errors are plotted in figure 5.13, also the response of the observer model is shown in figure 5.14. The response of the observer shows that the state for the pressure goes to zero asymptotically, but we find large values of gain for the short period of the DNS simulation, where we implement the control. This necissates the scaling of the final control introduced.

5.4 Conclusion

A feedback control law based on the estimation of the observer dynamics has been presented. The observer matrix is constructed using a linear stochastic estimation. A sensititivity study of the actuated dynamics has been performed to determine the relevant terms to be retained in the linearisation of the model. Finally an LQG based feedback law is obtained to find the optimal solution. The optimal control law is shown to have a single frequency, corresponding to the second Rossiter mode of the cavity flow. The LQG control provides stabilisation over infinite time horizon with a huge control

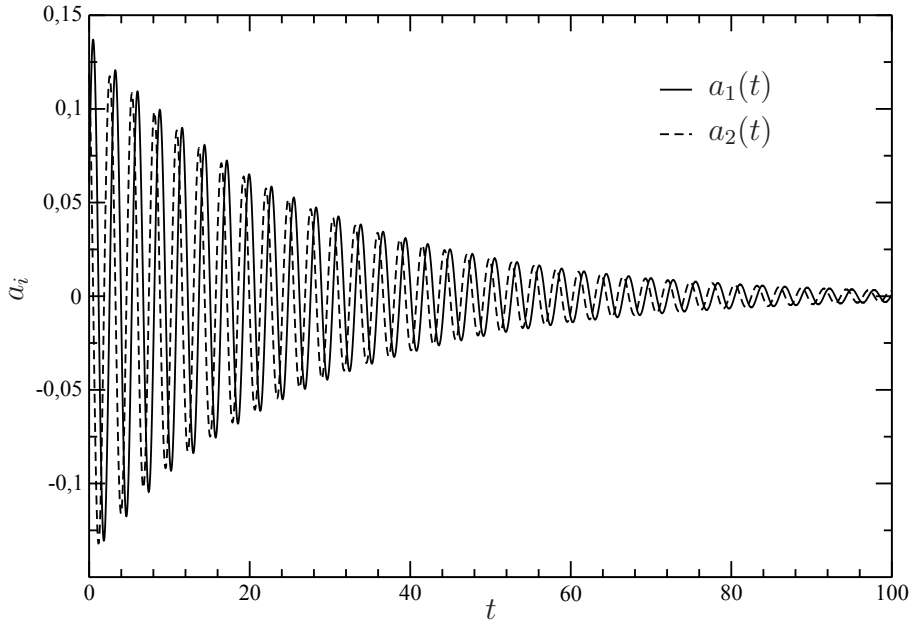

Figure 5.12 - *System response of the full system for the state components a_1 and a_2*

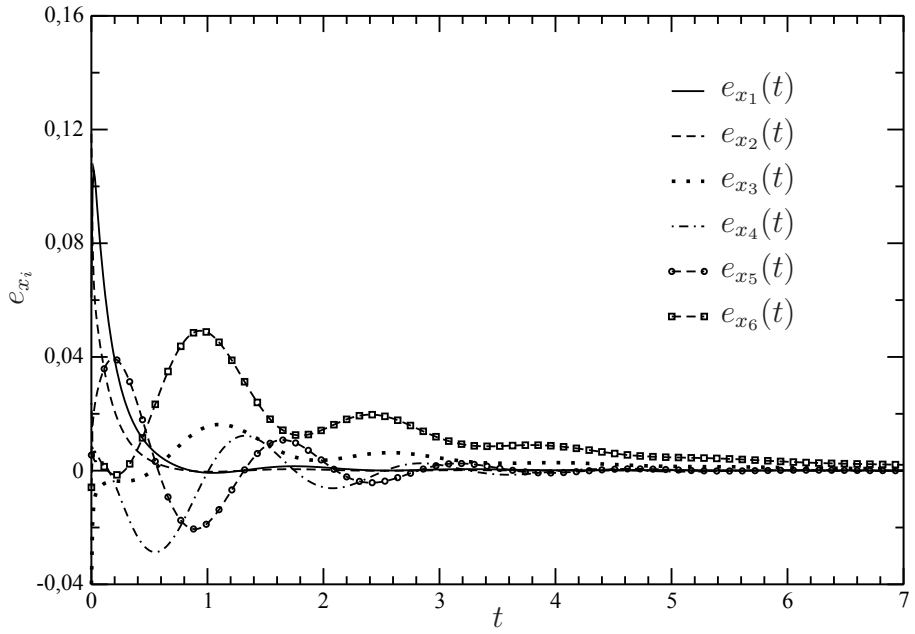

Figure 5.13 - *Error on the components of the state e_x*

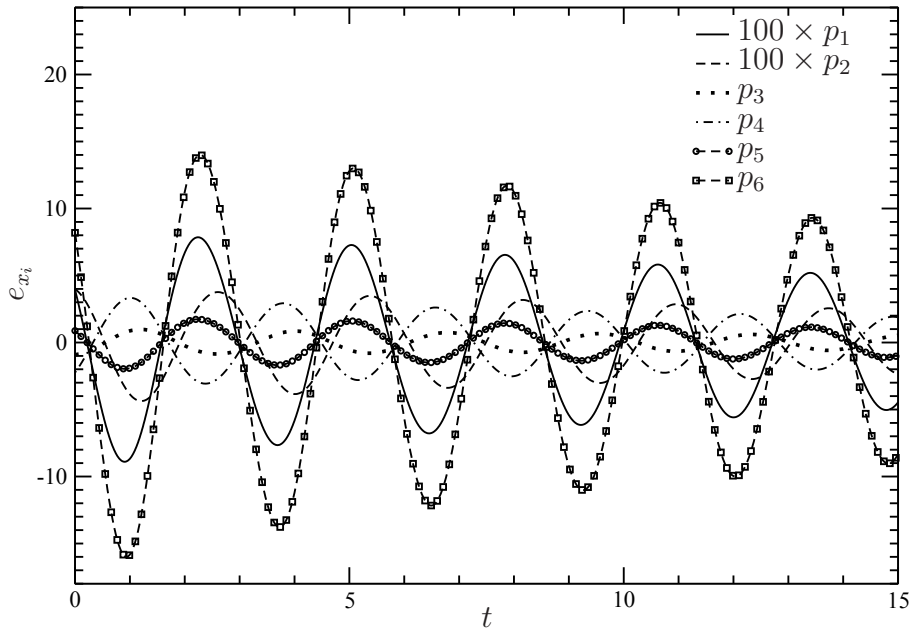

Figure 5.14 - *Output prediction y, the pressure fluctuations for the 6 modes. mode 1 and 2 have been rescaled by 100.*

amplitude, unrealistic to be utilised in the Direct Numerical Simulation which are solved over a short time interval. To resolve this problem, the control amplitude has been scaled down before introducing in Direct Numerical Simulation. The control provides a decrease in spectra corresponding to the second Rossiter mode.

Conclusions and Perspectives

Nous avons dans ce travail nous avons appliqué la réduction de modèle sur un écoulement de cavité puis nous l'avons étendu dans le cas d'un écoulement contrôlé dans le but ultime de réduire les émissions acoustiques. Les champs de vitesse et de pression sont déterminés, sans ou avec un forçage de type jet synthétique ou multifréquentiel par des simulations numériques directes, au voisinage du coin amont de la cavité, zone la plus sensible à une perturbation. Pour notre configuration, c'est le second mode de Rossiter qui est excité.

La base réduite est obtenue par décomposition orthogonal en modes propres, et un système dynamique d'ordre faible est déterminée par projection de Galerkin des équations isentropiques avec un produit scalaire basé sur l'énergie. Les quatre premiers modes représentent 98.5% *de l'énergie fluctuante totale La prise en compte, dans le modèle réduit du forçage est faite à partir d'un problème d'optimisation Kasnakoğlu et al. (2008), en déterminant un mode spatial spécifique orthogonal aux autres modes non forcés déjà connus. Dans ce cadre, il est supposé que l'écoulement moyen dans le cas forcé et non forcé sont identiques. Suite à l'introduction d'une erreur mesurant ce possiblè effet, l'hypothèse s'avère justifier pour des amplitudes du contrôle inférieur à* 10% *environ.*

Les modèles dynamiques obtenus par cette approche POD et projection de Galerkin sont connus pour être naturellement fortement instable. Nous avons donc stabilis les modèles en testant trois méthodes de calibration. L'approche de Couplet et al. (2005) qui met en oeuvre un problème d'optimisation o est minimisée l'erreur entre le champ des vitesse donné par la simulation numérique directe et celui obtenu par intégration du système dynamique. Suite aux travaux de Cordier et al. (2009), nous avons proposé d'ajouter une régularisation de la fonctionnelle coût à minimiser par une approche de Tikhonov dans laquelle nous avons introduit des poids basés sur la sensibilité la fonctionnelle par rapport aux coefficients temporels du système dynamique. Quoi qu'il en soit, on conclut qu'une régularisation sur un long temps d'intégration est nécessaire pour éviter toute divergence du système dynamique.

Le système dynamique forcé, après linéarisation a servi de base pour concevoir un contrôle linéaire quadratique Gaussien (loi de contrôle en boucle fermée). Un modéle d'observation liant la pression en certains points de l'écoulement et les variables d'état (vitesses) a été construit sur la base d'une estimation stochastique linéaire. A partir d'une loi de forçage multifréquentielle introduite dans les simulations numériques directes, et donc dans le mode de forçage du syst 'eme dynamique, nous obtenons une loi de contrôle optimale qui se révèle être parfaitement harmonique à une fréquence très proche du second mode de Rossiter. Cette nouvelle loi, introduite dans les simulations numériques directes a conduit à une réduction sensible des émissions acoustiques sur le second mode de Rossiter. Par contre, de faibles excitations sur d'autres fréquences subharmoniques

ou harmoniques sont visibles.

Apparemment, les modes POD tels qu'ils sont déterminés actuellement (critère énergétiques) ne sont pas les modes optimaux pour analyser ou réduire l'acoustique. Comme perspective de ce travail, il pourrait être judicieux de réfléchir sur l'introduction de l'approche de Jordan et al. (2007) basée sur une décomposition en des modes les plus observables vis-à-vis de l'acoustique en champ lointain. Il faudrait aussi certainement regarder l'influence de la taille du système dynamique (troncature) sur le contrôle aéroacoustique, les modes négligés pouvant jouer un grand rôle dans les émissions.

Une autre perspective serait d'étudier la réduction de modèle et la construction du mode de forçage sur la base d'un forçge stochastique plutôt que déterministe comme cela est fait actuellement.

Les études de sensibilités et l'utilisation d'opérateurs adjoints devraient aussi être accrues pour tenter d'amériorer soit le modèle réduit avec forçage, soit la calibration.

Le contrôle optimal en boucle ouverte avec région de confiance a été mené dans Bergmann et al. (2009) sur le cylindre et une extension à la cavité pourrait être explorée.

L'estimation d'état, qui est une partie du probléme de contrôle en boucle fermée pourrait être améliorée, par exemple en utilisant une estimation stochastique quadratique qui conduirait à une observateur non linéaire. La non linéarité apparaâit aussi dans le système dynamique forcé. On pourrait donc envisager d'appliquer un contrôle non linéaire dans ce cadre.

In this thesis we have developed and applied the various tools of a POD based reduced order modelling to study the self-sustained instabilities in a cavity. The ROM has been applied to perform control studies with the ultimate aim of reducing the noise level in the cavity.

Direct Numerical Simulation of the cavity flow has been performed. The cavity flow results has been validated with the results from literature. Control is introduced by means of a synthetic jet at the upstream edge of the cavity where the flow is more sensitive to perturbations. Analysis of the spectra shows a decrease in the amplitude corresponding to the second Rossiter mode of the cavity, which suggest the need of performing an optimal control study.

The basic theory of POD and their various properties which make them useful in the approximation of fluid flow has been discussed. The usual innerpoduct gives the natural definition of the norm of the energy of the fluid flow in case of incompressible flows. The choice of inner-product for the case of compressible, which gives the definition of energy has been discussed. The energy based inner-product as described in Rowley *et al.* (2003) has been used in this work to obtain the POD modes and for the Galerkin projection.

The eigen spectra demonstrates that the first 4 eigenmodes capture around 98.5% of the total fluctuation energy as shown by the Relative Information Content (RIC). A degenerate eigen spectrum showing eigenvalues which occur in pairs demonstrates the phasing behaviour of the flow. The vorticity modes mainly represent the hydrodynamic component and the dilatation the propagation of the acoustic waves. We note the energy cascade in the POD representation of the vorticity in terms of the size of the eddies represented. The vorticity being a hydrodynamic phenomenon represents the low frequency dynamics of the flow. The dilatation which represents the direction of the sound propagation, a high frequency phenomenon, is clearly depicted for the higher POD modes, where the angle of the wave propagation is distinctly visible thus indicating the presence of a multi-scale phenomenon.

ROM based on the isentropic Navier-Stokes equations which are used to model the cavity flows has been constructed. Extension of the ROM to include the effect of actuation, is done by constructing an actuated mode, obtained by solving an L_2 optimisation problem as demonstrated in Kasnakoğlu *et al.* (2008). The main feature of this approach is that the effect of actuation is explicitly available in our ROM and the un-actuated dynamics reproduced exactly in case the value of actuation tends to zero. The spatial modes exhibit a local behaviour capturing the effect of actuation. For small values of actuation (less than 10%) the mean value of the actuated and the un-actuated case can be assumed to be equal. In that case the difference in the average error can be interpreted as a translation of the reduced order subspace, which means that it is sufficient to consider the temporal coefficients of the un-actuated case. An error to take care of the difference in the average values while performing the Galerkin projections has been introduced, and shows a small errors for the most energetic modes.

The ROM compares well with the POD coefficients for the initial time and shows a divergence as time progresses. To take care of the divergence of the model, various techniques known as calibration techniques has been studied and a unified framework for the different calibration methods described in the literature is given. An application to the cavity flow demonstrates that the method of calibration which involves the solution of a constraint optimisation problem Bergmann & Cordier (2005) is better than the method of intrinsic stabilisation Kalb & Deanne (2007). The method of Couplet *et al.* (2005) based on the minimisation of functional based on the convex linear combination of terms which represent the normalised error and a measure of the variation of the coefficients of the model to

their values obtained from POD is found to be the better of the two above methods in terms of the normalised errors.

The only disadvantage of this method being the arbitrary parameter to be chosen while regularising the ill-conditioned linear system. The method presented in Cordier *et al.* (2009), remedies the problem by using the method of Tikhonov regularization, which chooses the parameter so as to balance between the solution norm and the residual norm. This is applied to the case of cavity flow and shown to perform better than the method of Couplet *et al.* (2005) for the normalised error. However the cost of calibration is more. The cost as argued out is shown to outweigh the benefits of a good model especially when we perform control studies.

A new contribution toward the calibration method has been the weighted Tikhonov regularization which takes care of the sensitivity of the modes with respect to a given cost functional, while defining the errors for calibration. The second way of introducing the weight matrix is to consider the spectra content of the POD decomposition. We compared the errors for the two type of Tikhonov regularization and it is found that the zeroth order regularization is the most effective among all the type of Tikhonov regularization considered. The proposed method outweighs the other methods in terms of errors. It is also shown that the model diverges for a long time of integration even after calibration, and it is necessary to calibrate over a long period of time, especially when performing control studies as shown in Nagarajan *et al.* (2009*b*).

A feedback control law based on the estimation of the observer dynamics has been presented. The observer matrix is constructed using a linear stochastic estimation. A sensititivity study of the actuated dynamics has been performed to determine the relevant terms in the linearisation of the model. Finally an LQG based feedback law is obtained to find the optimal solution. The optimal control law is shown to have a single frequency, corresponding to the second Rossiter mode of the cavity flow. The LQG control provides stabilisation over infinite time horizon with a huge control amplitude, unrealistic to be utilised in the Direct Numerical Simulation which are solved over a short time interval. To resolve this problem, the control amplitude has been scaled down before introducing in Direct Numerical Simulation. The control provides a decrease in spectra corresponding to the second Rossiter mode Nagarajan *et al.* (2009*a*).

As a future perspective it is observed that the POD modes which is an optimal representation of the energy fields is not suitable to resolve the far field acoustic, one of the extension of POD to include the effect of far field acoustic noise is the Most Observable Decomposition, as demonstrated in Jordan *et al.* (2007) which represent a good choice of bases to perform control studies for acoustics. Also it is interesting to minimise a cost functional which measures the acoustic propagation rather than the functional based on the energy. It will be interesting to note that the higher modes which are hydrodynamically in-significant will play a significant role in the acoustics, hence a comparison to determine the minimum number of POD modes to tackle the acoustics would be interesting (for a preliminary derivation for the open loop control see appendix H).

For the development of the reduced order model an interest would be to construct the ROM for a given random noise rather than the deterministic forcing we have used in this work. Sensitivity studies to external forcing to determine the position of the actuator is worth exploring. Open loop control by the method of trust regions is another area which can be explored. Improvement of the reduced order subspace during the optimisation process when the control parameter changes so that the first few

modes represent the dynamics of the new conf guration as demonstrated in Bergmann *et al.* (2009) can be applied to the study of the cavity f ow conf guration. It is also interesting to build and calibrate the ROM from experimental data.

For the application of the closed loop control the problem of estimation can be improved by a higher order Quadratic Stochastic Estimation (QSE) *i.e.* the by constructing a non-linear observer. It would also be interesting to consider the quadratic terms in the actuation and hence perform a non-linear control. The real challenge of a reduced order model is in using measurements from real time simulations (experimental or high turbulence simulation), to build up the control.

Annexes

Appendix A

Controllability and observability of linear systems

The equation of the plant with a feedback can be written as

$$\dot{x} = Ax + Bu \tag{A.1a}$$
$$y_c = Cx \tag{A.1b}$$

where $A \in \mathbb{R}^{n\times n}$, $B \in \mathbb{R}^{n\times m}$, $C \in \mathbb{R}^{p\times n}$

Theorem The following conditions for the controllability are equivalent

1. system (A.1) is controllable
2. An arbitrary state x is attainable from 0
3. The matrix $Q_T := \int_0^T e^{At}BB^T e^{A^T t}dt$ is non singular for any arbitrary $T > 0$. This condition is equivalent to determining the norm of the state matrix for an impulse response.
4. Rank of the matrix $[A|B] := [B, AB, \cdots A^{n-1}B] = n$, also reffered to as the Kalman's condition
5. Q_T satisfy the Lyapnov equation

$$AQ_T + Q_T A^T + BB^T = 0 \tag{A.2}$$

The above theorem can be reformulated for the Observibility by, considering the controllability of the dual system given by

$$\dot{z} = A^T z + C^T u \tag{A.3a}$$
$$y = B^T z \tag{A.3b}$$

where z is the dual state vector.

Appendix B

Galerkin projections for the full NS equations

As described in Rowley *et al.* (2003) the full Navier-Stokes equation can be written as

$$\begin{aligned}
\frac{D\rho}{Dt} + div\mathbf{u} &= 0 \\
\rho\frac{Du_i}{Dt} &= -\frac{\partial p}{\partial x_i} + \frac{1}{Re}\frac{\partial}{\partial x_j}\left(2S_{ij} - \frac{2}{3}\delta_{ij}div\mathbf{u}\right) \\
\rho\frac{DT}{Dt} + (\gamma-1)\rho T div\mathbf{u} &= \frac{\gamma}{Re}\left(2S_{ij}S_{ij} - \frac{2}{3}(div\mathbf{u})^2\right) + \frac{\gamma}{RePr}\nabla^2 T
\end{aligned} \tag{B.1}$$

The equations are non-dimensionalised using the length scale L, the speed of sound c_∞ and the ambient density ρ_∞. Temperature is non-dimensionalised by $\frac{c_\infty^2}{c_p}$ and pressure by ρc_∞^2. Here $P = (\gamma-1)\rho T$ and $S_{ij} = \frac{1}{2}(\frac{\partial u_i}{\partial x_j} + \frac{\partial u_i}{\partial x_j})$ is the symmetric part of the stress tensor, denoting the strain rate. On introducing the notation $q = (\rho, u_i, T)$ the above equations can be re-casted as

$$\frac{\partial\rho}{\partial t} = \mathcal{R}(q), \qquad \rho\frac{\partial u_i}{\partial t} = \mathcal{U}_i(q), \qquad \rho\frac{\partial T}{\partial t} = \theta(q)$$

where,

$$\begin{aligned}
\mathcal{R}(q) &= -(\mathbf{u}.\nabla)\rho - div\mathbf{u} \\
\mathcal{U}_i(q) &= -\rho(\mathbf{u}.\nabla)u_i - \frac{\partial p}{\partial x_i} + \frac{1}{Re}\frac{\partial}{\partial x_j}\left(2S_{ij} - \frac{2}{3}\delta_{ij}div\mathbf{u}\right) \\
\theta(q) &= -(\gamma-1)\rho T div\mathbf{u} + \frac{\gamma}{Re}\left(2S_{ij}S_{ij} - \frac{2}{3}(div\mathbf{u})^2\right) + \frac{\gamma}{RePr}\nabla^2 T
\end{aligned} \tag{B.2}$$

The equations can be further written in a concise form as

$$A(q)\dot{q} = f(q) \tag{B.3}$$

where $A(q) = diag(1, \rho, \rho, \rho)$ and $f(q) = (\mathcal{R}(q), \mathcal{U}_i(q), \theta(q))$ Since A is a aff ne function of q we can write

$$A(q) = B + L(q) = diag(1,0,0,0) + diag(0,\rho,\rho,\rho)$$

also since f is cubic it can be written as a sum of multi-linear forms f_i as

$$f(q) = f_1(q) + f_2(q,q) + f_3(q,q,q)$$

We now perform a Galerkin projection of the POD bases ϕ_k and expressing

$$q = \sum_k a_k(t)\phi_k$$

B.3 becomes

$$\left[B + L(\sum_l a_l\phi_l)\right] \sum_k \dot{a_k}\phi_k = f(q) \tag{B.4}$$

on taking the inner-product with ϕ_k we obtain:

$$\sum_k \dot{a}_k \left(\langle \phi_j, B\phi_k \rangle + \sum_l a_l \langle \phi_j, L(\phi_l)\phi_k \rangle \right) = \langle \phi_j, f(q) \rangle \tag{B.5}$$

In matrix form equation B.5 can be written as

$$M(a)\dot{a} = \tilde{f}(a) \tag{B.6}$$

where $a = (a_1, \ldots, a_n)$ and

$$M(a)_{jk} = \langle \phi_j, B\phi_k \rangle + \sum_l a_l \langle \phi_j, L(\phi_l)\phi_k \rangle$$

$$\begin{aligned} \tilde{f}_j(a) &= \langle \phi_j, f(q) \rangle \\ &= \sum_l a_l \langle \phi_j, f_1(\phi_l) \rangle + \sum_{l,m} a_l a_m \langle \phi_j, f_2(\phi_l, \phi_m) \rangle + \sum_{l,m,n} a_l a_m a_n \langle \phi_j, f_3(\phi_l, \phi_m, \phi_n) \rangle \end{aligned}$$

Note that all the coeff cients of the equation B.7 can be determined before solving the ODE's. In the case of constant density we have $B = I$, $L = 0$ also if we chose the spatial modes orthogonal *i.e.* we have $\langle \phi_i, \phi_j \rangle = \delta_{ij}$ and the mass matrix M is identity. Although equation B.7 is in principle not diff cult to solve the choice of the quadratic approximations with the isentropic equations simplif es the implementation. Also the choice of the energy based inner-product which preserves the energy is quite natural to the cold f ows we treat.

Appendix C

Specific volume formulations of ROM

As noted in the appendix A, the low-order model of the full Navier-Stokes equation has cubical implicit terms, Vigo (1998) suggests the use of a formulation by using the primitive variables (u, v, p) and the specif c volume $\varsigma = \frac{1}{\rho}$. The fully compressible Navier-Stokes equation in terms of these variables can be written as:

$$\begin{aligned}
\varsigma_t &= -u\varsigma_x + u_x\varsigma + v_y\varsigma - v\varsigma_y \\
u_t &= -uu_x - vu_y - \varsigma p_x + \frac{1}{Re}\varsigma\left[\left(\frac{4}{3}u_x - \frac{2}{3}v_y\right)_x + (u_x + u_y)_y\right] \\
v_t &= -uv_x - vv_y - \varsigma p_y + \frac{1}{Re}\varsigma\left[\left(\frac{4}{3}v_y - \frac{2}{3}u_x\right)_y + (v_x + u_y)_x\right] \\
p_t &= -up_x - vp_y - \gamma p(u_x + v_y) + \frac{\gamma}{RePr}[(p\varsigma)_{xx} + (p\varsigma)_{yy}] \\
&+ \frac{\gamma - 1}{Re}\left[u_x\left(\frac{4}{3}u_x - \frac{2}{3}v_y\right) + v_y\left(\frac{4}{3}v_y - \frac{2}{3}u_x\right) + (v_x + u_y)^2\right]
\end{aligned} \tag{C.1}$$

On introducing $q = (\varsigma, u, v, p)$ the above equation can be re-casted as

$$\dot{q} = \mathcal{Q}_1(q^1, q^2) + \frac{1}{Re}\mathcal{Q}_2(q^1, q^2) \tag{C.2}$$

with

$$\mathcal{Q}_1(q^1, q^2) = -\begin{pmatrix} u^1 v_x^2 - u_x^2\varsigma^1 - v_y^2\varsigma^1 + v^1\varsigma_y^2 \\ u^1 u_x^2 + v^1 u_y^2 + \varsigma^1 p_x^2 \\ u^1 v_x^2 + v^1 v_y^2 + \varsigma^1 p_y^2 u^1 p_x^2 + v^1 p_y^2 + \gamma p^1(u_x^2 + v_y^2) \end{pmatrix}$$

$$\mathcal{Q}_2(q^1, q^2) = \begin{pmatrix} 0 \\ \varsigma^1\left[\left(\frac{4}{3}u_x^2 - \frac{2}{3}v_y^2\right)_x + \left(u_x^2 + u_y^2\right)_y\right] \\ \varsigma^1\left[\left(\frac{4}{3}v_y^2 - \frac{2}{3}u_x^2\right)_y + \left(v_x^2 + u_y^2\right)_x\right] \\ \frac{\gamma}{Pr}[(p^2\varsigma^1)_{xx} + (p^2\varsigma^1)_{yy}] + \\ (\gamma - 1)\left[u_x^1\left(\frac{4}{3}u_x^2 - \frac{2}{3}v_y^2\right) + v_y^1\left(\frac{4}{3}v_y^2 - \frac{2}{3}u_x^2\right) + \left(v_x^1 + u_y^1\right)\left(v_x^2 + u_y^2\right)\right] \end{pmatrix}$$

The above formulation preserves the quadratic dynamics and hence the deriving a ROM is straight forward as in the case of the isentropic case. If q is expressed in terms of the POD bases as:

$$q(\mathbf{x},t) = \overline{q(\mathbf{x})} + \sum_{i}^{N} a_i(t)\phi_i(\mathbf{x}) \tag{C.3}$$

with the def nition of inner product for the non-dimensional variables given by:

$$\langle q^1, q^2 \rangle = \int_\Omega \left(\varsigma^1\varsigma^2 + u^1u^2 + v^1v^2 + p^1p^2 \right) d\Omega \tag{C.4}$$

inserting C.3 in C.2 we have the ROM as:

$$\begin{aligned}
\dot{a}_k &= \sum_{i=1}^{N} a_i \langle \mathcal{Q}_1(\overline{q},\phi_i) + \mathcal{Q}_1(\phi_i,\overline{q}),\phi_k\rangle + \sum_{i,j=1}^{N} a_i a_j \langle \mathcal{Q}_1(\phi_i,\phi_j),\phi_k\rangle \\
&+ \sum_{i=1}^{N} a_i \langle \mathcal{Q}_2(\overline{q},\phi_i) + \mathcal{Q}_2(\phi_i,\overline{q}),\phi_k\rangle + \sum_{i,j=1}^{N} a_i a_j \langle \mathcal{Q}_1(\phi_i,\phi_j),\phi_k\rangle \qquad \text{(C.5)} \\
&= \sum_{i=1}^{N} (L^1_{ik} + L^2_{ik}) a_i + \sum_{i,j=1}^{N} (\mathcal{Q}^1_{ijk} + \mathcal{Q}^2_{ijk}) a_i a_j \qquad \text{(C.6)}
\end{aligned}$$

where

$$\begin{aligned}
\mathcal{Q}^1_{ijk} &= \langle \mathcal{Q}_1(\phi_i,\phi_j),\phi_k\rangle \\
\mathcal{Q}^2_{ijk} &= \langle \mathcal{Q}_2(\phi_i,\phi_j),\phi_k\rangle \\
L^1_{ik} &= \langle \mathcal{Q}_1(\overline{q},\phi_i) + \mathcal{Q}_1(\phi_i,\overline{q}),\phi_k\rangle \\
L^2_{ik} &= \langle \mathcal{Q}_2(\overline{q},\phi_i) + \mathcal{Q}_2(\phi_i,\overline{q}),\phi_k\rangle
\end{aligned}$$

The system above can be solved with or without the subtraction of the mean in the latter case we have $L^1_{ik} = L^2_{ik} = 0$

Appendix D

Actuated POD by the method of stochastic estimation

The method as described in Caraballo *et al.* (2008) relies on a POD expansion, followed by a stochastic estimation to correlate the time coeff cients with the actuation input. The method can be summarized as follows

Algorithm:

1. To start , let the actuated snapshot sets be denoted as $\{q_k^{ac}, \gamma_k\}_{k=1}^{M}$, where $\gamma_k = \gamma(t_k)$ is the value of the actuation, $q_k^{ac} = q^{ac}(\mathbf{x}, t_k)$ and M is the number of actuated snapshots

2. We subtract the mean $\overline{q}$ of the un-actuated base f ow from the snapshot set. We def ne a new set of realisations by an innovation operator given as

$$\tilde{q_k} = q_k^{ac} - P_{\mathcal{S}} q_k^{ac} = q_k^{ac} - \sum_{i=1}^{n} \langle q_k^{ac}, \phi_{\mathbf{i}} \rangle \, \phi_{\mathbf{i}}$$

3. Perform the POD on the innovative snapshots $\{\tilde{q_k}\}$ to obtain an expansion for the f ow f eld of the form.

$$q(\mathbf{x}, t) = \sum_{i=1}^{N} a_i(t)\phi_i(x) + \sum_{i=1}^{M} a_i^{ac}(t)\phi_i^{ac}(x) \tag{D.1}$$

   where $a_i^{ac}(t) = \langle q, \phi_i^{ac} \rangle$

4. We wish to correlate the coeff cient $a_i^{ac}(t)$ to the input signal $\gamma(t)$ by means of a linear stochastic estimation of the form

$$a_i^{ac}(t) \approx A_i \gamma(t) + B_i \gamma^2(t) \tag{D.2}$$

where A_i and B_i are the linear and quadratic terms of the estimator. Substituting D.2 in D.1 we have

$$q(\mathbf{x},t) = \sum_{i=1}^{N} a_i(t)\phi_i(\mathbf{x}) + \gamma(t)\psi_1(\mathbf{x}) + \gamma(t)\psi_1(\mathbf{x})$$

where

$$\psi_1(\mathbf{x}) := \sum_{i=1}^{M} \phi_i^{ac}(\mathbf{x})A_i \quad \text{and} \quad \psi_2(\mathbf{x}) := \sum_{i=1}^{M} \phi_i^{ac}(\mathbf{x})B_i$$

The Galerkin model with the above expansion is of the form

$$\begin{aligned} \dot{a_k} &= C_k + L_{jk}a_j + Q_{ijk}a_i a_j + h_{1k}\gamma + h_{2ik}a_i\gamma \\ &+ (h_{3k} + g_{1k})\gamma^2 + g_{2ik}a_i\gamma^2 + g_{3k}\gamma^4 + g_{4k}\gamma^3 \end{aligned} \tag{D.3}$$

where

$$\begin{aligned} C_k &= \langle L(\overline{q}), \phi_k\rangle + \langle Q(\overline{q},\overline{q}), \phi_k\rangle \\ L_{jk} &= \langle L(\phi_j), \phi_k\rangle + \langle Q(\overline{q},\phi_j), \phi_k\rangle + \langle Q(\phi_\mathbf{j},\overline{\mathbf{q}}), \phi_k\rangle \\ h_{1k} &= \langle L(\psi_1), \phi_k\rangle + \langle Q(\overline{q},\psi_1), \phi_k\rangle + \langle Q(\psi_1,\overline{q}), \phi_k\rangle \\ Q_{ijk} &= \langle Q(\phi_i,\phi_j), \phi_k\rangle \\ h_{2ik} &= \langle Q(\phi_i,\psi_1), \phi_k\rangle + \langle Q(\psi_1,\phi_i), \psi_1\rangle \\ h_{3k} &= \langle Q(\psi_1,\psi_1), \phi_k\rangle \\ g_{1k} &= \langle L(\psi_2), \phi_k\rangle \\ g_{2ik} &= \langle Q(\phi_k,\psi_2), \phi_k\rangle + \langle Q(\psi_2,\phi_k), \phi_k\rangle \\ g_{3k} &= \langle Q(\psi_1,\psi_2), \phi_k\rangle \\ g_{4k} &= \langle Q(\psi_2,\psi_2), \phi_k\rangle \end{aligned}$$

The above method involves an additional procedures of determining the extra POD actuation modes combined with a stochastic estimation technique and is more complicated than the L_2 optimisation method described in chapter 2, but is much simpler than the sub-domain separation method which involves the identif cation of the control region.

Appendix E

Theorem concerning actuated mode

Theorem . Let $\mathcal{J}(\psi) = E\left[\|\tilde{q}_k - \gamma_k \psi\|^2\right]$

1. The minimum value of $\mathcal{J}(\psi)$ is achieved at

$$\psi^* = \frac{E[\gamma_k \tilde{q}_k]}{E[\gamma_k^2]}$$

2. $\psi^* \in \mathbf{X}$

3. $\psi^* \perp \phi_i$ for $i = 1, \ldots, n$

Proof: Note

1.

$$\begin{aligned} \mathcal{J}(\psi) &= E\left[\|\tilde{q}_k - \gamma_k \psi\|^2\right] \\ &= E\left[\|\tilde{q}_k\|^2 - 2\gamma_k \langle \tilde{q}_k, \psi \rangle + \gamma_k^2 \|\psi\|^2\right] \end{aligned}$$

$\mathcal{J}$ is quadratic with positive leading coeff cient $E[\gamma_k^2]$ and hence has a unique minimum, given by f nding the variation of $\mathcal{J}$ with respect to $\xi \in \mathbf{X}$ given by

$$\begin{aligned}
\frac{d}{d\delta}|_{\delta=0}\mathcal{J}(\psi+\delta\xi) &= \frac{d}{d\delta}|_{\delta=0}E\left[\|\tilde{q_k}\|^2 - 2\gamma_k\langle\tilde{q_k},\psi+\delta\xi\rangle + \gamma_k^2\|\psi+\delta\xi\|^2\right] \\
&= E\left[-2\gamma_k\langle\tilde{q_k},\xi\rangle + \gamma_k^2\langle\psi+\delta\xi,\xi\rangle + \gamma_k^2\langle\xi,\psi+\delta\xi\rangle\right]|_{\delta=0} \\
&= E\left[-2\gamma_k\langle\tilde{q_k},\xi\rangle + \gamma_k^2\langle\psi,\xi\rangle + \gamma_k^2\langle\xi,\psi\rangle\right] \\
&= E\left[-2\gamma_k\langle\tilde{q_k},\xi\rangle + 2\gamma_k^2\langle\psi,\xi\rangle\right] \\
&= E\left[\langle-2\gamma_k\tilde{q_k} + 2\gamma_k^2\psi,\xi\rangle\right] \\
&= \langle E\left[-2\gamma_k\tilde{q_k} + 2\gamma_k^2\psi\right],\xi\rangle
\end{aligned}$$

for ψ to be an extremum its f rst variation must vanish $\forall\xi \in \mathbf{X}$ hence we have

$$E\left[-2\gamma_k\tilde{q_k} + 2\gamma_k^2\psi\right] = 0$$

which by linearity of E implies

$$\psi^* = \frac{E[\gamma_k\tilde{q_k}]}{E[\gamma_k^2]}$$

2. $\psi^* \in \mathbf{X}$ follows from the linearity of E and noting that $\gamma_k\tilde{q_k} \in \mathbf{X}$ and $E(\gamma_k^2) \in \mathbb{R}$

3. To show that $\psi^* \perp \phi_i$ for $i = 1,\ldots,N$, we note that $\tilde{q_k} \in \text{Span}\{\phi_i\}$ we have for any i and k

$$\begin{aligned}
\langle\tilde{q_k},\phi_i\rangle &= \langle q_k^{ac} - \sum_{i=1}^{n}(q_k^{ac},\phi_{\mathbf{i}})_\Omega\,\phi_{\mathbf{i}},\phi_i\rangle \\
&= \langle q_k^{ac},\phi_i\rangle - \sum_{i=1}^{N}\langle q_k^{ac},\phi_i\rangle\langle q_k^{ac},\phi_j\rangle \\
&= \langle q_k^{ac},\phi_i\rangle - \langle q_k^{ac},\phi_i\rangle \\
&= 0
\end{aligned}$$

Using the linearity of the averaging operator E and the inner product we have

$$\begin{aligned}
\langle \psi^*, \phi_i \rangle &= \left\langle \frac{E[\gamma_k \tilde{q}_k]}{E[\gamma_k^2]}, \phi_i \right\rangle \\
&= \frac{E\left[\gamma_k \langle \tilde{q}_k, \phi \rangle\right]}{E[\gamma_k^2]} \\
&= \frac{E[0]}{E[\gamma_k^2]} \\
&= 0
\end{aligned}$$

Hence we have $\phi_i \perp \psi^*$ for $i = 1, \ldots, N$

Appendix F

Generalized Singular Value Decomposition (GSVD)

Let $A \in \mathbb{R}^{m\times n}$ and $L \in \mathbb{R}^{p\times n}$ be given with $m \geq n \geq p$. There exists orthogonal matrices $U \in \mathbb{R}^{m\times n}$ and $V \in \mathbb{R}^{p\times p}$ and a nonsingular matrix $X \in \mathbb{R}^{n\times n}$ such that

$$A = U \begin{pmatrix} \Sigma & 0 \\ 0 & I_{n-p} \end{pmatrix} X^{-1} \quad L = V(M, 0)X^{-1}$$

Where $\Sigma = diag(\sigma_1, \cdots, \sigma_p)$ and $M = diag(\mu_i, \cdots, \mu_p)$ with $0 \leq \sigma_1 \leq \cdots \leq \sigma_p \leq 1$ and $1 \geq \mu_1 \geq \cdots \geq \mu_p \geq 0$. Also we have $\sigma_j^2 + \mu_j^2 = 1$ for $j = 1, \cdots, p$.The values $\gamma_j = \frac{\sigma_j}{\mu_j}$ $(j = 1, \cdots, p)$ are called the generalised singular values of (A, L). The j^{th} column x_j of X is the right singular vector associated with σ_j

Appendix G

Open loop control

G.1 Open loop control of cavity flows

Regarding the use of ROM for optimal control studies using an open loop one can refer to Bergmann & Cordier (2005) where the optimal control has been applied for the control of wake flows behind a cylinder. Since the ROM is designed for a particular flow condition Fahl (2000) propose a method where the model is refined during the optimisation process, to take care of the validity of the model to the variation of control parameters. This method has been applied for the optimal control of wake flows by Bergmann & Cordier (2008).

In this Appendix the basic equations and results are given for the open loop control. The aim is to reduce the noise level in the cavity, for which as a first step, a control based on cost functional which reduces the total energy of the system hence also reduces the noise level. Mathematically this is equivalent to minimising the functional given by

$$\begin{aligned} \mathcal{J}(\tilde{q},\gamma(t)) &= \int_0^T \int_\Omega J(q(x,t),\gamma(t))d\Omega dt \\ &= \frac{\alpha}{2}\int_0^T \int_\Omega \|q(x,t)\|_2^2 d\Omega dt + \frac{\beta}{2}\int_0^T \gamma^2(t)dt \end{aligned} \tag{G.1}$$

Where $\alpha > 0$ and $\beta > 0$ represents the regularising term and serves as a measure of the cost of the control we would like to utilise in our optimisation process. The minimisation of the cost functional is subjected to the constraint satisfying the ROM, given here for the sake of convenience as

$$\begin{aligned} \dot{a}_k &= \mathcal{N}(a,\gamma(t)) \\ &= C_k + L_{jk}a_j + Q_{ijk}a_i a_j + h_{1k}\gamma + h_{2ik}a_i\gamma + h_{3k}\gamma^2 \end{aligned} \tag{G.2}$$

Using the expression for the POD expansion

$$q(\mathbf{x},t) = \overline{q}(\mathbf{x}) + \sum_{i=1}^{n} a_i(t)\phi_{\mathbf{i}}(\mathbf{x}) + \gamma(t)\psi(\mathbf{x}) \tag{G.3}$$

the above objective functional becomes

$$\begin{aligned}\mathcal{J}(a,\gamma(t)) &= \int_0^T \int_\Omega J(a,\gamma(t))d\Omega dt \\ &= \frac{\alpha}{2}\int_0^T \sum_{i=1}^{n}(a(t))^2 dt + \frac{\beta}{2}\int_0^T \gamma^2(t)dt\end{aligned} \tag{G.4}$$

The optimisation problem to be resolved can be written in a concise form as

$$\begin{cases} \min_{\gamma(t)} \mathcal{J}(a,\gamma(t)) \\ \text{s.t.} \\ \mathcal{N}(a,\gamma(t)) = 0 \end{cases}$$

The constrained optimisation problem can be reduced to an unconstrained by the method of Lagrange multipliers by introducing the adjoint variable ξ and def ning a new functional given by

$$\begin{aligned}\mathcal{L}(a,\gamma,\xi) &= \mathcal{J}(a,\gamma(t)) - \langle \xi, \mathcal{N}(a,\gamma)\rangle \\ &= \mathcal{J}(a,\gamma(t)) - \sum_{i=1}^{n}\int_0^T \xi_i(t)\mathcal{N}_i(a,\gamma)dt\end{aligned} \tag{G.5}$$

The above optimisation problem is solved for stationary values of the above functional given as

$$\delta\mathcal{L} = \frac{\partial\mathcal{L}}{\partial a_i}\delta a_i + \frac{\partial\mathcal{L}}{\partial\gamma}\delta\gamma + \frac{\partial\mathcal{L}}{\partial\xi_i}\delta\xi_i = 0$$

where δa, $\delta\gamma$ and $\delta\xi$ we also suppose that all the arguments of $\mathcal{L}$ is independent and the optimal system is determined by equating each term of the above to zero. On resolving the equation $\frac{\partial\mathcal{L}}{\partial\xi_i}\xi_i = 0$ we recover the equation of state $\mathcal{N}(a,\gamma(t)) = 0$. On equating the derivative with respect to the state variable a we recover the adjoint system of equation given by

$$\frac{d\xi_i(t)}{dt} = -\alpha a_i(t) - \sum_{i=1}^{n}\left(L_{ij} + \gamma(t)h_{2ij} + \sum_{j=1}^{n}\left(Q_{jik} + Q_{jki}\right)a_k(t)\right)\xi_j(t) \tag{G.6}$$

with the terminal condition given by

$$\xi_i(T) = 0$$

Finally on cancelling the derivative with respect to the control we obtain the optimality condition given as

$$\delta\gamma(t) = \beta\gamma + \sum_{i=1}^{n}\left(h_{1i} + \sum_{j=1}^{n}h_{2ij}a_j + 2h_{3i}\gamma(t)\right)\xi_i \tag{G.7}$$

G.2 Resolving the optimal system

An iterative method which uses the method of conjugate gradient coupled with the Armijo method is used to resolve the above optimal system for which the f nal algorithm can be summarized as follows

Algorithm We initialise the control $\gamma(t)$

1. Solve the direct system (G.2) to resolve the equation of state $a(t)$

2. We utilise the state obtained from the step 1, to solve the adjoint equation (G.6) to obtain the adjoint variables $\xi_i(t)$

3. We use the state and the adjoint variable obtained in step 1 and step 2 to evaluate the optimality condition (G.7)

4. The new control law is obtained as $\gamma_{new}(t) = \gamma_{old}(t) + \omega d(t)$ where $d(t)$ is the direction of descent which is obtained by solving the optimality system $\frac{d\mathcal{J}}{d\gamma} = \delta\gamma$ where ω is the direction of descent given by the Armijo method

5. We verify a convergence criteria, and return to step 1

The whole procedure can be summarized as follows

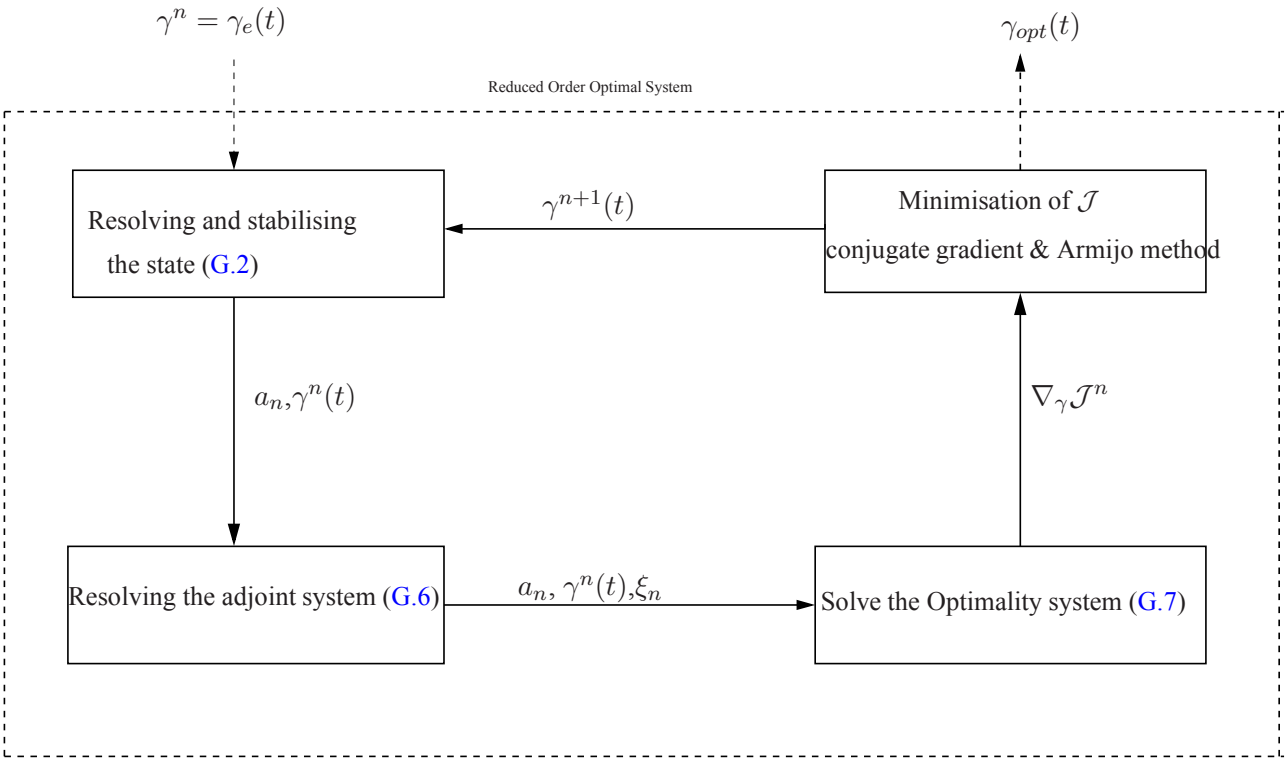

Figure G.1 - *optimal algorithm.*

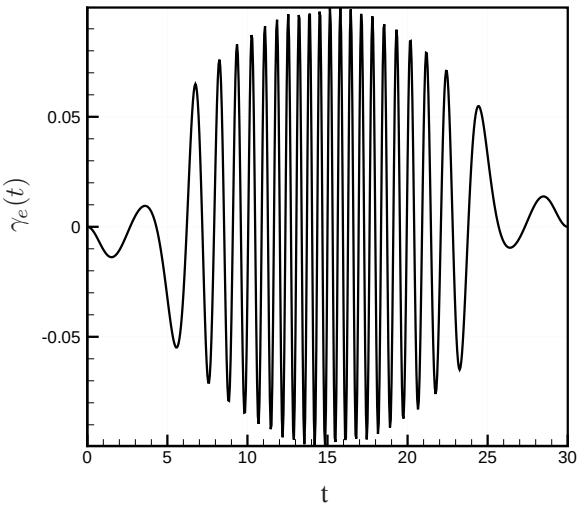

Figure G.2 - *Chirp excitation γ_e : forcing the DNS.*

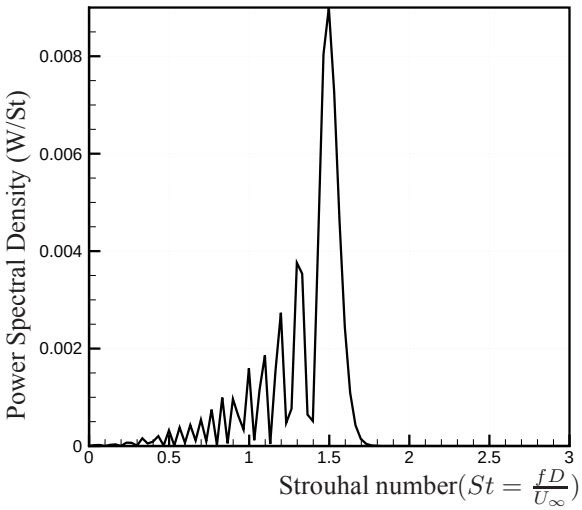

Figure G.3 - *Spectra of the initial chirp.*

G.3 Open loop control of cavity

In this study we build the actuation mode explained in section §3.13 by introducing a chirp excitation of the form.

$$A_1 \sin(2\pi St_1 t) \times \sin\left(2\pi St_2 t - A_2 \sin(2\pi St_3 t)\right) \tag{G.8}$$

where $A_1 = 0.1, A_2 = 27, St_1 = 1/60, St_2 = 2/3, St_3 = 1/30$. Figure G.2, shows the spectra of the excitation as shown in the f gure G.3 shows a frequency width in the range between $0.2 - 1.5$ with a concentration around the frequency 1.5. The Navier Stokes equation is excited with this frequency and about 300 snapshots are sampled which corresponds to the period of excitation $T = 15$ which corresponds to half the period of excitation for the full signal. The actuated mode is constructed with the help of these realisations The parameters $\alpha = 16.0$, $\beta = 0.015$ is chosen in this study. The Algorithm is repeated until we satisfy the convergence criteria for the cost functional given by $|\Delta\mathcal{J}(a,\gamma)| = |\mathcal{J}_{new}(a,\gamma) - \mathcal{J}_{old}(a,\gamma) \leq 10^{-5}|$. The Evolution of the cost functional is as shown in the f gure G.6 and shows a reduction of 10^{-2}, over a period of 1800 iteration of the algorithm. The cpu time of the algorithm is about $900s$. The optimal solution and the spectra of the optimal solution is shown in f gure G.4, and G.5 showing a typical amplitude of 0.08 and a frequency of 0.36, which corresponds to the natural frequency of f ow oscillation. We take this value of amplitude and frequency and introduce in the DNS and compare the value of the velocity spectra taken a point in the shear layer at the downstream edge of the cavity as shown in f gure G.7. At this stage it is worthwhile to note that the initial actuated mode we have added has a rich dynamics, of various frequencies, and hence our solution is only optimal for these range of frequencies and nothing can be said about the global optimality of the NS equation, until we have a fair idea about the sensitivities of the full NS equations. This represents a drawback in the utility of the reduced order model for control purposes

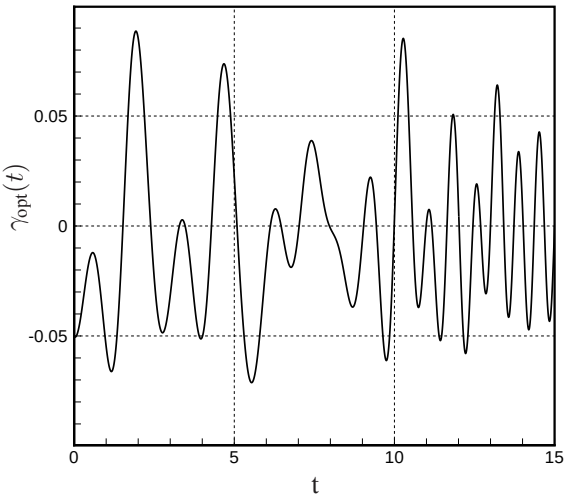

Figure G.4 - *Optimal solution* γ_{opt}.

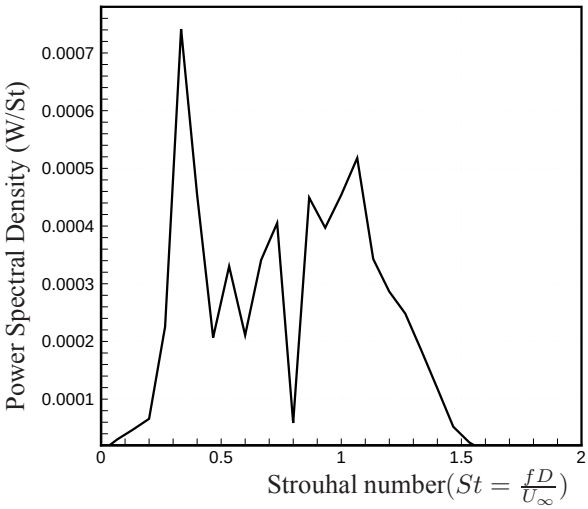

Figure G.5 - *Spectra of the optimal solution.*

when the global optimality of the full system is unknown. However given the time required for the computation of ROM, we can conclude that a coupling of the High f delity model and ROM is an essential part for the successful application of control.

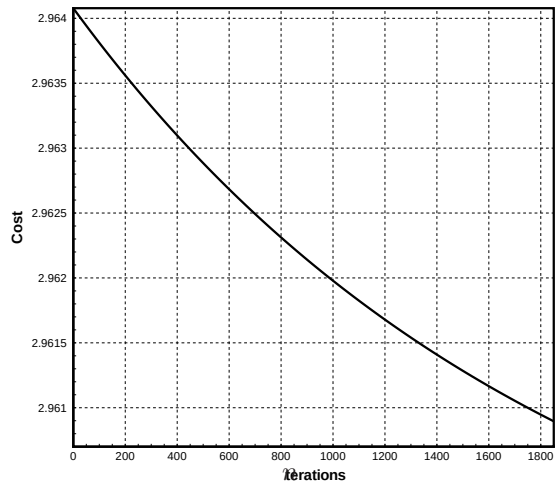

Figure G.6 - *Evolution of the cost functional $\mathcal{J}$.*

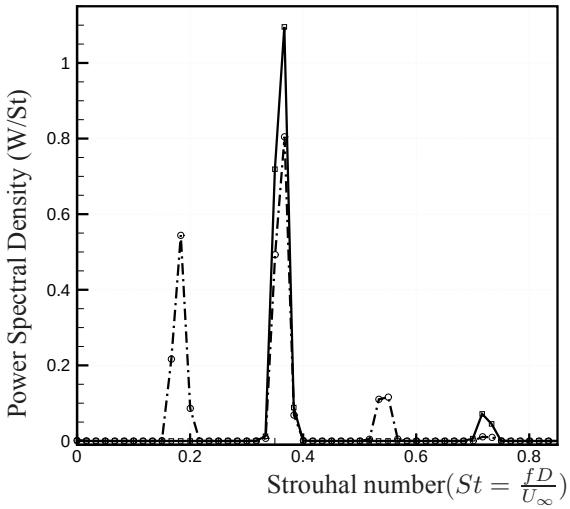

Figure G.7 - *Comparison of Spectra of the original solution and the optimal solution.*

Appendix H

An open loop approach to handle the acoustic terms in ROM

To minimise the acoustic noise it is natural to def ne a functional based on the dilatation operator def ned by

$$\begin{aligned} \mathcal{D} \quad &: \quad H^2(\Omega) \longrightarrow \mathbb{R} \\ (u, v, c) \quad &\longrightarrow \quad \int_\Omega (u_x + v_y)^2 d\Omega \end{aligned} \tag{H.1}$$

The f ow f eld expansion for the actuated case can be written as

$$q = \overline{q} + \gamma(t)\psi + \sum_{i=1}^{n} a_i(t)\phi_i \tag{H.2}$$

On applying the operator $\mathcal{D}$ we obtain

$$\begin{aligned} \mathcal{D}(q) &= \mathcal{D}(\overline{q}) + \gamma(t)\mathcal{D}(\psi) + \sum_{i=1}^{n} a_i(t)\mathcal{D}(\phi_i) \\ &= P + \gamma(t)M + \sum_{i=1}^{n} a_i(t)N_i \end{aligned} \tag{H.3}$$

For the optimisation problem we propose to minimise the functional given by

$$\begin{aligned} \tilde{\mathcal{J}}(a) &= \int_0^T \mathcal{J}(a)dt \quad \text{where} \\ \mathcal{J}(a) &= \sum_{i=1}^{n} a_i(t)N_i \end{aligned} \tag{H.4}$$

The above def nition of the functional gives the time average of the dialation over the period of optimisation. Also note that the above def nition of our functional is not quadratic unlike the def nition

we have used before and hence the process does not guarantee a minimiser. This choice of functional is utilised in Bergmann & Cordier (2008) to minimise the drag around a cylinder. The constraint for our minimisation as in appendix G written here for the sake of convenience as

$$\begin{aligned} \dot{a}_k &= \mathcal{N}(a,\gamma(t)) \\ &= C_k + L_{jk}a_j + Q_{ijk}a_i a_j + h_{1k}\gamma + h_{2ik}a_i\gamma + h_{3k}\gamma^2 \end{aligned} \tag{H.5}$$

The problem then can be written in a compact form as

$$\begin{cases} \min_{(\gamma,a)} \tilde{\mathcal{J}}(a,\gamma) \\ \text{s.t.} \\ \mathcal{N}(a,\gamma) = 0 \end{cases}$$

The Lagrangian for the above problem can be def ned as can be def ned by introducing the adjoint variable ξ

$$\begin{aligned} \mathcal{L}(a,\gamma,\xi) &= \tilde{\mathcal{J}}(a,\gamma) - \langle \xi, \mathcal{N}(a,\gamma)\rangle \\ &= \tilde{\mathcal{J}}(a,\gamma) - \sum_{i=1}^{n}\int_0^T \xi_i(t)\mathcal{N}_i(a,\gamma)dt \end{aligned} \tag{H.6}$$

minimisation of the above functional with respect to the state variable a gives the adjoint equations

$$\frac{d\xi_i(t)}{dt} = -\sum_{i=1}^{n}\left(L_{ij} + \gamma(t)h_{2ij} + \sum_{j=1}^{n}\left(Q_{jik} + Q_{jki}\right)a_k(t)\right)\xi_j(t) - N_i \tag{H.7}$$

with the terminal condition given by

$$\xi_i(T) = 0$$

Finally the optimality system s obtained by f nding the stationary value with respect to the control parameter γ as

$$\Delta_\gamma \mathcal{L} = \int_0^T \sum_{i=1}^{n} P_i \nabla\gamma \mathrm{dt} \tag{H.8}$$

where

$$P_i = \sum_{i=1}^{n}\left(h_{1i} + \sum_{j=1}^{n} h_{2ij}a_j + 2h_{3i}\gamma(t)\right)\xi_i$$

For the form of the forcing $\gamma(t) = A\sin(\omega t)$ which we have used the optimality condition with respect to the amplitude A and the frequency ω can be written as

$$\begin{aligned} \frac{\partial \mathcal{L}}{\partial A} &= \int_0^T (\sum_{i=1}^{n} P_i)\sin(\omega t)\mathrm{dt} \\ \frac{\partial \mathcal{L}}{\partial \omega} &= \int_0^T \omega A t(\sum_{i=1}^{n} P_i)\cos(\omega t)\mathrm{dt} \end{aligned} \tag{H.9}$$

Bibliography

ADRIAN, R. J. & MOIN, P. 1998 Stochastic estimation of organized turbulent structure: homegeneous shear f ow. *J. Fluid Mech* **190**, 531–559. 117

AHUJA, S. & ROWLEY, C. W. 2009 Feedback control of unstable steady states of f ow past a f at plate using reduced-order estimators. *J. Fluid Mech.* p. In Press. 45

ALGAZI, V. R. & SARKINSON, D. J. 1969 On the optimality of the karhunen loève expansion. *IEEE. Trans. Inform. Theory.* **15**, 319–321. 54

ANDREWS, C. A., DAVIES, J. M. & SCHWARTZ, G. R. 1967 Adaptive data compression. *Proc. IEEE.* **55**, 267–277. 54

AUBRY, N., HOLMES, P., LUMLEY, J. L. & STONE, E. 1988 The dynamics of coherent structures in the wall region of a turbulent boundary layer. *J. Fluid Mech.* **192**, 115–173. 48, 51, 68, 71, 92

BAGHERI, S., BRANDT, L. & HENNINGSON, D. S. 2009*a* Input-output analysis, model reduction and control of the f at-plate boundary layer. *J. Fluid Mech.* **620**, 263–298. 45

BAGHERI, S., HENNINGSON, D. S., HOEPFFNER, J. & SCHMID, P. J. 2009*b* Input-output analysis and control design applied to a linear model of spatially developing f ows. *Appl. Mech. Review* **62** (2). 25, 28, 45, 126

BARBAGALLO, A., SIPP, D., JACQUIN, L. & SCHMID, P. J. 2008 Control of an incompressible cavity f ow using a reduced model based on global modes. 5^th*,AIAA Theoretical Fluid Mechanics Conference.* p. 3904. 54

BARBAGALLO, A., SIPP, D. & SCHMID, P. J. 2009 Closed-loop control of an open cavity f ow using reduced-order models. *J. Fluid Mech.* p. In Press. 45

BARDOS, C. & PIRONNEAU, O. 2003 Derivatives and control in presence of shocks. *J. Comput. Fluid. Dyn* **11**, 383–392. 36

BERGMANN, M., BRUNEAU, C. H. & IOLLO, A. 2009 Enablers for robust POD models. *J. Comput. Phys.* **228** (2), 516–538. 51, 55, 134, 137

BERGMANN, M. & CORDIER, L. 2005 Optimal rotary control of the cylinder wake using Proper Orthogonal Decomposition reduced-order model. *Phys. Fluids* **17** (9), 097101. 66, 68, 73, 92, 94, 115, 117, 135, 155

BERGMANN, M. & CORDIER, L. 2008 Optimal control of the cylinder wake in the laminar regime by trust-region methods and pod reduced-order models. *J. Comput. Phys.* **227**, 7813–7840. 48, 55, 117, 155, 162

BERKOOZ, G., HOLMES, P. & LUMLEY, J.L. 1993 The Proper Orthogonal Decomposition in the analysis of turbulent f ows. *Annu. Rev. Fluid Mech.* **25**, 539–575. 56

BEWLEY, T. R. & AGARWAL, R. 1996 Optimal and robust control of transition. *Tech. Rep.*. Summer program, Center for Turbulence Research. 25, 28, 38

BEWLEY, T. R. & LIU, S. 1998 Optimal and robust control and estimation of linear paths to transition. *J. Fluid. Mech* **365**, 305–349. 25, 28, 37, 125

BOURGET, R., BRAZA, M. & DERVIEUX, A. 2007 Reduced-order modelling for unsteady transonic f ows around an airfoil. *Phys. Fluids* **19**, 111704. 51, 68, 94

BRES, G. & COLONIUS, T. 2008 Three-dimensional instabilities in compressible f ows over open cavities. *J. Fluid Mech.* **599**, 305–349. 10

BUCHOT, J. M. & RAYMOND, J. P. 2009*a* Feedback stabilization of a boundary layer equation, part 1: Homogeneous state equations. *ESAIM: COCV* p. to appear. 46

BUCHOT, J. M. & RAYMOND, J. P. 2009*b* Feedback stabilization of a boundary layer equation, part 2: Nonhomogeneous state equations and numerical simulations. *App. Math. Res.* **to appear**. 46

BUFFONI, M., CAMARRI, S., IOLLO, A., LOMBARDI, E. & SALVETTI, M. V. 2008 A non-linear observer for unsteady three-dimensional f ows. *J. Comput. Phys.* **227**, 2626–2643. 117

BUI-THANH, T., WILLCOX, K. & GHATTAS, O. 2008 Parametric reduced-order models for probabilistic analysis of unsteady aerodynamic applications. *AIAA* **46** (10), 2520–2529. 51, 55

BURKARDT, J., GUNZBURGER, M. D. & LEE, H. C. 2006 POD and CVT-based reduced-order modeling of navier-stokes f ows. *Computer Methods in Applied Mechanics and Engineering.* **196**, 337–355. 69

CARABALLO, E., KASNAKOĞLU, C., SERRANI, A. & SAMIMY, M. 2008 Control input separation methods for reduced-order model-based feedback f ow control. *AIAA Journal* **46(9)**, 2306–2322. 74, 147

CASTRO, C., PALACIOS, F. & ZUAZUA, E. 2008 An alternating descent method for the optimal control of the inviscid burgers equation in the presence of shocks. *Mathematical Models and Methods in Applied Sciences* **18** (3), 369–416. 36

CAZEMIER, W., VERSTAPPEN, R. & VELDMAN, A. 1998 Proper Orthogonal Decomposition and low-dimensional models for driven cavity f ows. *Phys. Fluids* **10** (7), 1685–1699. 68, 92

CHATARJEE, A. 2000 An introduction to the Proper Orthogonal Decomposition. *Current Science* **78** (7), 808–817. 48, 55

CHEVALIER, M., HOEPFFNER, J., AKERVIK, E. & HENNINGSON, D.S. 2007 Linear feedback control and estimation applied to instabilities in spatially developing boundary layers. *J. Fluid Mech.* **588**, 163–187. 45

CIZMAS, P. G., PALACIOS, A., O'BRIENC, T. & SYAMLAL, M. 2003 Proper orthogonal decompositions of spatio temporal patterns in f uidized beds. *Chemical Engineering Science* **59**, 4417–4427. 55

CORDIER, L., ABOU-EL-MAJD., B. & FAVIER., J. 2009 Calibration of POD Reduced-Order models by Tikhonov regularization. *Int. J. Numer. Meth. Fluids* **In Press**. 1, 6, 89, 90, 93, 97, 133, 136

CORDIER, L. & BERGMANN, M. 2002 Proper Orthogonal Decomposition: an overview. In *Lecture series 2002-04 on the post-processing of experimental and numerical data.*. Von Karman Institut for Fluid Dynamics. 48, 49, 50, 55, 65

COUPLET, M., BASDEVANT, C. & SAGAUT, P. 2005 Calibrated reduced-order POD-galerkin system for f uid f ow modelling. *J. Comput. Phys.* **207**, 192–220. 89, 90, 92, 93, 94, 95, 96, 97, 98, 113, 133, 135, 136

COUPLET, M., SAGAUT, P. & BASDEVANT, C. 2003 Intermodal energy transfers in a proper orthogonal decomposition-galerkin representation of a turbulent seperated f ow. *J. Fluid Mech.* **491**, 275–284. 68

COURANT, R. & HILBERT, D. 1953 *Methods of mathematical physics. Vol 1.*. John. Wiley. and Sons, N.Y. 58

DEBBAGH, K., CATHALIFAUD, P. & AIRIAU, C. 2007 Optimal and robust control of small disturbances in a channel f ow with a normal magnetic f eld. *Phys. Fluids* **19**, 014103. 45

DELPRAT, N. 2006 Rossiter's formula: A simple spectral model for a complex amplitude modulation process. *Phys. Fluids* p. 071703. 18

DELVILLE, J., CORDIER, L. & BONNET, J. P. 1998 Large scale structure identif cation and control in turbulent shear f ows. *Flow control fundamentals and practices, M. Gad-el-Hak, A. Pollard. and J. P. Bonnet, lecture notes in physics, , Springer* **m 53**, 199–273. 48, 55

DELVILLE, J., UKEILEY, L., CORDIER, L. & BONNET, J. P. 1999 Examination of large scale structures in turbulent mixing layer. part 1. *J. Fluid Mech.* **391**, 91–122. 48, 50, 54, 65

EC, EUROPEAN COMMISION REPORT 2001 European aeronautics: A vision for 2020. 2

EVANS, C. LAWRENCE. 1983 An introduction to mathematical optimal control theory. In *Lecture notes University of California, Berkeley*. http://math.berkeley.edu/ evans/. 28

FAHL, M. 2000 Trust-region methods for f ow control based on reduced order modelling. PhD thesis, Trier University. http://www.mathematik.uni-trier.de:8080/ fahl/. 48, 55, 117, 155

FIEDLER, H. E. 1998 Control of free turbulent shear f ows. *Flow control fundamentals and practices, M. Gad-el-Hak, A. Pollard. and J. P. Bonnet, lecture notes in physics, Springer.* **m 53**, 336–429. 48, 55

GALETTI, B., BRUNEAU, C., ZANETTI, L. & IOLLO, A. 2004 Low-order modelling of laminar f ow regimes past a conf ned cylinder. *J. Fluid Mech.* **503**, 161–170. 68, 92, 94

GAVARINI, M.I., BOTTARO, A. & NIEUWSTADT, F.T.M. 2005 Optimal and robust control of streaks in pipe f ow. *J. Fluid Mech.* **537**, 187–219. 46

GLOERFELT, X. 2008 Compressible Proper Orthogonal Decomposition/Galerkin reduced order model of self sustained oscillations in a cavity. *Phys. Fluids* **20**, 115105. 1, 5, 48, 51, 55, 67, 68

GORDEYEV, S. 1999 Investigation of coherent structure in the similarity region of the planar turbulent jet using pod and wavelet analysis. PhD thesis, University of Notre Dame. http://www.nd.edu/ sgordeye/research.html. 55

GOTTLIEB, D & TURKEL, E. 1975 Dissipative two-four method for time dependent problem. *Tech. Rep.*. Courant Instite of Mathematical Sciences, Newyork University, No. 75-22. 12

GRAHAM, W. R., PERAIRE, J. & TANG, K.Y. 1999a Optimal control of vortex shedding using low-order models part i-open loop development. *Int. J. Numer. Meth. Fluids* **44(7)**, 945–972. 68, 115, 117

GRAHAM, W. R., PERAIRE, J. & TANG, K.Y. 1999b Optimal control of vortex shedding using low-order models part ii-model based control. *Int. J. Numer. Meth. Fluids* **44(7)**, 973–990. 68, 115, 117

GUGERCIN, S. & ANTOULAS, A. C. 2004 A survey of model reduction by balanced truncation and some new results. *Comput. Optim. Applic.* **77** (8), 748–766. 54

GUNZBURGER, M. D. 1997a Introduction into mathematical aspects of f ow control and optimization. In *Lecture series 1997-05 on inverse design and optimzation methods*. Von Karman Institut for Fluid Dynamics. 29

GUNZBURGER, M. D. 1997b Lagrange multiplier techniques. In *Lecture series 1997-05 on inverse design and optimzation methods*. Von Karman Institut for Fluid Dynamics. 29

GUNZBURGER, M. D. 1997c Approximate solutions via sensitivities. In *Lecture series 1997-05 on inverse design and optimzation methods*. Von Karman Institut for Fluid Dynamics. 29, 30

HANSEN, P. C. 1994 Regularization tools: A Matlab package for analysis and solution of discrete ill-posed problems. *Numerical Algorithms* **6**, 1–35. 99, 102, 104

HAY, A., BORGGAARD, J. T. & PELLETIER, D. 2009 Local improvements to reduced-order models using sensitivity analysis of the proper orthogonal decomposition. *J. Fluid Mech.* **629**, 41–72. 51, 55

HIGHAM, N. J. 1989 *Matrix nearness problems and applications.* In Applications of matrix theory . Glover and Barnett editors, Clarendon Press. 63

HINZE, M. 2000 Optimal and instantaneous control of the instationary navier-stokes equation, accredition to supervise research dissertation. PhD thesis, Berlin University. http://www.math.tu-berlin.de/ hinze/. 55

HINZE, M. & SLAWING, T. 2003 Adjoint gradients compared to gradients from algorithmic differentiation in the instantaneous control of the navier-stokes equations. *Optimization Methods and Software* **18**, 299–315. 35

HOLMES, P., LUMLEY, J. L. & BERKOOZ, G. 1996 *Turbulence, Coherent Structures, Dynamical Systems and Symmetry*. Cambridge University Press, Cambridge, U.K. 48, 54, 55, 59

IOLLO, A. 1997 Remarks on the approximation of the Euler equations by a low order model. *Tech. Rep.* 3329. INRIA. 67

IOLLO, A., LANTERI, S. & DÉSIDÉRI, J. A. 1998 Stability properties of POD Galerkin approximations for the compressible navier-stokes equations. *Tech. Rep.* 3589. INRIA. 67

IOLLO, A., LANTERI, S. & DÉSIDÉRI, J. A. 2000 Stability properties of POD Galerkin approximations for the Compressible NavierStokes equations. *Theor. Comp. Fluid Dyn.* (13), 377–396. 92

JOLIFFE, I.T. 1986 *Principle Component Analysis.*. Springer-Verlag, N.Y. 50, 63

JORDAN, P., SCHLEGEL, M., STALNOV, O., NOACK, B. R. & TINNEY, C.E. 2007 Identifying noisy and quiet modes in a jet. *AIAA* p. 3702. 60, 108, 134, 136

JUTTIJUDATA, V., LUMLEY, J.L.. & REMPFER, D. 2005 Proper orthogonal decomposition in squire's coordinate system for dynamical models of channel turbulence. *J. Fluid Mech.* **534**, 195–225. 68

KALB, V.L. & DEANNE, A. E. 2007 An intrinsic stabilization scheme for proper orthogonal based low-dimensional models. *Phys. Fluids* **17(9)**, 1–21. 93, 135

KARAMANOS, G. S. & KARNIADAKIS, G. E. 2000 A spectral vanishing viscosity method for large-eddy simulations. *J. Comput. Phys.* **163(1)**, 22–50. 92

KARHUNEN, K. 1946 Zur spektral theorie stochasticher prozesse. *Ann. Acad. Sci. Fennicae.* **A1**, 34. 54

KASNAKOĞLU, C. 2007 Reduced Order Modeling, nonlinear analysis and control methods for f ow control. PhD thesis, Ohio State University. 1, 6, 48, 51, 52, 55, 69, 74

KASNAKOĞLU, C., SERRANI, A. & EFE, M. O. 2008 Control input separation by actuation mode expansion for f ow control problems. *International Journal of Control.* **81** (9), 1475–1492. 51, 74, 133, 135

KESTENS, TIM. 1999 Etude numérique du contrôle adaptif multivoies des instabilités aéroacoustiques des cavitiés. PhD thesis, INP, Toulouse. 21

KIM, J. & BEWLEY, T. R. 2007 A linear systems approach to f ow control. *Annu. Rev. Fluid Mech.* **39**, 383–417. 25, 28, 38, 45

KOSAMBI, D.D. 1943 Statistics in function space. *J. Indian. Math. Soc.* **7**, 76–88. 54

KRISHNAMURTHI, K. 1956 Sound radiation from surface cutouts in high speed f ow. PhD thesis, California Institute of Technology. 8, 17

LARCHEVÊQUE, LIONEL., SAGAUT, PIERRE., LE, THIÊN-HIÊP. & COMTE., PIERRE. 2004 Large-eddy simulation of a compressible f ow in a three-dimensional open cavity at high reynolds number. *J. Fluid Mech.* **516**, 265–301. 10

LEWIS, F.L. & SYRMOS, V.L. 1995 *Optimal Control.*. John Wiley and Sons. 38, 44, 45

LOÈVE, M. 1945 Fonctions aléotoires du second ordre. *Compte Rend. Acad. Sci. Paris* p. 220. 54

LUCHTENBURG, D. M., GÜNTHER, B., NOACK, B. R., KING, R. & TADMOR, G. 2009 A generalized mean-f eld model of the natural and high frequency actuated f ow around a high lift conf guration. *J. Fluid Mech.* **623**, 283–316. 48, 55, 68

LUCIA, D. J. & BERAN, P. S. 2003 Projection methods for reduced order models of compressible f ows. *J. Comput. Phys.* **188(1)**, 252–280. 55, 68

LUMLEY, J. L. 1967 The structure of inhomogeneous turbulence. *Atmospheric turbulence and wave propogation ed (A. M. Yaglom and V. I. Tatarski).* pp. 167–178. 48, 50, 56, 61, 64

MA, X. & KARNIADIKIS, G. 2002 A low-dimensional modelling for simulating 3d cylinder f ows. *J. Fluid Mech.* **458**, 181–190. 68

MAKINEN, R., PERIAUX, J. & TOIVANEN, J. 1999 Multidisciplinary shape optimization in aerodynamics and electromagnetics using genetic algorithms. *Int. J. Numer. Meth. Fluids* **30**, 149–159. 31

MARQUET, O., SIPP, D. & JACQUIN, L. 2008 Sensitivity analysis and passive control of cylinder flow. *J. Fluid Mech.* **615**, 221–252. 37

MOHAMMADI, B. 2007 Global optimization, level set dynamics, incomplete sensitivity and regularity control. *Int. J. Comput. Fluid D.* **21** (2), 61–68. 31

MOHAMMADI, B. & PIRONNEAU, O. 2004 Shape optimization in fluid mechanics. *Annu. Rev. Fluid Mech.* **361**, 255–279. 31

MOORE, B. 1981 Principal component analysis in linear systems: Controllability, observability, and model reduction. *IEEE Trans. Automat. Contr.* pp. 17–32. 54

MORET-GABARRO, LAIA. 2009 Aeroacoustic investigation and adjoint analysis of subsonic cavity flows. PhD thesis, INP, Toulouse. 21

NAGARAJAN, K. K., CORDIER, L., AIRIAU, C. & KOURTA, A. 2009*a* Development and application of a reduced order model for the control of self-sustained instabilities in cavity flows . *non-linear dynamics.* p. communicated. 136

NAGARAJAN, K. K., CORDIER, L., AIRIAU, C. & KOURTA, A. 2009*b* POD based reduced order modelling of a compressible forced cavity flow. In 19^{th} *Congrès Français de Mécanique, Marseille, France*. 136

NOACK, A. & WALTHER, A. 2007 Adjoint concepts for the optimal control of burgers equation. *Comput. Optim. Applic.* **36**, 109–133. 37

NOACK, B.R., AFANASIEV, K., MORZYNSKI, M., TADMOR, G. & THIELE, F. 2003 A hirerarchy of low-dimensional models for the transient and post-transient cylinder wake. *J. Fluid Mech.* **497**, 335–363. 68, 89, 92

NOACK, B.R., PAPAS, P. & MONKEWITZ, P.A. 2005 The need for a pressure-term representation in empirical galerkin models of incompressible shear flows. *J. Fluid Mech.* **523**, 339–365. 71, 92

NOACK, B.R., SCHLEGEL, M., AHLBORN, B., MUTSCHKE, G., MORZYNSKI, M., COMTE, P. & TADMOR, G. 2008 A finite-time thermodynamics formalism for unsteady flows. *J. Non-Equib. Thermodyn.* **33** (2), 103–148. 104

OBAYASHI, S. 1997 *Pareto Genetic Algorithm for aerodynamic design using the Navier-Stokes equations.*. Chichester: Wiley. 31

OWENS, R. E. 1979 Energy Efficient Engine Performance System-Aircraft Integration Evaluation. *Tech. Rep.*. NASA. 3, 173

PASTOOR, M., HENNING, L., NOACK, B.R., KING, R. & TADMOR, G. 2008 Feedback shear layer control for bluff body drag reduction. *J. Fluid Mech.* **608**, 161–196. 45

PERRET, L., COLLIN, E. & DELVILLE, J. 2006 Polynomial identif cation of pod based low order dynamical system. *J. Turb* **7(17)**, 1–15. 93, 95

PERRIN, R., CID, E., CAZIN, S., SÉVRAIN, A., BRAZA, M., MORADEI, F. & HARRAN, G. 2007 Phase averaged measurements of the turbulence properties in the near wake of a circular cylinder at high reynolds number by 2c-piv and 3c-piv. *Exp. Fluids* **42**, 93–109. 48, 55

PODVIN, B. 2001 On the adequacy of the ten-dimensional model for the wall layer. *Phys. Fluids* **13** (1), 210–224. 92

POINSOT, T. J. & LELE, S. K. 1992 Boundary condition for direct simulation of compressible viscous f ows. *J. Comput. Phys.* **101**, 104–129. 8, 14, 16

QUAGLIARELLA, D. & VICINI, A. 1997 *Coupling Genetic Algorithms and Gradient Based Optimization Techniques.*, pp. 289–309. Chichester: Wiley. 31

RAJAEE, M., KARLSSON, S. & SIROVICH, L. 1994 Low dimensional description of fre-shear-f ow coherent structures and their dynamical behaviour. *J. Fluid Mech.* **258**, 1. 68

RATHINAM, M. & PETZOLD, L. R. 2003 A new look at proper orthogonal decomposition. *SIAM, Journal on Numerical Analysis* **41(5)**, 1893 – 1925. 51, 55

RAVINDRAN, S. S. 1999 Proper Orthogonal Decomposition in optimal control of f uids. *NASA Report* **TM 1999-209113**. 68

RAVINDRAN, S. S. 2000a Reduced-order adaptive controllers for f uid f ows using POD. *J. Sci. Comput.* **15(4)**, 457–478. 48, 55

RAVINDRAN, S. S. 2000b A reduced-order approach for optimal control of f uids using proper orthogonal decomposition. *int. J. Numer. Meth. Fluids* **34**, 425–448. 48, 55

RAYMOND, J. P. & THEVENET, L. 2009 Boundary feedback stabilization of the two dimensional navier-stokes equations with f nite dimensional controllers. *Discrete and Continious Dynamical Systems (A)* p. submitted. 46

REMPFER, D. 1996 Investigations of boundary layer transition via galerkin projections on empirical eigenfunctions. *Phys. Fluids* **8**, 175–188. 68, 82

REMPFER, D. 2000 On low dimensional galerkin models for f uid f ows. *Theor. Comput. Fluid. Dyn* **14** (2), 75–88. 68, 89, 92

RIESZ, F. & NAGY, B.S. 1955 *Functional Analysis.*. Ungar, N.Y. 57

ROBINSON, J. C. 2007 *Infinite Dimensional Dynamical Systems:An Introduction to Dissipative Parabolic PDE's and the Theory of Global Attractor.*. Cambridge University Press, Cambridge, U.K. 69

ROWLEY, C.W. 2005 Model reduction for fuids using balanced proper orthogonal decomposition. *Int. J. Bifurcation and Chaos.* **15** (3), 997–1013. 54

ROWLEY, C.W., COLONIUS, T. & BASU, A. J. 2002 On self-sustained oscillations in two-dimensional comprssible fow over rectangular cavities. *J. Fluid Mech.* **445**, 315–346. 8, 10, 17

ROWLEY, C.W., COLONIUS, T. & MURRAY, R. M. 2003 Model reduction for compressible fows using pod and galerkin projection. *Phys. D* **189(1-2)**, 115–129. 1, 5, 48, 51, 55, 67, 68, 72, 135, 143

ROWLEY, C. W. 2002 Modelling, simulation and control of cavity fow oscillations. PhD thesis, California Institute of Technology. *http://www.princeton.edu/ cwrowley*. 67, 72

ROWLEY, C. W. & JUTTIJUDATA, V. 2005 Model-based control and estimation of cavity fow oscillations. *44, IEEE conference on decision and control.* pp. 512–571. 115, 117

ROWLEY, C. W. & WILLIAMS, D. R. 2006 Dynamics and control of high-reynolds-number fow over open cavities. *Annu. Rev. Fluid Mech.* **38**, 251–276. 10

SAMIMY, M., DEBIASI, M., CARABALLO, E., SERRANI, A., YUAN, X., LITTLE, J. & MYATT, J. H. 2007 Feedback control of subsonic cavity fows using reduced-order models. *J. Fluid. Mech* **579**, 315–346. 1, 6, 21, 45, 48, 51, 55, 69, 115, 116, 117, 127

SHRIF., ALI EL 2008 Contrôle optimal par simulation aux grand echelles d'un ecoulement de canal turbulent. PhD thesis, INP, Lorraine. 37

SHUTIAN, D., LI, J. & LIU, C. 2007 DNS for fow seperation control around an airfoil by pulsed jets. *cf* **36** (6), 1040–1060. 21

SIRISUP, S & KARNIADAKIS, G. E. 2004 A spectral viscosity method for correcting the long-term behaviour of pod model. *J. Comput. Phys.* **194**, 92–116. 112

SIROVICH, L. 1987*a* Turbulence and the dynamics of coherent structures. part1: Coherent structures. *Quarterly of Applied Mathematics XLV* **3**, 561–571. 54

SIROVICH, L. 1987*b* Turbulence and the dynamics of coherent structures. part2: Symmetries and transformations. *Quarterly of Applied Mathematics XLV* **3**, 573–582. 50, 54, 64, 65

SMITH, T. R., MOEHLIS, J. & HOLMES, P. 2005 Low-dimensional models for turbulent plane couette fow in a minimal fow unit. *J. Fluid Mech.* **538**, 71–110. 68

SPAGNOLI, B. & AIRIAU, C. 2008 Adjoint analysis for noise control in a two-dimensional compressible mixing layer. *Computers and Fluids* **37**, 475–486. 37

TEMAM, R. 1988 *Infinite-dimensional dynamical systems in Mechanics and Physics.*. Springer-Verlag, N.Y. 59

THOMPSON, K. W. 1987 Time dependent boundary layer conditions for hyperbolic systems. *J. Comput. Phys.* **68**, 1–. 16

UKEILEY, L., CORDIER, L., MANCEAU, R., DELVILLE, J., GLAUSER, M. & BONNET, J. P. 2001 Examination of large-scale structures in a turbulent mixing layer: part 2. dynamical systems model. *J. Fluid Mech.* **441**, 67–108. 48, 50, 55, 65, 68, 117

VIGO, G. 1998 La décomposition orthogonale propre appliquée aux équations de navier-stokes compressibles instationnaires . *Tech. Rep.* 3385. INRIA. 68, 72, 145

VOLKWEIN, S. 1999 Proper orthogonal decomposition and singular value decomposition. *Tech. Rep.* 153. Institut für mathematik, Graz university, *http://www.kfunigraz.ac.at/immawww/volkwein/publist.html*. 55

WALTHER, S., AIRIAU, C. & BOTTARO, A. 2001 Optimal control of toll-schlichting waves in a developing boundary layer.. *Phys. Fluids* **13** (7), 2087–2096. 37

WELLER, J., CAMARRI, S. & IOLLO, A. 2009*a* Feedback control by low-order modelling of the laminar f ow past a bluff body. *J. Fluid Mech.* **634**, 405–418. 45, 115, 117

WELLER, J., LOMBARDI, E. & IOLLO, A. 2009*b* Robust model identif cation of actuated vortex wakes. *Physica D* **238** (4), 416–427. 48, 55, 68, 73, 117

ZABCZYK, J. 1996 *Mathematical Control Theory: An Introduction.*. Birkhauser. 28

ZHOU, K., DOYLE, J. C. & GLOVER, K. 1996 *Robust and optimal control.*. Prentice Hall. 38, 44

ZUCCHER, S., LUCHINI, P. & BOTTARO, A. 2004 Algebraic growth in a blasius boundary layer: optimal and robust control by mean suction in the nonlinear regime. *J. Fluid Mech.* **513**, 135–160. 46

List of Figures

Résumé

On considère un écoulement compressible bidimensionnel, autour d'une cavité ouverte. Des d'instabilité, auto-entretenues par l'effet de rétroaction de l'écrasement de la couche de cisaillement sur le bord aval de la cavité, génèrent des émissions acoustiques qu'il faut réduire. Des simulations numériques directes (DNS) permettent d'obtenir, avec ou sans actionnement, un modèle précis de l'écoulement. A partir des champs issus de la simulation, des décompositions orthogonales de modes propres (POD) sont proposèes pour bâtir, par projection de Galerkin sur les équations isentropiques, des modèles d'ordre réduit non linéaires en prenant en compte l'actionnement (le contrôle). Pour éviter la divergence temporelle, les coeff cients du système dynamique non forcé sont calibrés par diverses approches originales dont une basée sur la sensiblité modale. A partir du système dynamique forcé par un actionnement multifréquentiel (présent aussi dans les DNS), un contrôle en boucle fermée linéaire quadratique gaussien est proposé sur un système linéarisé. La reconstruction de l'état est basée sur une estimation stochastique linéaire sur 6 points de pression. Le contrôle optimal obtenu s'avére être périodique à la fréquence du second mode de Rossiter, qui est exactement celles des instabilits auto-entretenues dans la cavité. Par introduction de ce contrôle dans les simulations numériques directes, nous avons obtenu une réduction du bruit (faible) sur la fréquence du contrôle.

Mots clefs: Ecoulements en cavité, Modélisation d'ordre réduit, contrôle rétroactif

Abstract

We consider a two dimensional compressible f ow around an open cavity. The Flow around a cavity is characterised by a self-sustained mechanism in which the shear layer impinges on the downstream edge of the cavity resulting in an acoustic feedback mechanism which must be reduced. Direct Numerical Simulations (DNS) of the f ow at a representative Reynolds number has been carried to obtain pressure and velocity f elds, both for the case of unactuated and multi frequency actuation. These f elds are then used to extract energy ranked coherent structures also called as the Proper Orthogonal Decomposition (POD) modes. A Reduced Order Model is constructed by a Galerkin projections of the isentropic compressible equations. The model is then extended to include the effect of control. To avoid the divergence of the model while integrating in time various calibration techniques has been utillized. A new method of calibration which minimizes a linear functional of error, based on modal sensitivity is proposed. The calibrated low order model is used to design a feedback control of the Linear Quadratic Gaussian (LQG) type, coupled with an observer. For the experimental implementation of the controller, a state estimate based on the observed pressure measurements at 6 different locations, is obtained through a Linear Stochastic Estimation (LSE). The optimal control obtained is periodic with a frequency corresponding to the second Rossiter mode of the cavity. Finally the control obtained is introduced into the DNS to obtain a decrease in spectra of the cavity acoustic mode.

Keywords: Cavity flows, Reduced Order Modelling, feedback control